

**Immunomodulatory Activity of *Lacticaseibacillus rhamnosus* R0011:
Analysis of Secretome-Mediated Impacts on Innate Immune Outcomes
in Intestinal Epithelial Cells and Antigen Presenting Cells**

by

Michael P. Jeffrey

A thesis submitted to the
School of Graduate and Postdoctoral Studies in partial
fulfillment of the requirements for the degree of

Doctor of Philosophy in Applied Bioscience

The Faculty of Science

University of Ontario Institute of Technology (Ontario Tech University)

Oshawa, Ontario, Canada

December 2021

© Michael P. Jeffrey, 2021

Thesis Examination Information

Submitted by: **Michael Jeffrey**

Doctor of Philosophy in Applied Bioscience

Thesis title: Immunomodulatory Activity of <i>Lactocaseibacillus rhamnosus</i> R0011: Analysis of Secretome-Mediated Impacts on Innate Immune Outcomes in Intestinal Epithelial Cells and Antigen Presenting Cells

An oral defense of this thesis took place on November 19th, 2021 in front of the following examining committee:

Examining Committee:

Chair of Examining Committee	Dr. Robert Bailey
Research Supervisor	Dr. Julia Green-Johnson
Examining Committee Member	Dr. Janice Strap
Examining Committee Member	Dr. Holly Jones Taggart
University Examiner	Dr. Dario Bonetta
External Examiner	Dr. Carole Creuzenet, University of Western Ontario

The above committee determined that the thesis is acceptable in form and content and that a satisfactory knowledge of the field covered by the thesis was demonstrated by the candidate during an oral examination. A signed copy of the Certificate of Approval is available from the School of Graduate and Postdoctoral Studies.

Abstract

Certain lactic acid bacteria (LAB), such as *Lactocaseibacillus rhamnosus* R0011, are associated with immune modulatory activities including down-regulation of pro-inflammatory gene transcription and expression. While host intestinal epithelial cells (IECs) and antigen-presenting cells (APCs) can interact directly with both commensal and pathogenic bacteria through innate immune pattern recognition receptors, recent evidence indicates indirect communication mediated by soluble mediators may be important in shaping host immune outcomes at the gut-mucosal interface. However, many questions remain about how soluble mediators derived from LAB can influence functional immune outcomes in IECs and APCs, especially in the context of pro-inflammatory challenge as over-expression and dysregulation of the inflammatory mediators they produce also contributes to numerous inflammatory disease pathologies. Genome-wide transcriptional profiling revealed context-dependent regulation of Tumor Necrosis Factor α and *Salmonella enterica* subsp. *enterica* serovar Typhimurium secretome-induced pro-inflammatory mediator transcription and production by the *Lactocaseibacillus rhamnosus* R0011 secretome (LrS) in human IEC, indicating a potential for modulation of pro-inflammatory immune activity with minimal IEC impact in the absence of a pro-inflammatory challenge. This modulation may be mediated through induction of negative regulators of innate immunity (*ATF3*, *TRIB3*, *DUSP1*) and through changes in global histone acetylation patterns, events important in maintaining immune regulation. THP-1 human monocytes conditioned with the LrS showed functional, transcriptional, and immunometabolic signatures consistent with M2 immunoregulatory activity, with increased production of immunoregulatory cytokines IL-10, IL-1Ra, and IL-4 and a cell-

surface expression profile of CD11b, CD11c^{lo}, and CX₃CR₁, features shared with subsets of gut macrophages. The LrS was able to attenuate STS-induced damage to IEC monolayer integrity and pro-inflammatory mediator production in Transwell co-cultures of human IECs and APCs, indicating that the LrS retains immunoregulatory activity in a context which more closely mimics that which occurs *in vivo*. Biochemical characterization of the soluble components found in the LrS revealed unique protein, amino acid, and metabolomic profiles warranting future experimentation to determine components with immunoregulatory bioactivity. Taken together, the results reported here provide insight into novel routes for indirect host-microbe communication mediated via secretome components and the subsequent impact on multiple immune regulatory mechanisms integral for IEC and APC function and activity.

Keywords: *Lacticaseibacillus rhamnosus* R0011; secretome; innate immune regulation; MIF; immunometabolism

Author's Declaration

I hereby declare that this thesis consists of original work of which I have authored. This is a true copy of the thesis, including any required final revisions, as accepted by my examiners.

I authorize the University of Ontario Institute of Technology (Ontario Tech University) to lend this thesis to other institutions or individuals for the purpose of scholarly research. I further authorize University of Ontario Institute of Technology (Ontario Tech University) to reproduce this thesis by photocopying or by other means, in total or in part, at the request of other institutions or individuals for the purpose of scholarly research. I understand that my thesis will be made electronically available to the public.

Michael P. Jeffrey

Statement of Contributions

Some of the work described in **Chapters 1, 2, and 3** was performed at the Rosell Institute for Microbiome and Probiotics (RIMAP), in Montreal, QC, Canada, and some of the measures presented in **Chapter 4** were carried out by research scientists at the Hospital for Sick Children SPARC Biocentre in Toronto, Ontario (amino acid analyses), Applied Biomics in California, U.S.A (2-D gel protein analyses), and Metabolon in North Carolina, U.S.A (metabolomic analyses). I was responsible for designing and performing the experiments as well as the analysis and interpretation of the data. RIMAP, in particular Dr. Thomas Tompkins and Chad Macpherson, provided technical support and expertise as well as access to equipment and tools required to perform most of the experiments¹.

The work described in **Chapter 1** has been published in the Journal of Immunology²:

Jeffrey, M. P., C. W. MacPherson, O. Mathieu, T. A. Tompkins, and J. M. Green-Johnson. 2020. Secretome-Mediated Interactions with Intestinal Epithelial Cells: A Role for Secretome Components from *Lactobacillus rhamnosus* R0011 in the Attenuation of *Salmonella* enterica Serovar Typhimurium Secretome and TNF-alpha-Induced Proinflammatory Responses. *J Immunol* 204: 2523-2534 available at <https://www.jimmunol.org/>

The work in **Chapters 2, 3 and 4** is being prepared for submission as three separate manuscripts

¹This work was supported by the MITACS Accelerate program through a partnership with the Rosell Institute for Microbiome and Probiotics (RIMAP) and by the Natural Sciences and Engineering Research Council of Canada (NSERC).

²The microarray data presented in **Chapter 1** has been submitted to the National Center for Biotechnology Information Gene Expression Omnibus (<https://www.ncbi.nlm.nih.gov/geo/query/acc.cgi?acc=GSE145091>) under accession number GSE145091

Acknowledgements

A special heart-filled thanks to my supervisor, Dr. Julia Green-Johnson, for her help, support, and guidance throughout my time in graduate studies. Her enthusiasm and curiosity for science inspired me to stay positive and to always work hard – you have sincerely made this journey such an enjoyable experience. I would also like to extend my gratitude to my committee members, Dr. Holly Jones Taggart and Dr. Janice Strap, whose keen interest and invaluable expertise always led to fruitful discussions during our meetings.

I would also like to thank the Rosell Institute for Microbiome and Probiotics for providing me with the opportunity to gain invaluable research experience. In particular, I would like to thank Dr. Thomas Tompkins for his expertise, patient support, and insightful feedback – thank you for all of the opportunities I was given. A sincere thank you to Chad MacPherson for always believing in me. I will always value our friendship and I look forward to many more conversations about science and philosophy.

To my lab mates, and in particular Dr. Padmaja Shastri and Dr. Sandra Clarke, thank you for your friendship.

Finally, to my friends and family who continued to support me during the completion of this project – thank you!

TABLE OF CONTENTS

Thesis Examination Information	ii
Abstract	ii
Author’s Declaration	iv
Statement of Contributions	v
Acknowledgements	vi
TABLE OF CONTENTS	vii
LIST OF TABLES	xi
LIST OF FIGURES	xii
LIST OF ABBREVIATIONS AND SYMBOLS	xx
INTRODUCTION	1
Host-Microbe Immune Communication and The Innate Immune System.....	1
The Mucosal Immune System and the Gut Microbiome.....	7
CHAPTER 1: Secretome-mediated interactions with intestinal epithelial cells: a role for secretome components from <i>Lactobacillus rhamnosus</i> R0011 in the attenuation of <i>Salmonella</i> enterica serovar Typhimurium secretome and TNF-α-induced pro-inflammatory responses	14
1.1 Introduction	14
1.2 Objectives	17
1.3 Methods	18
Bacterial Culture.....	18
Cell Culture and Challenge Assay and RNA extraction.....	19
Reverse Transcription (RT) of RNA and Direct-Method of Labelling	20
Microarray Analysis	20
Comparative RT-qPCR.....	21
Histone Extraction and H3/H4 Histone Acetylation Assay.....	22
Cytokine/Chemokine/Inflammation Marker Analysis	23
Measurement of Intracellular Reactive Oxygen Species (ROS) Generation.....	24
1.3 Results	25
The LrS attenuates TNF- α - and STS-induced changes in global gene expression profiles in HT-29 IECs	25
The LrS induces negative regulators of innate immunity in TNF- α and STS challenged IECs	27

The LrS attenuates TNF- α and STS-induced global histone acetylation	28
The LrS attenuates TNF- α - and ST-induced pro-inflammatory cytokine and chemokine protein production	29
The LrS reduces ROS generation from HT-29 IECs.....	30
1.4 Discussion	31
CHAPTER 2: <i>Lactocaseibacillus rhamnosus</i> R0011 secretome induces temporal transcriptional, functional, and immunometabolic signatures in THP-1 monocytes consistent with M2 immunoregulatory macrophage activity	68
2.1 Introduction	68
2.2 Objectives	71
2.3 Materials and Methods	72
Bacterial Culture	72
THP-1 Human Monocyte Conditioning and LPS Challenge	72
Reverse Transcription (RT) of RNA and Direct-Method of Labelling	73
Microarray Analysis	74
Global H3/H4 Histone Acetylation and DNA Methylation Determination	75
Chemokine and Cytokine Profiling	75
Morphological Characterization	76
Mitochondrial Function Assay	76
Analysis of Protein Lysine Acetylation.....	77
Flow Cytometry.....	77
2.4 Results	79
LrS conditioning induces differential and temporal gene expression profiles in THP-1 human monocytes	79
The LrS polarizes THP-1 monocytes into immunoregulatory M2 macrophages.....	80
Phenotypic characterization of LrS conditioned M2 macrophages	82
The LrS influences protein lysine acetylation patterns in THP-1 monocytes	83
LrS conditioned THP-1 macrophages respond robustly to LPS challenge	84
2.5 Discussion	86
CHAPTER 3: <i>Lactocaseibacillus rhamnosus</i> R0011 secretome impact on immune outcomes in intestinal epithelial and antigen-presenting cell interactions using an <i>in vitro</i> co-culture system	140
3.1 Introduction	140
3.2 Objectives	144

3.3 Materials and Methods	145
Bacterial Culture	145
Cell Culture and Challenge Assay and RNA extraction.....	145
Paracellular Flux Measurement	147
Comparative RT-qPCR.....	148
Morphological Characterization	148
Cytokine/Chemokine/Inflammatory Marker Analysis	149
3.4 Results	151
The LrS attenuates STS-induced pro-inflammatory cytokine and chemokine production from T84 IEC and THP-1 APC co-cultures	151
The LrS attenuates STS-induced pro-inflammatory gene expression in T84 IECs and THP-1 monocytes	152
The LrS reverses STS-induced damage to T84 IEC monolayer integrity via increased MIF production.....	153
3.5 Discussion	155
CHAPTER 4: Biochemical characterization and identification of components of the <i>Lactocaseibacillus rhamnosus</i> R0011 secretome	217
4.1 Introduction	217
4.2 Objectives	220
4.3 Materials and Methods	221
Bacterial Culture	221
Amino acid analyses	221
Two-dimensional difference gel electrophoresis (2D-DIGE) and protein identification via mass spectrometry	222
Metabolomic profiling	223
4.4 Results	224
The LrS has unique amino acid profiles when compared to secretomes derived from <i>L. helveticus</i> R0052 and R0389	224
Protein profiling identified unique proteins in the secretomes of exponential and stationary grown cultures.....	224
Metabolite composition of the three lactobacilli secretomes is species- and growth- phase-dependent	225
Tryptophan-derived AhR ligands and phenylalanine-derived metabolites were secreted by all strains.....	226
Methionine metabolism was altered between all bacterial strains.....	226

4.5 Discussion.....	227
GENERAL DISCUSSION AND CONCLUSIONS	241
APPENDIX.....	250
REFERENCES.....	255

LIST OF TABLES

CHAPTER 1

Table 1-I. Fold change difference in expression of genes encoding pro-inflammatory mediators and negative regulators of innate immunity in HT-29 IECs exposed to TNF- α , STS, the LrS, L-lactic acid, or a combination of the treatments.	39
Table 1-II. List of primers used for relative RT-qPCR for microarray validation.	40

CHAPTER 2

Table 2-I. Fold change differences in the amount of acetylation of proteins found in THP-1 human monocytes conditioned with the LrS versus medium controls for 24-, 48-, and 72-hours.	95
Table 2-II. Protein identification of spot IDs showing a fold change ≥ 3 in acetylation of lysine residues in proteins found within THP-1 human monocytes conditioned with the LrS when compared to controls.	97

CHAPTER 3

Table 3-I. List of primers used for relative RT-qPCR for determination of gene expression profiles in T84 IECs and THP-1 monocyte co-cultures.	160
--	------------

CHAPTER 4

Table 4-I. Protein identification via mass spectrometry of proteins found within the LrS from MRS-grown culture.	231
Table 4-II. Protein identification via mass spectrometry of proteins found within the LrS when grown in RPMI-1640 medium.	232

LIST OF FIGURES

INTRODUCTION

Figure I-1. Tissue macrophages exist as a heterogeneous population consisting of both M1 and M2 polarized macrophages each with their own unique repertoire of effector functions and are induced by different signals found within their microenvironments.	4
Figure I-2. M1 and M2 macrophages display distinct differences in their metabolic profiles.	6
Figure I-3. The GALT is a specialized area within the gut containing unique intestinal epithelial cells and other immune cells which help to facilitate gut microbiota-host immune communication.....	9

CHAPTER 1

Figure 1-1. Analysis of global gene expression data in HT-29 IECs exposed to TNF- α , the STS, the LrS alone, a combination of the LrS and either TNF- α or the STS, an L-lactic acid control, or a combination of the STS or TNF- α and L-lactic acid.....	41
Figure 1-2. Pathway analysis of TNF- α signaling pathways using IPA predictive modelling of the cellular outcomes of HT-29 IECs exposed to TNF- α challenge or TNF- α and the LrS.....	42
Figure 1-3. Gene-interaction maps of genes involved in the TNF- α signaling pathway in HT-29 IECs that were differentially modified relative to untreated cells as determined by the GeneDecks gene enrichment analysis and GeneMania	43
Figure 1-4. Gene-interaction maps of genes involved in the NF- κ B signaling pathway in HT-29 IECs that were differentially modified relative to untreated cells as determined by the GeneDecks gene enrichment analysis and GeneMania	44
Figure 1-5. Negative regulators of the innate immune response that were identified to be differentially transcribed in response to the different treatments.	45
Figure 1-6. RT-qPCR confirmation of the expression of Trib3, ATF3, DUSP1, and NF κ B1.....	46
Figure 1-7. Changes in global histone A. H3 or B. H4 acetylation patterns in challenged IECs.....	47
Figure 1-8. Cytokine and chemokine profiles from HT-29 IECs exposed to the different treatments for 6 hours.	48

Figure 1-9. Cytokine and chemokine profiles from HT-29 IECs challenged with the LrS, L-LA, TNF- α , or a combination of the different challenges for 6 hours	49
Figure 1-10. Cytokine and chemokine profiles from HT-29 IECs challenged with the LrS, L-LA, STS, or a combination of the different challenges for 6 hours.	59
Figure 1-11. String v 11.0 analysis reveals functional links between each of the different cytokines/chemokines measured in response to TNF- α , STS, LrS + TNF- α , L-LA + TNF- α , LrS + STS and L-LA + STS	65
Figure 1-12. MIF production is induced in HT-29 IECs by the LrS.....	66
Figure 1-13. IPA Upstream Regulator analytics identification of reactive oxygen species as a potential regulator explaining the observed gene expression changes when HT-29 IECs are exposed to the LrS and either TNF- α or STS.....	67

CHAPTER 2

Figure 2-1. The LrS induces unique temporal transcriptional profiles in THP-1 human monocytes distinct from L-LA controls.....	99
Figure 2-3. Changes in global histone H3 or H4 acetylation patterns and DNA methylation in THP-1 human monocytes conditioned with the LrS.....	101
Figure 2-4. THP-1 human monocytes conditioned with the LrS show similar transcription profiles to those seen in immunoregulatory macrophage activation.....	102
Figure 2-5. LrS conditioning of THP-1 human monocytes results in unique temporal cytokine and chemokine production profiles.....	103
Figure 2-6. Cytokine and chemokine profiles from THP-1s conditioned with the LrS (20% v/v) or L-LA controls for 24-, 48-, or 72-hours.....	104
Figure 2-8. Conditioning with the LrS induces distinct morphological changes in THP-1 monocytes when compared to secretomes derived from <i>S. enterica</i> serovar Typhimurium and <i>S. thermophilus</i> R0083.	128
Figure 2-9. Conditioning with the LrS induces distinct morphological changes and increases the cell-surface expression of CD11b, CD11c, CX3CR1 and CD86 in THP-1 human monocytes.	129
Figure 2-10. The LrS induces metabolic functional changes in THP-1 monocytes.	130
Figure 2-11. The LrS induces unique temporal changes in protein acetylation patterns in THP-1 human monocytes following conditioning for 24-, 48-, and 72-hours.	131
Figure 2-12. LPS-challenge of THP-1 monocytes conditioned with the LrS reveals heightened responsiveness.....	132
Figure 2-13. Cytokine and chemokine profiles from THP-1s conditioned with the LrS (20% v/v) 72-hours followed by challenge with LPS (125ng/mL) or LPS challenge alone for 6 hours.	133

CHAPTER 3

Figure 3-1. Transwell in vitro co-culture systems allow for the investigation of interactions between bacteria, IECs, and APCs in an environment which closely mimics the intestinal environment 144

Figure 3-2. Two-dimensional hierarchical clustering analysis of cytokine and chemokine production profiles from the apical and basolateral chambers of T84 IEC/THP-1 human monocytes in response to apically delivered LrS, STS, a combination of the LrS and the StS, or medium controls for 24 hours 162

Figure 3-3A. Apical and basolateral production of CCL1 by T84 IEC and THP-1 monocyte co-cultures following challenge with the LrS, STS, or a combination of the secretomes for 24 hours..... 163

Figure 3-3B. Apical and basolateral production of CCL2 by T84 IEC and THP-1 monocyte co-cultures following challenge with the LrS, STS, or a combination of the secretomes for 24 hours..... 164

Figure 3-3C. Apical and basolateral production of CCL3 by T84 IEC and THP-1 monocyte co-cultures following challenge with the LrS, STS, or a combination of the secretomes for 24 hours..... 165

Figure 3-3D. Apical and basolateral production of CCL13 by T84 IEC and THP-1 monocyte co-cultures following challenge with the LrS, STS, or a combination of the secretomes for 24 hours. 166

Figure 3-3E. Apical and basolateral production of CCL15 by T84 IEC and THP-1 monocyte co-cultures following challenge with the LrS, STS, or a combination of the secretomes for 24 hours. 167

Figure 3-3F. Apical and basolateral production of CCL19 by T84 IEC and THP-1 monocyte co-cultures following challenge with the LrS, STS, or a combination of the secretomes for 24 hours. 168

Figure 3-3G. Apical and basolateral production of CCL20 by T84 IEC and THP-1 monocyte co-cultures following challenge with the LrS, STS, or a combination of the secretomes for 24 hours. 169

Figure 3-3H. Apical and basolateral production of CCL21 by T84 IEC and THP-1 monocyte co-cultures following challenge with the LrS, STS, or a combination of the secretomes for 24 hours. 170

Figure 3-3I. Apical and basolateral production of CCL22 by T84 IEC and THP-1 monocyte co-cultures following challenge with the LrS, STS, or a combination of the secretomes for 24 hours. 171

Figure 3-3J. Apical and basolateral production of CCL23 by T84 IEC and THP-1 monocyte co-cultures following challenge with the LrS, STS, or a combination of the secretomes for 24 hours. 172

Figure 3-3K. Apical and basolateral production of CCL24 by T84 IEC and THP-1 monocyte co-cultures following challenge with the LrS, STS, or a combination of the secretomes for 24 hours.	173
Figure 3-3L. Apical and basolateral production of CCL25 by T84 IEC and THP-1 monocyte co-cultures following challenge with the LrS, STS, or a combination of the secretomes for 24 hours	174
Figure 3-3M. Apical and basolateral production of CCL26 by T84 IEC and THP-1 monocyte co-cultures following challenge with the LrS, STS, or a combination of the secretomes for 24 hours.	175
Figure 3-3N. Apical and basolateral production of CCL27 by T84 IEC and THP-1 monocyte co-cultures following challenge with the LrS, STS, or a combination of the secretomes for 24 hours.	176
Figure 3-3O. Apical and basolateral production of CD163 by T84 IEC and THP-1 monocyte co-cultures following challenge with the LrS, STS, or a combination of the secretomes for 24 hours.	177
Figure 3-3P. Apical and basolateral production of CX3CL1 by T84 IEC and THP-1 monocyte co-cultures following challenge with the LrS, STS, or a combination of the secretomes for 24 hours.	178
Figure 3-3Q. Apical and basolateral production of CXCL1 by T84 IEC and THP-1 monocyte co-cultures following challenge with the LrS, STS, or a combination of the secretomes for 24 hours.	179
Figure 3-3R. Apical and basolateral production of CXCL2 by T84 IEC and THP-1 monocyte co-cultures following challenge with the LrS, STS, or a combination of the secretomes for 24 hours.	180
Figure 3-3S. Apical and basolateral production of CXCL3 by T84 IEC and THP-1 monocyte co-cultures following challenge with the LrS, STS, or a combination of the secretomes for 24 hours.	181
Figure 3-3T. Apical and basolateral production of CXCL5 by T84 IEC and THP-1 monocyte co-cultures following challenge with the LrS, STS, or a combination of the secretomes for 24 hours	182
Figure 3-3U. Apical and basolateral production of CXCL8 by T84 IEC and THP-1 monocyte co-cultures following challenge with the LrS, STS, or a combination of the secretomes for 24 hours.	183
Figure 3-3V. Apical and basolateral production of CXCL9 by T84 IEC and THP-1 monocyte co-cultures following challenge with the LrS, STS, or a combination of the secretomes for 24 hours.	184
Figure 3-3W. Apical and basolateral production of CXCL10 by T84 IEC and THP-1 monocyte co-cultures following challenge with the LrS, STS, or a combination of the secretomes for 24 hours.	185

Figure 3-3X. Apical and basolateral production of CXCL11 by T84 IEC and THP-1 monocyte co-cultures following challenge with the LrS, STS, or a combination of the secretomes for 24 hours.	186
Figure 3-3Y. Apical and basolateral production of CXCL12 by T84 IEC and THP-1 monocyte co-cultures following challenge with the LrS, STS, or a combination of the secretomes for 24 hours.	187
Figure 3-3Z. Apical and basolateral production of CXCL16 by T84 IEC and THP-1 monocyte co-cultures following challenge with the LrS, STS, or a combination of the secretomes for 24 hours.	188
Figure 3-3AA. Apical and basolateral production of gp130 by T84 IEC and THP-1 monocyte co-cultures following challenge with the LrS, STS, or a combination of the secretomes for 24 hours.	189
Figure 3-3BB. Apical and basolateral production of IFN- β by T84 IEC and THP-1 monocyte co-cultures following challenge with the LrS, STS, or a combination of the secretomes for 24 hours.	190
Figure 3-3CC. Apical and basolateral production of IFN- γ by T84 IEC and THP-1 monocyte co-cultures following challenge with the LrS, STS, or a combination of the secretomes for 24 hours.	191
Figure 3-3DD. Apical and basolateral production of IL-1 β by T84 IEC and THP-1 monocyte co-cultures following challenge with the LrS, STS, or a combination of the secretomes for 24 hours.	192
Figure 3-3EE. Apical and basolateral production of IL-6 by T84 IEC and THP-1 monocyte co-cultures following challenge with the LrS, STS, or a combination of the secretomes for 24 hours.	193
Figure 3-3FF. Apical and basolateral production of IL-6RA by T84 IEC and THP-1 monocyte co-cultures following challenge with the LrS, STS, or a combination of the secretomes for 24 hours.	194
Figure 3-3GG. Apical and basolateral production of IL-10 by T84 IEC and THP-1 monocyte co-cultures following challenge with the LrS, STS, or a combination of the secretomes for 24 hours.	195
Figure 3-3HH. Apical and basolateral production of IL-16 by T84 IEC and THP-1 monocyte co-cultures following challenge with the LrS, STS, or a combination of the secretomes for 24 hours.	196
Figure 3-3II. Apical and basolateral production of IL-26 by T84 IEC and THP-1 monocyte co-cultures following challenge with the LrS, STS, or a combination of the secretomes for 24 hours.	197
Figure 3-3JJ. Apical and basolateral production of IL-27(p28) by T84 IEC and THP-1 monocyte co-cultures following challenge with the LrS, STS, or a combination of the secretomes for 24 hours.	198

Figure 3-3KK. Apical and basolateral production of IL-32 by T84 IEC and THP-1 monocyte co-cultures following challenge with the LrS, STS, or a combination of the secretomes for 24 hours.	199
Figure 3-3LL. Apical and basolateral production of IL-34 by T84 IEC and THP-1 monocyte co-cultures following challenge with the LrS, STS, or a combination of the secretomes for 24 hours.	200
Figure 3-3MM. Apical and basolateral production of IL-35 by T84 IEC and THP-1 monocyte co-cultures following challenge with the LrS, STS, or a combination of the secretomes for 24 hours.	201
Figure 3-3NN. Apical and basolateral production of MIF by T84 IEC and THP-1 monocyte co-cultures following challenge with the LrS, STS, or a combination of the secretomes for 24 hours.	202
Figure 3-3OO. Apical and basolateral production of Osteopontin by T84 IEC and THP-1 monocyte co-cultures following challenge with the LrS, STS, or a combination of the secretomes for 24 hours.	203
Figure 3-3PP. Apical and basolateral production of Pentraxin by T84 IEC and THP-1 monocyte co-cultures following challenge with the LrS, STS, or a combination of the secretomes for 24 hours.	204
Figure 3-3QQ. Apical and basolateral production of TNF- α by T84 IEC and THP-1 monocyte co-cultures following challenge with the LrS, STS, or a combination of the secretomes for 24 hours.	205
Figure 3-3RR. Apical and basolateral production of TNFR1 by T84 IEC and THP-1 monocyte co-cultures following challenge with the LrS, STS, or a combination of the secretomes for 24 hours.	206
Figure 3-3SS. Apical and basolateral production of TNFR2 by T84 IEC and THP-1 monocyte co-cultures following challenge with the LrS, STS, or a combination of the secretomes for 24 hours.	207
Figure 3-3TT. Apical and basolateral production of TNFRSF8 by T84 IEC and THP-1 monocyte co-cultures following challenge with the LrS, STS, or a combination of the secretomes for 24 hours.	208
Figure 3-3UU. Apical and basolateral production of TNFSF13 by T84 IEC and THP-1 monocyte co-cultures following challenge with the LrS, STS, or a combination of the secretomes for 24 hours.	209
Figure 3-3VV. Apical and basolateral production of TNFSF13B by T84 IEC and THP-1 monocyte co-cultures following challenge with the LrS, STS, or a combination of the secretomes for 24 hours.	210
Figure 3-3WW. Apical and basolateral production of C3L1 by T84 IEC and THP-1 monocyte co-cultures following challenge with the LrS, STS, or a combination of the secretomes for 24 hours.	211

Figure 3-4. Gene expression profiles of T84 IECs in T84 IEC/THP-1 monocyte co-cultures challenged with the LrS, STS, or a combination of the secretomes.	212
Figure 3-5. Gene expression profiles of THP-1 monocytes in T84 IEC/THP-1 monocyte co-cultures challenged with the LrS, STS, or a combination of the secretomes.....	213
Figure 3-6. The LrS attenuates STS-induced damage to T84 IEC monolayer integrity and permeability.	214
Figure 3-7. The LrS attenuates STS-induced damage to T84 IEC monolayer and integrity by antagonizing STS damage to ZO-1.....	215
Figure 3-8. The impact of the LrS on T84 IEC barrier function and integrity is abrogated by the addition of a MIF blocking antibody	216

CHAPTER 4

Figure 4-1. Free amino acid profiling of the secretomes of <i>L. rhamnosus</i> R0011, <i>L. helveticus</i> R0052, and <i>L. helveticus</i> R0389 when grown to stationary phase in RPMI-1640 medium.	233
Figure 4-2. 2D DIGE analysis of differentially expressed proteins found within RPMI-1640 grown stationary-phase and exponential-phase LrS and or MRS grown stationary-phase and exponential-phase LrS.....	2344
Figure 4-3. 2D DIGE analysis of differentially expressed proteins found within RPMI-1640 grown stationary-phase and exponential-phase LrS of two biological replicates	2355
Figure 4-4. BLAST Tree View of the multiple species alignment of NCBI BLASTp results using the <i>L. rhamnosus</i> R0011 GAPDH as the query search.	2366
Figure 4-5. PCA analysis, overview heat map representation, and summary counts of statistically significant biochemicals secretomes derived from exponential and stationary phase derived cultures of <i>L. rhamnosus</i> R0011, <i>L. helveticus</i> R0052, and <i>L. helveticus</i> R0389	2377
Figure 4-6. Heat map, boxplots, and Cytoscape visualizations of tryptophan metabolites found within the Lr-R0011, Lh-R0052, and the Lh-R0389 secretomes.	2388
Figure 4-7. Heat map, boxplots, and Cytoscape visualizations of phenylalanine metabolites found within the Lr-R0011, Lh-R0052, and the Lh-R0389 secretomes.	23939
Figure 4-8. Heat map, boxplots, and Cytoscape visualizations of methionine metabolites found within the Lr-R0011, Lh-R0052, and the Lh-R0389 secretomes.	2400

DISCUSSION

- Figure D-1.** Proposed mechanism of action behind the observed immunomodulatory activity of the LrS on HT-29 IECs challenged with the STS or TNF- α 242
- Figure D-2.** The LrS differentiates THP-1 human monocytes into macrophages which display functional similarities to M2-like macrophages. 244
- Figure D-3.** Post-translational modifications by the LrS to key enzymes involved in glycolysis may reveal mechanism(s) of action behind the observed immunometabolic shift towards an M2-like phenotype in LrS-conditioned macrophages. 246
- Figure D-4.** LrS-induced MIF production by T84 IECs antagonizes STS-induced damage to IEC monolayer integrity and subsequent inflammatory activity by the underlying APC population. 247

APPENDIX

- Appendix A1.** Sample readout obtained from the Agilent 2000 Bioanalyzer to determine RNA quality prior to cDNA synthesis for qRT-PCR and microarray experiments. 250
- Appendix A2.** Sample MA plot with LOWESS normalization of microarray gene expression data taken from HT-29 IECs challenged with TNF- α 251
- Appendix A3.** Volcano plot analysis of gene expression data taken from HT-29 IECs conditioned with the LrS, conducted using MeV software..... 252
- Appendix A4.** Cytokines/chemokines examined and their associated functions..... 253

LIST OF ABBREVIATIONS AND SYMBOLS

2D-DIGE	Two-dimensional Difference gel Electrophoresis
ANOVA	Analysis of Variance
AP-1	Activator Protein-1
APC	Antigen-presenting Cell
ATCC	American Type Culture Collection
ATF3	Activating Transcription Factor 3
CCL	Chemokine (C-C motif) Ligand
CD	Cluster of Differentiation
CXCL	Chemokine (C-X-C motif) Ligand
DUSP1	Dual Specificity Phosphatase 1
ELISA	Enzyme-Linked Immunosorbent Assay
FAO	Fatty Acid Oxidation
FAS	Fatty Acid Synthesis
FITC	Fluorescein Isothiocyanate
GALT	Gut-Associated Lymphoid Tissue
GI	Gastrointestinal
HDAC	Histone Deacetylase
IEC	Intestinal Epithelial Cell
IL-#	Interleukin-#
LA	Lactic Acid
LAB	Lactic Acid Bacteria

LPS	Lipopolysaccharide
LrS	<i>Lactocaseibacillus rhamnosus</i> R0011 secretome
LTA	Lipoteichoic Acid
MAMPs	Microbe-Associated Molecular Patterns
MAPK	Mitogen-Activated Protein Kinases
MIF	Macrophage Inhibitory Factor
MIQE	Minimum Information for Publication of Quantitative Real-Time PCR Experiments
MFI	Mean Fluorescence Intensity
MyD88	Myeloid Differentiation Factor 88
NF- κ B	Nuclear Factor Kappa-light-chain- enhancer of Activated B cells
NLR	NOD-like Receptor
NOD#	Nucleotide-Binding Oligomerization Domain
PAMPs	Pathogen-Associated Molecular Patterns
PRR	Pattern Recognition Receptor
ROS	Reactive Oxygen Species
RT-qPCR	Quantitative Reverse Transcription PCR
ST	<i>Salmonella enterica</i> serovar Typhimurium
STS	<i>Salmonella enterica</i> serovar Typhimurium secretome

TCA	Tricarboxylic acid cycle
TER	Transepithelial Resistance
TLR#	Toll-like Receptor-#
TNF α	Tumor Necrosis Factor α
TRAM	TRIF Adaptor Molecule
TRIB3	Tribbles Pseudokinase 3
TRIF	TIR Domain-Containing Adaptor- Inducing Interferon- β

INTRODUCTION

Host-Microbe Immune Communication and The Innate Immune System

Commensal gut bacteria play a crucial role in the development and maintenance of the mammalian immune system (Gensollen *et al.*, 2016; Zheng *et al.*, 2020). A causal relationship between commensal gut bacteria and host immune activity was first described in early studies utilizing germ-free animal models. These studies outlined the importance of host-microbe immune communication in shaping functional outcomes within the immune system as lack of a diverse gut microbiota leads to dysfunctional immune activity and structural defects in immune lymphoid tissues (Bauer *et al.*, 1963). Reciprocal interactions between the host and resident microbiota suggest a multi-faceted role for gut microbes in maintaining a state of immune homeostasis and tolerance within the gut, while still allowing the immune system to detect and respond to pathogens (Ayres, 2016; Cheng *et al.*, 2019; Mowat, 2018; Mowat *et al.*, 2014). However, many questions remain regarding mechanistic evidence defining the roles of gut-associated microbes in facilitating host-microbe immune crosstalk.

Cells of the innate immune system are the primary participants in facilitating bidirectional host-microbe immune communication. Although non-specific, the mammalian innate immune system responds rapidly to initiate this host-microbe communication by recognizing conserved microbe-associated molecular patterns (MAMPs) present on the surface or within the intracellular environment of pathogens and commensal microorganisms. In order to recognize these MAMPs, cells of the innate immune system express pattern-recognition receptors (PRRs) which include the toll-like receptors (TLR), the nucleotide-binding oligomerization domain (NOD)-like receptors

(NLRs), and the C-type lectin receptors (CLRs). TLRs induce a signalling cascade through the recruitment of several adaptor molecules including myeloid differentiation factor 88 (MyD88), TIR domain-containing adaptor-inducing interferon- β (TRIF), and TRIF-related adaptor molecule (TRAM). TLRs use different combinations of adaptor molecules in order to elicit different cellular responses terminating with the activation of the nuclear factor kappa-light-chain-enhancer of activated B cells (NF- κ B) transcription factor, the interferon regulatory factors (IRF), the activator protein (AP-1) family of proteins, or the mitogen-activated protein kinases (MAPKs) (Pandey *et al.*, 2014). Once activated, these transcription factors induce the transcription of different pro-inflammatory mediators which act in concert to recruit cells of the immune system to eliminate the invading pathogen. Unlike the TLRs, NLRs are solely intracellular PRRs which recognize peptidoglycan motifs present in cell walls of Gram-positive and Gram-negative bacteria. nucleotide-binding oligomerization domain-containing protein 1 (NOD1) detects d-glutamyl-meso-diaminopimelic acid (DAP), found in Gram negative and certain Gram-positive bacteria, while Nucleotide-binding oligomerization domain-containing protein 2 (NOD2) detects muramyl dipeptide (MDP), present in both Gram negative and Gram-positive bacteria (Girardin *et al.*, 2003). Activation of NODs induces a similar intracellular signalling pathway as the TLRs, terminating with the activation of the NF- κ B transcription factor and increased transcription of pro-inflammatory cytokines and chemokines (Moreira *et al.*, 2012).

Different cell types within the innate immune system have their own unique repertoire of PRRs to recognize specific MAMPs. The majority of these cells are derived from pluripotent hematopoietic stem cells in the bone marrow, which give rise to a common

myeloid progenitor able to further differentiate into monocytes, neutrophils, eosinophils, and basophils (Janeway *et al.*, 2002). Monocytes can further differentiate into various types of tissue macrophages upon stimulation with specific cytokines and chemokines or exposure to certain pathogens. Once differentiated, macrophages are tasked with scavenging, pathogen recognition and elimination, and antigen presentation to the adaptive arm of the immune system (Janeway *et al.*, 2002).

Differentiated tissue macrophages exist as a heterogeneous population, broadly divided and classified into M1 or M2 phenotypes. M1 macrophages, or classically activated macrophages, are activated by TLR stimulation or microbial challenge. As such, these macrophages produce a wide array of pro-inflammatory mediators and possess bactericidal activities to facilitate the host response to the invading microbial challenge. Conversely, M2 macrophages, or alternatively activated macrophages, are characterized as having immunoregulatory activity and are often associated with the resolution of the inflammatory response following immune challenge and are equipped with tissue remodelling processes to repair inflammation-induced tissue damage (**Figure I-1**). M2 macrophages have been further phenotypically characterized into distinct subtypes, each with their own range of effector mechanisms (Colin *et al.*, 2014; Mantovani *et al.*, 2004; Martinez *et al.*, 2014; Martinez *et al.*, 2006). However, this phenotype classification system often does not reflect the paradigm of macrophage activation states and diverse functional specializations of macrophages *in vivo* as these subtypes exhibit a high degree of phenotypic plasticity depending on signals in their microenvironments (Guilliams *et al.*, 2018).

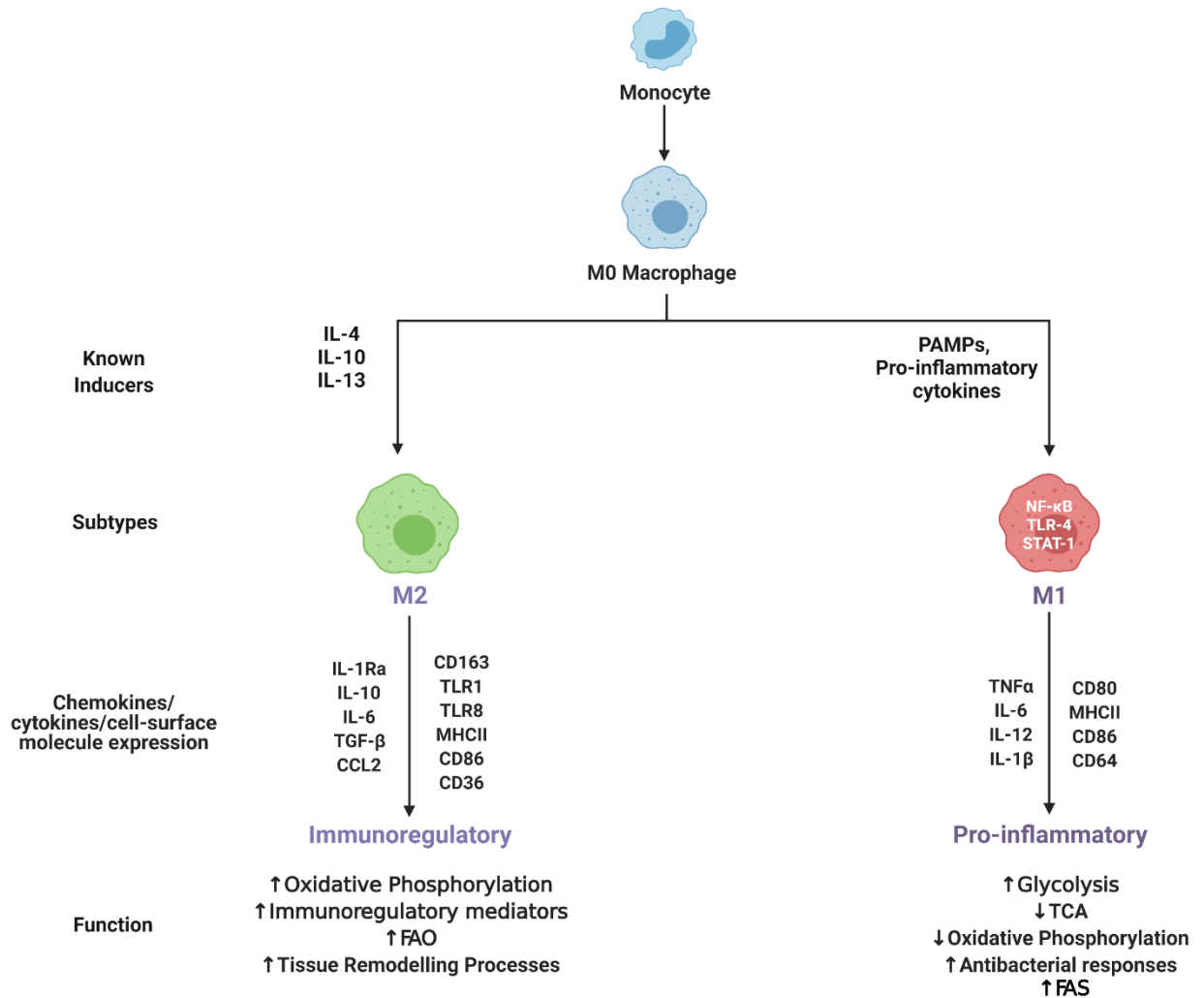


Figure I-1. Tissue macrophages exist as a heterogeneous population consisting of both M1 and M2 polarized macrophages. Within these polarized populations, there exists a continuum of phenotypes and activation states, each with their own unique repertoire of effector functions. These cells react to their microenvironment and exhibit a high degree of phenotypic plasticity. Image created with BioRender.

Activated macrophages undergo metabolic reprogramming in order to support their diverse effector functional states. Studies utilizing lipopolysaccharide (LPS)-challenged macrophages were the first to report changes in metabolic activity due to microbial recognition by macrophages via increased production of nitric oxide through enhanced arginine metabolism (MacMicking *et al.*, 1997). Since then, others have demonstrated that

M1 macrophages often display enhanced flux through glycolysis, allowing them to generate ATP quickly to support microbicidal activity. Coupled with this increased reliance on glycolysis for ATP generation, M1 macrophages display reduced oxidative phosphorylation and a truncated tricarboxylic acid cycle (TCA), leading to the accumulation of succinate and citrate (Jha *et al.*, 2015; O'Neill *et al.*, 2016; Van den Bossche *et al.*, 2017). Within M1 macrophages, succinate inhibits the activity of pyruvate dehydrogenase and stabilizes the activity of hypoxia inducible factor 1 α (HIF1 α) (Tannahill *et al.*, 2013), a transcription factor involved in up-regulating the expression of glycolytic enzymes and inflammatory mediators, providing a link between metabolic reprogramming and changes in immune effector functions. Moreover, excess citrate is shuttled into the cytoplasm where it serves as a precursor for the generation of acetyl-CoA and subsequently used for inflammatory mediator production via fatty acid synthesis, as well as used for acetylation of histones to activate the promoter regions of inflammatory gene loci (Lauterbach *et al.*, 2019). (**Figure I-2**). Although the mechanisms behind this shift in macrophage metabolism remain poorly understood, recent evidence has suggested that LPS-induced nitric oxide in macrophages can inhibit the activity of aconitase 2, a key enzyme involved in the TCA cycle, and several components of the electron transport chain (Palmieri *et al.*, 2020). This may result in immunometabolic polarization of resting macrophages into an inflammatory phenotype by effectively shunting the flow of carbon through the TCA cycle and inhibiting subsequent ATP generation via oxidative phosphorylation and shifting metabolic flux through glycolysis following recognition of pathogen associated MAMPs.

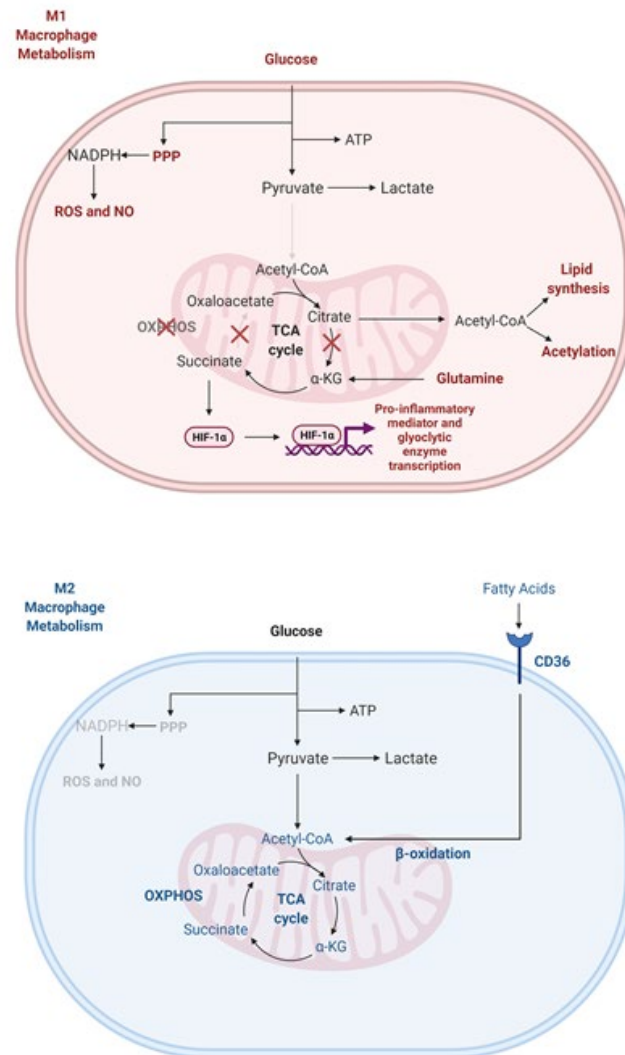


Figure I-2. M1 and M2 macrophages display distinct differences in their metabolic profiles. M1 macrophages are characterized as having a truncated TCA and reduced oxidative phosphorylation. In M1 macrophages, succinate can be used to enhance the activity of HIF1 α , leading to increased transcription of pro-inflammatory mediators to help support microbicidal activities. In contrast, M2 macrophages utilize FAO and oxidative phosphorylation for ATP generation. Image created with BioRender.

In contrast, M2 macrophages are characterized as having reduced reliance on glycolysis and exhibit enhanced oxidative phosphorylation and fatty acid oxidation via an intact TCA to meet energy demands of the cell (**Figure I-2**)(Van den Bossche *et al.*, 2017). To date, a causal relationship between this shift in metabolic activity and subsequent impact

on immune effector functions in M2 macrophages remains poorly defined. Evidence points to some cellular consequences of this glycolytic reprogramming and sequestration of TCA intermediates for ATP generation via oxidative phosphorylation. For example, during periods of reduced glycolytic flux in APCs, glyceraldehyde-3-phosphate (GAPDH), a key enzyme in glycolysis, exhibits moonlighting activity by binding to tumor necrosis factor α (TNF α) and interferon- γ (IFN- γ) mRNA, two potent proinflammatory mediators, inhibiting their translation into functional protein (Chang *et al.*, 2013; Millet *et al.*, 2016). More research is needed to delineate the functional consequences of this altered metabolic phenotype on immune activity, especially in the context of host-microbe interactions with LAB.

The Mucosal Immune System and the Gut Microbiome

Intestinal epithelial cells (IECs) along the GI tract are in frequent contact with both pathogenic and non-pathogenic bacteria and provide both a mechanical and chemical barrier that prevents most bacteria from entering systemic circulation (Artis, 2008). IECs are connected to one another through tight junctions and are covered with a thick layer of glycosylated proteins known as the mucin layer, providing additional protection from invading pathogens and commensal microorganisms (Sansonetti, 2004). IECs also express PRRs, including TLRs and NLRs, which are used to recognize bacteria and other microorganisms. Several NLRs act as sensor molecules able to activate assembly of inflammasomes, multimeric protein complexes that optimize cellular responses to pathogens and damage-associated molecular patterns by facilitating caspase-mediated activation of pro-inflammatory cytokines interleukin-1 β (IL-1 β) and IL-18 (Guo *et al.*, 2015). If the mucin layer is breached, PRR activation rapidly induces IECs to produce pro-

inflammatory cytokines and chemokines, such as interleukin-8 (IL-8), which acts as a potent chemoattractant protein for neutrophils and other members of the immune system (Pitman *et al.*, 2000). While NOD-mediated responses to intracellular bacteria are important for host defence, NOD signalling is also involved in maintaining immune homeostasis (Philpott *et al.*, 2014). For example, NOD1 ligands from gut microbes act to prime innate immune activity at the systemic level through effects on neutrophils (Clarke *et al.*, 2010). Activation of NOD2 by gut microbiota components contributes to intestinal barrier maintenance by NF- κ B-mediated induction of mucin and antimicrobial peptide production, (Jiang *et al.*, 2013) and is involved in regulating mucosal damage induced by T cell activation (Zanello *et al.*, 2016). TLR-mediated interactions with the gut microbiota however are also important for maintenance of the IEC barrier, through induction of cytoprotective heat shock proteins and of cytokines such as IL-6, which is involved in epithelial repair (Rakoff-Nahoum *et al.*, 2004). Paneth cells, specialized secretory epithelial cells located in intestinal crypts, also respond to the gut microbiota through TLR-mediated interactions by producing antimicrobial peptides, which in turn play a role in host defense and in shaping the gut microbiota (Salzman *et al.*, 2008; Vaishnava *et al.*, 2008).

Within the small intestine, there are also organized lymphoid structures, collectively called the gut-associated lymphoid tissues (GALT), which optimize antigen-presenting cell (APC) (macrophages and dendritic cells), T cell and B cell interactions. Key structures in the GALT are the Peyer's patches, specialized lymphoid tissues containing high numbers of B cells, T cells, and APCs which help to facilitate this bidirectional crosstalk between the innate and adaptive arms of the immune response. Directly above the Peyer's patches are microfold cells (M cells), epithelial cells which allow for direct

transport of dietary and microbial-associated antigens and soluble mediators across the IEC layer into the underlying lymphoid tissues. Here, APCs process antigens and present them to the surrounding T cells. Antigen sampling can also be carried out by APCs by using dendrites extended through the epithelial layer to sample intestinal luminal contents (Cerovic *et al.*, 2014; Mowat *et al.*, 2011). These activated T and B cells can leave the Peyer's patches via the mesenteric lymph node and provide protection and shape immune outcomes at other systemic mucosal locations (Mowat *et al.*, 2014) (**Figure I-3**).

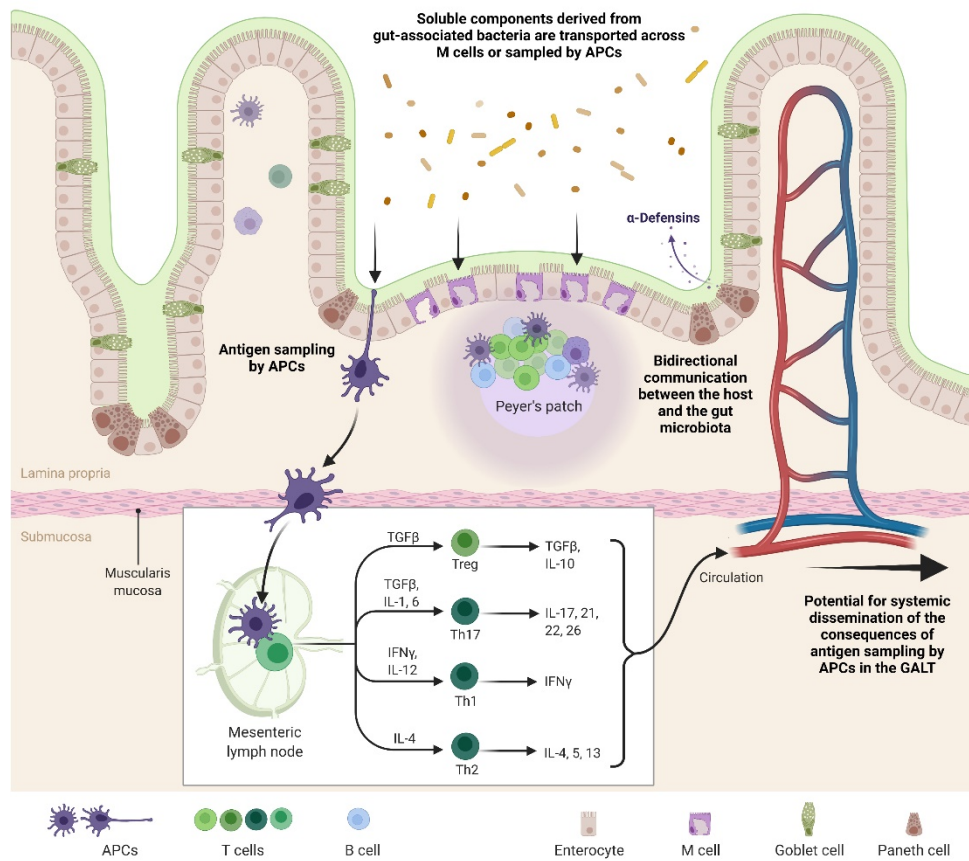


Figure I-3. The GALT is a specialized area within the gut containing unique intestinal epithelial cells and other immune cells which help to facilitate gut microbiota-host immune bidirectional communication. Soluble mediators derived from LAB and other commensals can interact with immune cell populations below the intestinal epithelial barrier leading to local and potentially systemic diverse physiological and immunological outcomes. Image created with BioRender.

The GALT faces challenges unique to its location in the body. Due to the continual barrage of stimuli in the form of food components, normal gut microbiota and pathogens, the GALT must distinguish between signals it should mount a response against and those to which it should remain nonresponsive (Smith *et al.*, 2005). When an antigen is associated with a pathogen, usually through PRR activation, there is an increase in pro-inflammatory cytokine, chemokine, and antibody production by surrounding immune cells, usually resulting in the eventual clearance of the invading pathogen. Once the invading pathogen or danger signal is cleared, the inflammatory signal is terminated and there is an increase in the transcription of regulatory cytokines and other immunoregulatory proteins to return to physiological homeostasis (Paludan *et al.*, 2021). However, if the sampled component is derived from a commensal microorganism, there is often a muted immune response. Although mechanistic evidence for how constituents of the host gut microbiota can shape and alter these immune outcomes remain elusive, some have suggested that the differences in the magnitude of the immune response to commensal microorganisms lie within evolutionary changes to structural components recognized by host PRRs. For example, lipoproteins derived from Gram-positive bacteria, such as the noncommensal *Staphylococcus carnosus*, often elicit a robust immune response via TLR2 signaling and NF- κ B activation, while the same lipoprotein derived from commensal *Staphylococcus epidermidis* elicits a muted TLR2-mediated response. This is due primarily to post-translational modifications to these lipoproteins via acylation of long-chain fatty acids to specific lipid moieties which renders it unrecognizable by the TLR2-TLR6 signaling complex (Nguyen *et al.*, 2017).

While signals delivered through pattern recognition receptors (PRRs) have been examined extensively in bidirectional host-microbe communication, recent evidence points to roles for microbial metabolites and soluble components as key mediators in host-microbe immune communication (Blacher *et al.*, 2017; Zargar *et al.*, 2015). However, mechanistic evidence for the roles of soluble mediator-driven changes to host immune outcomes has remained elusive, with few studies describing the role of lactic acid bacteria (LAB)-derived soluble mediators in host-microbe immune communication. Most notably, the secreted p75 and p40 proteins, first identified in *L. rhamnosus* GG have been shown to protect against TNF α -induced IEC death by activating the Akt cellular pathway and through the induction of cytoprotective heat-shock proteins (Seth *et al.*, 2008; Yan *et al.*, 2007). Production of amino acids and their derivatives have also been shown to be responsible for some of the effects attributed to LAB. For example, lactobacilli can convert dietary tryptophan into indoles and other tryptophan metabolites, which by acting through the aryl hydrocarbon receptors present on host immune cells, can elicit a wide array of immunomodulatory activity (Vogel *et al.*, 2014; Zelante *et al.*, 2013). Moreover, *L. reuteri* 6475 produces histamine which has been associated with inhibiting TNF α production in human monocytes via inhibition of the MAPK signaling pathway (Thomas *et al.*, 2012). More novel mechanisms of action behind LAB immunoregulatory activity involve epigenetic and post-translational effects on gene expression. Lactic acid, a major metabolite of lactobacilli, has been shown to have histone deacetylase (HDAC) activity (Garrote *et al.*, 2015; Latham *et al.*, 2012), a mechanism by which some lactobacilli may exert effects on gene expression by modulating histone deacetylation patterns (Ghadimi *et al.*, 2012). Taken together, these

studies emphasize the need to examine the role of LAB-derived soluble components in host-microbe immune communication.

Although inflammation is important for activation of host defence within the GALT, excessive activation or dysregulation of this process can lead to tissue damage and contributes to diseases associated with chronic inflammation. Regulation of innate immune activation is thus an important element of host-microbe interactions, especially at the gut mucosal interface, where microbes are constantly encountered. Certain strains of gut-associated bacteria can act to down-regulate effects of pro-inflammatory stimuli, and shape host immune outcomes by participating in maintenance of a state of immune homeostasis in the gut mucosa. *Lactobacillus rhamnosus* R0011, a commercially available LAB originally isolated in 1976 by Edouard Brochu from a dairy starter culture (Tompkins *et al.*, 2012), has been shown to modulate genes involved in TLR, NOD, MAPK, and cytokine-chemokine receptor interactions in HT-29 IECs under basal conditions following exposure to live bacteria for 3-hours (Audy *et al.*, 2012). *L. rhamnosus* R0011 has also been shown to antagonize the activity of several gut-associated pathogenic microbes such as *Campylobacter jejuni*, *Helicobacter pylori*, and *Escherichia coli* via direct and indirect mechanisms of action (Alemka *et al.*, 2010; Johnson-Henry *et al.*, 2004; Sherman *et al.*, 2005). Moreover, *L. rhamnosus* R0011 has the capacity to modulate basal cytokine production from HT-29 IECs (Wallace *et al.*, 2003), to down-regulate TLR-induced IL-8 production from HT-29 IECs *in vitro* (Wood *et al.*, 2007), and can inhibit pathogen-induced formation of neutrophil extracellular traps (NETs) (Vong *et al.*, 2014), providing mechanisms through which *L. rhamnosus* R0011 may limit damage to surrounding tissues. However, these studies have only examined the interactions between

live or dead *L. rhamnosus* R0011 with HT-29 IECs necessitating the need for studies examining the potential immunomodulatory capacity and the mechanism(s) of action of soluble components derived from *L. rhamnosus* R0011 in IECs, as well as other key cell types involved in innate immunity which participate in shaping host immune outcomes at the gut-mucosal interface.

CHAPTER 1: Secretome-mediated interactions with intestinal epithelial cells: a role for secretome components from *Lactobacillus rhamnosus* R0011 in the attenuation of *Salmonella* enterica serovar Typhimurium secretome and TNF- α -induced pro-inflammatory responses

1.1 Introduction

Lactic acid bacteria (LAB) have been shown to influence the activity of different key cell types involved in both innate and adaptive immunity. These interactions occur predominately at mucosal interfaces and in gut-associated lymphoid tissues where bacteria can exert immunomodulatory effects via direct interactions with immune cells or indirectly through the production and secretion of bioactive molecules (Suez *et al.*, 2019). Although the precise nature of these host-microbe interactions remain largely unknown, *in vitro* studies have aimed to elucidate the cellular mechanisms behind the actions of LAB, with many modulating key cell signaling pathways in various cell types involved in innate immunity, including intestinal epithelial cells (IECs). One of the earliest defined mechanisms of action proposed for the immunomodulatory activity of commensal gut bacteria involves inhibition of NF- κ B transcription factor activity via inhibiting its nuclear translocation or by inhibiting the ubiquitination of the I κ B- α inhibitory protein complex in IECs (Neish *et al.*, 2000). Expanding on this work, others have demonstrated varied means of LAB-mediated inhibition of NF- κ B and its associated signaling pathways (Macpherson *et al.*, 2014; MacPherson *et al.*, 2017). For example, the anti-inflammatory activity of *Lactobacillus crispatus* M247 has been attributed to the upregulation of PPAR γ , a potent inhibitor of NF- κ B activation, while other species and strains of lactobacilli have been demonstrated to increase the expression of A20 (TNFAIP3), a transcription factor

responsible for terminating NF- κ B signaling in IECs (O'Callaghan *et al.*, 2012; O'Flaherty *et al.*, 2012; Tomosada *et al.*, 2013). More recently, novel mechanisms of action of LAB involving epigenetic and post-translational effects on IEC gene expression have been identified (Ghadimi *et al.*, 2012; Zhao *et al.*, 2015). Lactic acid, a major metabolite of lactobacilli, has also been shown to have histone deacetylase (HDAC) inhibitory activity (Garrote *et al.*, 2015; Latham *et al.*, 2012), suggesting another mechanism through which some lactobacilli may exert effects on gene expression by modulating histone deacetylation patterns.

The tumor necrosis factor (TNF) superfamily encompasses numerous effector molecules and protein receptors which have pleiotropic effects on cells of the immune system (Vanamee *et al.*, 2018). TNF- α , the most studied molecule of the TNF superfamily, is a potent pro-inflammatory cytokine with diverse effects on inflammatory and cell survival signaling pathways. Binding of TNF- α to membrane-bound TNFR1 present on HT-29 human IEC (Janes *et al.*, 2006) results in the activation of NF- κ B, JNK, and p38 MAPK signaling pathways through the recruitment of a protein complex involving tumor necrosis factor receptor type 1-associated death domain (TRADD), TNF receptor-associated factor (TRAF) 2, and receptor-interacting serine/threonine kinase 1 (RIPK1) (Leppkes *et al.*, 2014). Activation of these signaling pathways through prolonged exposure to TNF- α leads to excessive production of inflammatory mediators and has been implicated in several human disease pathologies including intestinal infections with Gram negative enteropathogens such as those from the genus *Salmonella* (Hotamisligil, 2017). Growing evidence suggests that LAB secrete or shed bioactive molecules with differential immunomodulatory activity on TNF- α -mediated signaling pathways. Kim *et al.* (2012)

have shown that lipoteichoic acid, a key component of the Gram-positive bacterial cell wall, derived from *Lactobacillus plantarum* K8 can down-regulate TNF- α -induced pro-inflammatory cytokine production from HT-29 human IECs (Kim *et al.*, 2012), while soluble proteins derived from *Lactocaseibacillus rhamnosus* GG inhibit TNF- α -mediated intestinal epithelial cell damage (Yan *et al.*, 2007).

Pathogens at the gut-mucosal interface can activate pro-inflammatory signaling pathways in host IECs through direct recognition of bacterial components via innate immune receptors such as the toll-like receptors (TLRs) or the nucleotide-binding oligomerization domain-like receptors (NLRs), activating well characterized signaling pathways. Detection of pathogenic bacteria by TLRs and NLRs expressed on or within IECs usually results in the up-regulation of pro-inflammatory mediators via NF- κ B activation. However, less is known about how secreted molecules from pathogens influence host immune cells, although recent findings suggest that this is also an important route for pathogenicity. For example, *Neisseria meningitidis* secretes bioactive molecules which serve multiple roles in host-pathogen interactions (Tomassen *et al.*, 2017). Probiotic LAB have been shown to antagonize gut-pathogen activity through direct inhibition (Sherman *et al.*, 2005) and through the secretion of bioactive molecules (Fayol-Messaoudi *et al.*, 2005), suggesting the potential for complex and multi-faceted host-microbe interactions mediated by soluble molecules. Many questions currently remain regarding the roles of probiotic-derived secreted bioactive molecules in these host-pathogen interactions.

1.2 Objectives

The *Lactocaseibacillus rhamnosus* R0011 secretome (LrS) down-regulates the production of interleukin (IL)-8 from IECs challenged with a wide array of innate immune stimulants including TNF- α , TLR and NOD1 agonists (Jeffrey *et al.*, 2018). In the present study, we aimed to further interrogate the signaling pathways modulated by the LrS in HT-29 IECs exposed to TNF- α to better understand the mechanism(s) of action behind the observed bioactivity, as TNF- α induction is a common feature of many PRR-mediated pathways. Furthermore, secretome components from *Salmonella enterica* subsp. *enterica* serovar Typhimurium (ST), a known gut pathogen, were examined for the ability to influence IEC innate immune activity as was the impact of the LrS in this context. TNF- α signaling is well defined in HT-29 human IECs (Janes *et al.*, 2006) and their use as an IEC model to study the impacts of both TNF- α and invasive pathogens at the gut-mucosal interface is well established (Jung *et al.*, 1995; Rousset, 1986). Using genome-wide gene expression microarrays and cytokine/chemokine production analysis, the following results provide novel insights into the complex multi-faceted role of bacterial secretome components in interdomain communication as mediated through the respective secretomes of LAB and ST.

1.3 Methods

Bacterial Culture

Lyophilized *Lactobacillus rhamnosus* R0011 was obtained from RIMAP (Montreal, Quebec, Canada). The LrS was prepared as previously described (Jeffrey *et al.*, 2018). Briefly, bacteria were grown in deMan, Rogosa and Sharpe (MRS) medium (Difco, Canada) at 37°C for 17 hours in a shaking incubator and then diluted in non-supplemented RPMI-1640 medium and allowed to further propagate for an additional 23 hours under the same conditions. The pH of the LrS was measured and the pH of the control was adjusted to that of the bacterial culture using L-lactic acid and HCl. To determine the L-lactic acid concentration within the LrS, the Megazyme D-/L-lactic acid kit was used following manufacturer's protocols. Both the bacterial culture and controls were centrifuged at 3000 x g for 20 minutes and filtered through a 0.22 µm filter (Progene, Canada) to remove any bacteria. The filtered supernatant samples were also subjected to size fractionation using < 10 kDa Amicon Ultra – 15 centrifugal filter (EMD Millipore, MA, USA). This < 10 kDa fraction was used for all experiments as this was previously determined to be the fraction which retained the observed bioactivity (Jeffrey *et al.*, 2018).

For preparation of the STS, bacteria were propagated overnight in tryptone soya broth (Oxoid) in a shaking incubator at 37°C. Overnight cultures were centrifuged at 3000 X g for 20 minutes at 4°C and filtered through a 0.22 µm filter and the secretome was stored at -80°C.

Cell Culture and Challenge Assay and RNA extraction

The HT-29 human colorectal adenocarcinoma cell line was obtained from the American Type Culture Collection (ATCC, #HTB-38) and was maintained in RPMI-1640 medium supplemented with 10% bovine calf serum and 0.05 mg/mL gentamicin (Sigma-Aldrich, MO, USA) and were grown in 75 cm² tissue culture flasks (Greiner-Bio-One, NC, USA) at 37°C, 5% CO₂ in a humidified incubator (Thermo Fisher, MA, USA) as described previously (Jeffrey *et al.*, 2018). HT-29 IECs were enumerated and viability determined using Trypan Blue following sub-culturing. Cells were then resuspended in complete culture medium (RPMI-1640 medium supplemented with 10% bovine calf serum and 0.05 mg/mL gentamicin) and 2.0 x 10⁶ cells were seeded into 25 cm² cell tissue culture flasks (Greiner-Bio-One, NC, USA). This cell concentration has been shown to yield sufficient amounts of RNA for subsequent microarray analyses (MacPherson *et al.*, 2017). Seeded HT-29 IECs were incubated for 48 hours at 37°C, 5% CO₂ in a humidified incubator in order to obtain confluent monolayers prior to challenge. HT-29 IEC cell culture medium was aspirated and replaced with fresh non-supplemented (no calf serum) RPMI-1640 medium containing the LrS, L-lactic acid controls, TNF- α (50ng/mL), STS (1% v/v), or a combination of the challenges concurrently. Total RNA was harvested after 3 hours of exposure to the various challenges using the phenol-based TRIzol method of RNA extraction (Chomczynski, 1993) following manufacturer's protocols (ThermoFisher Scientific, MA, USA). Briefly, 2 mL of TRIzol reagent was added to each culture flask to lyse the IEC. Cell culture homogenates were added to Phase Lock Gel-Heavy tubes for phase separation of total RNA. Total extracted RNA was then purified using the RNeasy Plus Mini Kit (Qiagen, Hilden, Germany). The purity and quality of RNA was determined

using both the ND100 NanoDrop and an Agilent 2000 Bioanalyzer, respectively. Only samples with an RNA Integrity Number (RIN) greater than 9.0 were used for microarray analysis (**Appendix A1**).

Reverse Transcription (RT) of RNA and Direct-Method of Labelling

Control and experimental total RNA (15µg) was reverse transcribed with Superscript IV (Invitrogen, MA, USA) and labelled with Cy3-dCTP and Cy5-dCTP (GE Healthcare, Amersham Biosciences) using the direct method of dye labelling as previously described (MacPherson *et al.*, 2017). Briefly, 3 µg of oligo dT23 primers were added to the RNA and samples were heated to 70°C for 30 min in order to reduce secondary structure formation. A cDNA synthesis master mix containing 5X First Strand Buffer, 0.1M DTT, dNTPs, 200U of SuperScript IV, and either 1mM of Cy3 or Cy5 dye was added, and the samples were heated at 42°C for 3 hours in order to allow the RT to occur. Dye swaps between treated and control RNA were done in order to eliminate bias of dye labelling. Purification of the cDNA product was done using the QIAQuick PCR purification kit following manufacturer's protocols (Qiagen, Hilden, Germany). Labelling efficiency was determined by calculating the dye incorporation rate to ensure consistency between experiments.

Microarray Analysis

Hybridization of the labelled cDNA to the microarray was done using previously established protocols (MacPherson *et al.*, 2017). Following hybridization, the microarrays were scanned using the ScanArray 5000 instrument from Perkin-Elmer (Waltham, MA, USA) and spot intensities were quantified using ImaGene® version 9.0 (BioDiscovery,

CA, USA). Normalization was done using locally weighted scatterplot smoothing (LOWESS) (Berger *et al.*, 2004) (**Appendix A2**).

Statistical analyses and two-dimensional hierarchical clustering analyses was performed with Multi-Experiment Viewer (MeV, version 4.2) (**Appendix A3**). Genes with statistically significant changes in expression levels were selected based on a t-test yielding a p -value < 0.05 (indicating reproducible changes in fluorescence ratios between biological replicates) and a 1.5-fold-change gene expression cut-off. Set Distiller from GeneDecks, Cytoscape, and Ingenuity Pathway Analysis (IPA) pathway enrichment analyses were used in order to ascertain the pathways in which genes were significantly modified by the different treatments. Set Distiller groups gene sets into statistically significant ($p < 0.05$) and biologically relevant pathways and descriptors (Stelzer *et al.*, 2009), while GeneMANIA in Cytoscape determines functional links between genes in gene sets (Shannon *et al.*, 2003; Warde-Farley *et al.*, 2010). Gene networks were generated through the use of IPA (Qiagen, <https://www.qiagenbioinformatics.com/products/ingenuity-pathway-analysis>) (Kramer *et al.*, 2014).

Comparative RT-qPCR

RT-qPCR to determine transcript abundance of differentially expressed genes was performed to validate microarray expression data as per the Minimum Information for Publication of Quantitative Real-Time PCR Experiments (MIQE) guidelines. DNase-treated RNA (1 μ g) from controls and each challenge were reverse transcribed with Superscript IV following manufacturer's protocols as previously described (Macpherson *et al.*, 2014). Reverse-transcribed cDNA was diluted 1:4 prior to amplification and 2.5 μ l of diluted cDNA was used in RT-qPCR using gene-specific primers (Table II) and

SsoAdvanced Universal SYBR Green Supermix (Bio-Rad, CA, USA) per the manufacturer's instructions. An initial incubation of 5 min at 95°C was performed, followed by 40 cycles consisting of template denaturation (15 s at 95°C) and one-step annealing and elongation (30 s at 60°C), with a Bio-Rad CFX Connect instrument (Bio-Rad, CA, USA). Four biological replicates were analyzed for each gene tested, and fold change expression levels were normalized to the expression levels of two reference genes (*RPLPO* and *B2M*) and negative controls using Bio-Rad CFX Manager 3.1 software.

Histone Extraction and H3/H4 Histone Acetylation Assay

H3 and H4 global acetylation patterns in HT-29 IECs were determined using the EpiQuik Global Histone H4 (P-4009) and H3 (P-4008) Acetylation Assay Kits following manufacturer's protocols (Epigentek, NY, USA). Briefly, histones were extracted from HT-29 IECs following 3 hours of challenge and total protein concentrations in each sample were determined using the Coomassie Plus Protein Assay Reagent (Thermo Fisher Scientific, MA, USA). A total of 2 µg of protein from both untreated and challenged IEC histone extracts were spotted into strip wells and assayed for the amount of acetylation using antibodies specific for acetylated H3 or H4 histones. Standards with known concentrations of acetylated histones were included and % histone acetylation was determined by comparing treated and untreated controls. Statistical analysis was done using GraphPad Prism's (Version 8) one-way analysis of variance (ANOVA) and Tukey's multiple comparison test when the ANOVA indicated significant differences were present. All data are shown as the mean % change in histone acetylation ± standard error of the mean (SEM).

Cytokine/Chemokine/Inflammation Marker Analysis

Cell culture supernatants were collected following 6 hours of challenge in order to allow sufficient time for the production of key inflammatory cytokines and chemokines. Cytokine and chemokine profiling was performed using the Bio-Plex Pro™ 40-Plex Human Chemokine Panel (Bio-Rad #171ak99mr2) and the Bio-Plex Pro™ Human Inflammation Panel 1, 37-Plex (Bio-Rad #171AL001M). All 40 chemokines (CCL21, BCA-1 / CXCL13, CTACK / CCL27, ENA-78 / CXCL5, Eotaxin / CCL11, Eotaxin-2 / CCL24, Eotaxin-3 / CCL26, Fractalkine / CX3CL1, GCP-2 / CXCL6, GM-CSF, Gro- α / CXCL1, Gro- β / CXCL2, I-309 / CCL1, IFN- γ , IL-1 β , IL-2, IL-4, IL-6, IL-8 / CXCL8, IL-10, IL-16, IP-10 / CXCL10, I-TAC / CXCL11, MCP-1 / CCL2, MCP-2 / CCL8, MCP-3 / CCL7, MCP-4 / CCL13, MDC / CCL22, MIF, MIG / CXCL9, MIP-1 α / CCL3, MIP-1 δ / CCL15, MIP-3 α / CCL20, MIP-3 β / CCL19, MPIF-1 / CCL23, SCYB16 / CXCL16, SDF-1 α + β / CXCL12, TARC / CCL17, TECK / CCL25, TNF- α) or 37 cytokines (APRIL/TNFSF13, BAFF/ TNFSF13B, sCD30/TNFRSF8, sCD163, Chitinase-3-like 1, gp130/sIL-6R β , IFN- α 2, IFN- β , IFN- γ , IL-2, sIL-6R α , IL-8, IL-10, IL-11, IL-12 (p40), IL-12 (p70), IL-19, IL-20, IL-22, IL-26, IL-27 (p28), IL-28A/IFN- λ 2, IL-29/IFN- λ 1, IL-32, IL-34, IL-35, LIGHT/TNFSF14, MMP-1, MMP-2, MMP-3, Osteocalcin, Osteopontin, Pentraxin-3, sTNF-R1, sTNF-R2, TSLP, TWEAK/TNFSF12) (**Appendix A4**) were multiplexed on the same 96-well plate. Chemokine/cytokine standards were serially diluted and chemokine profiling from all cell challenges was done following manufacturer's instructions (Bio-Rad, CA, USA) with 4 biological replicates. Quality controls were also included to ensure the validity of the concentrations that were obtained. The Bio-Plex Manager™ software was used to determine the concentration of the analytes within each

sample using the generated standard curves and concentration was expressed in pg/mL (concentration in range). Statistical analysis was done using GraphPad Prism's (Version 8) one-way analysis of variance (ANOVA) and Tukey's multiple comparison test when the ANOVA indicated significant differences were present. All data are shown as the mean pg/mL \pm standard error of the mean (SEM). String v 11.0 analysis was also done to determine functional links between each of the different cytokines/chemokines measured (Szkłarczyk *et al.*, 2019).

Measurement of Intracellular Reactive Oxygen Species (ROS) Generation

Intracellular ROS production was determined by using 2', 7'-Dichlorofluorescein Diacetate (DCFH-DA) (Sigma-Aldrich, MO, USA). HT-29 IECs were pre-treated with 100 μ M DCFH-DA for 30 minutes at 37°C, 5% CO₂ to allow sufficient time for cellular uptake. Cells were washed twice with fresh medium and challenged with the LrS, TNF- α (50 ng/mL), STS (1% v/v), L-lactic acid matched controls, or a combination of the treatments for 45 minutes. Fluorescence of DCF due to the oxidation of DCFH-DA by ROS was quantified using a Synergy HT Microplate Reader (BioTek Instruments) set to 485/20 excitation and a 528/20 emission filter pair and a photomultiplier tube (PMT) sensitivity of 55.

1.3 Results

The LrS attenuates TNF- α - and STS-induced changes in global gene expression profiles in HT-29 IECs

Genome-wide transcriptional profiling of HT-29 IECs treated with TNF- α , STS, LrS, L-LA, or a combination of these was performed to evaluate the global changes in the IEC transcriptome in response to these challenges (data can be found at <https://www.ncbi.nlm.nih.gov/geo/query/acc.cgi?acc=GSE145091> under accession number GSE145091). Two-dimensional hierarchical heat-map cluster analysis revealed that TNF- α and STS challenges do not cluster closely together, suggesting differences between these treatments. Interestingly, L-LA appears to have a distinct effect on gene expression profiles when combined with either pro-inflammatory challenge, with the co-challenges of L-LA and either TNF- α or STS clustering closely with the TNF- α and STS challenges, respectively. In contrast, the LrS and co-challenge of the LrS with either TNF- α or the STS cluster together, indicating distinct and unique global gene expression profiles (**Figure 1-1A**). TNF- α challenge had a large impact on the global IEC transcriptomic response, with a total of 1531 differentially modulated genes (886 up-regulated and 645 down-regulated) ($n = 4$; $p < 0.05$). When combined with the LrS, this was reduced to a total of 820 genes, indicating that the LrS attenuated the impact of TNF- α on IEC global gene expression ($n = 4$; $p < 0.05$). A similar effect was observed on STS-induced changes in IEC global gene expression, with the LrS reducing the total number of differentially expressed genes from 618 to 342 ($n = 4$; $p < 0.05$) (**Figure 1-1B**).

To interrogate the cellular pathways impacted by the different challenges, gene enrichment analysis was performed using GeneDecks Set Distiller analysis. This analysis

revealed that treatment of HT-29 IECs with TNF- α led to the increased transcription of genes involved in immune related pathways including the innate immune response (88), TNF- α (36), MAPK (43), and NF- κ B (31) signaling pathways ($p < 0.001$) (**Figure 1-1C**). Further analysis revealed that TNF- α challenge led to increased transcription of key pro-inflammatory mediators common to these immune pathways such as *CXCL1* (13.2 fold-change), *CXCL10* (29.6 fold-change), *CCL20* (35.9 fold-change), *BIRC3* (15.4 fold-change), *PTGS2* (11.0 fold-change), *CXCL8* (23.6 fold-change) and *NF κ BI* (4.1 fold-change) (Table I). Other cellular pathways identified as being impacted by TNF- α challenge involved apoptosis (65), p21-Activated Protein Kinases (PAK) (77), and TWEAK pathways (30) ($p < 0.001$) (**Figure 1-1D**). Consistent with the changes observed in global gene expression profiles, co-challenge of IECs with the LrS resulted in attenuation of TNF- α -induced transcription of genes involved in the innate immune response (38), TNF- α (20), MAPK (13), NF- κ B (11), apoptosis (36), PAK (36), and TWEAK (19) ($p < 0.001$), an effect that was independent of L-lactic acid (**Figure 1-1C and 1-1D; Table 1-I**).

The STS also induced transcriptional changes leading to the activation of genes involved in immune-related pathways, with the greatest impact on those involved in regulating innate immune activity (28), NF- κ B (16), TLR signaling (21), and NLR signaling (21) ($p < 0.001$) (**Figure 1C**). As was seen with the TNF- α challenge, the STS also induced the expression of *CXCL1* (7.9 fold-change), *CCL20* (6.4 fold-change), *BIRC3* (2.5 fold-change), *PTGS2* (1.7 fold-change), and *NF κ BI* (1.8 fold-change). Concurrent challenge of IECs with the LrS and the STS resulted in the attenuation of all ST-secretome-induced transcription of genes involved in the aforementioned immune-related pathways

($p < 0.001$, **Figure 1-1C**; **Table 1-I**), suggesting that the LrS attenuates both TNF- α and STS-induced transcriptional changes in IEC.

The LrS induces negative regulators of innate immunity in TNF- α and STS challenged IECs

IPA was used to further interrogate the underlying mechanism(s) of action of the LrS on TNF- α - and STS-induced transcriptional responses in IECs. Using molecular activity prediction, pathway analysis revealed that treatment of TNF- α -challenged IECs with the LrS results in the attenuation of components of the TNF- α receptor complex (*TNFR*, *FADD*, and *RIPP*), the IKK complex (*IKK α* , *IKK β* , and *IKK γ*), as well as the NF- κ B signalling complex (*NF κ B1*, *NF κ B2*, *RELA* and *RELB*) (**Figure 1-2**). GeneMania gene enrichment analysis confirmed these findings, as the LrS significantly attenuated STS- and TNF- α -induced transcription of *NF κ B1*, *NF κ B2*, *RELA* and *RELB*, TNFR2-TRAF signaling complex protein (*BIRC3*), *CASP8* and FADD like apoptosis regulator (*CFLAR*), *IRAK-2*, and several genes involved in the MAPK signaling pathway (**Figures 1-3 and 1-4**).

To elucidate how the LrS was attenuating the activation of these cellular pathways in response to TNF- α challenge, HT-29 IECs treated with the LrS were examined for differential activation of negative regulators of the innate immune response. Interestingly, treatment of HT-29 IECs with the LrS alone resulted in decreased expression of dual specificity phosphatase 1 (*DUSP1*) (-4.5 fold-change), a key regulator of the MAPK pathway, and of activating transcription factor 3 (*ATF3*) (-3.4 fold-change) and tribbles pseudokinase 3 (*TRIB3*) (-5.8 fold-change), negative regulators of innate immunity (**Figure 1-5A-D**). However, when HT-29 IECs were co-challenged with the LrS and TNF-

α , there was a 15.7 fold-change in *DUSP1* expression, 12.7 fold-change in *ATF3* expression, and 5.5 fold-change in *TRIB3* expression (**Figure 1-5**). This pattern of up-regulation of negative regulator expression was also seen in HT-29 IECs co-challenged with the LrS and STS, where a 7.4 fold-change in *DUSP1* expression, 6.37 fold-change in *ATF3* expression, and 7.0 fold-change in *TRIB3* expression was observed (Figure 3C). Effects on expression of these negative regulators were confirmed by RT-qPCR (**Figure 1-6**). Predictive modeling of these negative regulators (using IPA's upstream regulator analysis software) suggest that they play key roles in the modulation of TNF- α or STS-induced activation of the NF- κ B, MAPK, and TNF- α signalling pathways when HT-29 IECs are treated with the LrS (**Figure 1-5F**) suggesting a possible mechanism of action behind the observed immunoregulatory activity of the LrS. Moreover, a similar trend was observed for heat shock protein family A (Hsp70) member 6 (*HSPA6*) (15.0 and 4.1 fold-change) and growth arrest and DNA-damage-inducible β (*GADD45 β*) (10.1 and 5.1 fold-change), key cellular players in mediating oxidative and cellular stressors, in response to the combination of LrS and TNF- α or STS (**Table I**).

The LrS attenuates TNF- α and STS-induced global histone acetylation

The ability of the LrS to modulate global histone acetylation patterns was examined to determine if the observed reduction in pro-inflammatory gene expression correlated with decreased histone acetylation. To this end, analysis of the amount of acetylated H3 and H4 histones indicated that the LrS significantly reduced TNF- α and STS-induced H3 histone acetylation (n = 4; $p < 0.05$) (**Figure 1-7A**). In addition, the LrS also attenuated STS-induced acetylation of H4 histones (n = 4; $p < 0.05$) (**Figure 1-7B**) in IECs.

The LrS attenuates TNF- α - and ST-induced pro-inflammatory cytokine and chemokine protein production

To determine whether the observed effects of the LrS on STS and TNF- α -induced pro-inflammatory mediator gene expression translated into effects at the protein level, the impact on production of several cytokines and chemokines were measured. Of the 74 different pro-inflammatory and regulatory protein markers examined, TNF- α challenge resulted in significant production of 55 different cytokines/chemokines and markers of inflammation ($n = 4$; $p < 0.05$) (**Figures 1-8A-D, 1-9, 1-11**). Consistent with the observed attenuation of TNF- α -induced transcriptional changes in HT-29 IECs co-challenged with the LrS, production of 48 of the observed TNF- α -induced cytokines/chemokines and markers of inflammation was significantly attenuated to constitutive levels by the addition of the LrS ($n = 4$; $p < 0.05$).

Of the 74 different protein markers examined in this study, String protein analysis identified IFN- γ , GM-CSF, IL-1 β , CXCL8, and CXCL1 as being involved in responses to *Salmonella* spp. infection (**Figure 8E**). STS challenge resulted in significant increases in production of these 5 cytokines/chemokines and 24 other mediators of inflammation, providing further evidence of the ability of secretome components from this gut-associated pathogen to induce pro-inflammatory mediator production consistent with typical *Salmonella* spp.-induced cytokine and chemokine profiles in IECs. Co-challenge with the LrS attenuated the production of 17 STS-induced cytokines/chemokines and markers of inflammation, indicating that the immunomodulatory impact of the LrS on STS-induced transcriptional responses was correlated to functional protein levels in IECs (**Figures 1-8A-D, 1-10, 1-11**).

Again, L-lactic acid had marginal impacts on TNF- α or STS-induced pro-inflammatory mediator production from IECs, suggesting that the observed immunomodulatory activity of the LrS is not simply due to the presence of L-lactic acid. Co-challenge of HT-29 IECs with L-lactic acid resulted in a significant reduction in the production of CXCL10, CXCL1, and CCL2 from TNF- α challenged IECs (**Figures 1-8A-D, 1-9, 1-10**). Interestingly, treatment with the LrS alone or in combination with TNF- α did lead to the significant production of macrophage inhibitory factor (MIF) ($14,721.3 \pm 4693.9$ pg/mL) from constitutive levels (1934.4 ± 142.8) (**Figure 1-12**). This was the only instance in which challenge with the LrS induced the production of a cytokine/chemokine found within this panel.

The LrS reduces ROS generation from HT-29 IECs

IPA Upstream Regulator analytics identified nitric oxide and reactive oxygen species (ROS) as a potential upstream regulator that may explain the observed gene expression changes when HT-29 IECs are exposed to the LrS and either TNF- α or STS (**Figure 1-13A**). To this end, intracellular ROS production in response to the different treatments was examined using DHFA. HT-29 IECs treated with the LrS had significantly less ROS production than the other treatments (**Figure 1-13B**), suggesting that intracellular ROS is not responsible for the observed changes in the transcript abundance of these key negative regulators of innate immunity.

1.4 Discussion

While many studies support direct contact-mediated routes for immunomodulatory activity of lactobacilli in their interactions with IEC (Suez *et al.*, 2019; Thomas *et al.*, 2010), evidence for alternate modes of microbe-host interaction involving soluble mediators and secreted components point toward multiple potential mechanisms of action (Lebeer *et al.*, 2008, 2010). Earlier reports of antimicrobial and immunomodulatory effects of soluble mediators from conditioned media of lactobacilli suggesting the potential for secretome-mediated effects of these bacteria on IEC (Broekaert *et al.*, 2007; Ganguli *et al.*, 2013; Park *et al.*, 2013; Tao *et al.*, 2006) are supported by more recent studies reflecting the impact of microbial metabolites on the immune system (Kim, 2018; Postler *et al.*, 2017). Although several mechanisms of action behind the activity of LAB have been identified, few studies have investigated the effects of LAB secretome components on key signaling pathways involved in innate immune signaling in IECs. Based on our earlier observations indicating that the LrS attenuates TNF- α -induced IL-8 production by HT-29 IECs (Jeffrey *et al.*, 2018), we examined the effects on TNF- α -induced gene expression in order to gain insight into regulatory activity at the transcriptional level. Co-challenge of TNF- α -challenged HT-29 IECs with the LrS attenuated the activation of many genes involved in pro-inflammatory signaling activity, including those involved in NF- κ B activation. These findings are in keeping with previous transcriptomic analysis which revealed that live Lr R0011 modulates expression of genes involved in TLR, NOD, MAPK, and cytokine-chemokine receptor interactions in HT-29 IECs under basal conditions (Audy *et al.*, 2012) indicating a potential role for soluble mediators and metabolites in the immunomodulatory activity of live LAB.

Challenge of HT-29 IECs with the STS resulted in the up-regulation of several genes involved in pro-inflammatory activity and is, to our knowledge, the first report of the effects of secretome derived from ST grown under normal conditions on IECs. ST typically causes inflammation in the intestinal epithelium through the direct delivery of effector proteins via type III secretion systems (Keestra-Gounder *et al.*, 2015). However, the results presented here describe a potentially novel route of pathogenicity of this gut-associated pathogen via the shedding or secretion of bioactive molecules inducing pro-inflammatory signaling pathways. Recent reports have suggested that effector proteins encoded by the ST pathogenicity island-1 are packaged into outer membrane vesicles for long-distance delivery to host cells (S. I. Kim *et al.*, 2018) and several studies indicate that ST has strategies to exploit the host inflammatory response, contributing further to its pathogenic activity. ST requires intestinal inflammation in order to circumvent colonization resistance provided by the normal gut microbiota (Barman *et al.*, 2008; Stecher *et al.*, 2007). ST also utilizes tetrathionate generated by the host via the oxidation of free luminal thiosulfate by reactive oxygen species (ROS) produced by activated pro-inflammatory intestinal macrophages (Winter *et al.*, 2010). Tetrathionate acts as a respiratory electron acceptor and facilitates the ability of ST to respire ethanolamine released into the gut lumen during inflammation, providing a unique strategy for this intestinal pathogen to use the host inflammatory response to gain a growth advantage over other bacteria in the gut (LaRock *et al.*, 2015; Thiennimitr *et al.*, 2011). For this reason, we examined the ability of the LrS to attenuate STS-induced expression of pro-inflammatory mediators as a potential mechanism to counteract this pathogenic strategy. As was seen with TNF- α -challenged IECs, the LrS also attenuated ST-secretome-induced expression of

genes involved in NF- κ B, MAPK, TLR, and NLR signaling pathways, suggesting a novel route of LAB-mediated gut-pathogen antagonism at the IEC level.

Concurrent challenge of TNF- α - or STS-challenged HT-29 IECs with the LrS resulted in the up-regulation of *DUSP1*, *TRIB3*, and *ATF3*. DUSP1, a central regulator of the MAPK pathway which acts to dephosphorylate p38 α and Jun N-terminal kinases (Arthur *et al.*, 2013), has been well characterized in its role as a negative regulator of innate pro-inflammatory activity (Chi *et al.*, 2006; Hammer *et al.*, 2006; Ko *et al.*, 2009; Lang *et al.*, 2006; Salojin *et al.*, 2006). TRIB3, a negative regulator of NF- κ B-mediated signaling, acts as a pseudokinase to allosterically inhibit the phosphorylation of p65 by protein kinase A (Wu *et al.*, 2003). *TRIB3* transcription is activated by DDIT3/CHOP, a member of the CCAAT/enhancer-binding protein (C/EBP) family (Ohoka *et al.*, 2005), and the LrS up-regulated expression of this transcription factor in TNF- α or STS-challenged HT-29 IECs. In contrast, lipopolysaccharide derived from *Helicobacter pylori* down-regulates CHOP and TRIB3 expression in human gastric epithelial cell lines (Smith *et al.*, 2011), suggesting TRIB3 plays a complex role in IEC responses to gut bacteria.

ATF3 is a transcription factor also involved in the attenuation of NF- κ B-mediated signaling (Whitmore *et al.*, 2007). Its expression can be induced by ribosomal insults, which has been suggested as a mechanism through which NF- κ B activation is regulated in IEC to prevent excessive inflammation in response to commensal bacteria (Park *et al.*, 2013). Although there have been reports of differential modulation of ATF3 in response to bacterial challenge (Lee *et al.*, 2018; Nguyen *et al.*, 2016), to the best of our knowledge, this is the first report of induction of this transcriptional repressor in response to secretome components from LAB. ATF3 recruits HDAC1 to deacetylate the promoter regions of NF-

κ B target genes, such as IL-6 and IL-12 (Li *et al.*, 2010), hindering the activity of the p65 subunit of NF- κ B (Gilchrist *et al.*, 2006), or can deacetylate p65 directly (Kwon *et al.*, 2015). For this reason, the ability of the LrS to modulate global histone acetylation patterns was examined. Epigenetic reprogramming through changes in histone acetylation patterns is well documented and has been shown to be an important aspect of host-microbe interactions in the gut (Miro-Blanch *et al.*, 2019; Qin *et al.*, 2018). Furthermore, *Lactobacillus rhamnosus* MTCC 5897 and *Lactobacillus fermentum* MTCC 5898 have been shown to limit *E. coli*-induced increases in Caco-2 IEC H3 and H4 histone acetylation (Bhat *et al.*, 2019). In keeping with these findings, the LrS reduced TNF- α - and STS-induced H3 and H4 histone acetylation, suggesting a possible mechanism of action behind the observed immunomodulatory activity of the LrS on TNF- α and ST-secretome-induced pro-inflammatory gene transcription through chromatin structural remodeling. However, it is currently unknown if this reduction in histone acetylation is a direct result of increased ATF3 expression when IECs are co-challenged with the LrS and this warrants further investigation.

Interestingly, up-regulation of *DUSP1*, *TRIB3*, and *ATF3* by the LrS was observed when HT-29 IEC were also responding to either TNF- α or the STS, but not to the LrS alone. Impact on *GADD45 β* and *HSPA6* (*HSP70B*) expression followed a similar pattern and was significantly upregulated by the LrS only in IEC exposed to these pro-inflammatory stimuli. *GADD45 β* is a central regulator of many cellular functions in response to certain cellular stressors and has been shown to play a protective role against TNF- α -induced apoptosis by antagonizing JNK activation (Papa *et al.*, 2004). *HSP70B*' and other members of the HSP70 family of proteins also have diverse intracellular

functions within cells in response to stress by acting as molecular chaperones to prevent denaturation of proteins and refold and guide damaged proteins to their correct cellular localization. Moreover, the HSP70 family of proteins can inhibit NF- κ B activation by preventing the oligomerization of NEMO proteins and subsequent IKK activation (Ran *et al.*, 2004; Salminen *et al.*, 2008). Overall, this indicates context-dependent regulation of the production of pro-inflammatory biomarkers by the LrS and may provide insights into how some bacteria use soluble mediators to maintain homeostasis at the gut mucosal interface by counteracting effects of potential extracellular stressors and pro-inflammatory stimuli.

ATF3 and TRIB3 expression can be induced in response to endoplasmic reticulum stress and has been shown to be activated by ROS generation (Hoetzenecker *et al.*, 2011; Kanwar, 2010). As ROS plays a complex role in regulating IEC responses to pro-inflammatory stimuli and other cell stressors, we examined the impact of the LrS on ROS production by HT-29 IEC. LAB-induced ROS production has been reported as a potential immunomodulatory mechanism (Lin *et al.*, 2016), and varied roles for ROS in microbe-host communication are further illustrated by the ability of *Lactobacillus johnsonii* N6.2 to modulate immune activity through effects on 2,3-indoleamine dioxygenase (IDO) activity (Valladares *et al.*, 2015), and the impact of H₂O₂ produced by lactobacilli on *Citrobacter rodentium* pathogenicity in rodents (Pircalabioru *et al.*, 2016). ROS induction has been shown to be a route through which certain LAB inhibit NF- κ B activation in activated IEC, via the oxidation of ubiquitin conjugating enzyme 12 both *in vitro* and *in vivo* (Jones *et al.*, 2013; Kumar *et al.*, 2007; Wentworth *et al.*, 2011). Indeed, nitric oxide and ROS were identified as potential upstream regulators of the activation of DDIT3/CHOP, ATF3, and

DUSP1 when HT-29 IEC were co-challenged with the LrS and either pro-inflammatory challenge. However, excessive ROS production can lead to pathological inflammation through the activation of NF- κ B signaling pathways via stabilization of NEMO proteins, resulting in the production of pro-inflammatory mediators (Herb *et al.*, 2019; Reuter *et al.*, 2010). Recent reports indicate that HSP70 can inhibit mitochondrial ROS production in response to bacterial toxins in human lung microvascular endothelial cells (Li *et al.*, 2018), and others have demonstrated the ability of LAB to inhibit ROS production and exert antioxidant activity (Gaisawat *et al.*, 2019; Vong *et al.*, 2014). In keeping with these findings, intracellular ROS production was significantly lower in HT-29 IEC treated with the LrS, indicating that the induction of these negative regulators was not due to an increase in ROS production and that the LrS may reduce oxidative stress on IECs by induction of HSP70.

The ability of the LrS to attenuate production of TNF- α - and STS-induced pro-inflammatory cytokines and chemokines is in keeping with the observed effects on negative regulator expression. While down-regulation of IEC pro-inflammatory cytokine production has shown with other LAB (Bai *et al.*, 2004; Gao *et al.*, 2017; Tuo *et al.*, 2018; Wan *et al.*, 2018), to our knowledge, this is the first report of secretome components of LAB demonstrating this range of immunomodulatory bioactivity on pro-inflammatory mediator production by IECs. Interestingly, challenge with the LrS increased MIF production, while TNF- α or STS challenge and lactic acid controls did not, a finding consistent with previous reports suggesting that pro-inflammatory cytokines also do not induce MIF production by IECs (Maaser *et al.*, 2002). This was the only instance in which the LrS induced cytokine production from HT-29 IECs, and is to our knowledge the first report of secretome

components of LAB to stimulate MIF production. MIF is a pleiotropic cytokine (Harris *et al.*, 2019) and has been reported to be integral in the maintenance of IEC barrier function through its effects on colonic tight and adherens epithelial junctions (Vujicic *et al.*, 2018). It may also act to inhibit AP-1 activity (Kleemann *et al.*, 2000) resulting in the down-regulation of inflammatory gene expression. MIF's role in response to Gram-negative bacterial challenge is well established (Das *et al.*, 2014; Roger *et al.*, 2003) and it has been associated with increased macrophage-dependent pathogen clearance (Roger *et al.*, 2013), indicating that it may exert context-dependent regulation of the inflammatory response to bacteria. Although the precise nature of regulation of transcription and secretion of MIF remains to be fully elucidated, it has been shown that MIF is secreted when NF- κ B activation is inhibited (Cho *et al.*, 2009), suggesting a possible mechanism of action behind LrS-induced MIF secretion. Moreover, MIF has also been shown to increase M-cell mediated transport of luminal antigens, indicating that it plays a key role in facilitating the complex cross-talk between bacterial secretome components and the underlying immune cell population at the gut-mucosal interface (Man *et al.*, 2008).

L-lactic acid, a key metabolite produced by lactobacilli and present in the LrS, had distinct effects on IEC signaling pathways. Most notably, unique gene expression profiles were observed when HT-29 IECs were challenged with TNF- α and treated with L-lactic acid concentration-matched controls, indicating that L-lactic acid is not responsible for the observed bioactivity of the LrS. Although many of the cellular pathways involved in TNF- α signaling were unaffected by L-lactic acid, it did attenuate the production of TNF- α -induced CXCL10, CXCL1, and CCL2. Indeed, lactic acid has been shown to attenuate the production of some pro-inflammatory cytokines by human monocytes and T cells exposed

to challenge, through the transcriptional and post-transcriptional regulation of enzymes involved in glycolysis (Dietl *et al.*, 2010; Haas *et al.*, 2015). Moreover, L-lactic acid has been associated with HDAC inhibitory activity resulting in changes to gene expression profiles (Latham *et al.*, 2012), making it a potential immunomodulatory molecule of interest, although its actions on IEC were distinct from those mediated by the LrS.

The results presented in this study provide new insights into the role of soluble bioactive molecules derived from both pathogenic bacteria and lactobacilli in communication with host IECs. We propose a novel mechanism of LAB secretome-mediated effects on IEC signaling pathways through the induction of *ATF3*, *TRIB3*, *DUSP1*, negative regulators of the NF- κ B and MAPK signaling pathways, and through changes in global histone acetylation patterns. The LrS also induced the production of MIF, a cytokine which may exert context-dependent regulation of gut homeostasis by influencing IEC barrier integrity, M-cell dependent antigen uptake, and transcriptional responses to pro-inflammatory challenge. Taken together, these findings give novel insight into the complex mechanisms of action behind secretome-mediated interdomain communication at the gut-mucosal interface, and suggest new directions for approaches to delineate the activities of gut-associated bacteria *in vivo*. Future work to characterize the LrS and STS will be needed in order to determine which bioactive molecule(s) are responsible for the observed impacts of these bacteria on IECs, their roles in pathogenicity and host immune responses, and their potential roles in gut microbe-host interactions.

Table I. Fold change difference in expression of genes encoding pro-inflammatory mediators and negative regulators of innate immunity in HT-29 IECs exposed to TNF- α , STS, the LrS, L-lactic acid, or a combination of the treatments.

Gene Name	TNF- α	STS	LrS	L-lactic Acid	TNF- α + LrS	STS + LrS	TNF- α + L-lactic Acid	STS + L-Lactic Acid
Pro-inflammatory Mediator								
<i>CXCL1</i>	13.2	7.85	-1.62	-	13.72	-	10.35	-
<i>CXCL10</i>	29.62	-	-	-	-	-	17.1	-
<i>CXCL11</i>	13.2	-	-	-	-	-	4.17	-
<i>CCL20</i>	35.93	6.39	-1.54	-	8.77	-	6.75	14.38
<i>IL-1β</i>	2.134	-	-	-	-	-	2.48	-
<i>IL-8</i>	23.61	5.97	-	-	5.50	2.02	18.96	7.52
<i>IL-17C</i>	10.68	3.69	-	-	-	-	11.31	5.79
<i>IL-23A</i>	4.30	-	-	-	-	-	2.02	-
<i>IL-32</i>	5.28	-	-	-	-	-	8.32	-
<i>BIRC3</i>	15.39	2.47	-	-	-	-	4.46	6.65
<i>PTGS2</i>	10.99	1.67	-	-	-	-	14.41	2.98
<i>EGFR</i>	3.80	-	-	-	-	-	1.64	-
Negative Regulator of Innate Immunity								
<i>DUSP1</i>	2.86	-	-4.48	-	15.67	7.40	4.49	1.50
<i>ATF3</i>	2.47	-	-3.39	-	12.65	6.37	5.66	-
<i>TRIB3</i>	-	-	-5.75	-	5.50	7.00	2.00	-
<i>HSPA6</i>	-	-	-6.69	-	14.95	4.11	-	-
<i>GADD45β</i>	-	-	-5.67	-	10.06	5.05	2.07	-

Table II. List of primers used for relative RT-qPCR for microarray validation.

Gene	GenBank Accession Number	Amplicon Length (bp)	Primer Sequence (5' – 3')	Source
<i>B2M</i>	NM_004048	150	F: GTGCTCGCGCTACTCTCTC R: GTCAACTTCAATGTCGGAT	(Dydensborg <i>et al.</i> , 2006)
<i>RPLPO</i>	NM_001002	142	F: GCAATGTTGCCAGTGTCTG R: GCCTTGACCTTTTCAGCAA	(Dydensborg <i>et al.</i> , 2006)
<i>TRIB3</i>	NM_021158.4	184	F: TGGTACCCAGCTCCTCTACG R: GACAAAGCGACACAGCTTGA	(Jousse <i>et al.</i> , 2007)
<i>ATF3</i>	NM_001206484.3	71	F: AAGAACGAGAAGCAGCATTTGAT R: TTCTGAGCCCGGACAATACAC	(Bottone <i>et al.</i> , 2005)
<i>DUSP1</i>	NM_004417	80	F: GGCCCCGAGAACAGACAAA R: GTGCCCACTTCCATGACCAT	(Locati <i>et al.</i> , 2002)
<i>NFκB1</i>	NM_003998.3	130	F: GCAGCACTACTTCTTGACCACC R: TCTGCTCCTGAGCATTGACGTC	(Macpherson <i>et al.</i> , 2014)

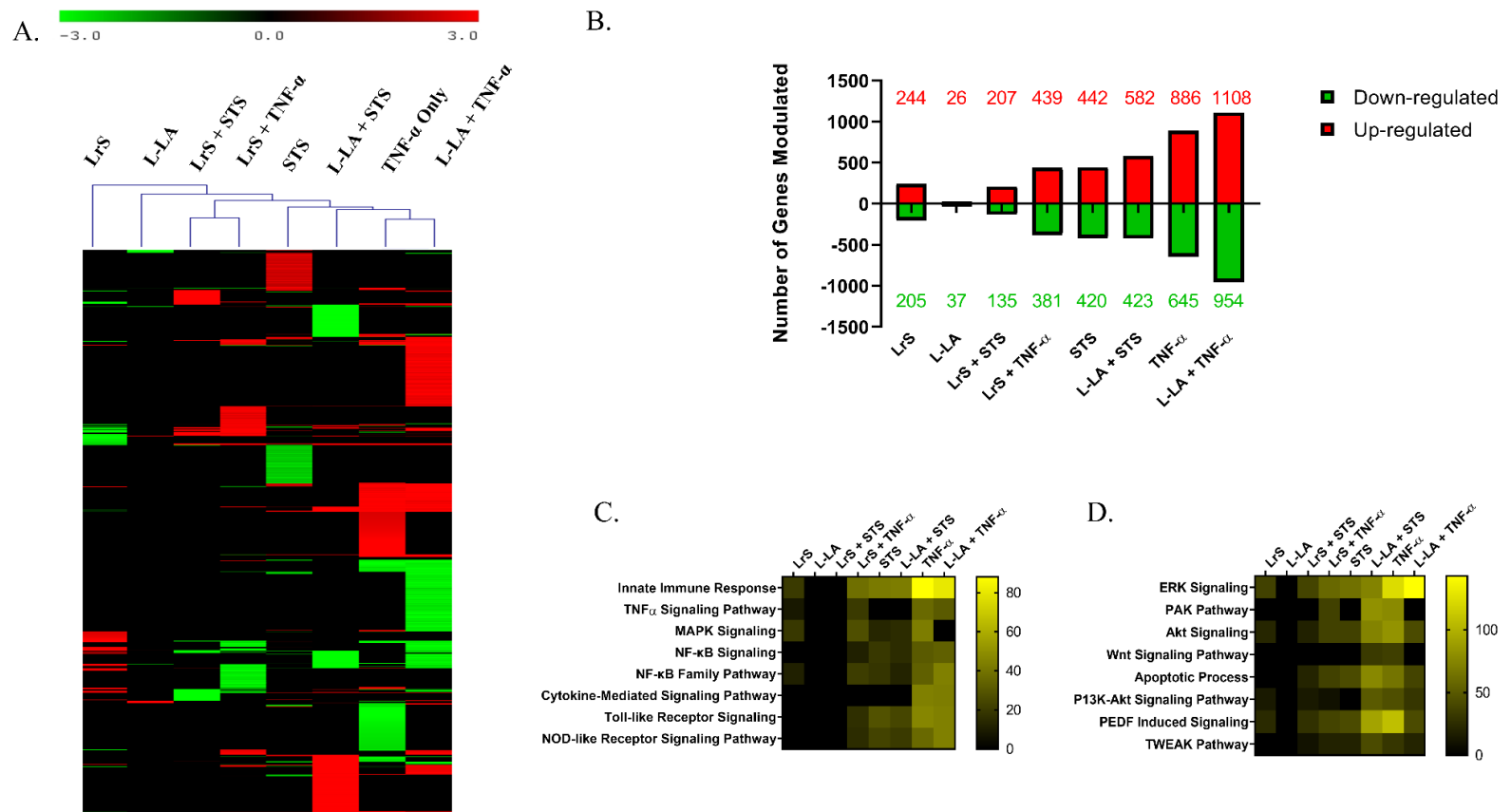


Figure 1-1. A. Two-dimensional hierarchical clustering analysis of global gene expression data in HT-29 IECs exposed to TNF- α , the STS, the LrS alone, a combination of the LrS and either TNF- α or the STS, an L-lactic acid control, or a combination of the STS or TNF- α and L-lactic acid (n = 4, P < 0.05, fold change difference > 1.5 vs untreated cells). **B.** Total number of up- and down-regulated genes in response to each different challenge. Gene enrichment analysis using GeneDecks Set Distiller to delineate the number of genes in **C.** Immune-related or **D.** Cellular/Signaling related pathways differentially modified in HT-29 IECs exposed to TNF- α , the STS, the LrS, a combination of both, or to the STS or TNF- α + L-lactic acid control (n = 4, P < 0.05).

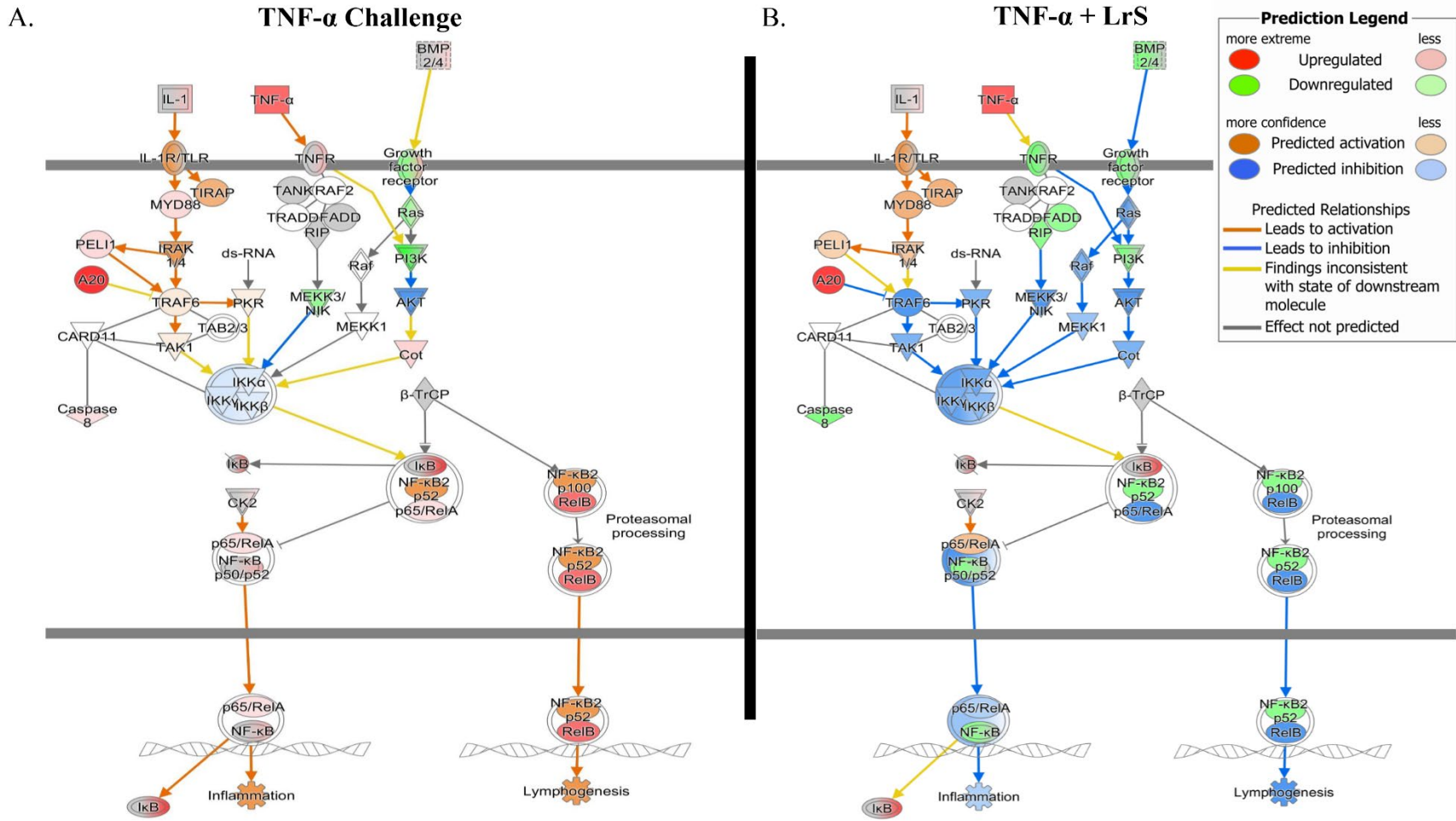


Figure 1-2. Pathway analysis of TNF- α signaling pathways using IPA predictive modelling of the cellular outcomes of HT-29 IECs exposed to **A.** TNF- α challenge or **B.** TNF- α + the LrS.

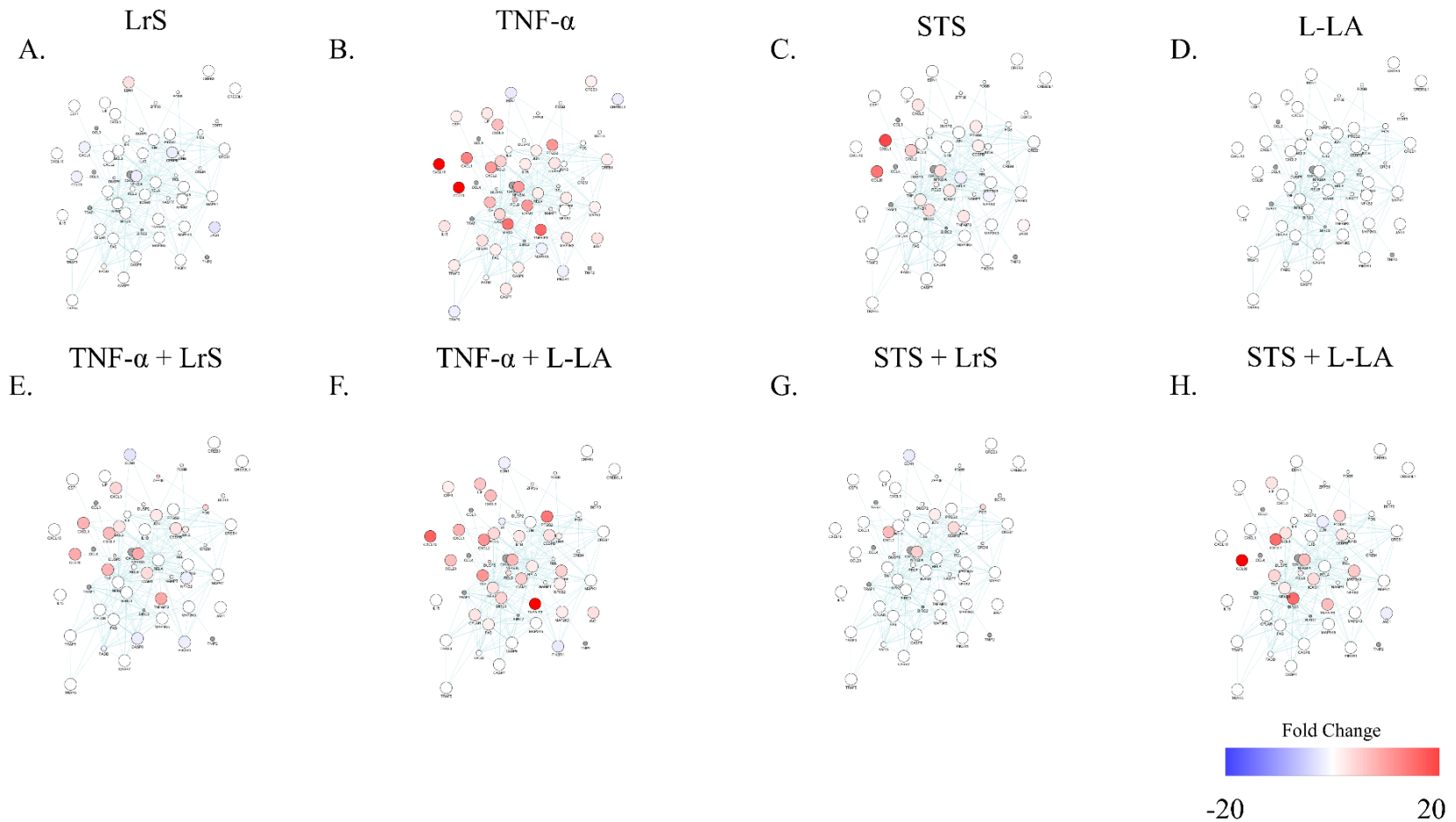


Figure 1-3. Gene-interaction maps of genes involved in the TNF- α signaling pathway in HT-29 IECs that were differentially modified relative to untreated cells as determined by the GeneDecks gene enrichment analysis and GeneMania ($P < 0.05$) by **A.** LrS **B.** TNF- α **C.** STS **D.** L-lactic acid controls **E.** TNF- α + the LrS **F.** TNF- α + L-lactic acid controls **G.** STS + the LrS or **H.** STS and L-lactic acid controls.

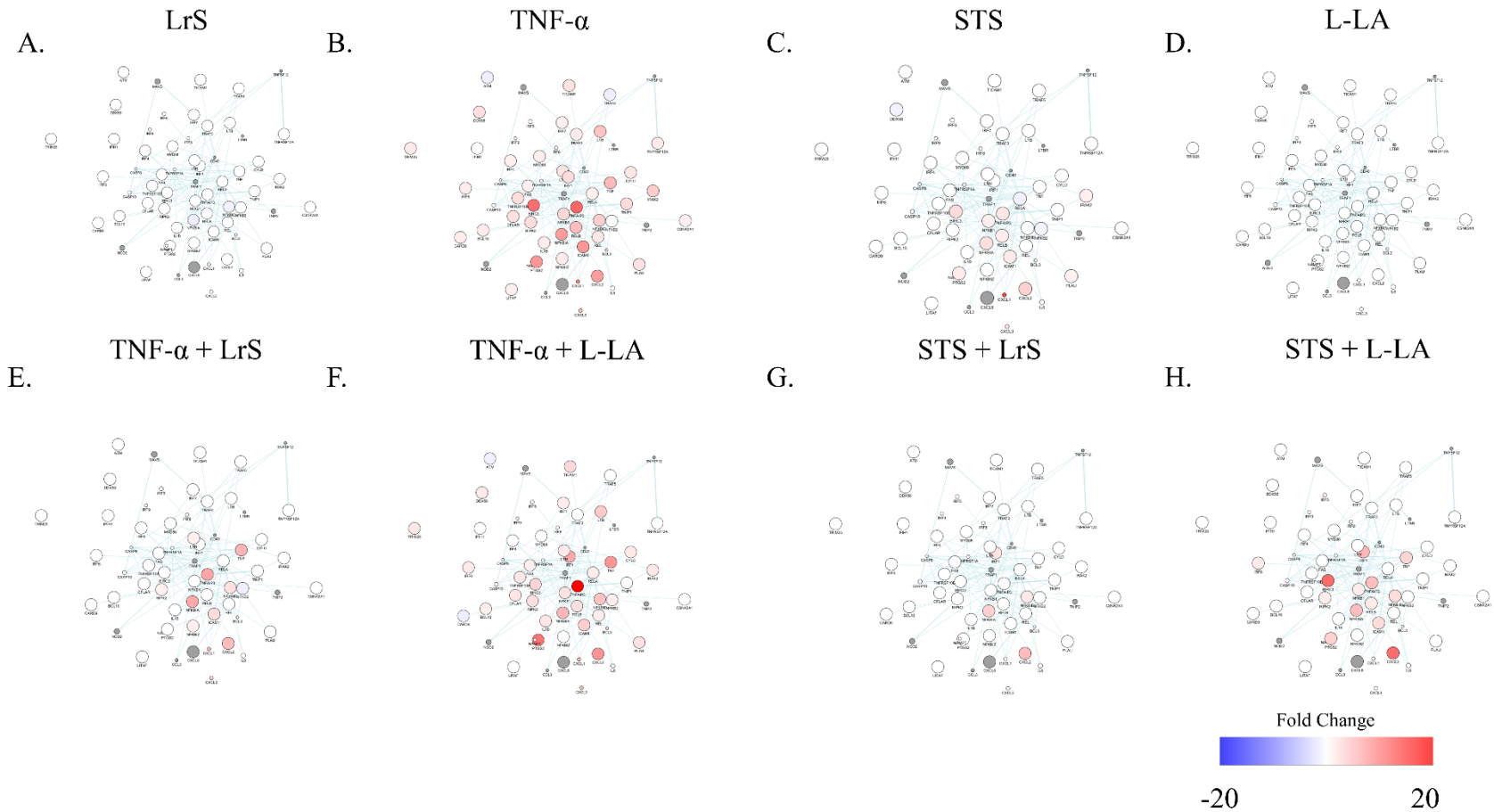


Figure 1-4. Gene-interaction maps of genes involved in the NF- κ B signaling pathway in HT-29 IECs that were differentially modified relative to untreated cells as determined by the GeneDecks gene enrichment analysis and GeneMania ($p < 0.05$) by **A.** LrS **B.** TNF- α **C.** STS **D.** L-lactic acid controls **E.** TNF- α + the LrS **F.** TNF- α + L-lactic acid controls **G.** STS + the LrS or **H.** STS and L-lactic acid controls.

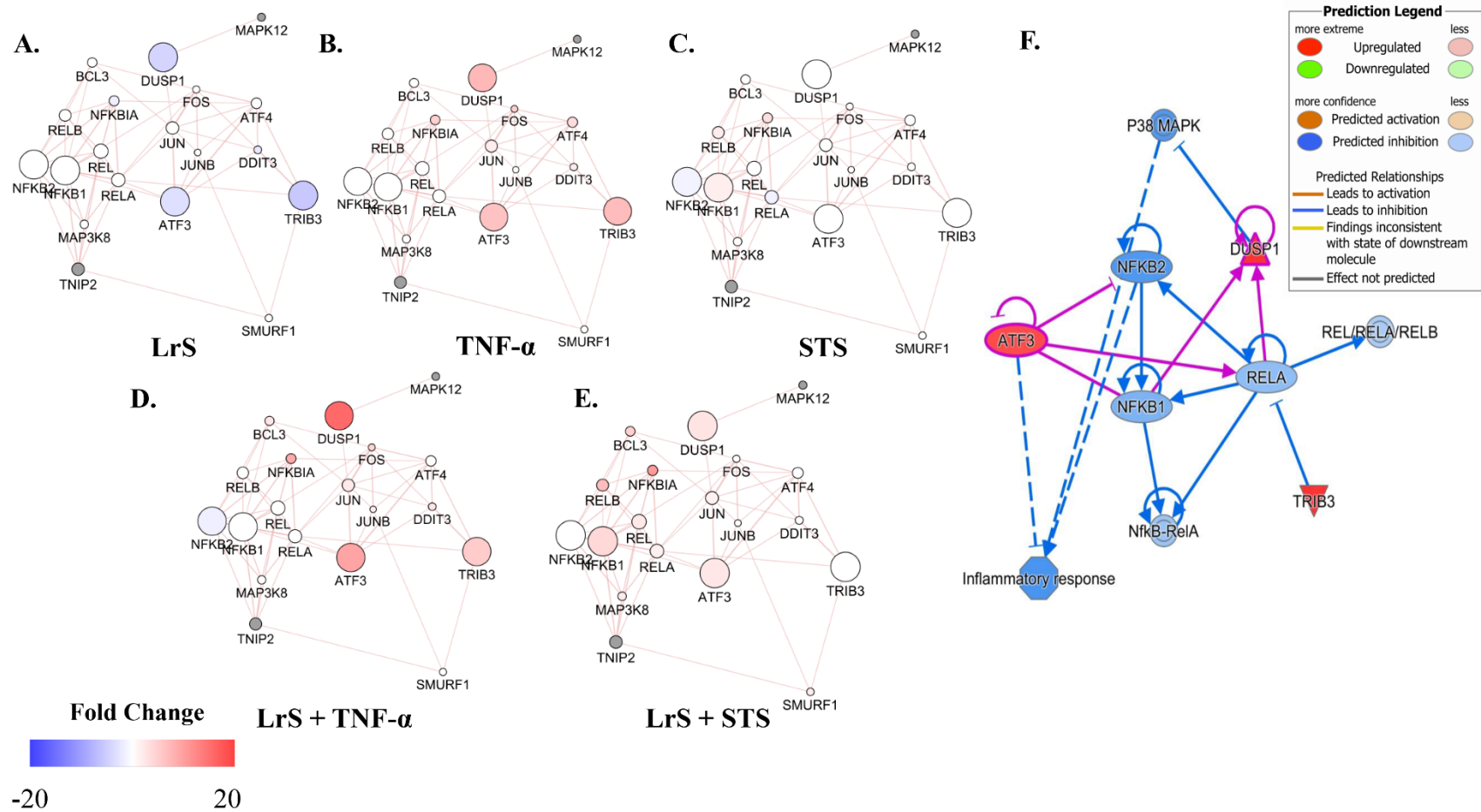


Figure 1-5. Negative regulators of the innate immune response that were identified to be differentially transcribed in response to the different treatments. Gene interaction maps using CytoScape and GeneMania showing genes which have been reported to interact directly with each other in response to treatment with **A.** LrS **B.** TNF- α **C.** STS **D.** TNF- α + the LrS or **E.** STS + the LrS **F.** IPA pathway analysis using predictive modelling to determine the interactions between the identified negative regulators and the NF- κ B and MAPK signaling pathways.

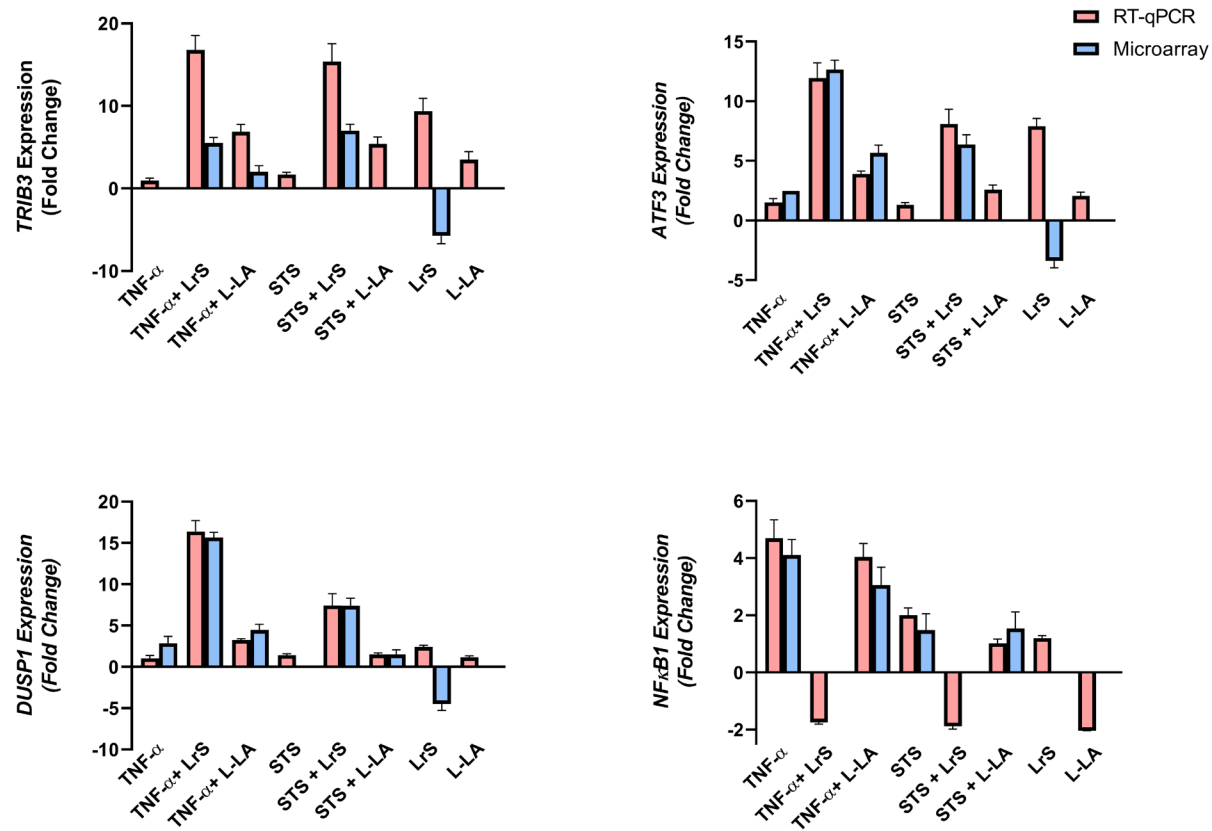
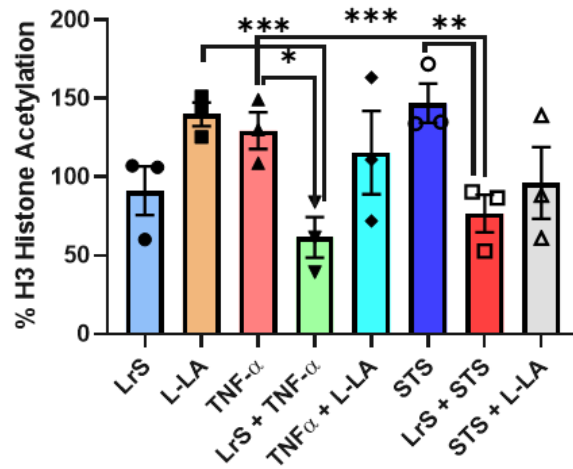


Figure 1-6. RT-qPCR confirmation of the expression of Trib3, ATF3, DUSP1, and NFκB1. Data shown is the mean relative fold-change ± SEM (n = 4).

A.



B.

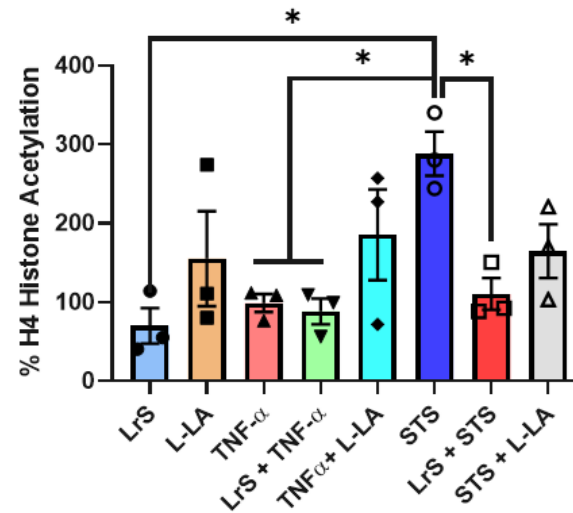


Figure 1-7. Changes in global histone **A.** H3 or **B.** H4 acetylation patterns in challenged IECs. Data shown is the mean change in % acetylation compared to untreated controls \pm SEM (n = 4). Significance is indicated as * $p < 0.05$, ** $p < 0.01$, *** $p < 0.001$ as determined by one-way ANOVA and Tukey's post-hoc test.

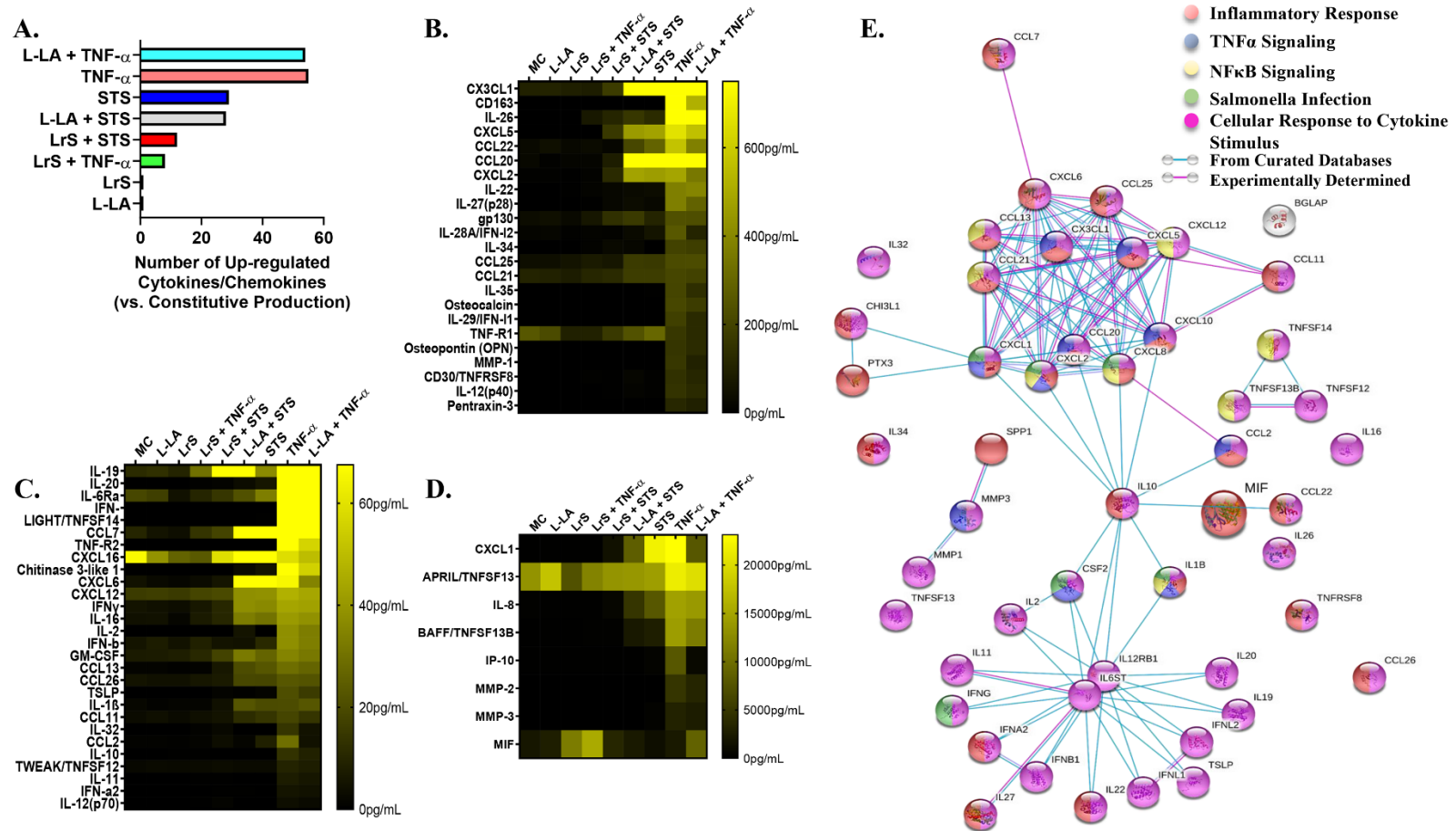


Figure 1-8. Cytokine and chemokine profiles from HT-29 IECs exposed to the different treatments for 6 hours. **A.** Total number of cytokines and chemokines showing significant levels of production relative to negative controls as determined by as determined by one-way ANOVA and Dunnett's post-hoc test ($n = 4$; $p < 0.05$). **B-D.** Cytokine and chemokine profiles from HT-29 IECs exposed to the different challenges for 6 hours. Data shown is the means cytokine/chemokine production (pg/mL) \pm SEM ($n = 4$). **E.** String v 11.0 analysis showing functional links between each of the different cytokines/chemokines measured based on reported literature and curated databases.

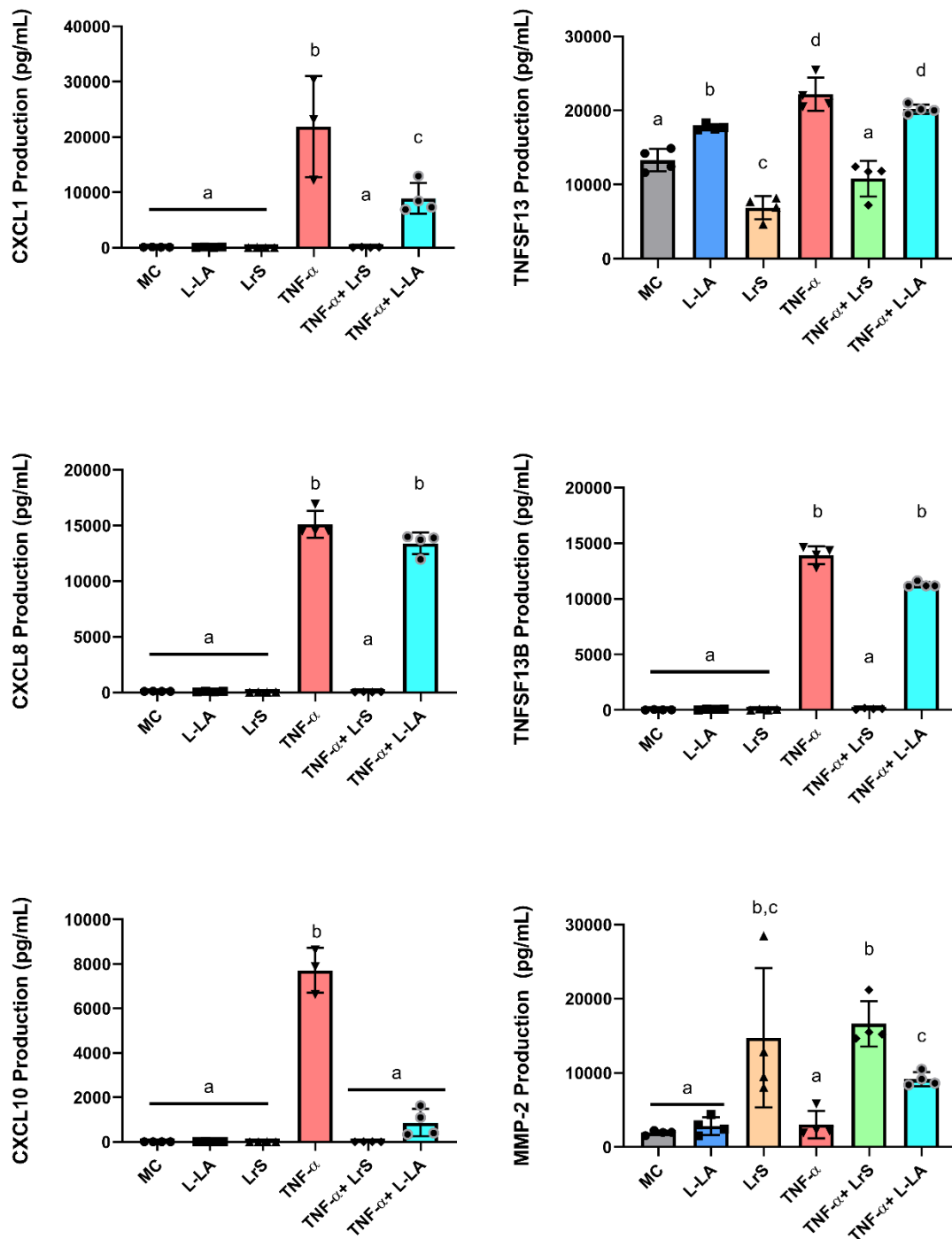
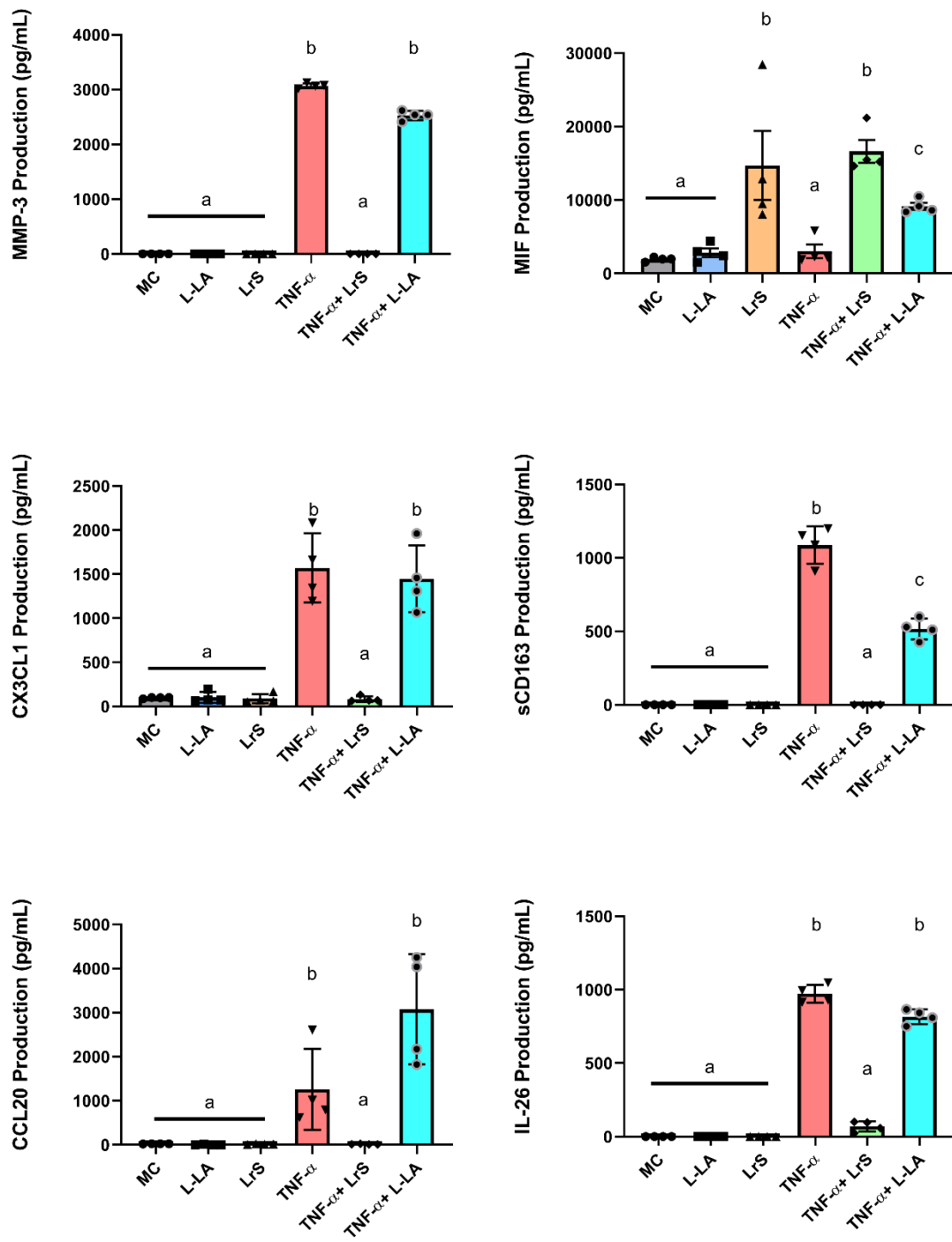
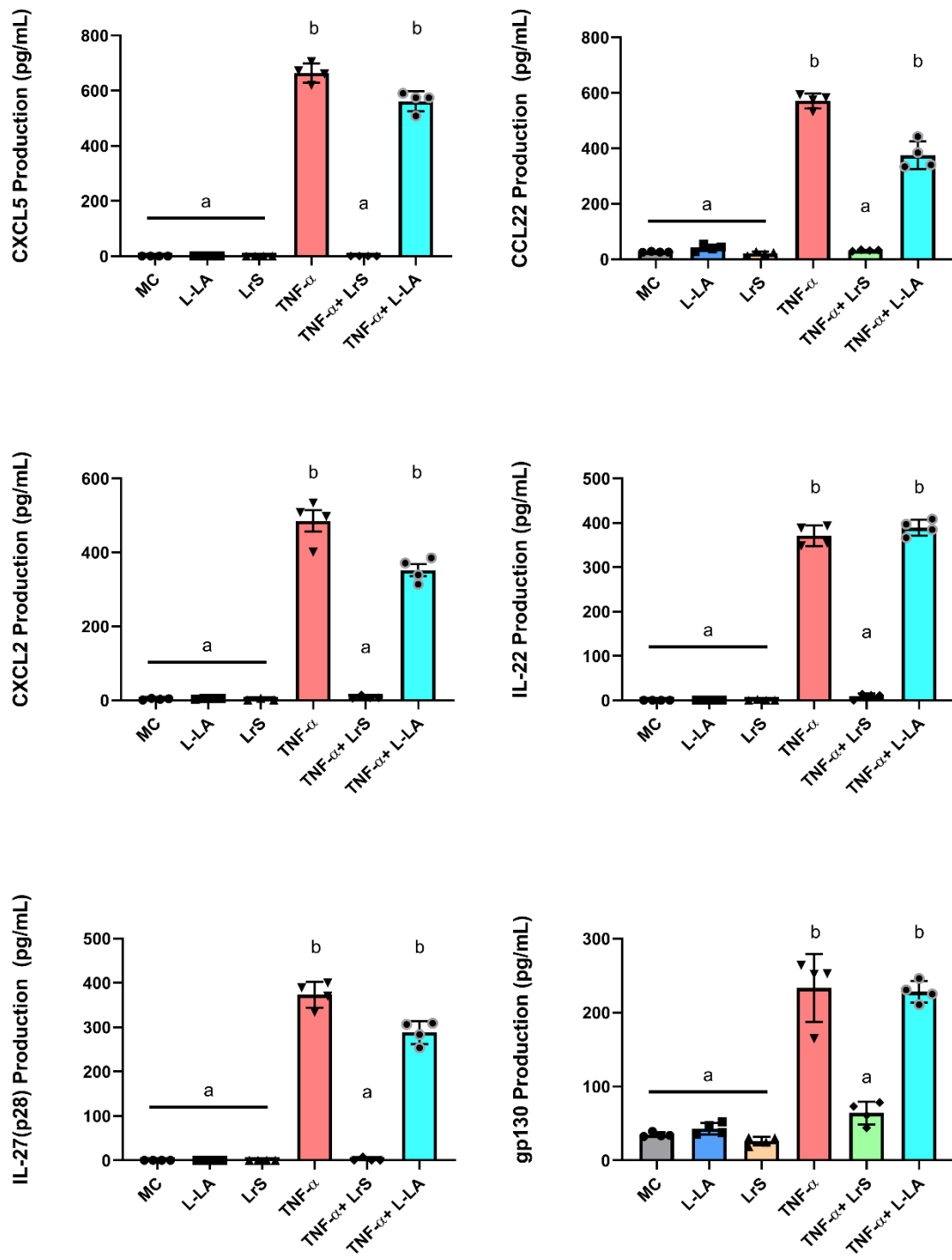


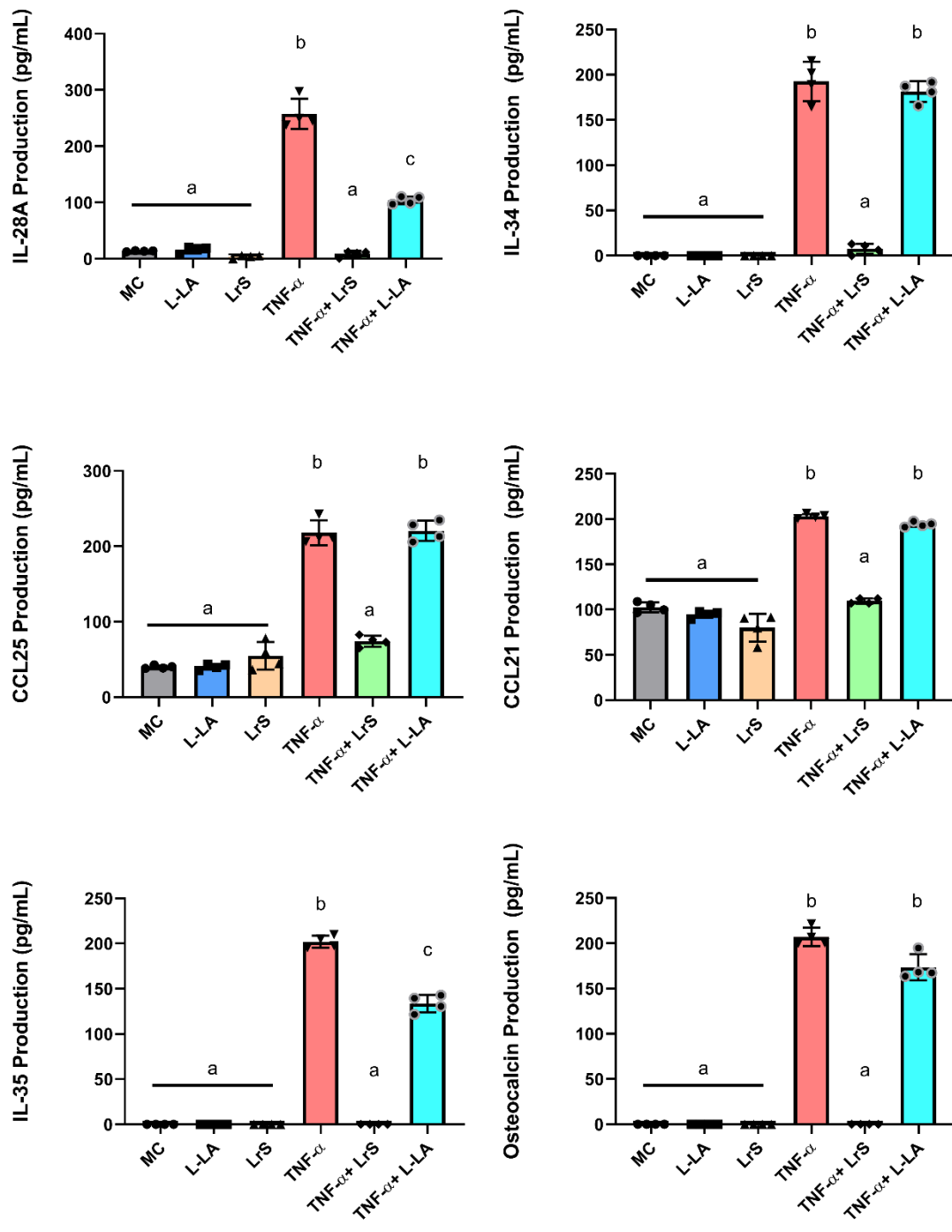
Figure 1-9. Cytokine and chemokine profiles from HT-29 IECs challenged with the LrS, L-LA, TNF- α , or a combination of the different challenges for 6 hours. Data shown is the means cytokine/chemokine production (pg/mL) \pm SEM (n = 4). Significance is denoted by different letters as determined by one-way ANOVA and Tukey's post-hoc test ($p < 0.05$).



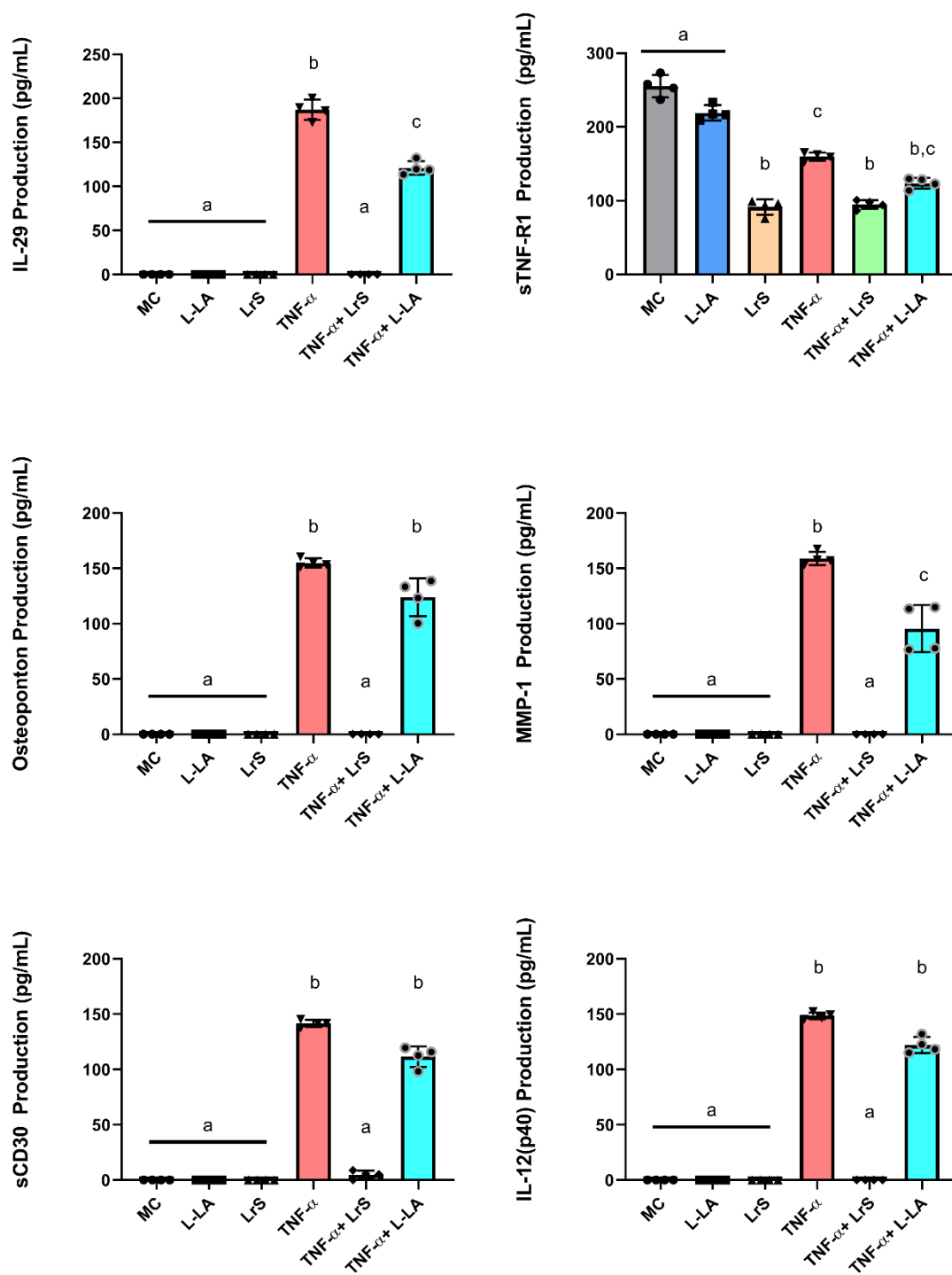
This is a continuation of Figure 1-9



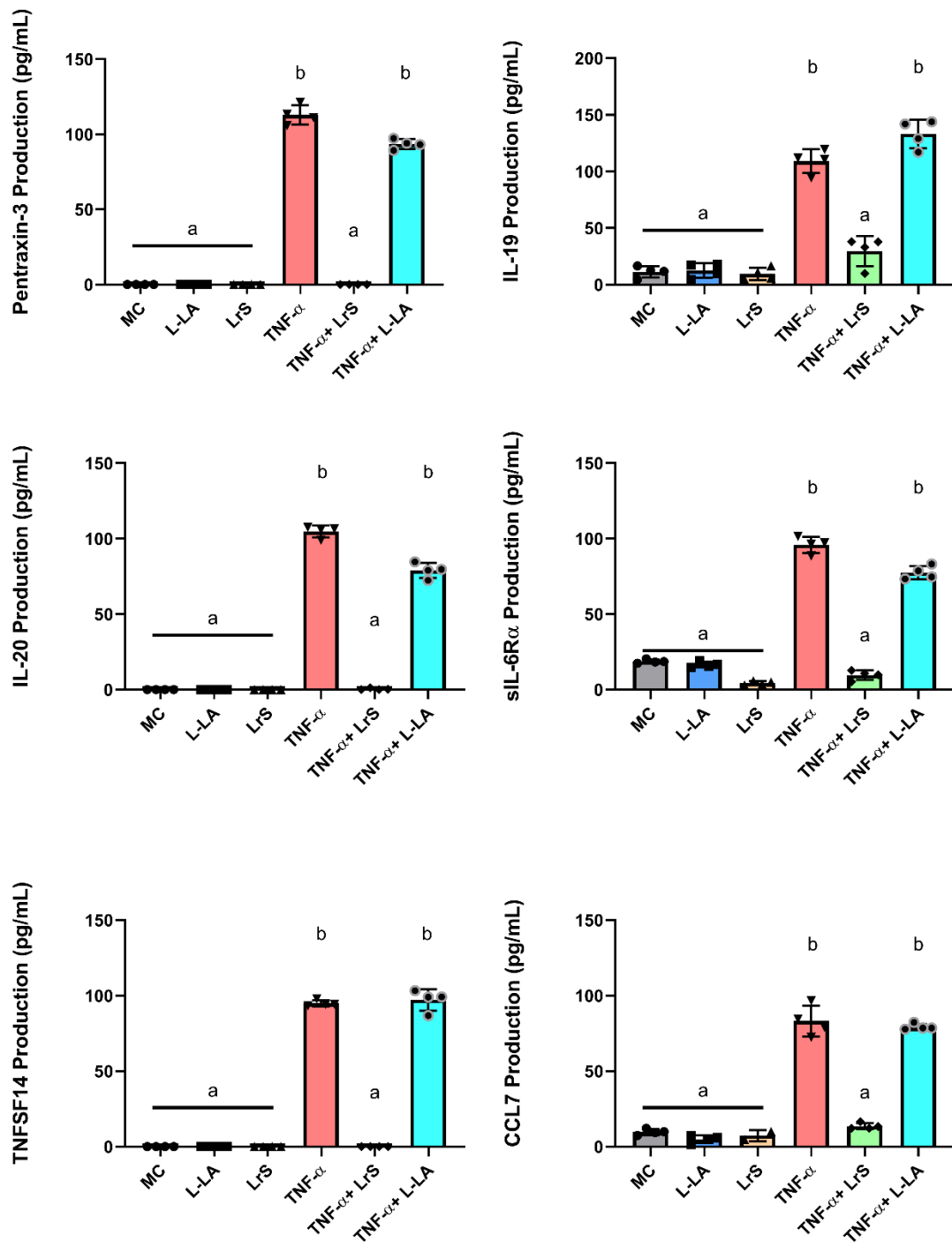
This is a continuation of Figure 1-9



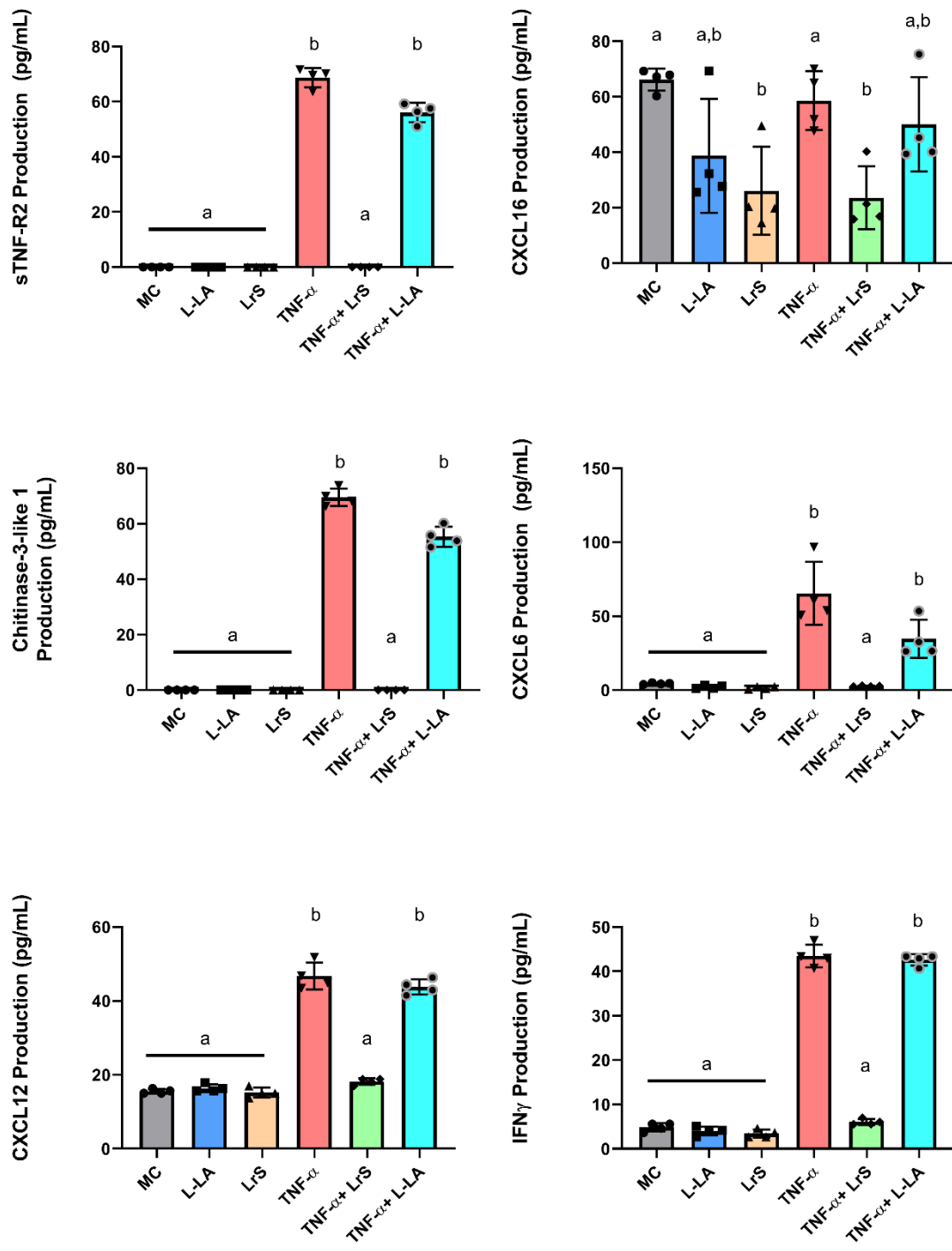
This is a continuation of Figure 1-9



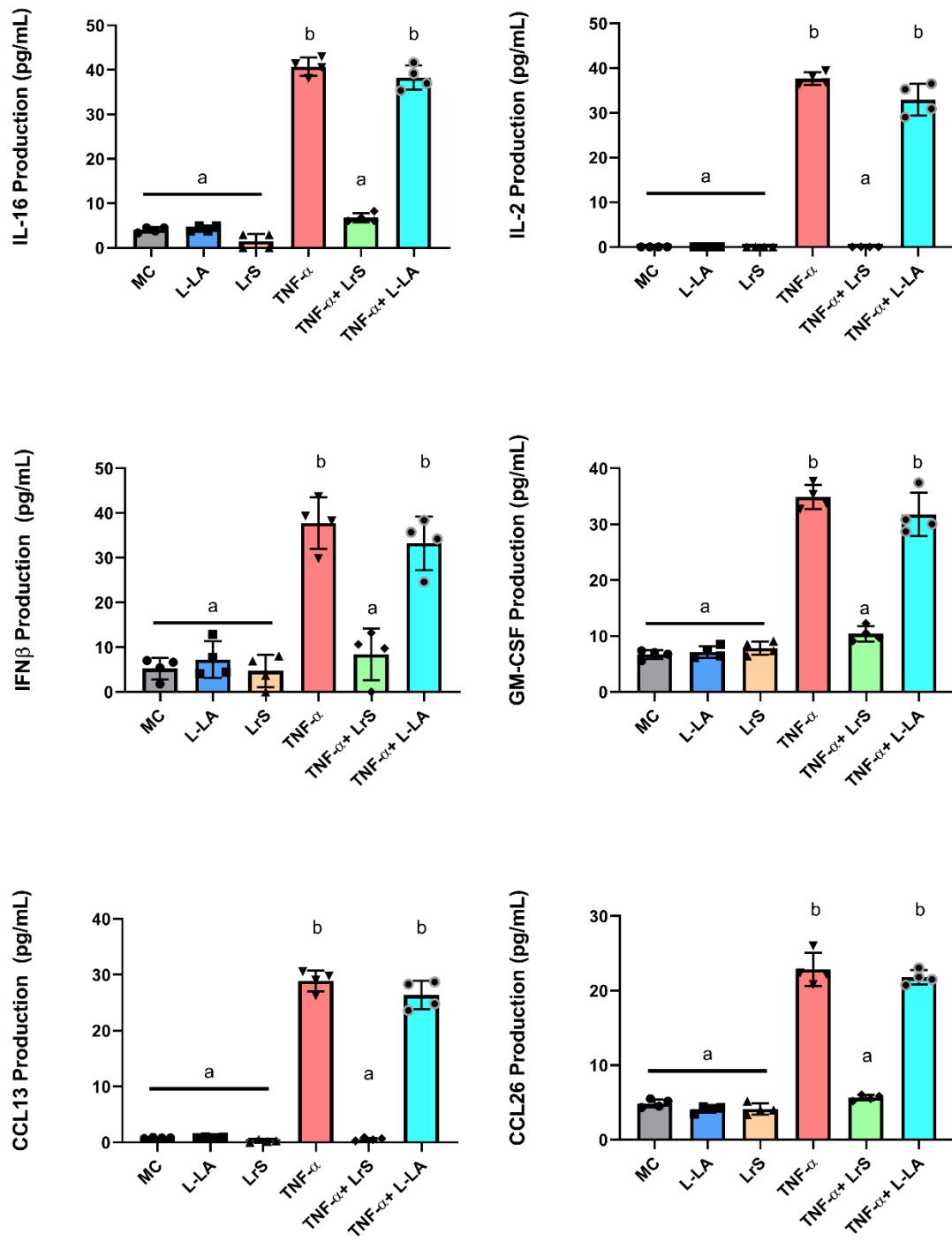
This is a continuation of Figure 1-9



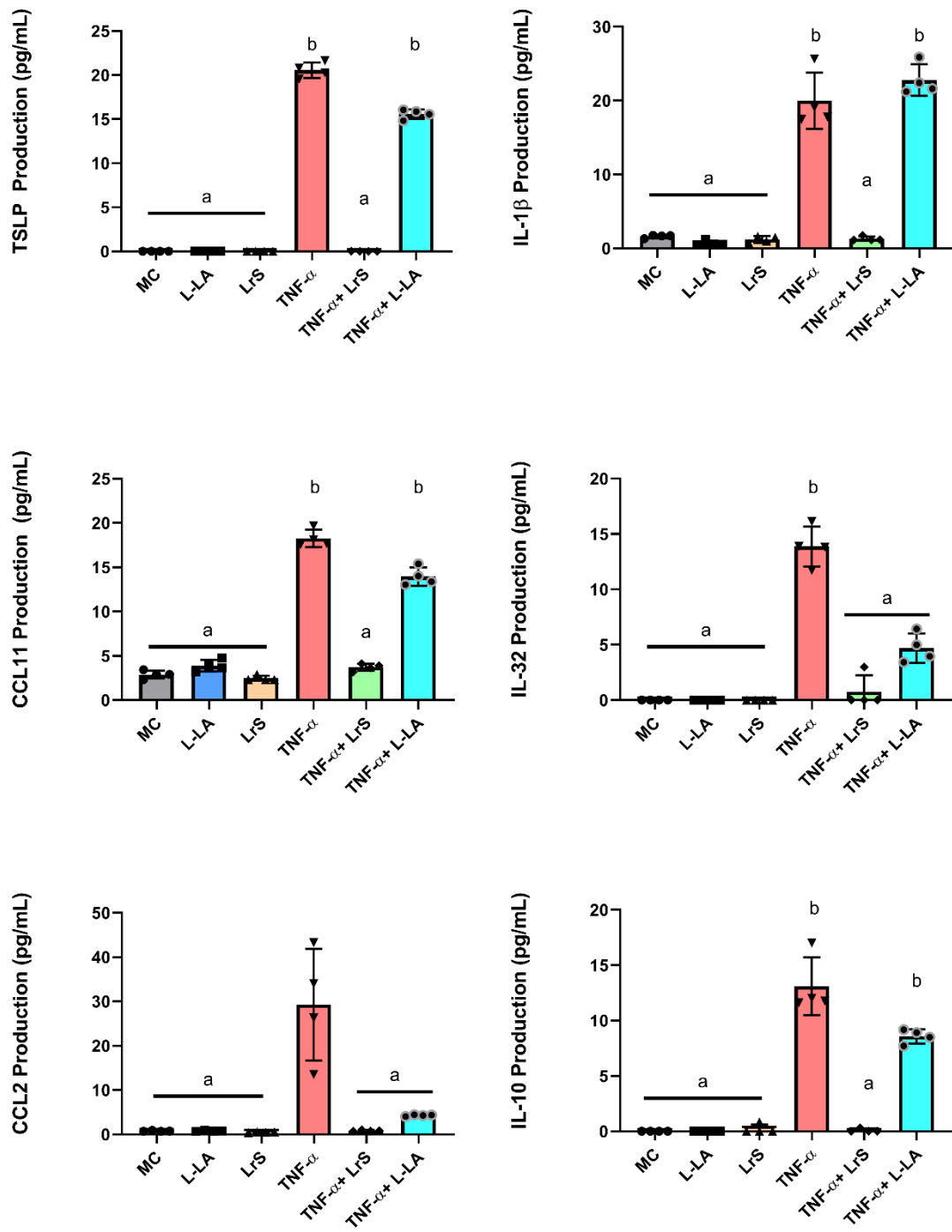
This is a continuation of Figure 1-9



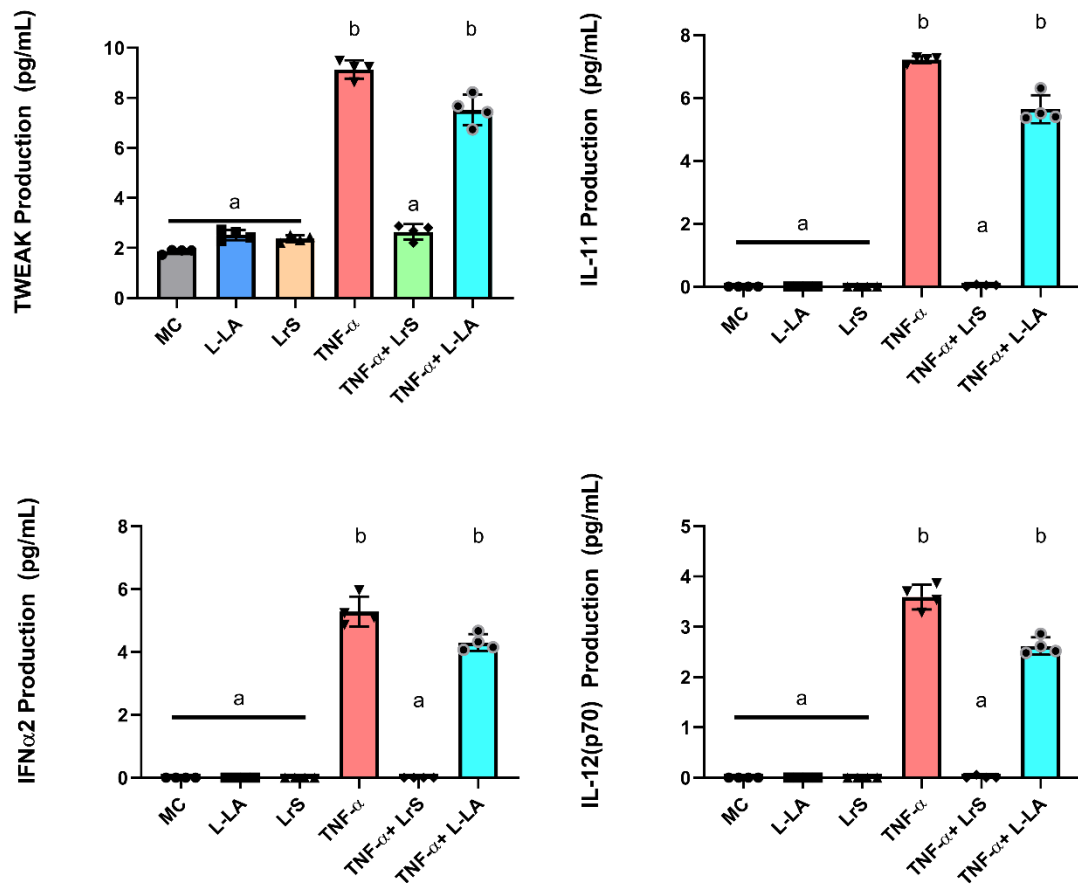
This is a continuation of Figure 1-9



This is a continuation of Figure 1-9



This is a continuation of Figure 1-9



This is a continuation of Figure 1-9

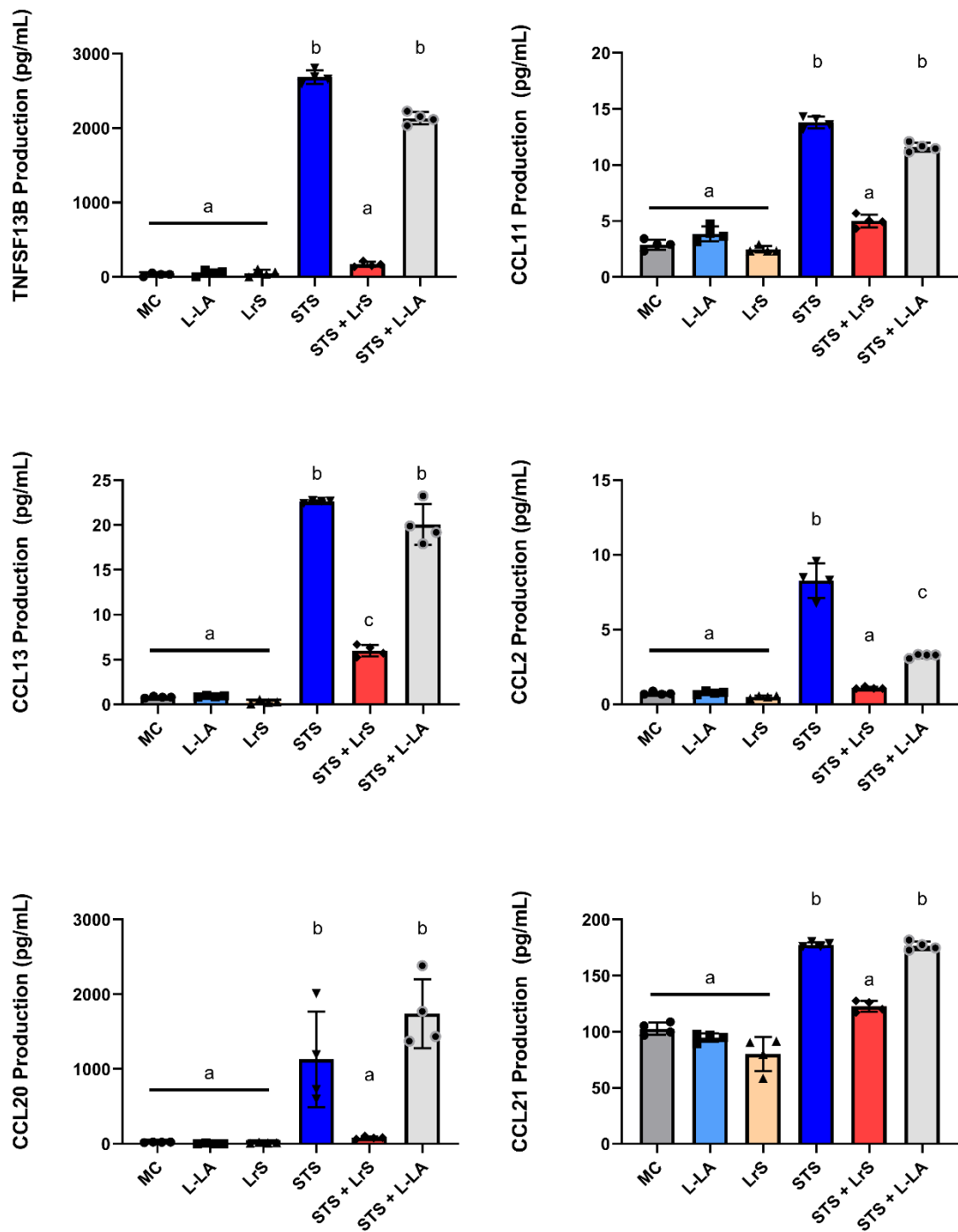
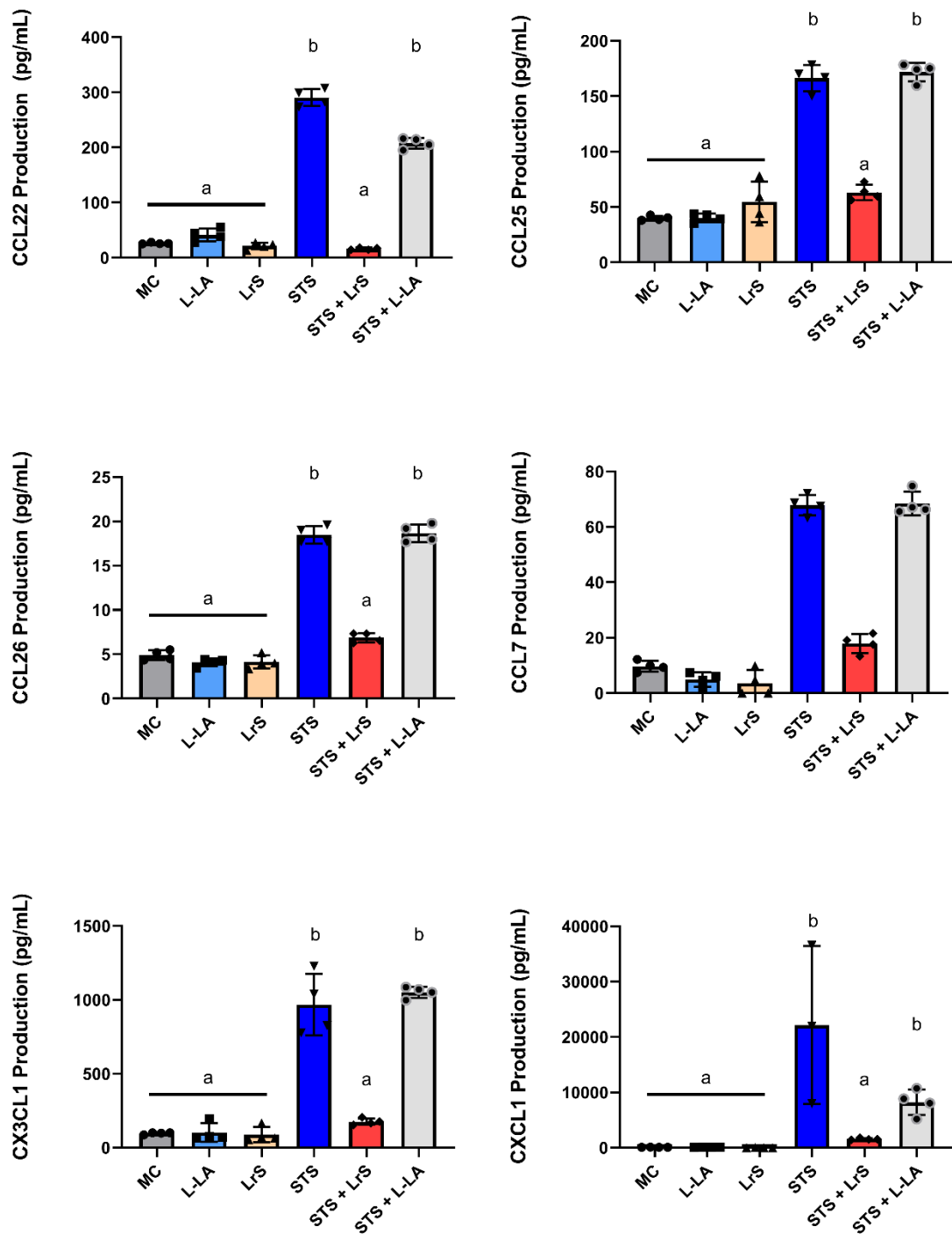
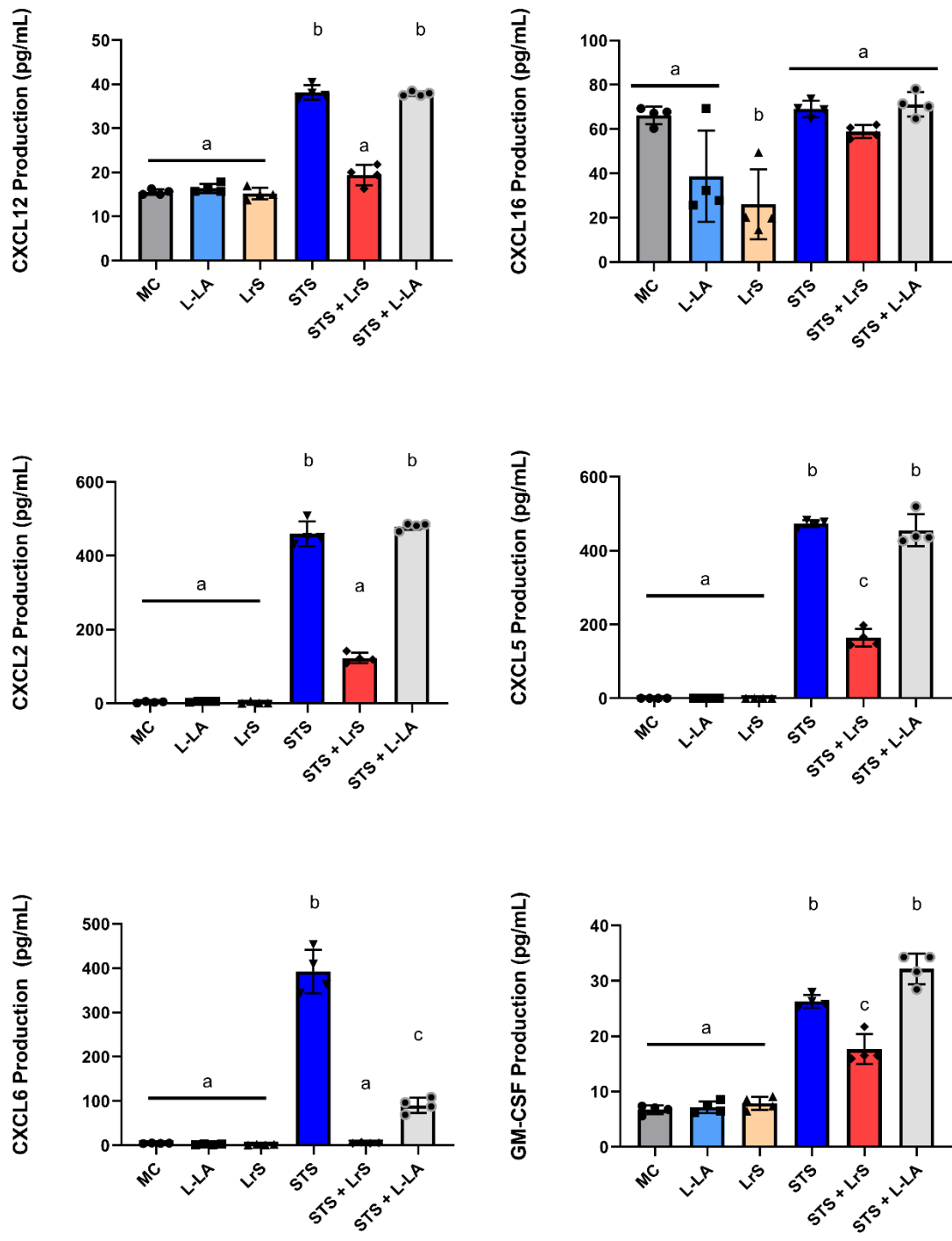


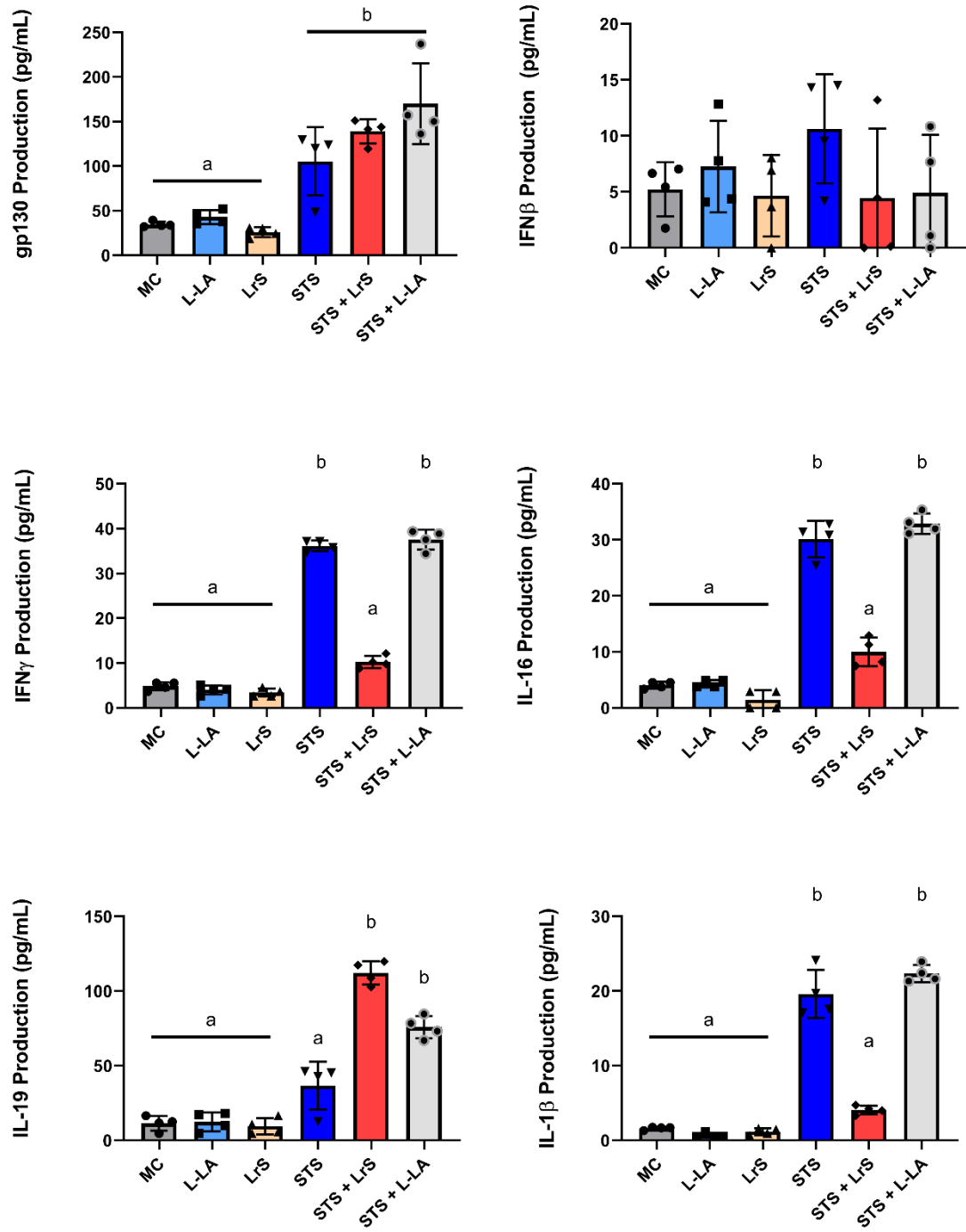
Figure 1-10. Cytokine and chemokine profiles from HT-29 IECs challenged with the LrS, L-Lactic Acid, STS, or a combination of the different challenges for 6 hours. Data shown is the means cytokine/chemokine production (pg/mL) \pm SEM (n = 4). Significance is denoted by different letters as determined by one-way ANOVA and Tukey's post-hoc test ($p < 0.05$).



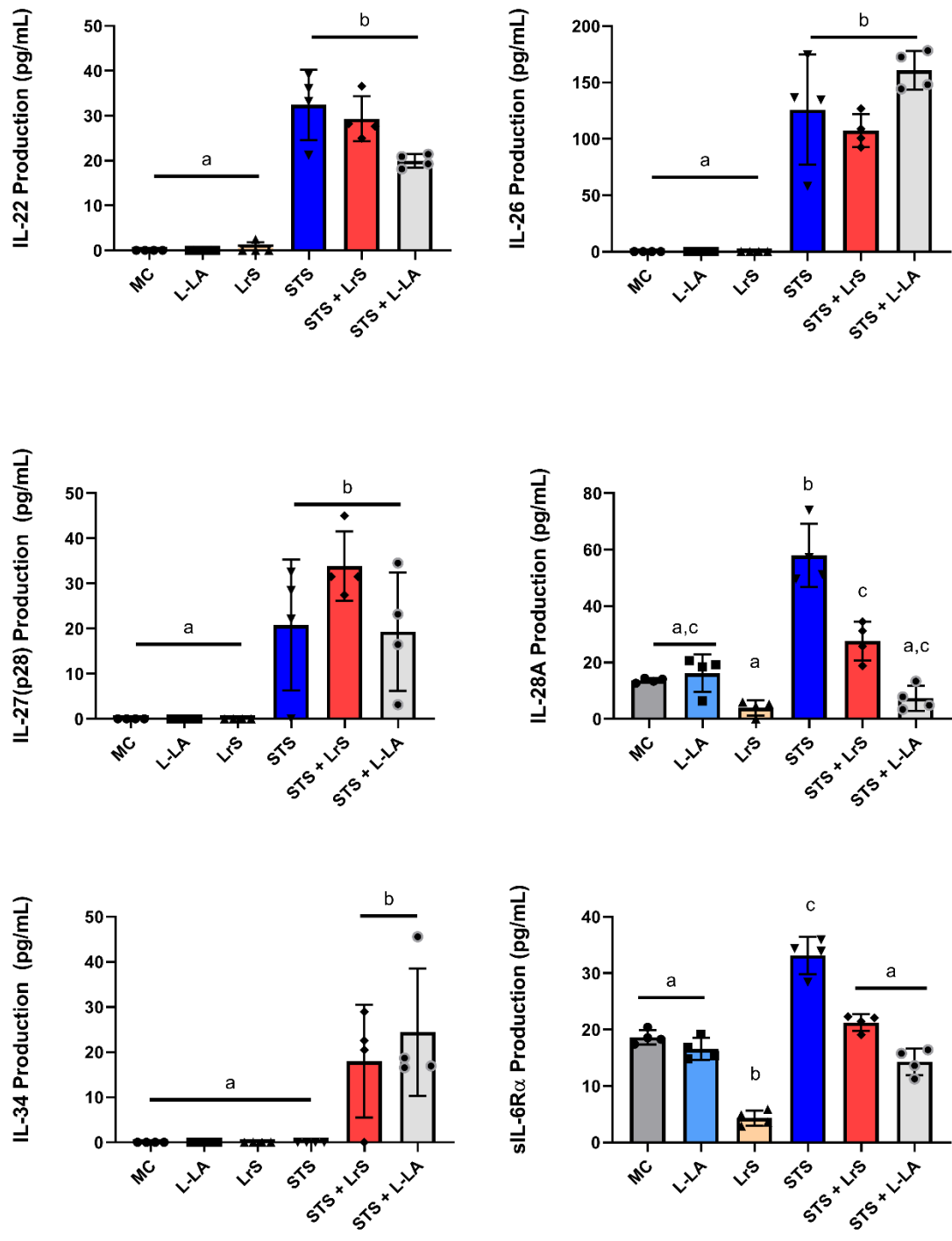
This is a continuation of Figure 1-10



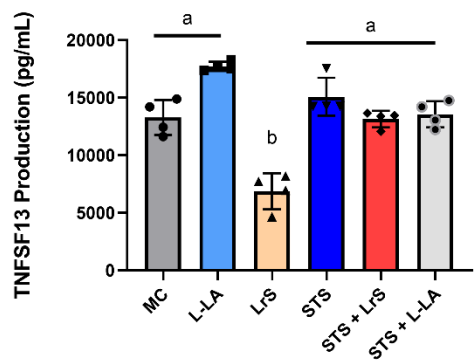
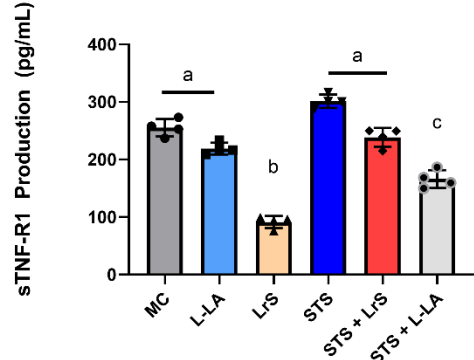
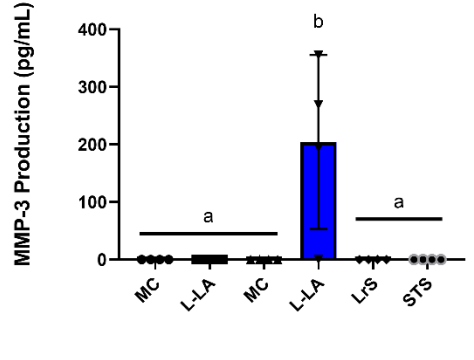
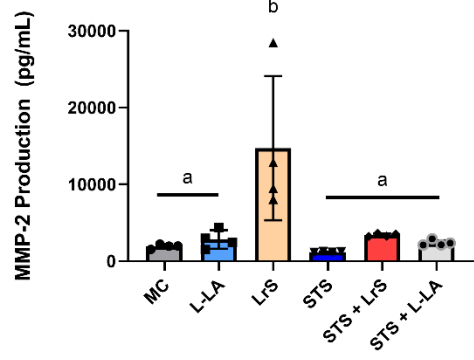
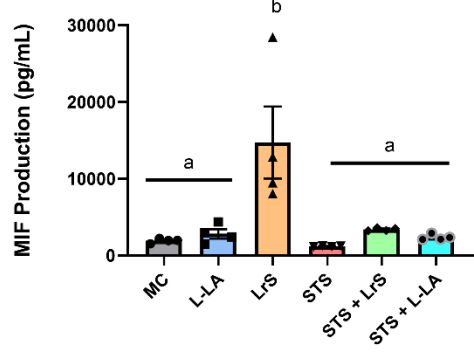
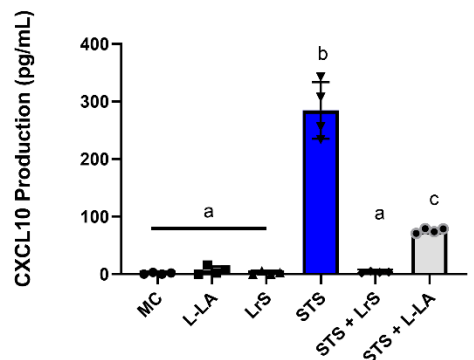
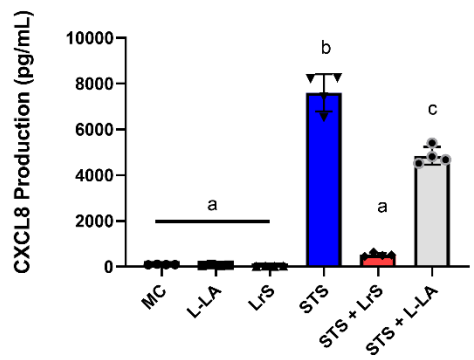
This is a continuation of Figure 1-10



This is a continuation of Figure 1-10



This is a continuation of Figure 1-10



This is a continuation of Figure 1-10

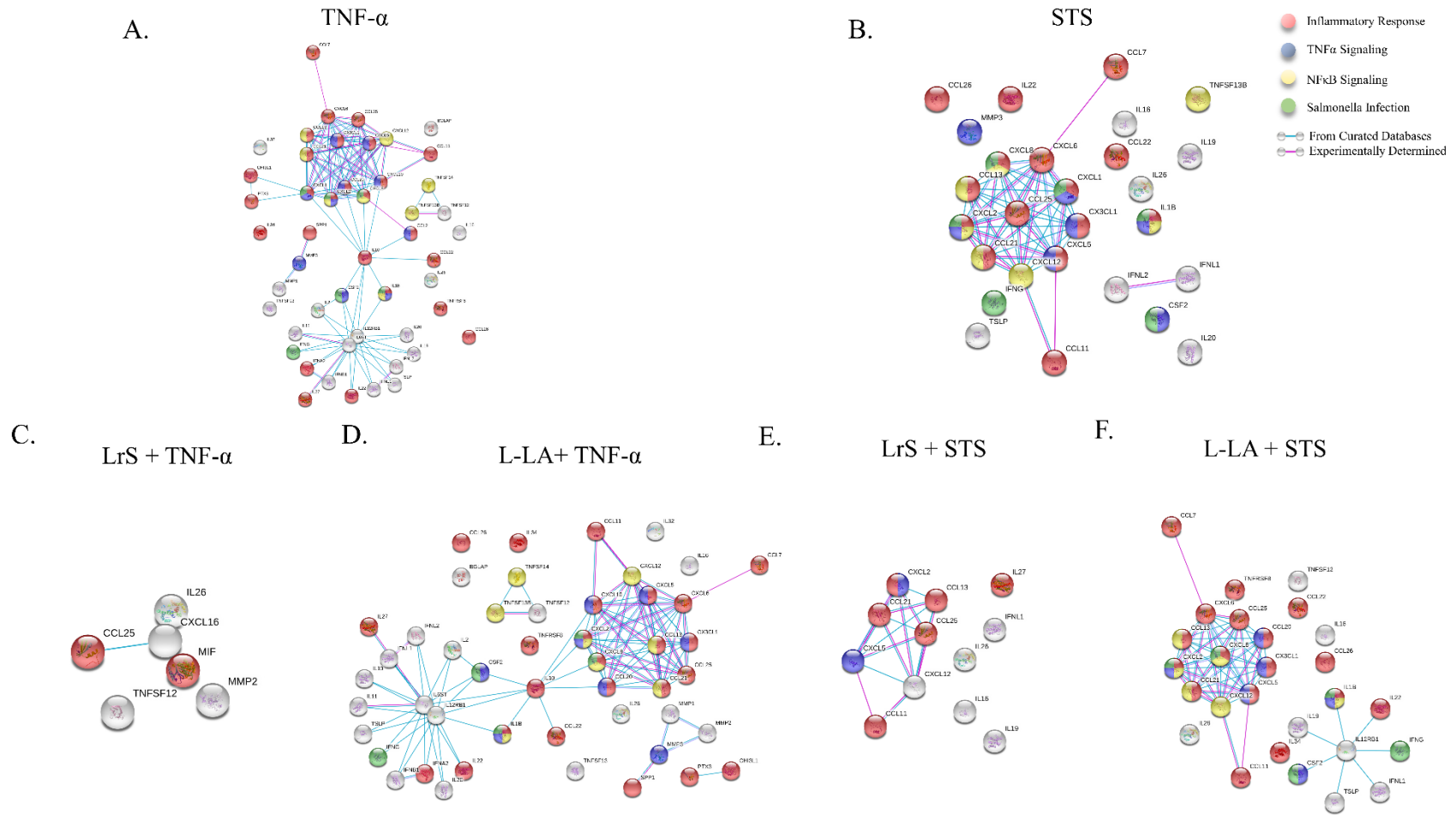


Figure 1-11. String v 11.0 analysis reveals functional links between each of the different cytokines/chemokines measured in response to **A. TNF- α** **B. STS** **C. LrS + TNF- α** **D. L-LA + TNF- α** **E. LrS + STS** and **F. L-LA + STS**

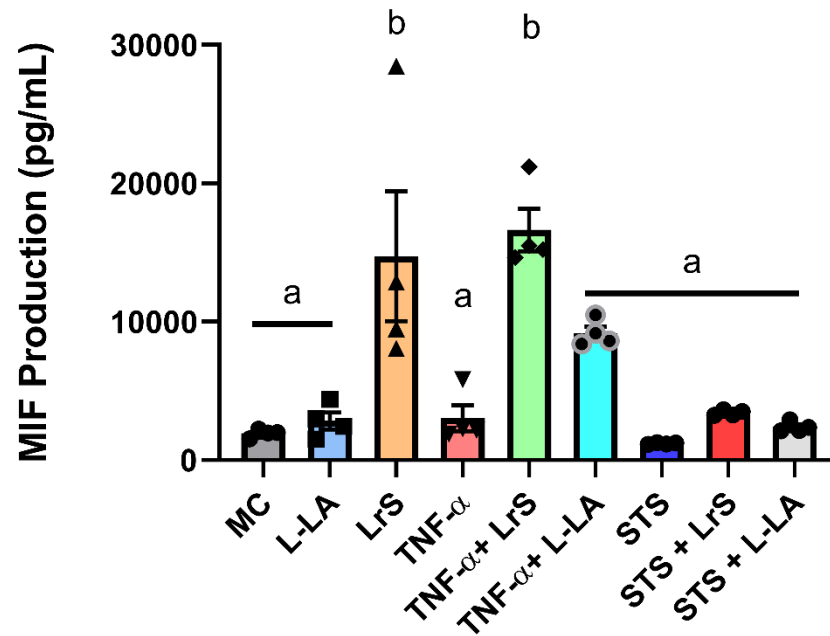


Figure 1-12. MIF production is induced in HT-29 IECs by the LrS. HT-29 IECs were exposed to the different challenges for 6 hours and the levels of MIF were quantified. Data shown is the means cytokine/chemokine production (pg/mL) \pm SEM (n = 4). Different letters denote significance between treatments as determined by one-way ANOVA and Tukey's post-hoc test.

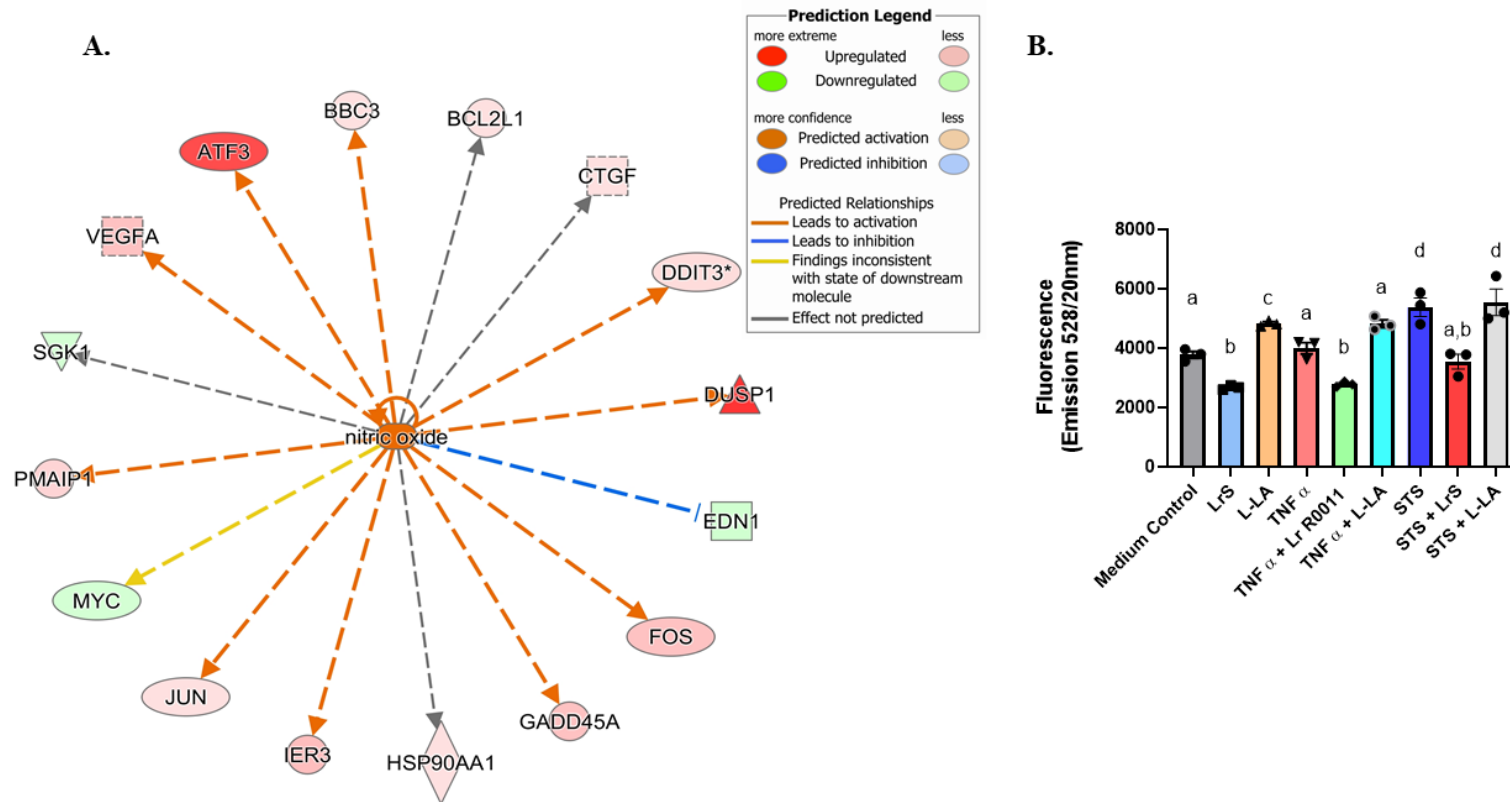


Figure 1-13A. IPA Upstream Regulator analytics identified reactive oxygen species as a potential regulator explaining the observed gene expression changes when HT-29 IECs are exposed to the LrS and either TNF- α or STS. **B.** Intracellular ROS production by HT-29 IECs in response to the different treatments (n = 3). Data shown is the mean fluorescence intensity of oxidized DCF-HA following 45 minutes of challenge.

CHAPTER 2: *Lactocaseibacillus rhamnosus* R0011 secretome induces temporal transcriptional, functional, and immunometabolic signatures in THP-1 monocytes consistent with M2 immunoregulatory macrophage activity

2.1 Introduction

Antigen-presenting cells (APC), such as macrophages and dendritic cells, participate in antigen processing and cytokine production, facilitating innate and adaptive immune interactions (Jakubzick *et al.*, 2017). Typically, macrophage activity varies with phenotype, with macrophages polarized to the M1, or classically activated phenotype, showing pro-inflammatory activities (increased phagocytic capacities and secretion of inflammatory mediators). In contrast, polarized M2 or alternatively activated macrophages are associated with immunoregulatory activity (tissue remodeling and secretion of immunoregulatory mediators), with current models reflecting a range of phenotypes within these categories (Cerovic *et al.*, 2014; Mowat *et al.*, 2011; Orecchioni *et al.*, 2020). These polarization states remain fluid and adaptive to macrophage microenvironments and in the small intestine, where the mucin layer covering intestinal epithelial cells (IEC) is porous, the sampling of antigens and contact with microbial components and products by the underlying APC cell populations helps to shape host immune outcomes. Consequences of these host-microbe interactions include certain epigenetic and immunometabolic modifications of APC associated with innate immune memory in the form of innate immune tolerance and trained innate immunity (Lachmandas *et al.*, 2016; Penkov *et al.*, 2019; Rodriguez *et al.*, 2019; Russell *et al.*, 2019). For example, initial contact of myeloid cells with β -glucan, a fungal structural

component, induces persistent epigenetic reprogramming, which primes the innate immune system to respond more robustly to subsequent challenge via increased trimethylation of H3K4 (Quintin *et al.*, 2012). Conversely, epigenetic silencing occurs in THP-1 human monocyte cells following prolonged exposure to lipopolysaccharide (LPS), resulting in a state of tolerance to subsequent LPS challenge (Rodriguez, R. M., et al., 2019).

Within gut-associated lymphoid tissues, a range of APC phenotypes act in order to maintain immune homeostasis yet remain responsive to pathogens, reacting to many microbial signals through pattern recognition receptor (PRR) activation. However, since the mucosal surface is covered with a mucin layer that can impede direct contact with gut microbes, secretion of biologically active mediators able to pass through the mucin layer and interact directly with IEC and APC may be an important route through which LAB, and potentially other gut microbes, influence the immune system at the mucosal interface.

Mechanistic evidence provides insight into the capacity of certain LAB for immune modulation and their impact on host immune outcomes (Jeffrey *et al.*, 2020; Macpherson *et al.*, 2014; MacPherson *et al.*, 2017; Suez *et al.*, 2019). As described in **Chapter I**, transcriptomic analysis revealed context-dependent regulation of TNF α and *Salmonella typhimurium* serovar Typhimurium secretome-induced pro-inflammatory mediator transcription and production by the *Lactocaseibacillus rhamnosus* R0011 secretome (LrS) in human IEC, indicating a potential for modulation of pro-inflammatory immune activity with minimal IEC impact in the absence of a pro-inflammatory challenge. These findings indicate that this modulation is mediated through induction of negative regulators of innate immunity and through changes in global histone acetylation patterns (Jeffrey *et al.*, 2020),

events important in maintaining immune regulation. However, the immunomodulatory activity of LAB is not limited to interactions with host IECs. Some studies have also focused on the effects of LAB on monocytes and macrophage activity (Wu *et al.*, 2016), many of which highlight key differences from the effects seen in IECs, with mounting evidence suggesting that LAB are highly immunostimulatory in APCs. For example, some LAB have been shown to induce the production of pro-inflammatory cytokines such as TNF- α , CXCL8, IL-12p70, and IL-1 β and enhance bactericidal activity of human macrophages (Rocha-Ramirez *et al.*, 2017). While certain bacteria can polarize already differentiated macrophages (Christoffersen *et al.*, 2014), the aforementioned studies focused primarily on direct contact of bacteria with host APCs. To date, few studies have outlined a clear mechanism for the role of LAB and their secretomes in the differentiation and subsequent polarization of monocytes into immunoregulatory APCs through transcriptional and immunometabolic reprogramming, a potential important route of host-microbe communication at the gut-mucosal interface.

2.2 Objectives

In the current study, we aimed to delineate the impacts of the LrS on macrophage activity by investigating the temporal transcriptional and functional reprogramming of macrophage activity and responses to subsequent LPS challenge of THP-1 human monocytes. THP-1 monocytes are a well-established model for studying monocyte and macrophage function *in vitro* and can readily be differentiated into macrophages with characteristics of either M1 or M2 phenotypes (Chanput *et al.*, 2014; Qin, 2012). LPS challenge of THP-1 monocytes results in a phenotype and transcriptional profile shared with LPS-challenged peripheral blood mononuclear cell-derived macrophages isolated from healthy donors (Chanput *et al.*, 2013; Sharif *et al.*, 2007), making THP-1s a useful cell model to study the impacts of LPS challenge and LrS conditioning on human monocyte activity. Using genome-wide transcriptional profiling, cytokine/chemokine production analysis, cell-surface protein expression and mitochondrial substrate utilization assays, the data presented here provides evidence supporting the potential for gut microbial secretome-mediated functional re-programming of macrophage activity into an immunoregulatory M2 phenotype.

2.3 Materials and Methods

Bacterial Culture

Lyophilized *Lactocaseibacillus rhamnosus* R0011 was obtained from the Rosell Institute for Microbiome and Probiotics (Montreal, QC). The LrS was prepared as previously described (Jeffrey *et al.*, 2020; Jeffrey *et al.*, 2018). Briefly, *Lactocaseibacillus rhamnosus* R0011 was grown in de Mann, Rogosa, and Sharpe broth (Oxoid, cat. # CM0359) overnight to stationary growth phase. Resulting cultures were further propagated in non-supplemented Roswell Park Memorial Institute (RPMI)-1640 (Sigma-Aldrich, cat. # R6504) to stationary phase, centrifuged at 3 000 x g and filtered through a 0.22 µm filter to remove the bacteria. The filtrate (LrS) was immediately frozen at -80°C. A medium control consisting of only MRS diluted in RPMI-1640 medium was included and subjected to the same culture conditions and filtration process. The pH of the LrS was measured and the pH of the medium control was adjusted to that of the bacterial culture using L-lactic acid and concentrated HCl. The Megazyme D-/L-lactic acid kit was used to determine the L-lactic acid concentration in the LrS secretome, and equal amounts of L-lactic acid were added to the medium control to account for this potentially bioactive metabolite.

THP-1 Human Monocyte Conditioning and LPS Challenge

The THP-1 human peripheral blood monocyte cell line (ATCC #TIB-202) was maintained in RPMI-1640 medium supplemented with 0.05 mM β-mercaptoethanol, 10% calf serum and 0.05 mg/mL gentamicin in a humidified incubator at 37°C and 5% CO². THP-1 monocytes were enumerated, and viability determined using Trypan Blue following sub-culturing. THP-1 monocytes were seeded into T25 tissue culture flasks or 96-well tissue culture plates at a concentration of 1 x 10⁶ cells/mL and used at a final concentration

of 5×10^5 cells/mL in non-supplemented RPMI-1640 medium. To determine the temporal effects of the LrS on monocyte differentiation, the LrS was added at a final concentration of 20% v/v to the THP-1 cells for 24-, 48-, and 72-hours of conditioning. A concentration of 20% v/v was selected based on preliminary analysis which revealed impacts on cytokine production profiles and morphological changes in THP-1 monocytes while not negatively impacting cell viability. In contrast to the work done in **Chapter I**, this preliminary work also suggested that the bioactive constituents within the LrS were > 10 kDa in size when using THP-1 human monocytes. L-lactic acid (LA) controls were also included to account for potential effects of this bioactive molecule, which is present in the LrS. For LPS challenges, THP-1 cells were cultured with lipopolysaccharide (LPS) (100 ng/mL) for 6 hours alone or following conditioning with the LrS for 72 hours. Total RNA was harvested using the phenol-based TRIzol method of RNA extraction following manufacturer's protocols (ThermoFisher Scientific, MA, USA). Briefly, 2 mL of TRIzol reagent was added to each culture flask to lyse the THP-1 cells. Cell culture homogenates were added to Phase Lock Gel-Heavy tubes for phase separation of total RNA. Total extracted RNA was then purified using the RNeasy Plus Mini Kit (Qiagen, Hilden, Germany). The purity and quality of RNA was determined using both the ND100 NanoDrop and an Agilent 2000 Bioanalyzer, respectively. Only samples with an RNA Integrity Number (RIN) greater than 9.0 were used for microarray analysis.

Reverse Transcription (RT) of RNA and Direct-Method of Labelling

Control and experimental total RNA (15 μ g) was reverse transcribed with Superscript IV (Invitrogen, MA, USA) and labelled with Cy3-dCTP and Cy5-dCTP (GE Healthcare, Amersham Biosciences) using the direct method of dye labelling as previously

described (Macpherson *et al.*, 2014; MacPherson *et al.*, 2017). Briefly, 3 µg/µL of oligo dT23 primers were added to the RNA and samples were heated to 70°C for 30 min in order to reduce secondary structure formation. A cDNA synthesis master mix containing 5X First Strand Buffer, 0.1M DTT, dNTPs, 200U of SuperScript IV, and either 1mM of Cy3 or Cy5 dye were added and the samples were heated at 42°C for 3 hours in order to allow the RT to occur. Dye swaps between treated and control RNA was done to eliminate bias of dye labelling. Purification of the cDNA product was done using the QIAQuick PCR purification kit following manufacturer's protocols (Qiagen). Labelling efficiency was determined by calculating the dye incorporation rate to ensure consistency between experiments.

Microarray Analysis

Hybridization of the labelled cDNA to the microarray was done using previously established protocols (Macpherson *et al.*, 2014; MacPherson *et al.*, 2017). Following hybridization, the microarrays were scanned using the ScanArray 5000 instrument from Perkin-Elmer (Waltham, MA, USA) and spot intensities were quantified using ImaGene® version 9.0 (BioDiscovery, CA, USA). Normalization was done using locally weighted scatterplot smoothing (LOWESS) (Berger *et al.*, 2004). Statistical analyses and two-dimensional hierarchical clustering analyses was performed with Multi-Experiment Viewer (MeV, version 4.2). Genes with statistically significant changes in expression levels were selected based on a t-test yielding a p-value < 0.05 and a 1.5-fold-change gene expression cut-off. gProfiler, Gene Set Enrichment Analysis (GSEA) and EnrichmentMap pathway enrichment analyses were used in order to ascertain the pathways in which genes were significantly modified by the different treatments (Reimand *et al.*, 2019; Shannon *et*

al., 2003). For some challenges, Metascape was used for circos plot generation and functional gene enrichment analyses (Y. Zhou *et al.*, 2019).

Global H3/H4 Histone Acetylation and DNA Methylation Determination

Global H3 and H4 histone acetylation patterns in THP-1 monocytes following conditioning with the LrS was determined as previously described (Jeffrey *et al.*, 2020) using the EpiQuik Global Histone H4 (P-4009) and H3 (P-4008) Acetylation Kits following manufacturer's protocols (EpiGentek). Global DNA methylation patterns were determined using the MethylFlash Methylated DNA Quantification kit (P-1034) following manufacturer's protocols (EpiGentek). Briefly, total DNA was extracted from THP-1 monocytes conditioned with the LrS or culture medium controls over 24-, 48-, or 72-hours, using the PureLink Genomic DNA Mini Kit (Invitrogen). A total of 100ng of DNA was spotted onto strip wells and assayed for methylated DNA. A positive control consisting of a known amount of methylated DNA was included, and the percentage of methylated DNA was calculated by comparing treated and untreated controls. Statistical analysis was done using GraphPad Prism (Version 8) one-way ANOVA and Tukey multiple comparison test when the ANOVA indicated significant differences were present. All data are shown as the mean percentage of change in histone acetylation or methylated DNA \pm SEM.

Chemokine and Cytokine Profiling

Cytokine and chemokine profiling was performed using the Bio-Plex Pro™ 40-Plex Human Chemokine Panel (Bio-Rad #171ak99mr2) and the Bio-Plex Pro™ Human Inflammation Panel 1, 37-Plex (Bio-Rad #171AL001M) were multiplexed on the same 96-

well plate. Cytokine standards were serially diluted and chemokine profiling from all cell challenges was done following manufacturer's instructions (Bio-Rad) with 4 biological replicates. Quality controls were also included to ensure the validity of the results obtained. The Bio-Plex Manager™ software was used to determine the concentration of the analytes within each sample using the generated standard curves and was expressed in pg/mL. Statistical analysis was done using GraphPad Prism's (Version 8) one-way analysis of variance (ANOVA) and further analysis was done using Tukey's multiple comparison test when the ANOVA indicated significant differences were present. All data are shown as the mean pg/mL \pm standard error of the mean (SEM). Z-scores were determined and visualized using R version 4.0.0 and package Bioconductor to determine the overall impact of each challenge on cytokine and chemokine production from THP-1 monocytes.

Morphological Characterization

Morphological changes in THP-1 human monocytes conditioned with the LrS, STS, or secretome derived from *Streptococcus thermophilus* R0083 was determined by staining actin filaments with phalloidin-CF568 (Biotum Inc. Cat. # 00044-T) following manufacturing protocols. Briefly, following conditioning, cells were fixed with 3.75% formaldehyde, permeabilized with 0.5% Triton X-100, and stained with phalloidin-CF568 (1 U/mL) for 20 minutes at room temperature. Cells were counter-stained and mounted using ProLong™ Diamond Antifade Mountant with DAPI (ThermoFisher Cat #: P36966). *S. thermophilus* R0083 was included to determine potential impacts of soluble components derived from other LAB.

Mitochondrial Function Assay

Mitochondrial function through mitochondrial substrate utilization was determined using the Mitoplate S-1 system following manufacturer's protocols (Biolog, Cat. # 14105). THP-1 human monocytes were seeded into a 96-well plate which was pre-coated with dried metabolic substrate probes at a final cell density of 40,000 cells per well. Saponin (100µg/mL) was used as a permeability agent to facilitate cellular uptake and mitochondrial utilization of the different substrates. Cells were treated with 20% LrS for 24 hours and the amount of dye reduction was quantified by measuring the absorbance of the colour change at OD₅₉₀. Fold changes in the utilization of the different metabolic substrates was determined by comparing the absorbance readings of LrS treated cells to an untreated control.

Analysis of Protein Lysine Acetylation

Protein lysine acetylation in THP-1 human monocytes conditioned with the LrS for 24-, 48-, and 72-hours was done using 2D-Western Blot and peptide mass fingerprinting analyses. Cell pellets were harvested following the different conditioning time points, supernatant decanted, and immediately frozen at -80°C prior to shipping to Applied Biomics (California, USA) for processing. Anti-acetyl lysine antibodies (Acetylated Lysine Monoclonal Antibody (1C6) Catalog # MA1-2021 from ThermoFisher) were used to detect proteins with acetylated lysine residues and a fold change > 5.0 between the LrS conditioned and corresponding medium controls was chosen as a cut-off for subsequent protein identification using peptide-mass fingerprinting.

Flow Cytometry

Differential cell-surface marker expression of THP-1s conditioned with the LrS or medium controls was determined using a BD Accuri C6 flow cytometer. THP-1 monocytes were conditioned with the LrS or medium controls for 24-, 48-, or 72-hours as described above. Following conditioning, 1×10^6 cells were resuspended in D-phosphate buffered saline (D-PBS) and cells were stained with the viability dye 7-Aminoactinomycin D (7-AAD) (Tonbo, 13-6993) for 10 minutes on ice while protected from light. Cells were washed with 1 mL of cell staining buffer (CSB) (4% calf serum, 5 mM EDTA in D-PBS) and centrifuged for 5 minutes at $400 \times g$ (4°C). Immediately following viability staining, non-specific Fc-mediated interactions were blocked by the addition of $100\mu\text{L}$ of blocking buffer (10% calf serum (heat inactivated) in D-PBS) to the cell suspension for 10 minutes. An antibody master mix containing anti-human FITC CD11c (Tonbo 35-0116, clone 3.9) (0.2ug/test), anti-human APC CD11b (Tonbo 20-0118, clone ICRF44) (0.2 ug/test), and anti-human PE CD86 (Tonbo 50-0869, clone B7-2 IT2.2) (0.2 ug/test) or anti-human APC CD64 (BioLegend, clone 10.1) and anti-human PE CX3CR1 (BioLegend, clone 2A9-1) was added to the cell suspension followed by incubation on ice and protected from light for 30 minutes. Cells were washed with CSB as described above, resuspended in $100 \mu\text{L}$ of fixation buffer (4% paraformaldehyde-PBS) and incubated for 30 minutes at room temperature protected from light. Data acquisition was done using the BD Accuri Plus flow cytometer and corresponding software package. 30,000 viable cells (as determined by incorporation of 7-AAD viability dye (Tonbo 13-6993)) were acquired for each experiment and subsequent analysis was done using FlowJo v. 10.

2.4 Results

LrS conditioning induces differential and temporal gene expression profiles in THP-1 human monocytes

Genome-wide transcriptional profiling of THP-1 human monocytes cultured with the LrS or LA matched controls was performed to evaluate global changes in the THP-1 transcriptome in response to LrS conditioning. Two-dimensional hierarchical heat-map cluster analysis revealed that conditioning THP-1s with the LrS resulted in unique temporal gene expression profiles, distinct from LA matched controls. In fact, LA had no significant impact on THP-1 expression profiles (**Figure 2-1A; 2-1B**) indicating that although this bioactive molecule is a key metabolite in the LrS, it is not responsible for the LrS-mediated impact on transcriptional activity. 48hrs of LrS conditioning had the largest impact on the THP-1 transcriptome, with a total of 4126 differentially expressed genes (2086 up-regulated and 2040 down-regulated) ($n = 4, p < 0.05$). Of the three different time points tested, 72hrs of conditioning with the LrS had the lowest impact on the THP-1 transcriptome, with only 813 differentially expressed genes (542 up-regulated and 271 down-regulated) ($n = 4, p < 0.05$), indicating a distinct temporal effect of LrS conditioning. (**Figure 2-1B**).

To interrogate the cellular pathways impacted in THP-1 monocytes following LrS conditioning, gene enrichment analysis was performed using GSEA and gProfiler. GSEA analysis revealed that the LrS induced differential expression of genes involved in key macrophage signaling pathways such as the activation of the immune response (Normalized Enrichment Score (NES) = 2.59, $p < 0.001$), cellular responses to external stimulus (NES = 3.30, $p < 0.001$), cell adhesion molecule expression (NES = 2.52, $p <$

0.001), and the up-regulation of genes associated with interleukin-10 signaling, myeloid leukocyte differentiation, and a tolerant macrophage phenotype (NES = 2.56, $p < 0.001$) when compared to cells treated with LA controls (**Figure 2-1C**).

The LrS polarizes THP-1 monocytes into immunoregulatory M2 macrophages

Although there were unique differential gene expression profiles induced by the LrS over the different time points (**Figure 2-2A**), gProfiler analysis identified a high degree of functional similarity of differential gene expression profiles and pathway activation between the different LrS conditioning time points, with most of the differential pathway activation occurring following 48hrs of conditioning (**Figure 2-2B**). EnrichmentMap visualization of activated functionally related pathways identified by gProfiler revealed overlap between the different LrS conditioning time-points with many of the activated cellular pathways belonging to cell cycle, transcription, metabolism, and the cellular response to molecules of bacterial origin (**Figure 2-2C**), confirming the results obtained by the GSEA analysis. Moreover, genes belonging to functional groups relating to cytoskeletal reorganization and metabolic and biosynthetic processes were largely influenced by 48-hours of LrS conditioning, indicating a significant impact on key macrophage cellular pathways (**Figure 2-2C**). Levels of global H3 and H4 acetylation confirmed these findings, with the LrS significantly increasing %H3 and %H4 histone acetylation following 48hrs of conditioning ($n = 3$; $p < 0.05$) (**Figure 2-3**). However, the LrS did not have an impact on levels of methylated DNA between the three different time points ($n = 3$; $p > 0.05$) (**Figure 2-3**).

Since GSEA analysis indicated that THP-1 monocytes conditioned with the LrS

share gene expression signatures consistent with a tolerant macrophage phenotype and gProfiler analysis identified activated cellular pathways belonging to cell differentiation and metabolism (**Figure 2-1C**), gene expression profiles were probed for increased transcription of genes associated with immunoregulatory macrophage activity (**Figure 2-4**). The LrS induced increased transcription of *ADAMDEC1*, *ZFP36L1*, and *RND3*, genes and transcription factors involved in differentiation of monocytes into mature macrophages ($n = 4$; $p < 0.05$) (**Figure 2-4**). Temporal changes in gene expression of a wide range of genes associated with an immunoregulatory macrophage transcriptional signature (*IL-10R*, *TDO2*, *CD36*, *CD163*, *TLR1*, *TLR8*, *DUSP1*, and *ATF3*) were also observed following LrS conditioning, suggesting that the LrS polarizes THP-1 monocytes into an immunoregulatory phenotype, an effect independent of lactic acid ($n = 4$; $p < 0.05$) (**Figure 2-4**). *IL1R2* (Interleukin 1 Receptor Type 2) was also highly up-regulated in THP-1s following 24 and 48 hours of LrS conditioning (13.18 and 78.47 fold change respectively) ($n = 4$; $p < 0.05$) (**Figure 2-4**).

Cytokine and chemokine profiling confirmed these findings, with increased temporal production of immunoregulatory macrophage-associated mediators IL-1Ra, IL-10, CCL1, CCL17, CCL20, CXCL1 and 2, IL-6, IL-4 and MMP-2 following conditioning with the LrS, an effect independent of LA and challenge with STS (**Figures 2-5, 2-6, 2-7**). There was also an increase in the production of some classical pro-inflammatory cytokines and chemokines following 48hrs of LrS conditioning, but not after 72 hours, and not to the level observed with STS challenge, highlighting key differences between conditioning with the LrS and the STS (**Figure 2-7**). This is similar to the results seen with transcriptional profiling and suggests that prolonged exposure to the LrS induces a tolerant

immunoregulatory phenotype in THP-1 human monocytes.

Phenotypic characterization of LrS conditioned M2 macrophages

Phenotypic and morphological characterization of THP-1 human monocytes conditioned with the LrS was done to confirm the insights gained from the transcriptional and cytokine and chemokine profiling. Indeed, the LrS induced morphological changes in THP-1s over the three different time points examined, with the majority of cells appearing as differentiated macrophages following 72 hrs of conditioning, an effect not seen in THP-1 monocytes conditioned with the STS or *S. thermophilus* R0083 (**Figure 2-8**). These morphological changes were in keeping with the transcriptional profiling, which indicated increased transcription of genes involved in myeloid leukocyte differentiation, cytoskeletal organization and adhesion (**Figure 2-1C and 2-2B**). Flow cytometric analysis indicated a substantial shift in the number of cells expressing CD11b and CD11c, indicative of monocyte differentiation into an antigen presenting cell (APC) phenotype (**Figure 2-9A**). Probing these patterns further, histogram analysis revealed a 72% and 73% increase in the number of cells expressing CD11b following 48- and 72-hours of LrS-conditioning (**Figure 4B**). This correlated to a significant increase in CD11b median fluorescent intensity (MFI) when cells were conditioned with the LrS for 48- or 72-hours, compared to medium controls (**Figure 2-9B**). Numbers of CD11c⁺ cells were much lower than CD11b⁺ cells, even after 72-hours of LrS conditioning (**Figure 2-9**). Cell surface expression of CD86, a co-stimulatory cell-surface molecule involved in T cell activation and survival, and of the fractalkine receptor CX₃CR1 was also increased in cells conditioned with the LrS in a time-dependent fashion (**Figure 2-9**). Conversely, CD64 expression was significantly reduced in cells conditioned with the LrS following 72-hours of conditioning (**Figure 2-9**).

gProfiling analysis identified multiple different metabolic pathways influenced by LrS conditioning, and increased transcription of genes associated with immunoregulatory macrophage fatty acid and tryptophan metabolism was observed (**Figure 2-2** and **2-4**). As such, the impacts of the LrS on THP-1 metabolic signatures was investigated to ascertain whether the changes at the transcriptional, protein, and cell-surface molecule expression level also correlated to a metabolic signature consistent with immunoregulatory macrophage activity. Indeed, the LrS increased the transcription of many genes involved in fatty acid oxidation such as *ABCD1* (2.1 fold-change), *ABCD4* (2.5 fold-change), *TWIST1* (3.7 fold-change), *CD36* (8.34 fold-change), and *FABP4* (35 fold-change), and tryptophan metabolism such as *KMO* (11.9 fold-change) and *TDO2* (47.6 fold-change), with no changes in the transcription of genes involved in glycolysis following 48-hours of conditioning ($n = 4, p < 0.05$) (**Figure 2-10A**). Consistent with these results, metabolic utilization assays indicated that LrS conditioning did not increase the utilization rate of glycolytic intermediaries, suggesting that the levels of glycolytic flux were not impacted (**Figure 2-10B**). However, LrS-conditioned macrophages had increased utilization of metabolites involved in the citric acid cycle, indicating an intact citric acid cycle (**Figure 2-10B**).

The LrS influences protein lysine acetylation patterns in THP-1 monocytes

To further interrogate the mechanism(s) of action behind the observed phenotypic changes induced by conditioning with the LrS, post-translational changes via acetylation of protein lysine residues was examined. 2-D Western Blot analysis determined that conditioning with the LrS resulted in post-translation modifications in 69 different proteins over the three different timepoints examined when compared to controls (**Table 2-I**;

Figure 2-11). Subsequent peptide mass fingerprinting revealed that conditioning with the LrS increases the acetylation of histones H3 and H4, confirming previously obtained results (**Table 2-II**). Moreover, the acetylation state of several proteins involved in mitochondrial and metabolic function in THP-1s were influenced by conditioning with the LrS. These included phosphoglycerate mutase 1, ATP synthase subunit O, mitochondrial superoxide dismutase, isocitrate dehydrogenase (NADP), and glyceraldehyde-3-phosphate (**Table 2-II**).

LrS conditioned THP-1 macrophages respond robustly to LPS challenge

LPS challenge of THP-1 monocytes was used to further examine overall immune effector function and cellular responses of macrophages to this key TLR4 ligand following conditioning with the LrS for 72 hours. Two-dimensional hierarchical heat-map cluster analysis revealed that LrS conditioning of THP-1s prior to LPS challenge resulted in unique global gene expression profiles, distinct from LPS challenge or LrS conditioning alone (**Figure 2-12A**). In fact, LrS-conditioned macrophages shared a very limited subset of differentially expressed genes and enriched pathway activation with LPS challenge alone (**Figure 2-12B and 12-C**). Moreover, the number of differentially expressed genes within key immune-related signaling pathways in macrophages was significantly lower in THP-1 monocytes conditioned with the LrS compared to LPS challenge alone (**Figure 2-12D**), indicating that the unique transcriptional signature in response to LrS conditioning in THP-1 macrophages is distinct from the signature induced by LPS challenge. LPS challenge of LrS-conditioned macrophages resulted in increased expression of genes in the Toll-like receptor signaling, NF- κ B signaling, regulation of the innate immune response, and cytokine-mediated pathways when compared to LPS or LrS conditioning alone (**Figure 2-**

12D). Cytokine and chemokine profiling confirmed these results, as LrS conditioning enhanced production of LPS-induced cytokine and chemokine production (**Figure 2-12E and 2-13**) coupled with increased production of immunoregulatory IL-10 and IL-1Ra, suggesting that conditioning of THP-1 monocytes with the LrS influences subsequent immune outcomes to LPS challenge.

2.5 Discussion

Regulation of macrophage activity at the gut-mucosal interface is integral for maintaining immune homeostasis and shaping host immune outcomes to subsequent pro-inflammatory challenge. Microbiota-induced innate immune memory has been described as a potential mechanism through which the resident microbiota induces immune tolerance, with some studies suggesting that these signals delivered through PRRs can also induce innate immune training to subsequent inflammatory signals (Clarke *et al.*, 2010; Honko *et al.*, 2006; Mitroulis *et al.*, 2018). Recent evidence suggests that these varied modes of communication may be an important route through which LAB and other members of the gut microbiota exert physiological and immunological changes at distal and systemic sites within the host (Kang *et al.*, 2020; Negi *et al.*, 2019; Zheng *et al.*, 2020). While the ability of LAB to influence macrophage activity has been reported (Madej *et al.*, 2017; Mata Forsberg *et al.*, 2019), little is known about the roles of secretome components derived from LAB in the transcriptional and functional reprogramming of macrophages, a potentially important route of communication between the host and the resident microbiota.

In the present study, we determined that the LrS induced a unique transcriptional profile in THP-1 monocytes depending on exposure time, with a high degree of differential gene transcription occurring after 48-hours and a substantial reduction in gene expression following 72-hours of LrS conditioning. This is, to our knowledge, the first report of temporal macrophage transcriptional reprogramming by prolonged exposure to a LAB-derived secretome. Transcriptional regulation of macrophage polarization is well documented, with many gene expression profiles recognized as associated with monocyte differentiation and immunoregulatory macrophage activation (Lawrence *et al.*, 2011;

Martinez *et al.*, 2006; Orecchioni *et al.*, 2020; Xue *et al.*, 2014). The LrS induced increased transcription of *ADAMDEC1*, *ZFP36L1*, and *RND3*, genes and transcription factors involved in monocyte differentiation into mature macrophages (Chen *et al.*, 2015; Jie *et al.*, 2015; Lund *et al.*, 2013) and gene enrichment analysis identified differential activation of cellular pathways involved in cytoskeletal rearrangement and myeloid leukocyte differentiation. Our previous analysis has indicated that the LrS may influence histone acetylation patterns in challenged intestinal epithelial cells by decreasing global histone acetylation and thereby attenuating pro-inflammatory gene transcription. Here we show that the LrS may increase H3 and H4 histone acetylation in a temporal fashion in THP-1 human monocytes. This may help to explain the observed increase in overall differential gene expression and subsequent changes in protein expression patterns and cell morphology. We also examined whether the LrS could influence DNA methylation patterns in these same cells. Unlike histone acetylation patterns, the LrS did not have an impact on global DNA methylation.

Morphological and flow cytometric analysis confirmed these findings, as LrS conditioning of THP-1 monocytes resulted in temporal morphological changes and an increase in the cell surface expression of CD11b and CD11c, indicative of monocyte to macrophage differentiation, and also increased expression of the fractalkine receptor CX₃CR1. CX₃CR1-expressing macrophages in the GALT have been shown to play an integral role in maintaining gut homeostasis by producing IL-10 and are involved in facilitating cross-talk between the resident gut microbiota and the underlying immune cell population (De Schepper *et al.*, 2018; Gross *et al.*, 2015; Hadis *et al.*, 2011; M. Kim *et al.*, 2018; Medina-Contreras *et al.*, 2011; Regoli *et al.*, 2017; Varol *et al.*, 2015). Conversely,

LrS-conditioned THP-1s had reduced cell-surface expression of CD64. Human peripheral blood mononuclear cell-derived macrophages treated with LPS or IFN- γ express high levels of membrane-bound CD64 and display a phenotype consistent with M1-macrophage activity (Ambarus *et al.*, 2012; Tarique *et al.*, 2015). Moreover, administration of an immunotoxin that targets CD64 led to the selective elimination of M1 macrophages in an inflammatory disease setting, illustrating the negative outcomes of dysregulated activity of M1 phenotype macrophages and highlighting the importance of CD64 in M1-associated macrophage activity (Akinrinmade *et al.*, 2017; Hristodorov *et al.*, 2015).

Changes in the gene expression of multiple immunoregulatory macrophage-associated genes was also observed following conditioning with the LrS, suggesting polarization of THP-1 monocytes into immunoregulatory macrophages. For example, the LrS induced the expression of *ATF3* and *DUSP1*, key regulators of innate immune activity, which is consistent with our previous results examining the LrS impact on TNF α and STS-challenged HT-29 IEC (Jeffrey *et al.*, 2020). Overexpression of ATF3 has been shown to inhibit inflammatory macrophage gene transcription and activate expression of immunoregulatory macrophage genes through the Wnt/ β -catenin signaling pathway (Sha *et al.*, 2017). Further, DUSP1 polarizes macrophages towards an M2 phenotype via inhibition of the AP-1 transcription factor complex, inhibiting inflammatory gene transcription (Lawrence *et al.*, 2011).

Cytokine and chemokine profiling confirmed these findings, as we observed increased production of immunoregulatory macrophage-associated cytokines such as IL-10 and IL-1Ra following conditioning with the LrS. IL-10 production is associated with immunoregulatory M2 macrophage activity and polarization as it serves multiple roles in

the regulation of inflammatory immune responses (Couper *et al.*, 2008). It binds to the IL-10 receptor (IL-10R), resulting in the phosphorylation of STAT3 and subsequent transcription of genes involved in immunoregulation and repression of pro-inflammatory cytokine production (Saraiva *et al.*, 2010). Indeed, IL-10 signaling was identified by GSEA analysis as being impacted by the LrS and *IL-10R* expression was increased following LrS conditioning. These cellular insights into LrS-mediated macrophage polarization into an immunoregulatory phenotype implicate enhanced IL-10 signaling in THP-1 monocytes. IL-1Ra antagonizes the activity of IL-1 α and IL-1 β by binding to the IL-1R1 receptor and is thought to play an integral role in the resolution of the inflammatory response as it is typically produced following IL-1 secretion. We also observed increased transcription of *IL1R2* (Interleukin 1 Receptor Type 2), a decoy receptor for IL-1 β / α and a known marker of immunoregulatory M2 macrophages (Viola *et al.*, 2019), following 24 and 48 hours of conditioning, suggesting that the LrS significantly alters IL-1 signaling outcomes. Additionally, LrS-conditioned THP-1 monocytes produced IL-4, an immunoregulatory and pleiotropic cytokine which inhibits the production and secretion of pro-inflammatory cytokines and can promote and shape adaptive immune responses (Hart *et al.*, 1989). As was seen with IL-10/*IL-10R* production and expression, the LrS also induced the expression of the IL-4 receptor, *IL4Ra*, as well as *IL4I1* (IL-4-induced gene 1), an L-amino acid oxidase and M2 immunoregulatory macrophage associated marker with inhibitory roles in T cell activation (Yue *et al.*, 2015). IL-4 signaling in macrophages promotes IL-1Ra production and *IL1R2* expression (Fenton *et al.*, 1992). We also observed increased production of Type I interferons from LrS-conditioned monocytes, suggesting enhanced anti-viral capacity. Evidence for microbiota-induced Type I interferon production in APCs

suggests that this is an important route for instructive transcriptional and metabolic programming, enabling robust responses to subsequent pathogen challenge by promptly activating the adaptive immune response (Schaupp *et al.*, 2020).

Macrophage immunometabolism plays an integral role in macrophage effector function. M1 macrophages are characterized by their increased reliance on aerobic glycolysis for energy, resulting in a substantially higher glycolytic flux and a shunted citric acid cycle in order to maintain sustained cytokine and inflammatory mediator production. In contrast, M2 macrophages rely on oxidative phosphorylation mediated through an intact citric acid cycle, highlighting key metabolic differences which can be used to distinguish macrophage phenotype and effector functions (Diskin *et al.*, 2018; Geeraerts *et al.*, 2017). For this reason, we examined the ability of the LrS to influence metabolic flux in THP-1 monocytes. We observed increased utilization of all citric acid cycle intermediates, without altered glycolytic metabolism, indicative of an immunoregulatory macrophage metabolic signature. Moreover, the LrS increased transcription of *CD36*, a cell-surface receptor involved in fatty acid uptake, and *FABP4* (Fatty Acid Binding Protein-4), a cytoplasmic protein involved in lipid transport and metabolism (Szanto *et al.*, 2010). Lipid metabolism was identified by gProfiler as one of the metabolic pathways within THP-1 monocytes that was influenced by the LrS and is a hallmark of immunoregulatory macrophage activity. *TDO2* (Tryptophan 2,3-Dioxygenase), a key enzyme involved in tryptophan metabolism and activation of the kynurenine pathway which plays an integral role in M2 macrophage activity (Campesato *et al.*, 2020), was also up-regulated in LrS-conditioned THP-1 monocytes, further suggesting that the LrS influences multiple macrophage metabolic pathways, and is, to our knowledge, the first report of immunometabolic reprogramming

of THP-1 human monocytes by LAB-secretome components.

To determine potential underlying mechanism(s) of action behind the observed changes in metabolic activity and functional outcomes in LrS-conditioned THP-1 monocytes, post-translational modifications of intracellular proteins was examined. This analysis revealed the deacetylation of phosphoglycerate mutase 1 (PGAM1) in THP-1s conditioned with the LrS. PGAM1 catalyzes a rate-limiting step of glycolysis in leukocytes by converting 3-phosphoglycerate (3-PG) to 2-phosphoglycerate (2-PG). When deacetylated, PGAM1 exhibits diminished activity (Hallows *et al.*, 2012), suggesting a possible mechanism of action through which the LrS alters metabolism in THP-1s by reducing glycolytic activity within the cell. Moreover, LrS conditioning led to deacetylation of GAPDH, another key enzyme involved in glycolysis. Deacetylation of cytosolic GAPDH results in decreased glycolytic activity in response to glucose (Li *et al.*, 2014), providing additional mechanistic evidence for reduced glycolytic flux in THP-1 monocytes conditioned with the LrS. In contrast, mitochondrial isocitrate dehydrogenase 2 (IDH2), a key enzyme involved in the oxidative decarboxylation of isocitrate to α -ketoglutarate, was acetylated following conditioning with the LrS. Unlike isocitrate dehydrogenase 3 (IDH3), the reaction catalyzed by IDH2 is reversible and uses NADP⁺ and NADPH instead of NAD⁺ and NADH as a redox couple. This leads to the accumulation of NADPH in the mitochondria, which can be used for scavenging mitochondrial ROS (mtROS) (Yu *et al.*, 2012). Moreover, IDH2 has also been implicated in the export of citrate from the mitochondria for lipid biosynthesis, a hallmark of M1 macrophage activity, following reductive carboxylation (Yoo *et al.*, 2008). When IDH2 becomes acetylated, it has reduced activity (Smolkova *et al.*, 2020), which may lead to

increased flux of isocitrate through IDH3 and a potential reduction in mtROS scavenging due to impaired NADPH generation. However, mitochondrial manganese superoxide dismutase (SOD2), an enzyme which typically displays dismutase activity by converting superoxide to O₂ or H₂O₂, was acetylated following conditioning with the LrS. Acetylated SOD2 displays peroxidase activity yet has increased capacity for the rapid generation of mitochondrial H₂O₂ through a mechanism which is still not fully understood (He *et al.*, 2019; Hjelmeland *et al.*, 2019). Increased levels of mitochondrial H₂O₂ within macrophages has been shown to drive M2 polarization (Griess *et al.*, 2020), potentially through the recruitment and stabilization of hypoxia-inducible factor-2 α (HIF-2 α) which can act to suppress nitric oxide synthesis (Takeda *et al.*, 2010). Although other proteins were identified with differential lysine acetylation patterns following conditioning with the LrS, more research is needed to ascertain the diverse functional outcomes of these post-translational modifications, especially in the context of host-microbe interactions. Indeed, post-translational modification of proteins involved in metabolism has emerged as a potential route through which metabolic activity is regulated (Baeza *et al.*, 2016), and the results presented here may represent a novel means of host-microbe communication through which soluble components derived from LAB can regulate the activity of many important cellular processes.

The ability of macrophages to respond robustly to pathogen-associated molecular patterns is integral to host defense and survival. LPS challenge of LrS-conditioned THP-1 monocytes revealed heightened responsiveness, suggesting a degree of innate immune priming, while maintaining an overall M2 phenotype. Evidence for alterations of macrophage responses to pro-inflammatory challenge indicate strain-specific impacts on

immune outcomes as some strains within the same species have antagonistic impacts on PRR-induced cytokine release (Drago et al., 2010). For example, *Lactobacillus paracasei* attenuates LPS-induced cytokine production by PMA-differentiated THP-1 cells (Sun et al., 2017) while exopolysaccharide isolated from *L. paracasei* DG stimulates cytokine production from THP-1 monocytes (Balzaretto et al., 2017). PRR-mediated recognition of microbiota-derived peptidoglycan by neutrophils has been shown to enhance and prime systemic immunity towards *Streptococcus pneumoniae* and *Staphylococcus aureus* infection (Clarke et al., 2010), suggesting that this priming of the innate immune system by LAB and other members of the microbiota can influence systemic immune responses and promote effective host defence against pathogens.

Taken together, the results presented here describe transcriptional and functional re-programming of THP-1 human monocytes mediated by secretome components of *L. rhamnosus* R0011. These secretome-conditioned macrophages showed functional, transcriptional, and immunometabolic signatures consistent with M2 immunoregulatory activity, with increased production of immunoregulatory cytokines IL-10, IL-1Ra, and IL-4 and a cell-surface expression profile of CD11b, CD11c^{lo}, and CX₃CR₁, features shared with subsets of gut macrophages (Bujko et al., 2018; Cipriani et al., 2016). Moreover, LrS-conditioning of THP-1 monocytes did not impair responses to subsequent LPS challenge, despite their overall homeostatic M2 phenotype. Gut-associated macrophages play a dynamic and multifaceted role in host-microbe interactions and are required to respond appropriately to diverse gut microbe-derived cues to shape subsequent immune effector signals. The results reported here provide insight into novel routes for indirect secretome-mediated microbe-host communication and the impact on activation of multiple

immune mechanisms integral for macrophage function and activity. Future work to examine the role of secretome-mediated communication in the impact of LAB and other gut microbes on the functionality at the gut mucosal interface and distal systemic immunological outcomes *in vivo* may aid in elucidating gut microbe-mediated effects on systemic immunity and in the selection of potential biomarkers for the design of future clinical studies.

Table 2-I. Fold change differences in the amount of acetylation of proteins found in THP-1 human monocytes conditioned with the LrS versus medium controls for 24-, 48-, and 72-hours.

Spot ID	24hr Acetyl Ratio (Secretome/Control)	48hr Acetyl Ratio (Secretome/Control)	72hr Acetyl Ratio (Secretome/Control)
1	1.3	-1.3	0.0
2	-4.3	2.5	0.0
3	1.0	-1.2	1.6
4	-1.3	-1.6	0.0
5	-1.5	-1.9	-2.0
6	-3.6	-2.9	-4.5
7	-2.9	1.2	-2.0
8	-1.2	-1.7	1.3
9	-1.5	1.0	1.1
10	-1.6	-2.2	0.0
11	-8.3	-7.9	-1.8
12	-1.6	-3.3	-3.0
13	-10.4	0.0	0.0
14	-1.5	-2.0	-3.3
15	1.0	-2.2	0.0
16	-3.6	-1.6	-2.2
17	-1.5	-3.4	-3.0
18	1.4	1.4	0.0
19	1.6	-2.3	-3.8
20	1.5	-2.5	-1.8
21	-2.8	-4.2	1.5
22	-3.7	-1.0	0.0
23	2.4	-2.1	0.0
24	1.5	-2.0	-5.8
25	-1.3	-1.4	-3.1
26	-1.7	-1.2	-1.9
27	2.2	-1.8	-3.8
28	2.2	-1.6	-2.5
29	-3.4	1.4	-4.2
30	2.4	1.6	-1.2
41	3.0	-1.1	-1.0
42	3.7	17.8	0.0
43	2.2	1.7	1.3
44	4.7	2.3	4.5
45	5.5	0.0	4.0
46	2.7	0.0	0.0
47	1.6	0.0	1.2
48	6.3	1.8	1.1
49	2.4	2.3	1.0
50	2.6	3.5	1.3
51	19.8	4.5	5.3
52	1.3	2.6	2.9

This table is continued on the following page

Table 2-I. *continued*

Spot ID	24hr Acetyl Ratio (Secretome/Control)	48hr Acetyl Ratio (Secretome/Control)	72hr Acetyl Ratio (Secretome/Control)
54	2.8	3.2	1.2
55	15.2	1.5	6.1
56	26.2	2.1	10.0
57	2.0	4.9	6.7
58	7.2	0.0	0.0
59	2.2	0.0	3.6
60	2.9	1.5	1.3
61	2.0	0.0	1.7
62	3.1	1.5	4.6
63	2.6	3.2	-1.1
64	30.7	5.2	19.5
65	37.0	308.5	113.3
66	53.4	39.1	50.1
67	37.1	20.0	3.3
68	7.0	1.7	3.7
69	3.5	1.1	3.1
70	11.0	6.0	4.0
71	5.6	35.1	43.4
72	10.6	12.3	7.2
73	2.0	2.4	3.1
74	0.0	3.0	0.0
75	0.0	0.0	7.2
76	0.0	0.0	1.6
77	0.0	0.0	3.8
78	0.0	0.0	1.6
79	0.0	0.0	2.7

Table 2-II. Protein identification of spot IDs showing a fold change ≥ 3 in acetylation of lysine residues in proteins found in THP-1 human monocytes conditioned with the LrS when compared to controls.

Spot #	Protein ID	Acetyl Ratio	Acetyl Ratio	Acetyl Ratio
		24hr	48hr	72hr
		Fold Change Secretome/Control	Fold Change Secretome/Control	Fold Change Secretome/Control
11	Phosphoglycerate mutase 1	-8.3	-7.9	-1.8
13	Cellular nucleic acid-binding protein	-10.4	0.0	0.0
21	40S ribosomal protein	-2.8	-4.2	1.5
24	T-complex protein 1 subunit epsilon	1.5	-2.0	-5.8
29	Glyceraldehyde-3-phosphate dehydrogenase	-3.4	1.4	-4.2
42	Vimentin/Tubulin alpha-1C chain	3.7	17.8	0.0
44	Catalase	4.7	2.3	4.5
45	Heterogeneous nuclear ribonucleoprotein H	5.5	0.0	4.0
48	Isocitrate dehydrogenase [NADP], mitochondria	6.3	1.8	1.1
51	Heterogeneous nuclear ribonucleoproteins A2/B1	19.8	4.5	5.3
53	Heterogeneous nuclear ribonucleoproteins A2/B1	5.8	1.6	9.0
55	Prohibitin-2	15.2	1.5	6.1
56	Heterogeneous nuclear ribonucleoprotein A1	26.2	2.1	10.0
57	40S ribosomal protein S4, X isoform	2.0	4.9	6.7

This is a continuation of Table 2-II

Spot #	Protein ID	Acetyl Ratio	Acetyl Ratio	Acetyl Ratio
		24hr	48hr	72hr
		Fold Change Secretome/Control	Fold Change Secretome/Control	Fold Change Secretome/Control
58	Chloride intracellular channel protein 1	7.2	0.0	0.0
59	Proteasome subunit beta type-4/Actin Fragment	2.2	0.0	3.6
64	ATP synthase subunit O, mitochondrial	30.7	5.2	19.5
65	Superoxide dismutase [Mn], mitochondrial (SOD2)	37.0	308.5	113.3
66	Superoxide dismutase [Mn], mitochondrial (SOD2)	53.4	39.1	50.1
67	60S ribosomal protein L12	37.1	20.0	3.3
68	Histone H2B type 1-M	7.0	1.7	3.7
70	Histone H3.3	11.0	6.0	4.0
71	Histone H4	5.6	35.1	43.4
72	Profilin-1	10.6	12.3	7.2
75	Heterogeneous nuclear ribonucleoprotein H	0.0	0.0	7.2
77	Uroporphyrinogen decarboxylase/Cactin Fragment	0.0	0.0	3.8

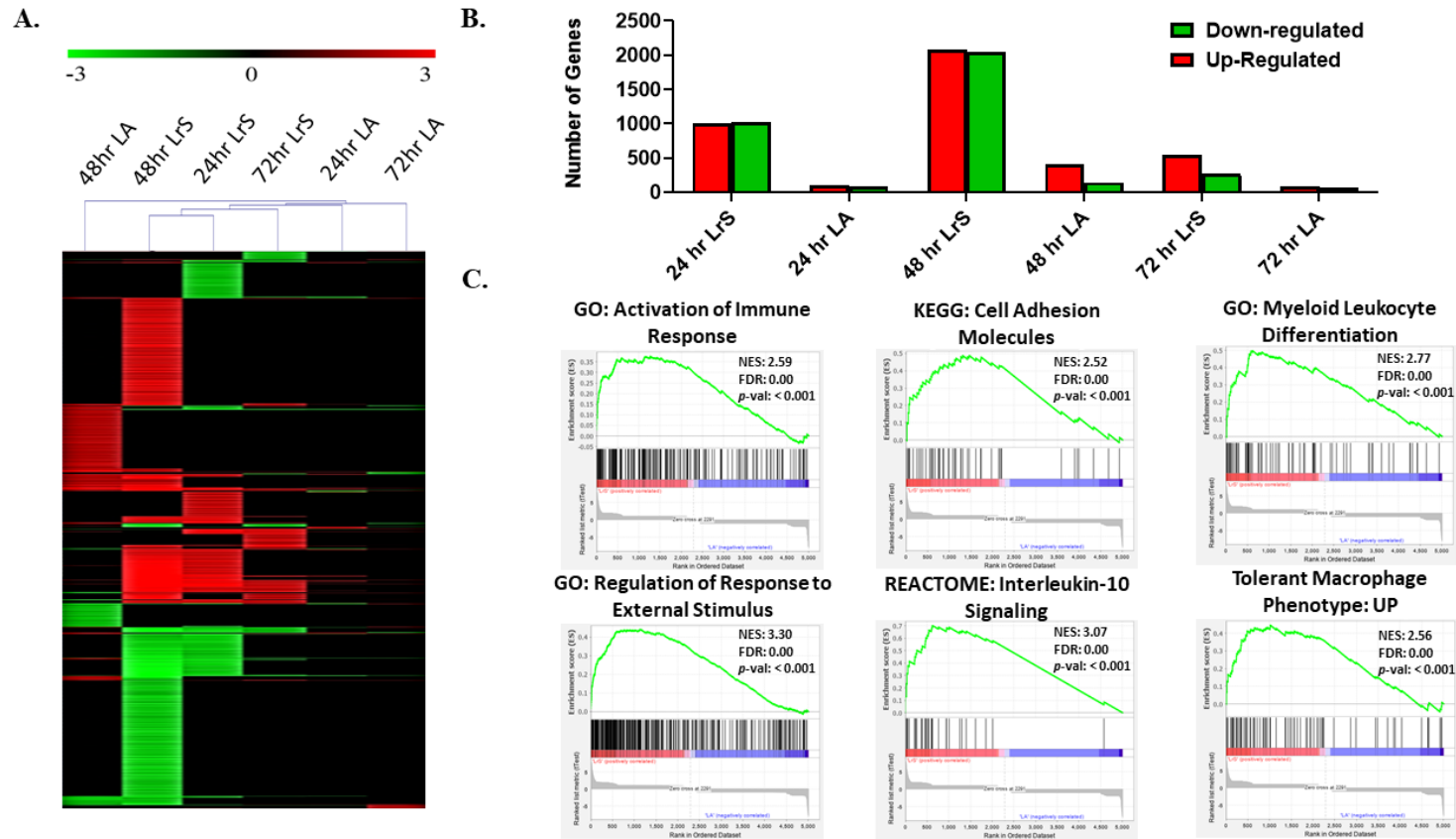
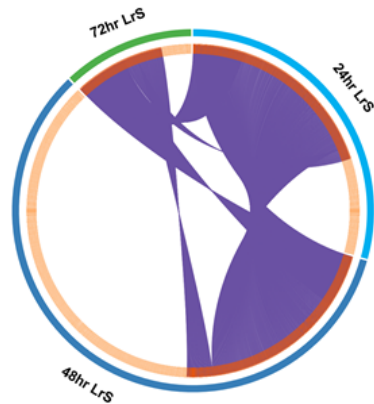
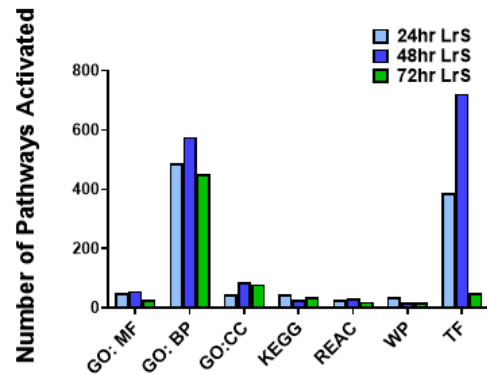


Figure 2-1. The LrS induces unique temporal transcriptional profiles in THP-1 human monocytes distinct from L-LA controls. **A.** Two-dimensional hierarchical clustering analysis of global gene expression patterns in THP-1 human monocytes conditioned with the LrS or LA-matched controls for 24-, 48-, or 72-hours ($n = 4$; $p < 0.05$; fold change different > 1.5 versus media-control treated cells). **B.** Total number of up- and down-regulated genes in response to each of the different challenges. **C.** Gene set enrichment analysis (GSEA) revealed the enrichment of key macrophage signaling pathways activated by conditioning with the LrS (red) when compared to LA-matched controls (blue) as determined by the ranked t-Test list metric over all tested time points. The green line represents the enrichment score and the black lines indicate where the genes within the gene set fall within the ranked pathway gene list.

A.



B.



C.

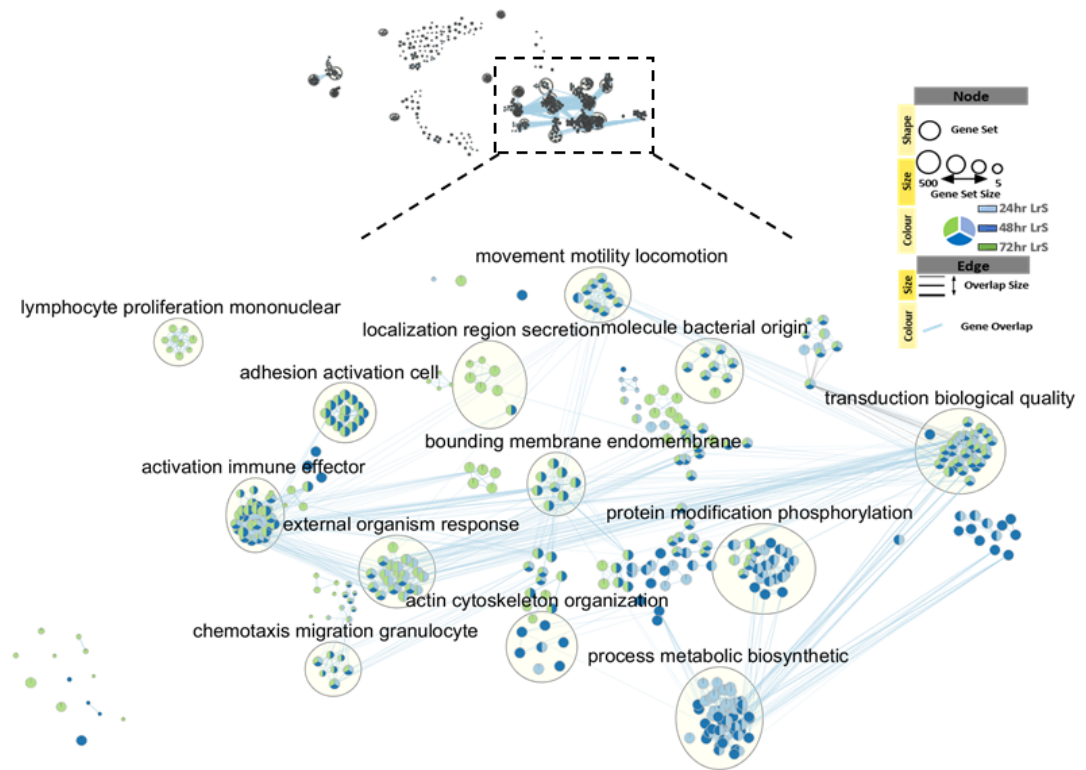


Figure 2-2. A. Venn-Diagram analysis identified unique temporal gene signatures in THP-1 monocytes conditioned with the LrS. B. gProfiler gene enrichment analysis revealed the activation of many key signaling pathways by the LrS in THP-1 monocytes (MF = molecular function; BP = biological process; REAC = Reactome pathways; WP = wikiPathways; TF = transcription factors). C. Visualization of the differential activation of key cellular pathways identified by gProfiler by EnrichmentMap analysis

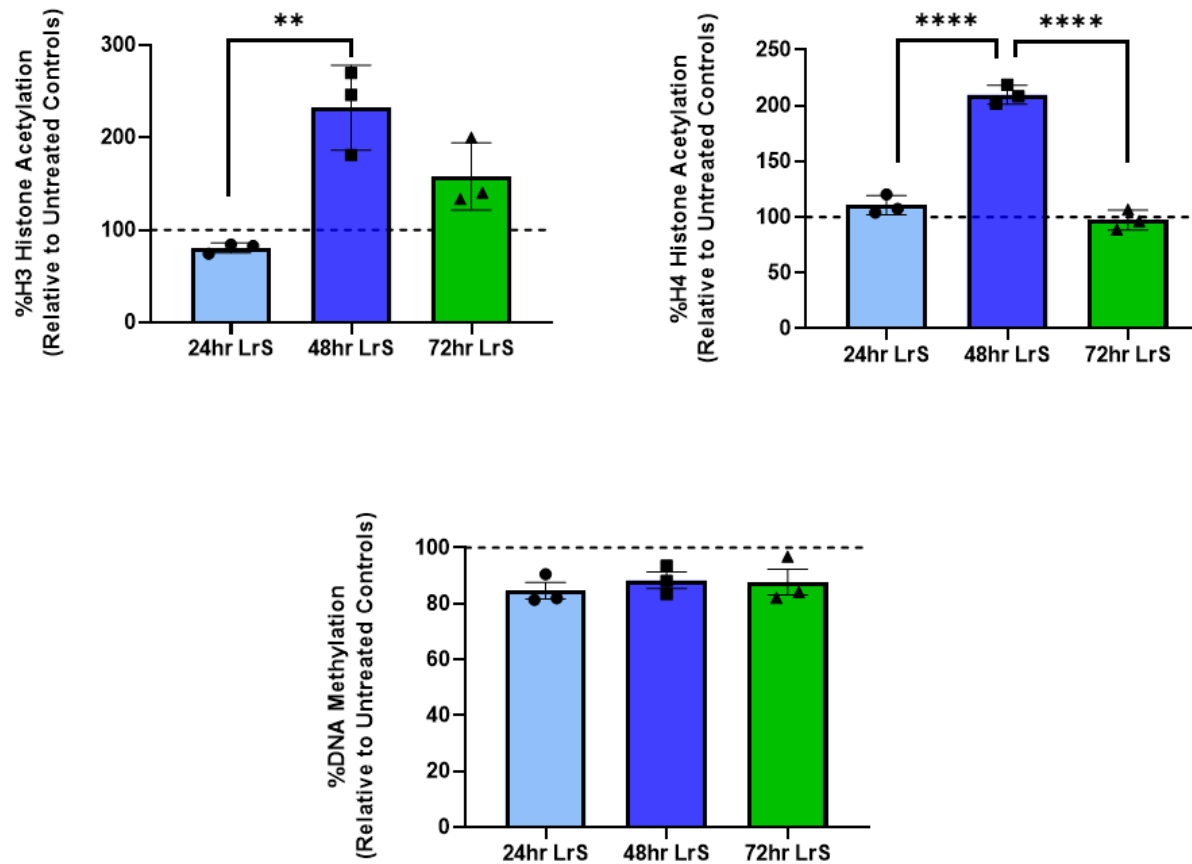


Figure 2-3. Changes in global histone H3 or H4 acetylation patterns and DNA methylation in THP-1 human monocytes conditioned with the LrS. Data shown are the mean change in percentage of acetylation or DNA methylation compared with untreated controls \pm SEM (n = 3). Significance is indicated as * $p < 0.05$, ** $p < 0.01$, *** $p < 0.001$ as determined by one-way ANOVA and Tukey's post-hoc test.

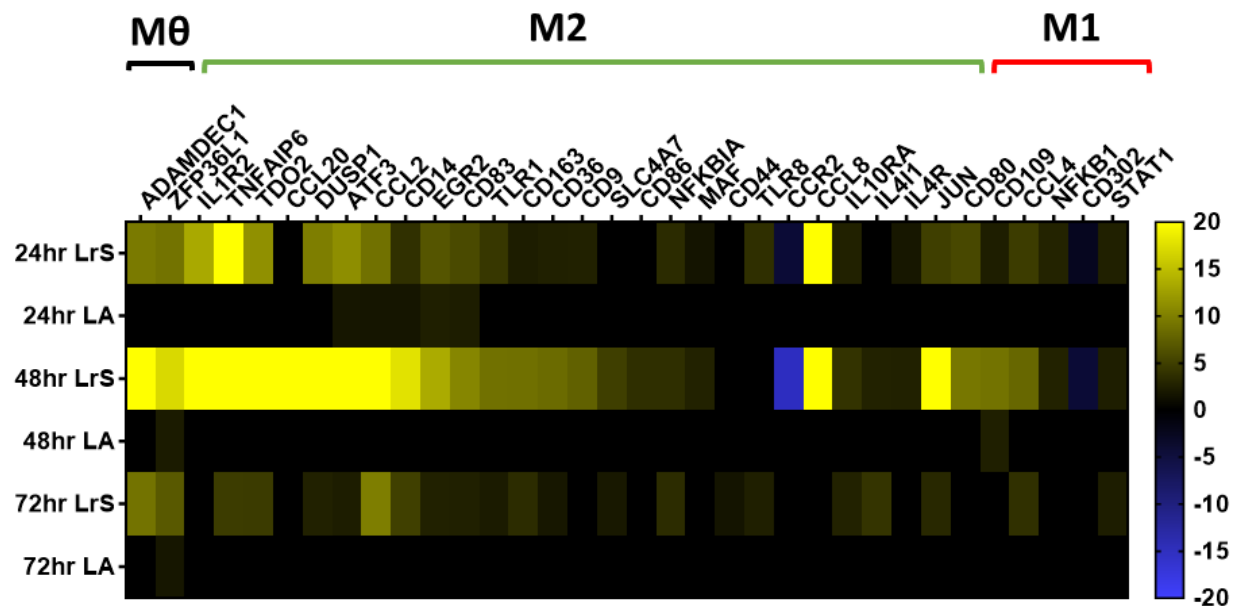
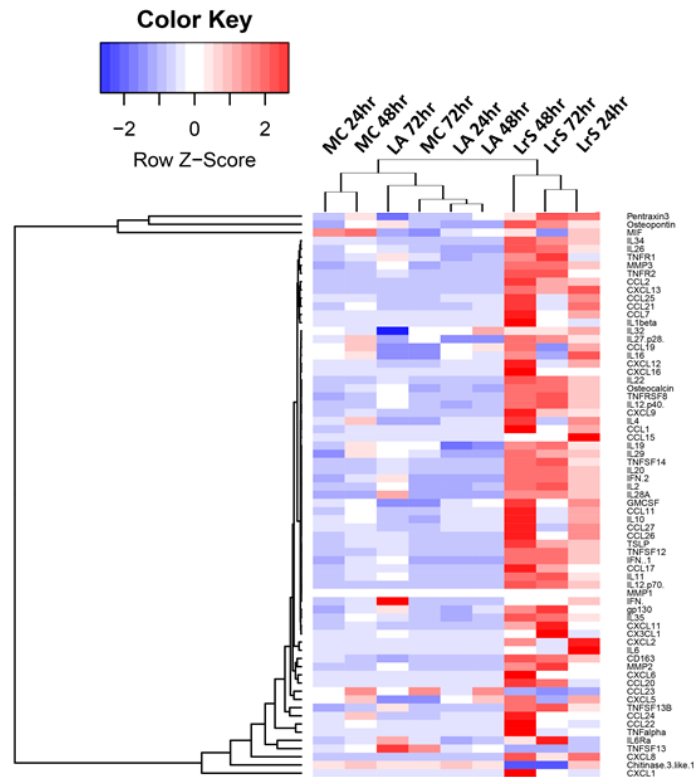


Figure 2-4. THP-1 human monocytes conditioned with the LrS show similar transcription profiles to those seen in immunoregulatory macrophage activation (n = 4; p < 0.05; fold change different > 1.5 versus untreated cells). Microarray data was probed for genes typically associated with monocyte to macrophage differentiation as well as those genes identified to be important in M1 and M2 polarization.

A.



B.

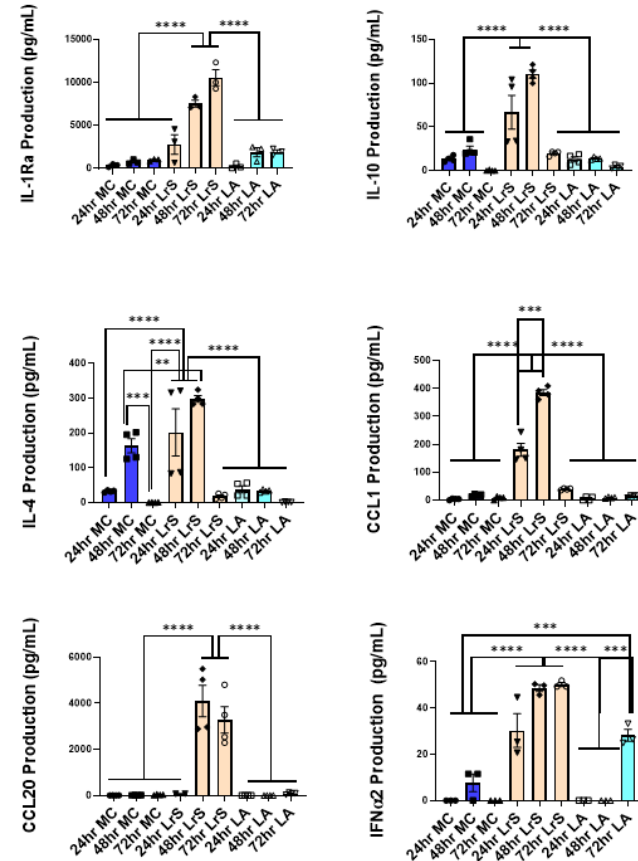


Figure 2-5. LrS conditioning of THP-1 human monocytes results in unique temporal cytokine and chemokine production profiles. **A.** Two-dimensional hierarchical clustering analysis of cytokine and chemokine production profiles from THP-1 human monocytes following conditioning with the LrS or LA-matched controls for 24-, 48-, or 72-hours. Data shown is the Z-score statistic for each cytokine and chemokine measured ($n = 4$). **B.** The LrS induces the production of key immunoregulatory cytokines from THP-1 human monocytes (IL-1Ra, IL-10, IL-4, CCL1, CCL20, IFN α 2). Data shown is the mean cytokine or chemokine production (pg/mL) \pm SEM ($n = 4$). Statistical significance is indicated as *** $p < 0.001$ or **** $p < 0.0001$ as determined by Tukey's one-way ANOVA.

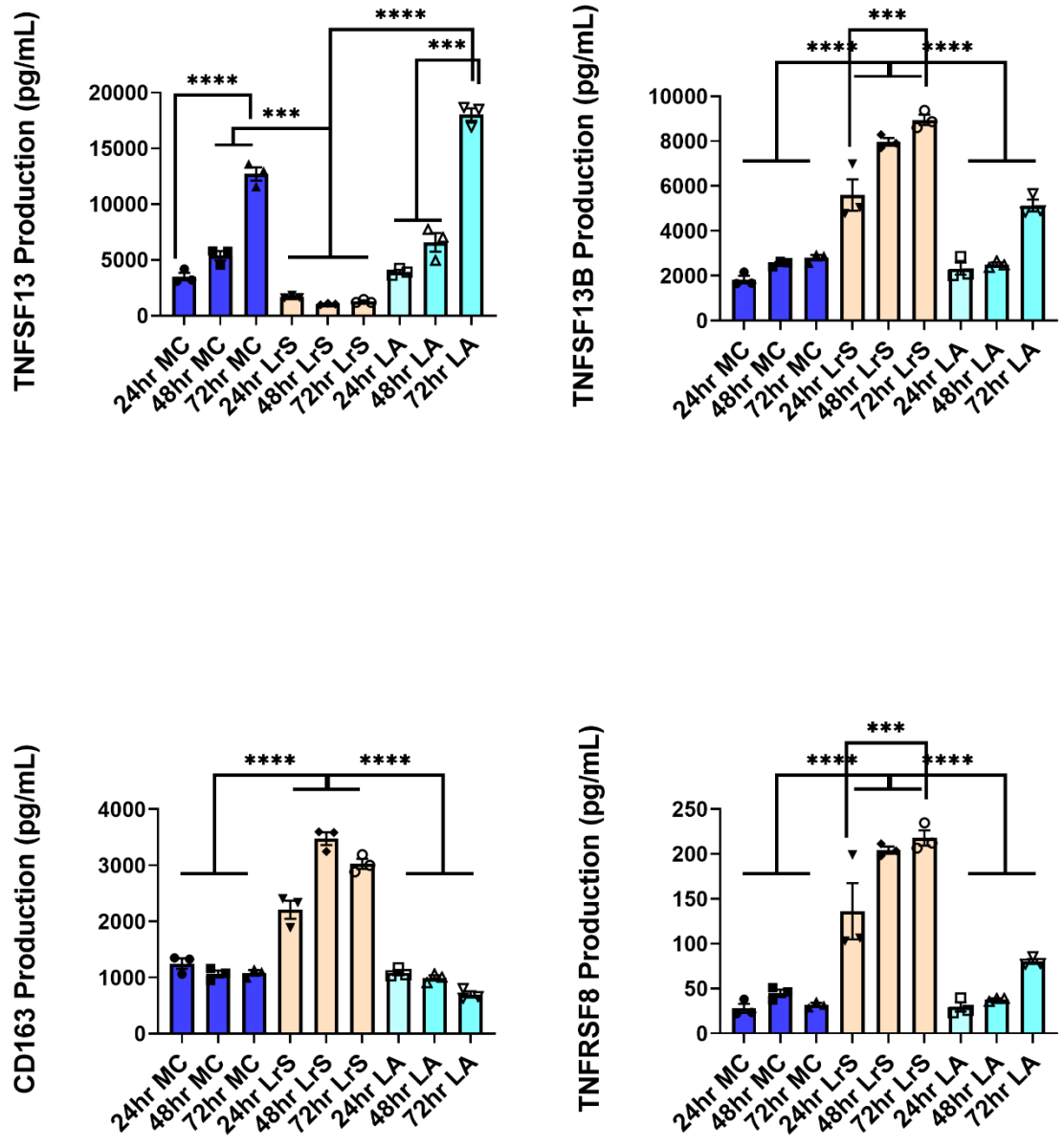
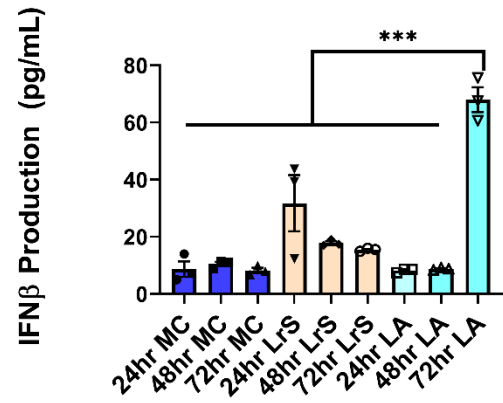
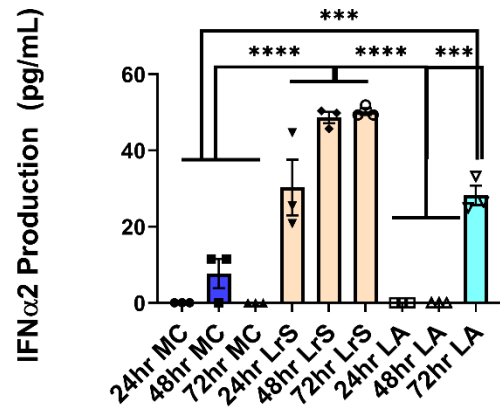
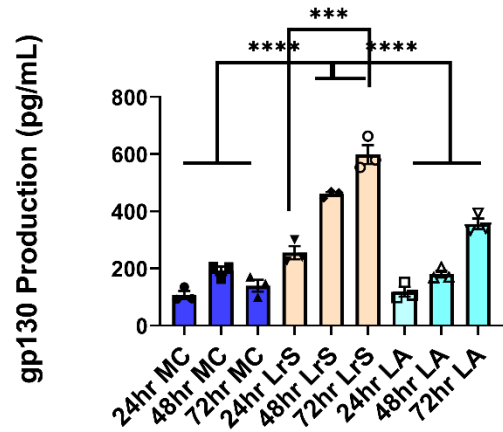
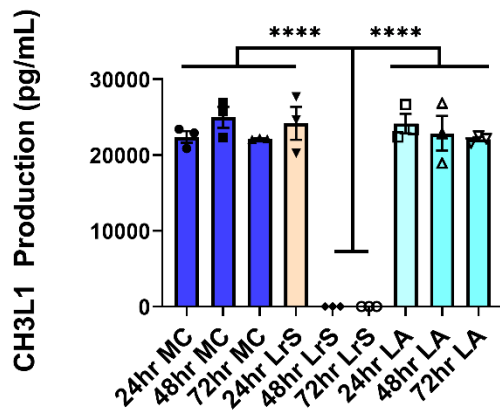
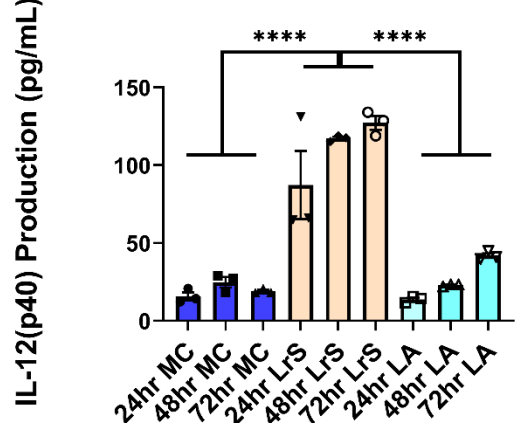
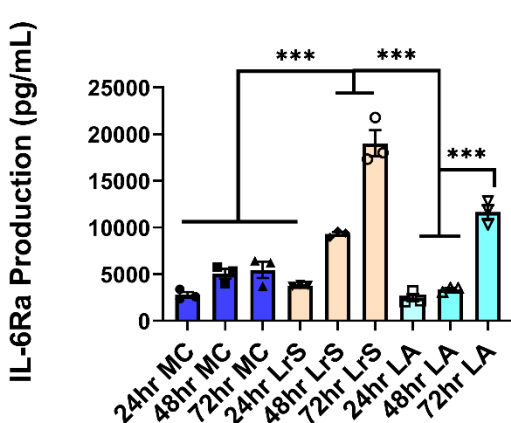
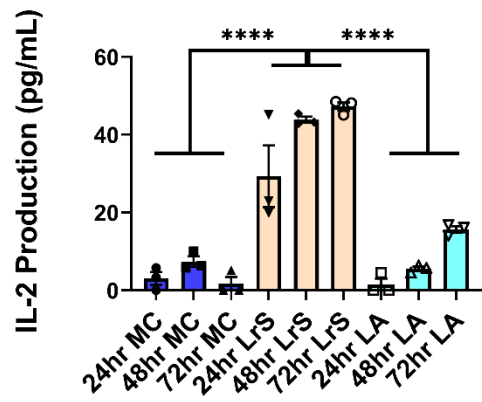
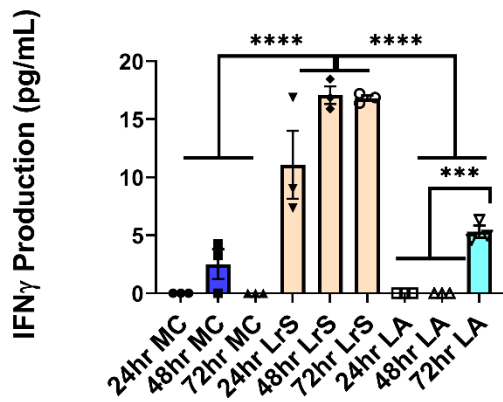


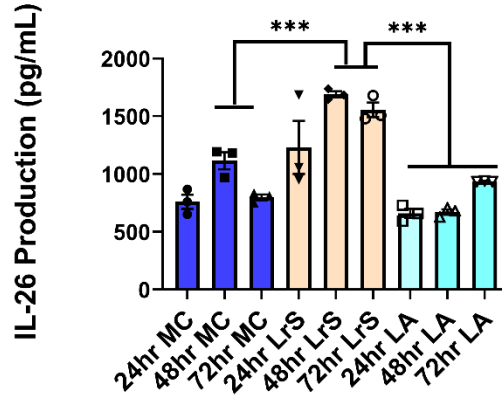
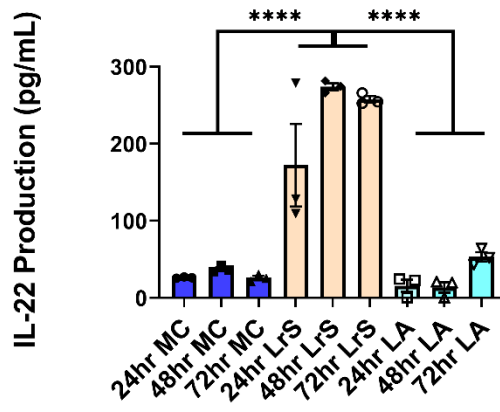
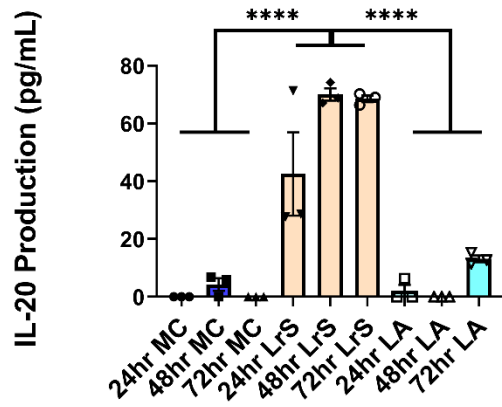
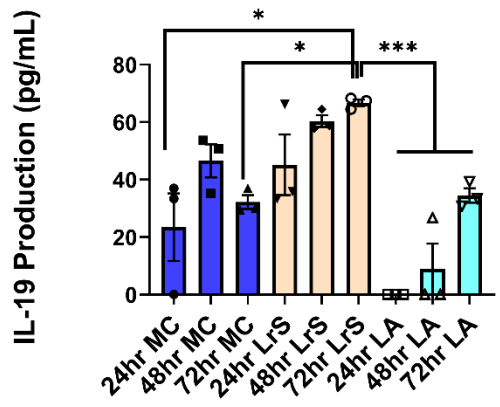
Figure 2-6. Cytokine and chemokine profiles from THP-1s conditioned with the LrS (20% v/v) or L-LA controls for 24-, 48-, or 72-hours. Data shown is the means cytokine/chemokine production (pg/mL) \pm SEM (n = 4). Significance is indicated as * $p < 0.05$, ** $p < 0.01$, *** $p < 0.001$ as determined by one-way ANOVA and Tukey's post-hoc test.



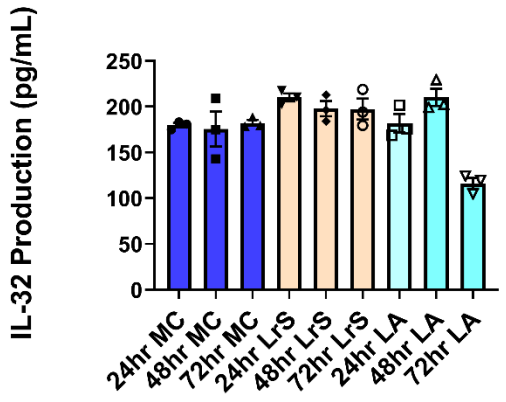
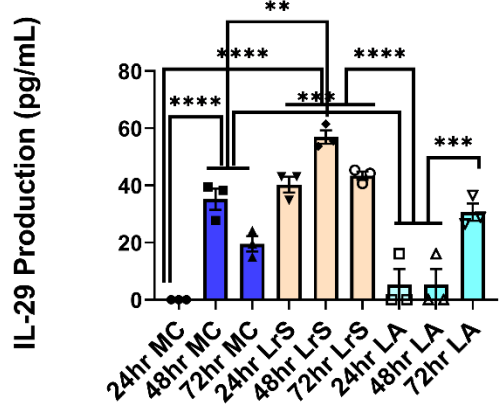
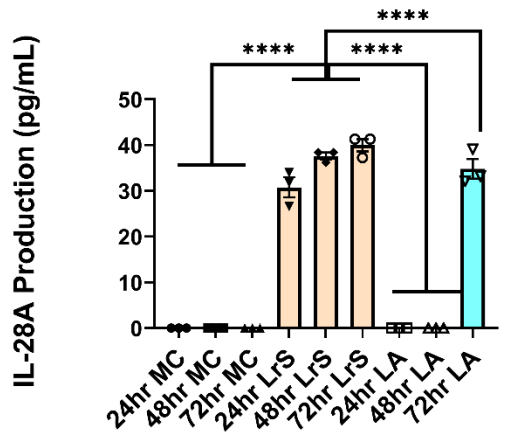
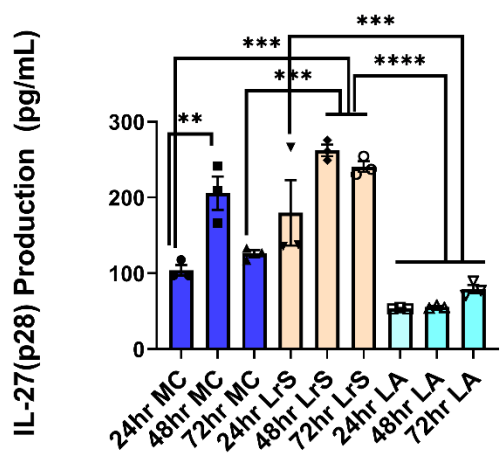
This is a continuation of Figure 2-6.



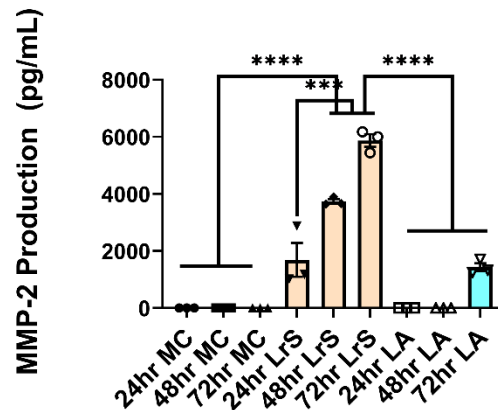
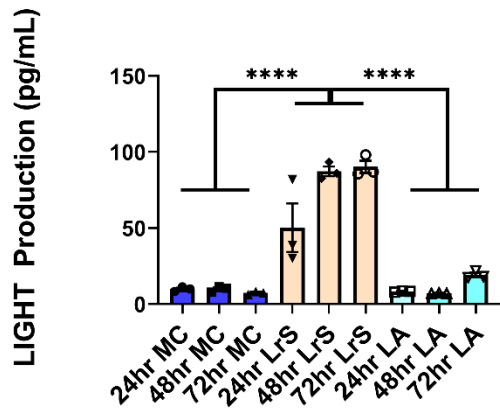
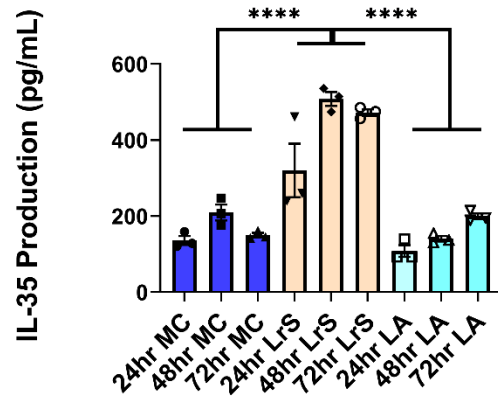
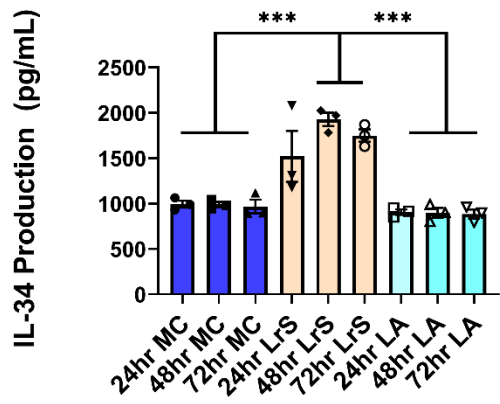
This is a continuation of Figure 2-6.



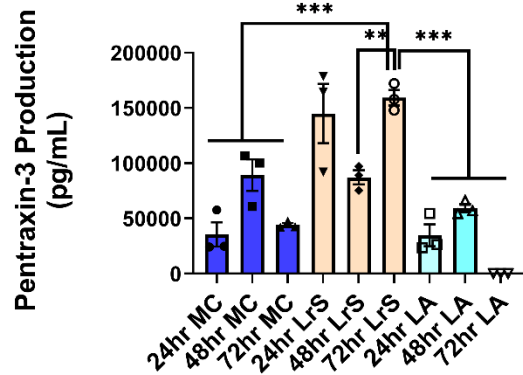
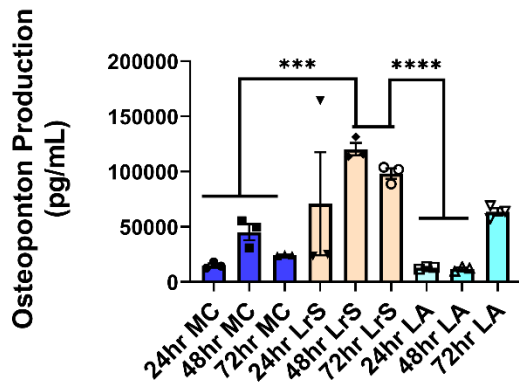
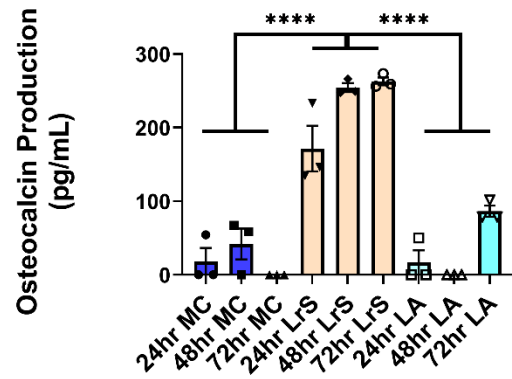
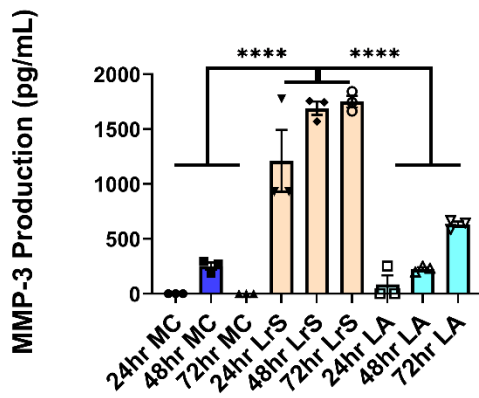
This is a continuation of Figure 2-6.



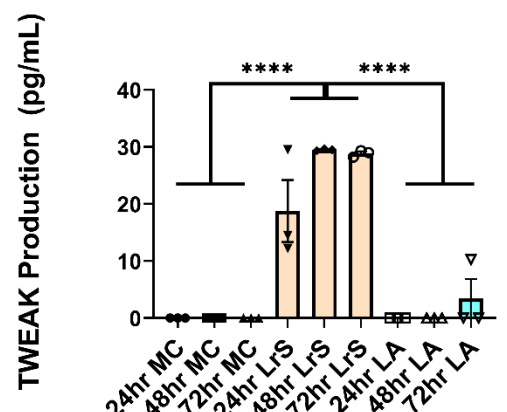
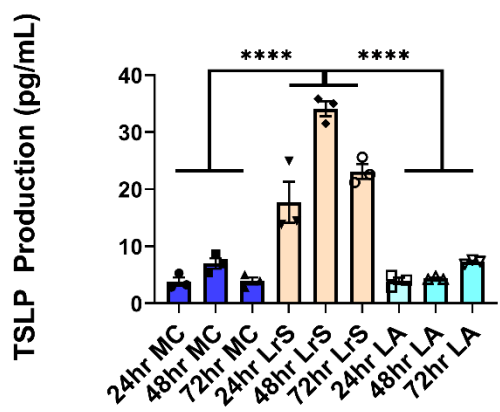
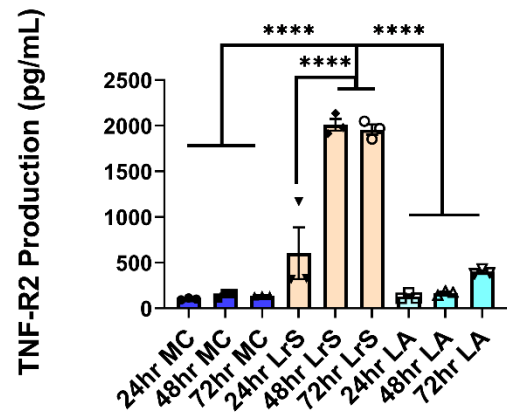
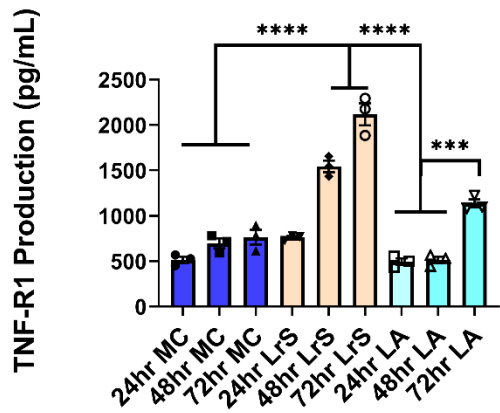
This is a continuation of Figure 2-6.



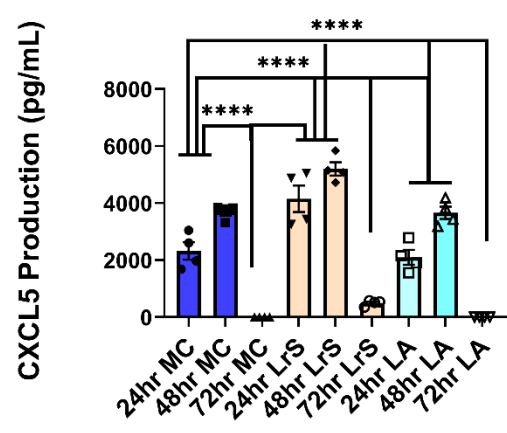
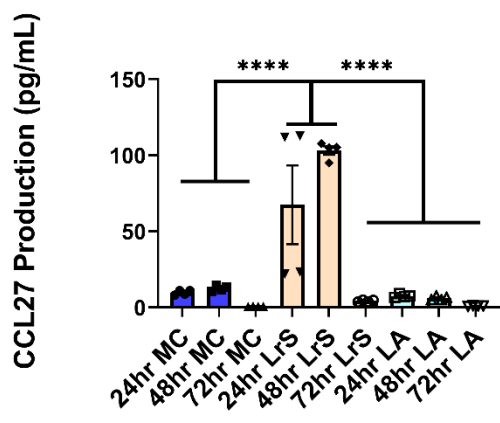
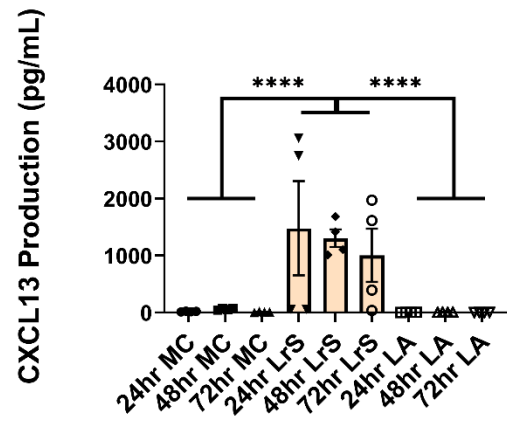
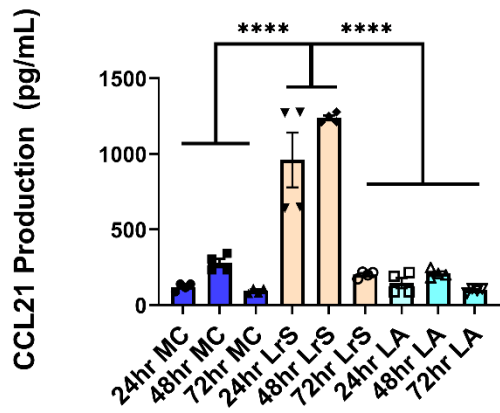
This is a continuation of Figure 2-6.



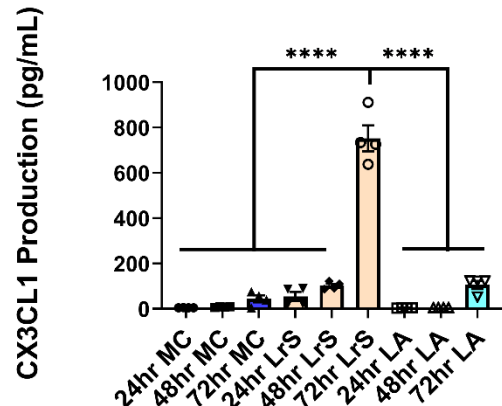
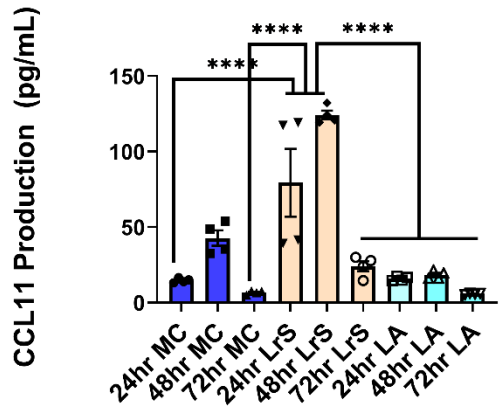
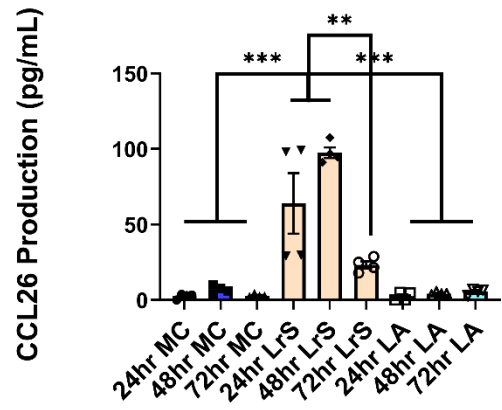
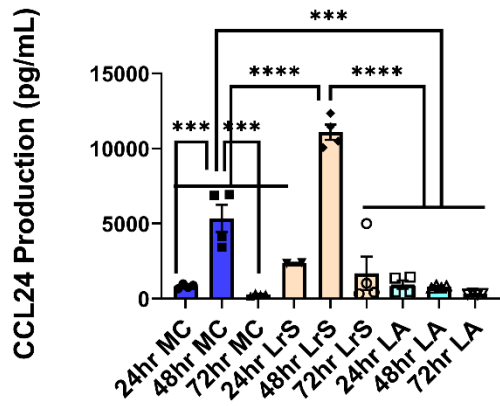
This is a continuation of Figure 2-6.



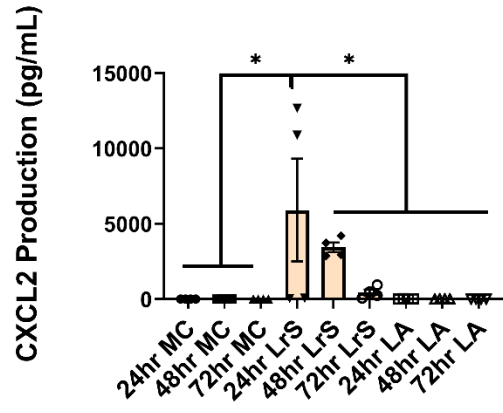
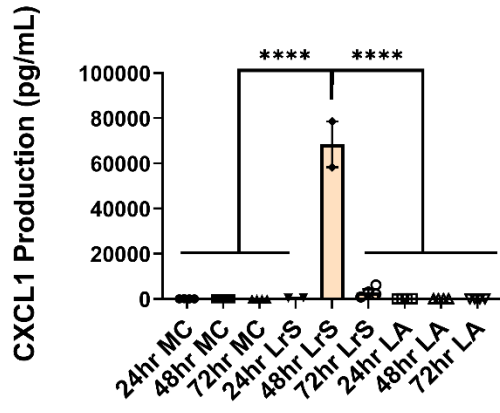
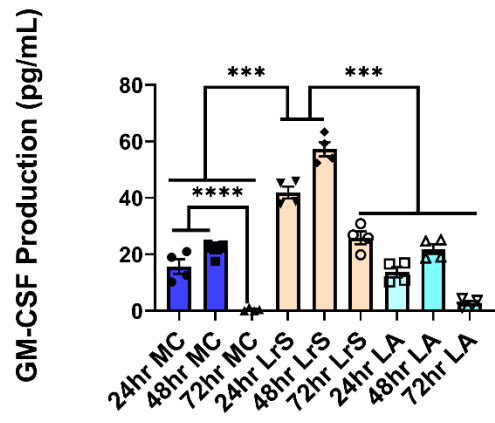
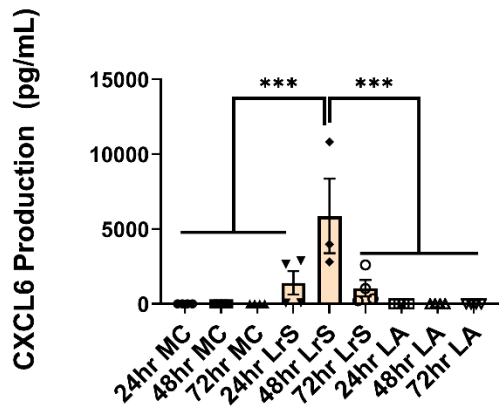
This is a continuation of Figure 2-6.



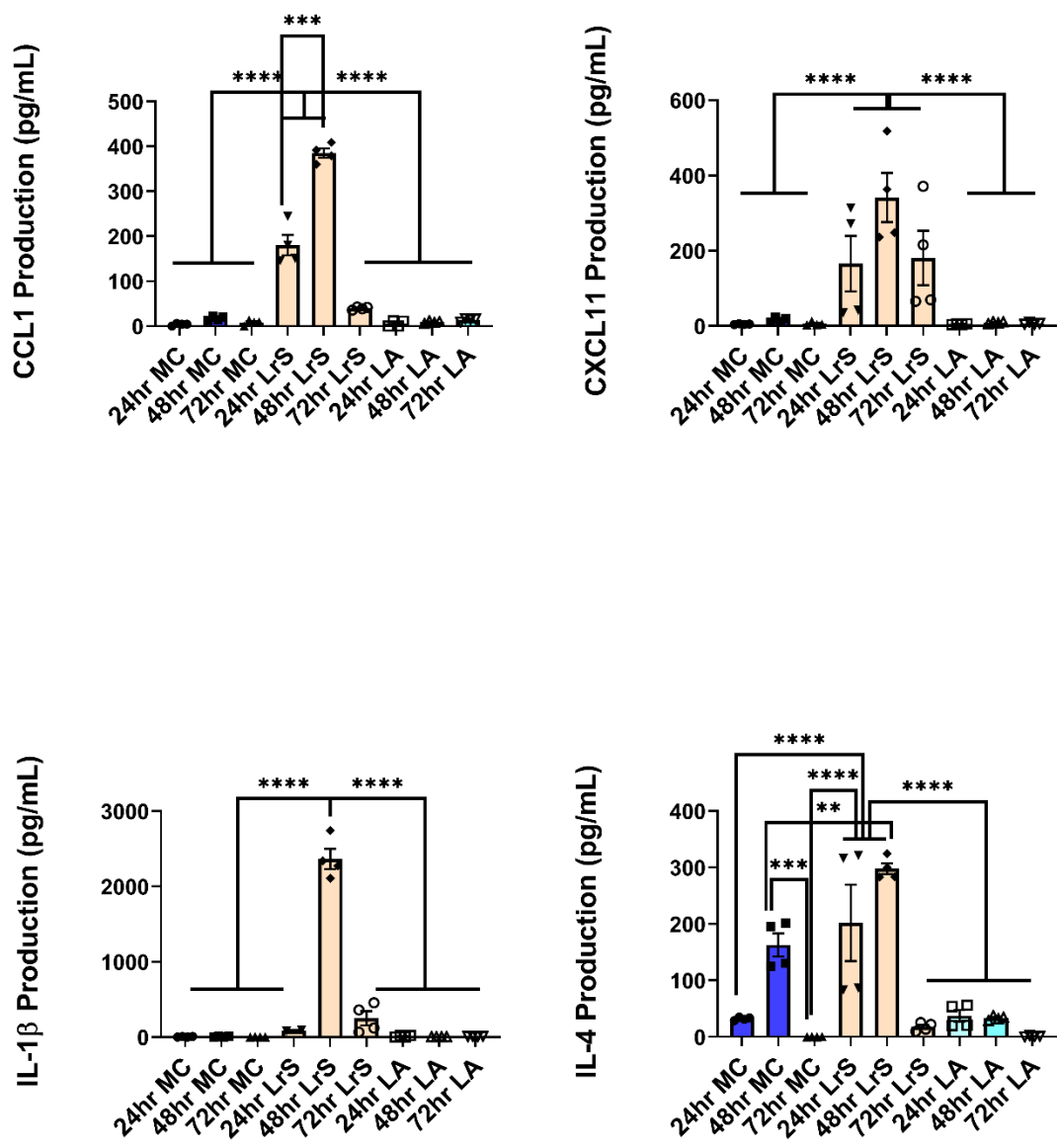
This is a continuation of Figure 2-6.



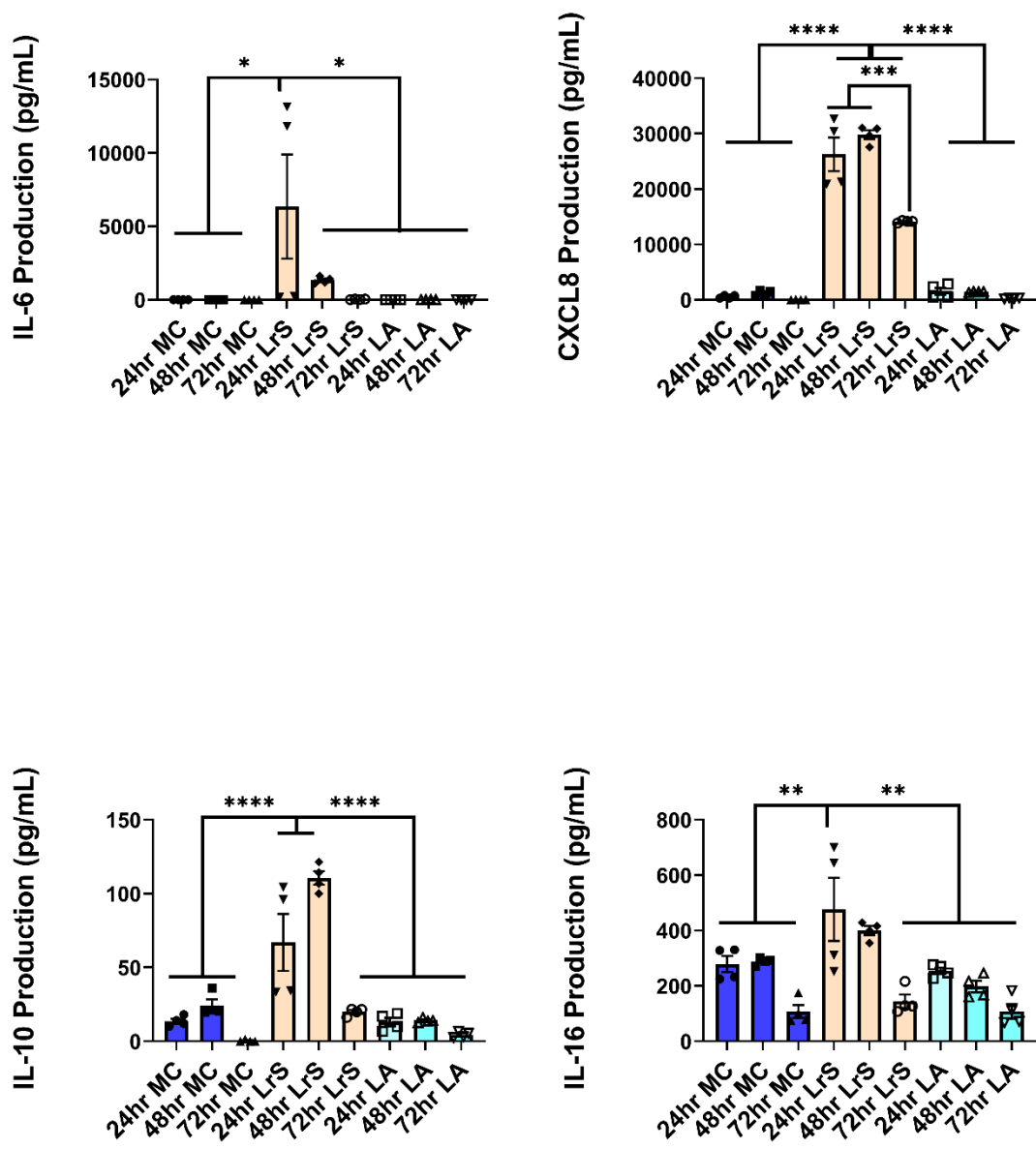
This is a continuation of Figure 2-6.



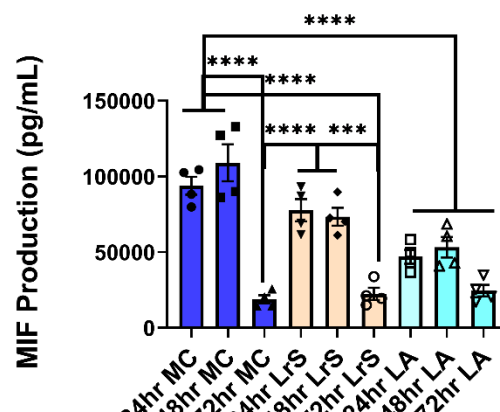
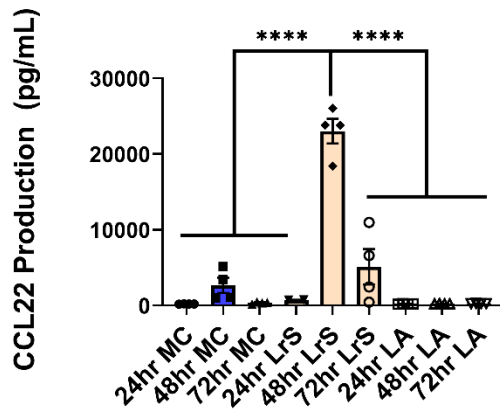
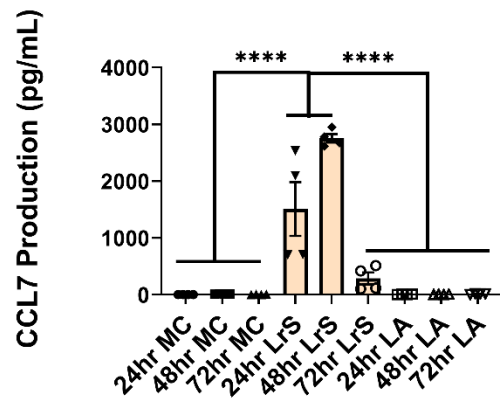
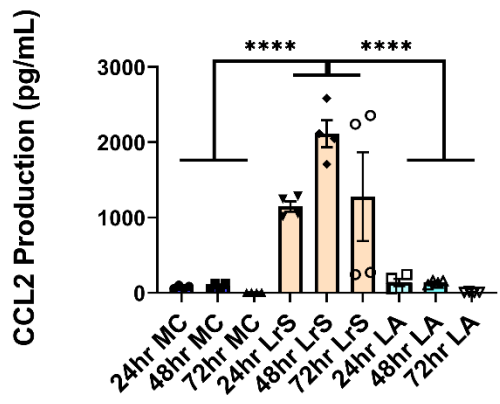
This is a continuation of Figure 2-6.



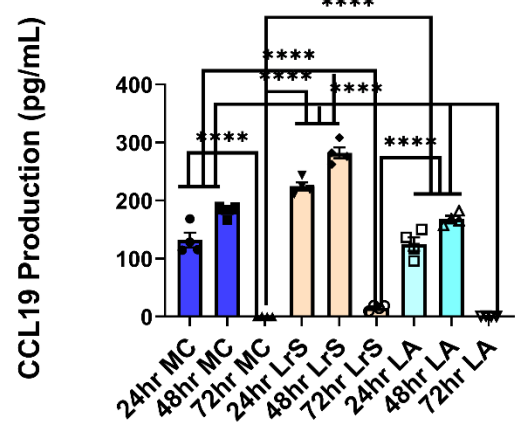
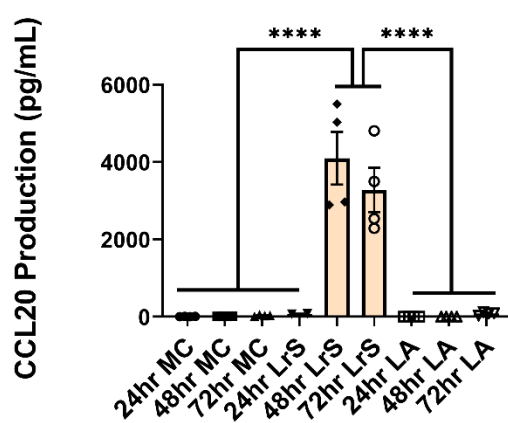
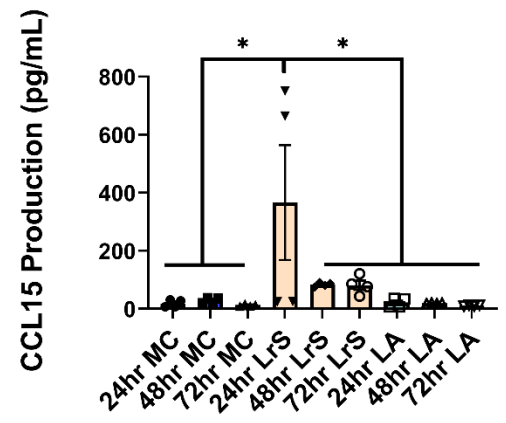
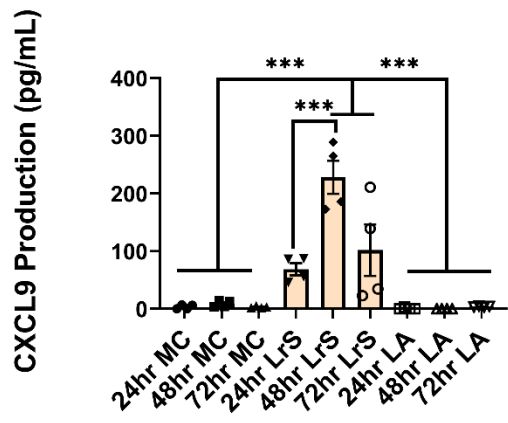
This is a continuation of Figure 2-6.



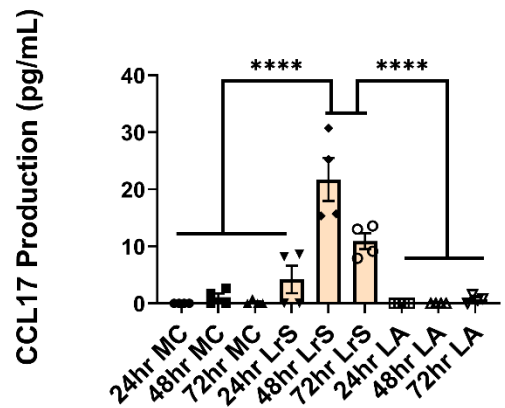
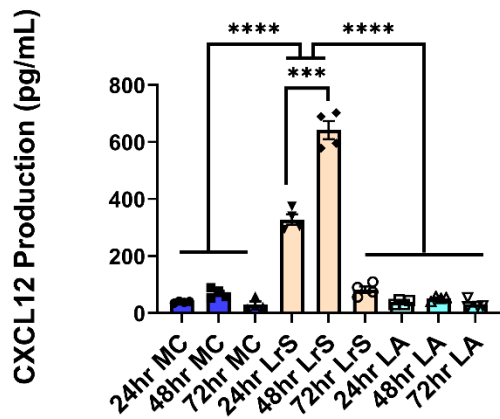
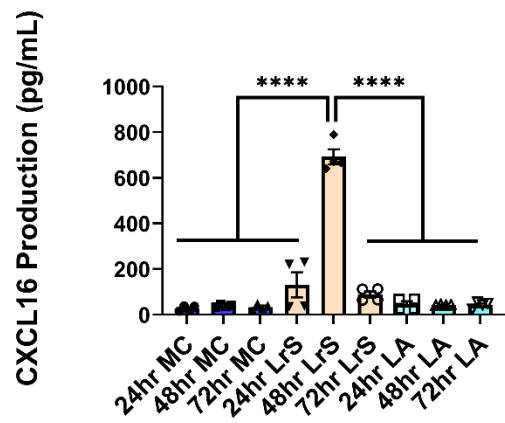
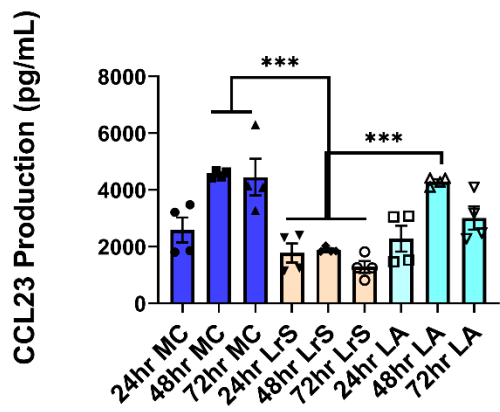
This is a continuation of Figure 2-6.



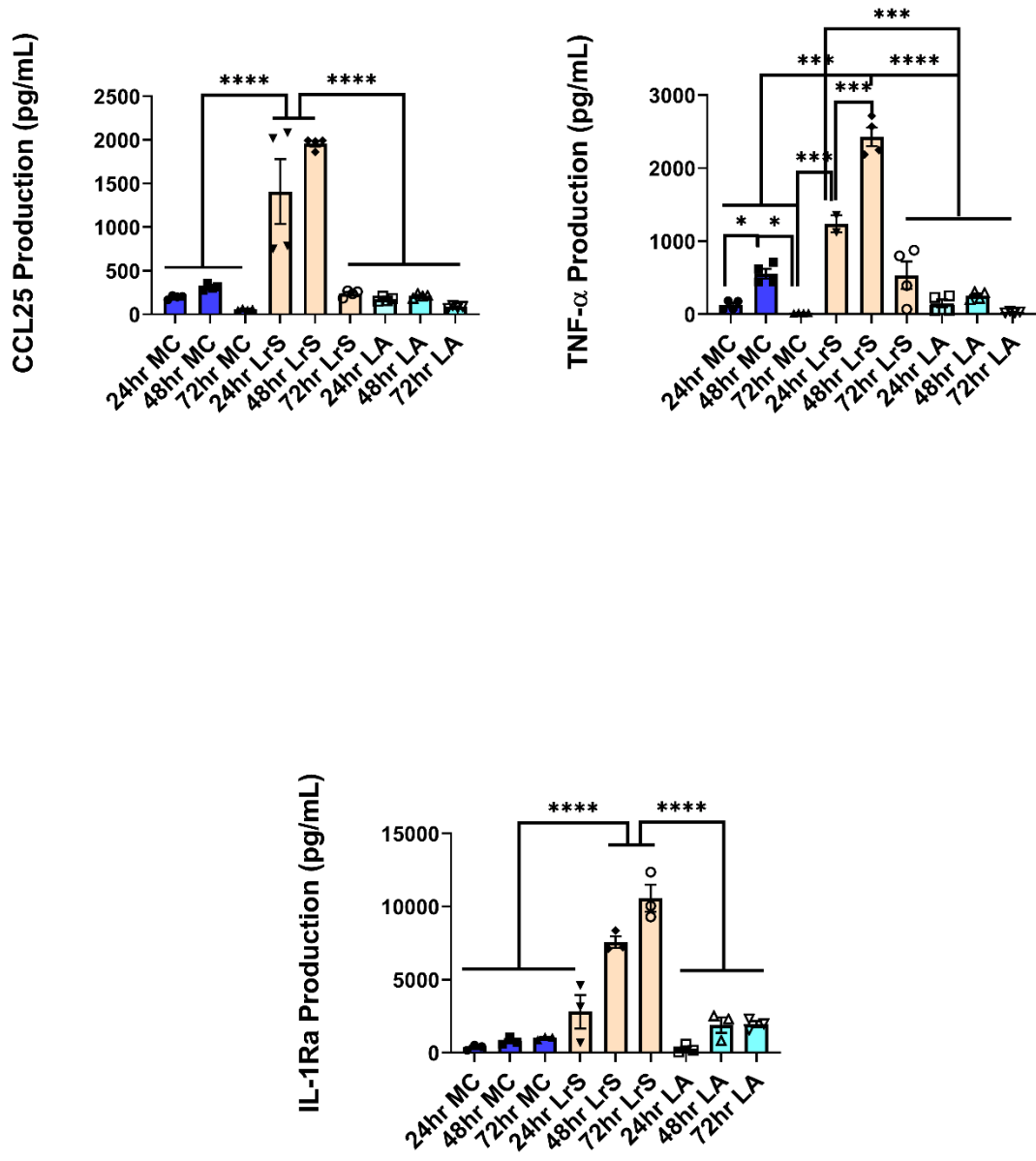
This is a continuation of Figure 2-6.



This is a continuation of Figure 2-6.



This is a continuation of Figure 2-6.



This is a continuation of Figure 2-6.

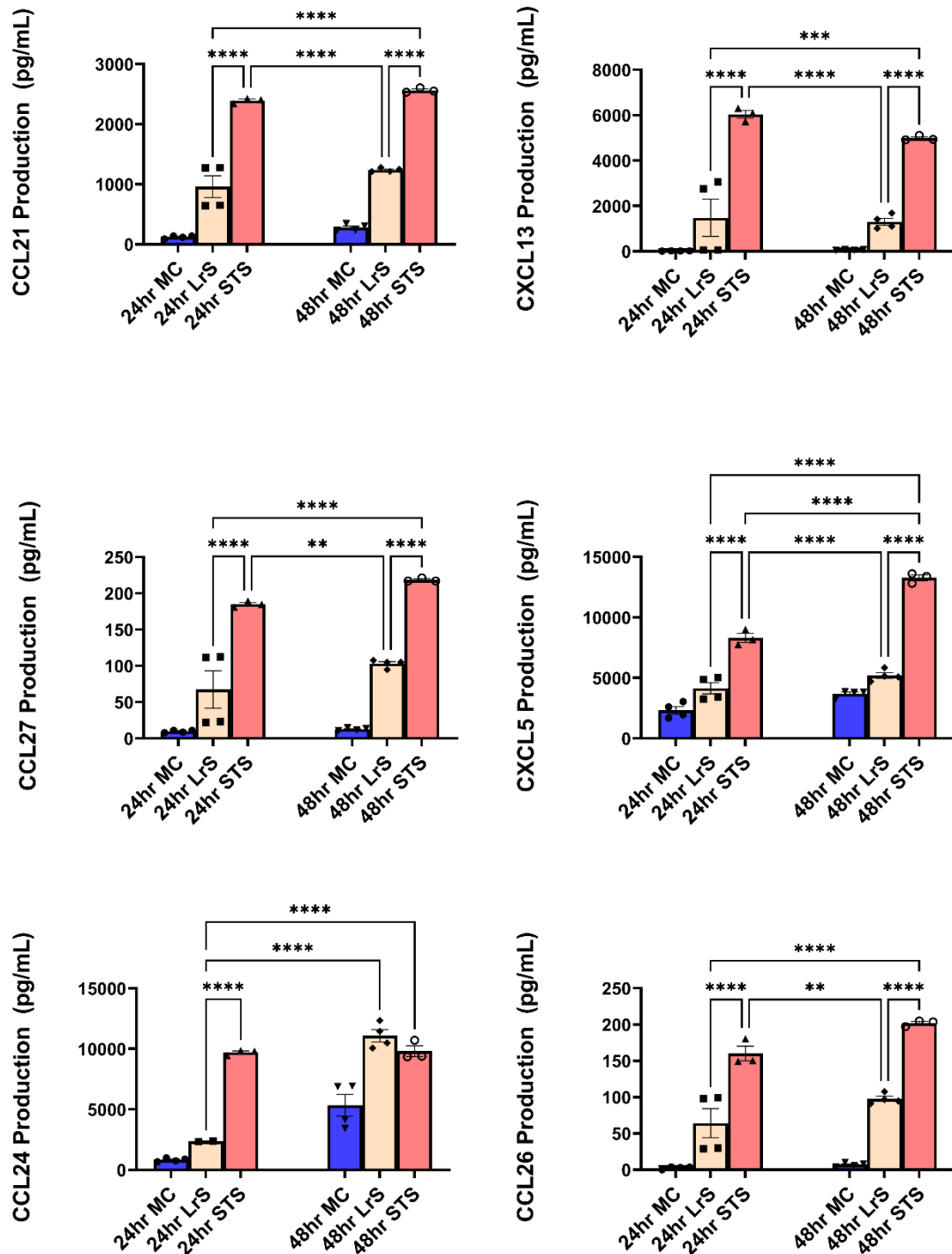
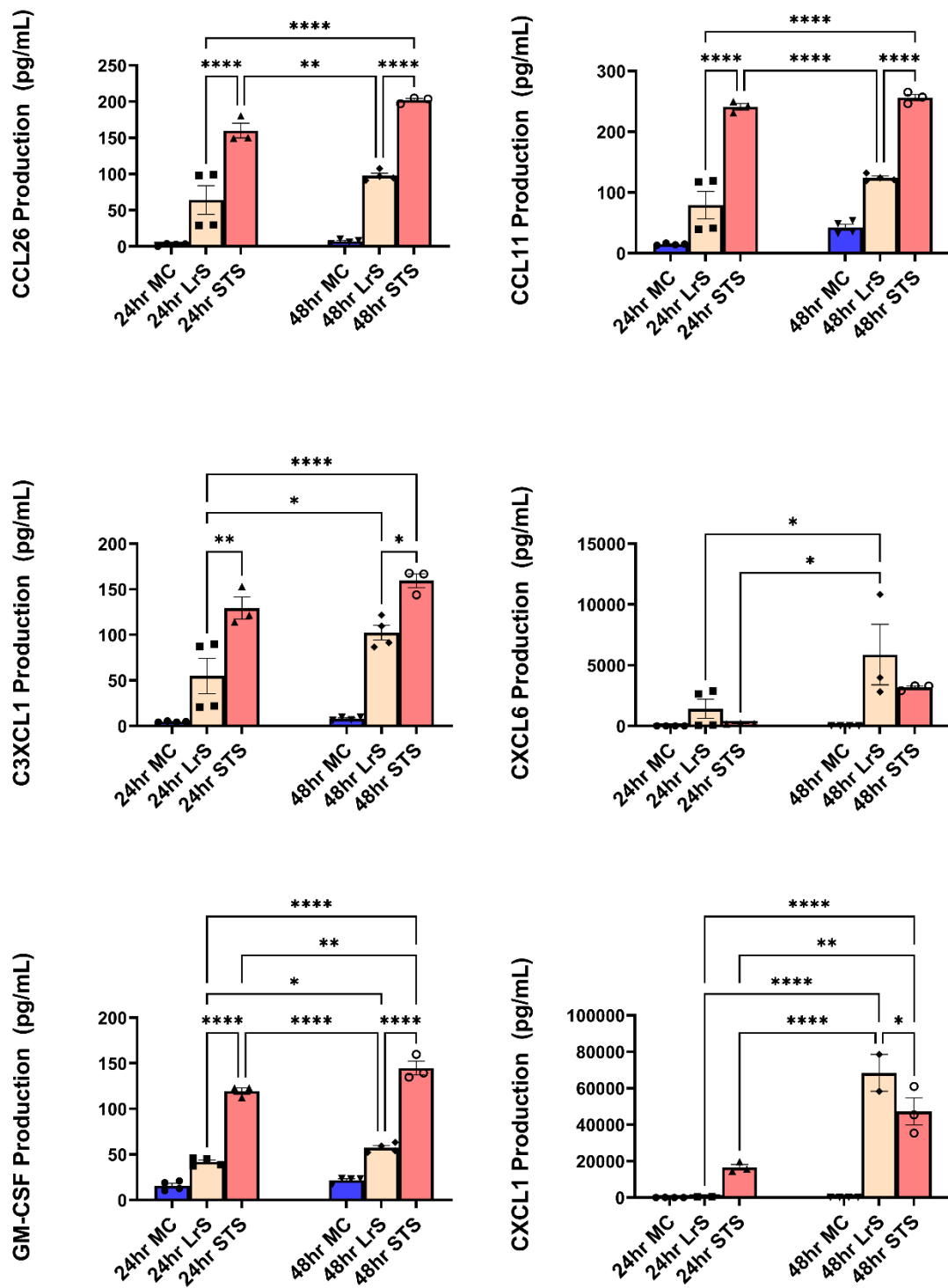
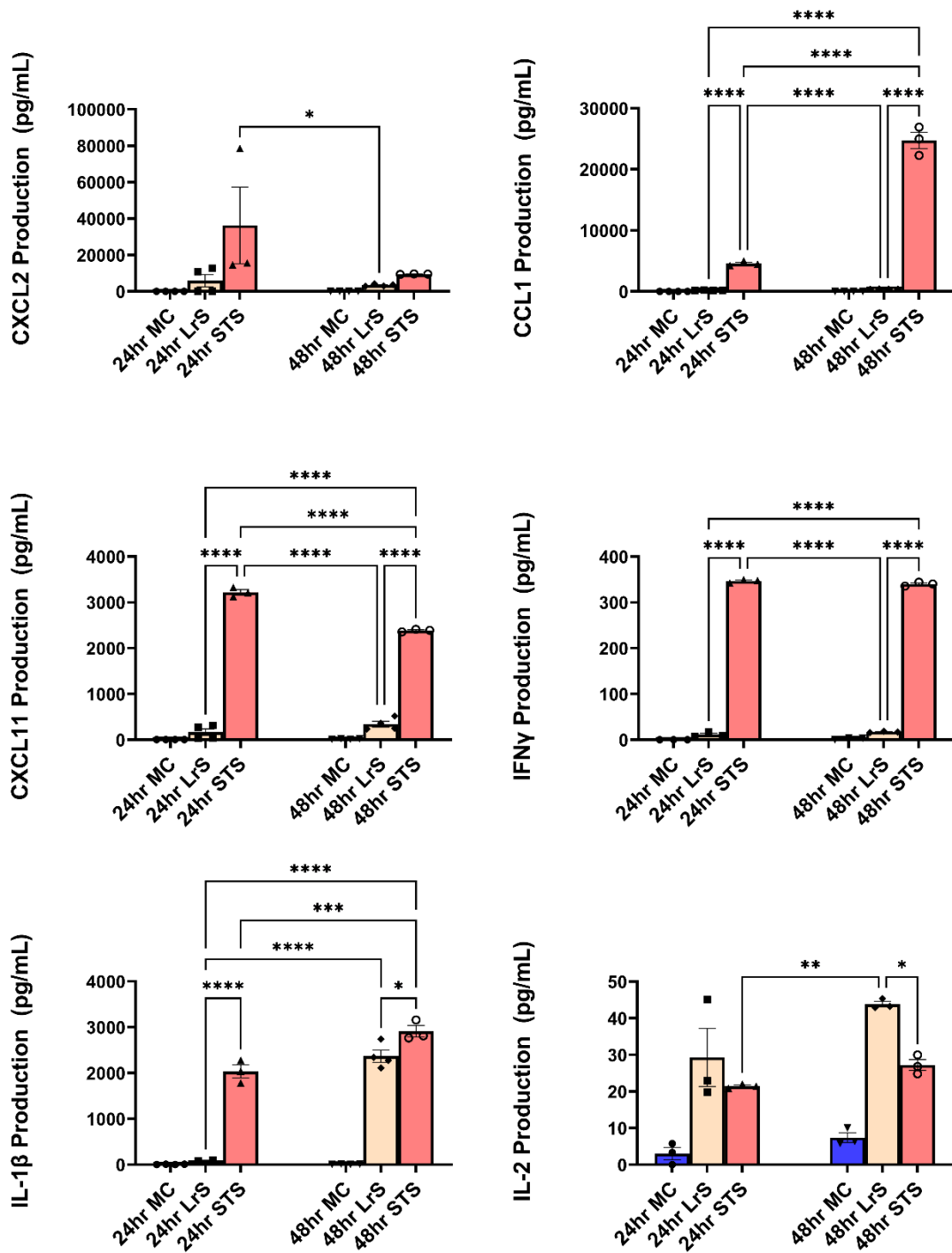


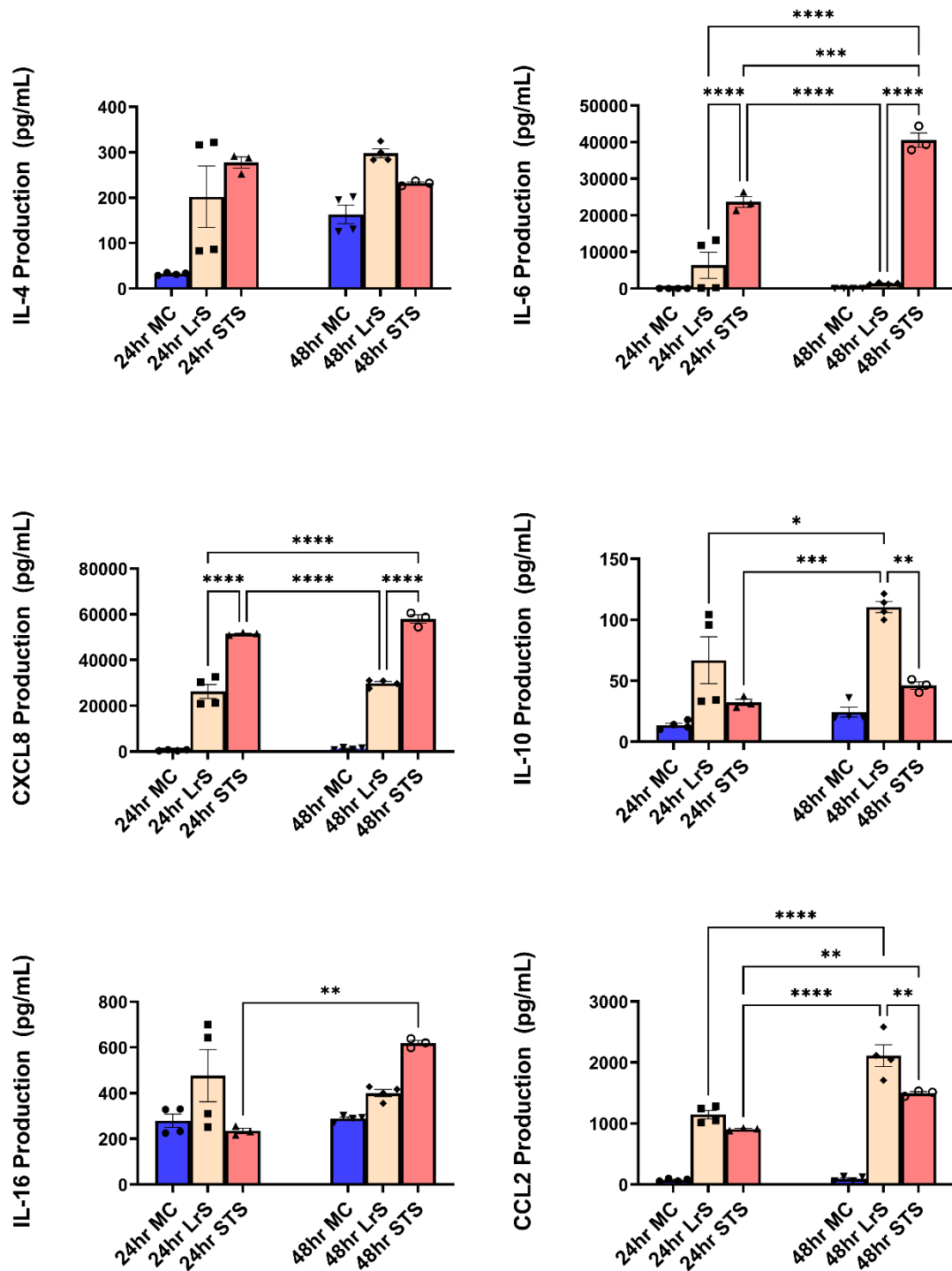
Figure 2-7. Cytokine and chemokine profiles from THP-1s conditioned with the LrS (20% v/v) or STS (1% v/v) for 24- or 48-hours. Data shown is the means cytokine/chemokine production (pg/mL) \pm SEM (n = 4). Significance is indicated as * $p < 0.05$, ** $p < 0.01$, *** $p < 0.001$ as determined by one-way ANOVA and Tukey's post-hoc test. 72-hour data is omitted as THP-1 monocytes conditioned with the STS following 48-hours were no longer viable.



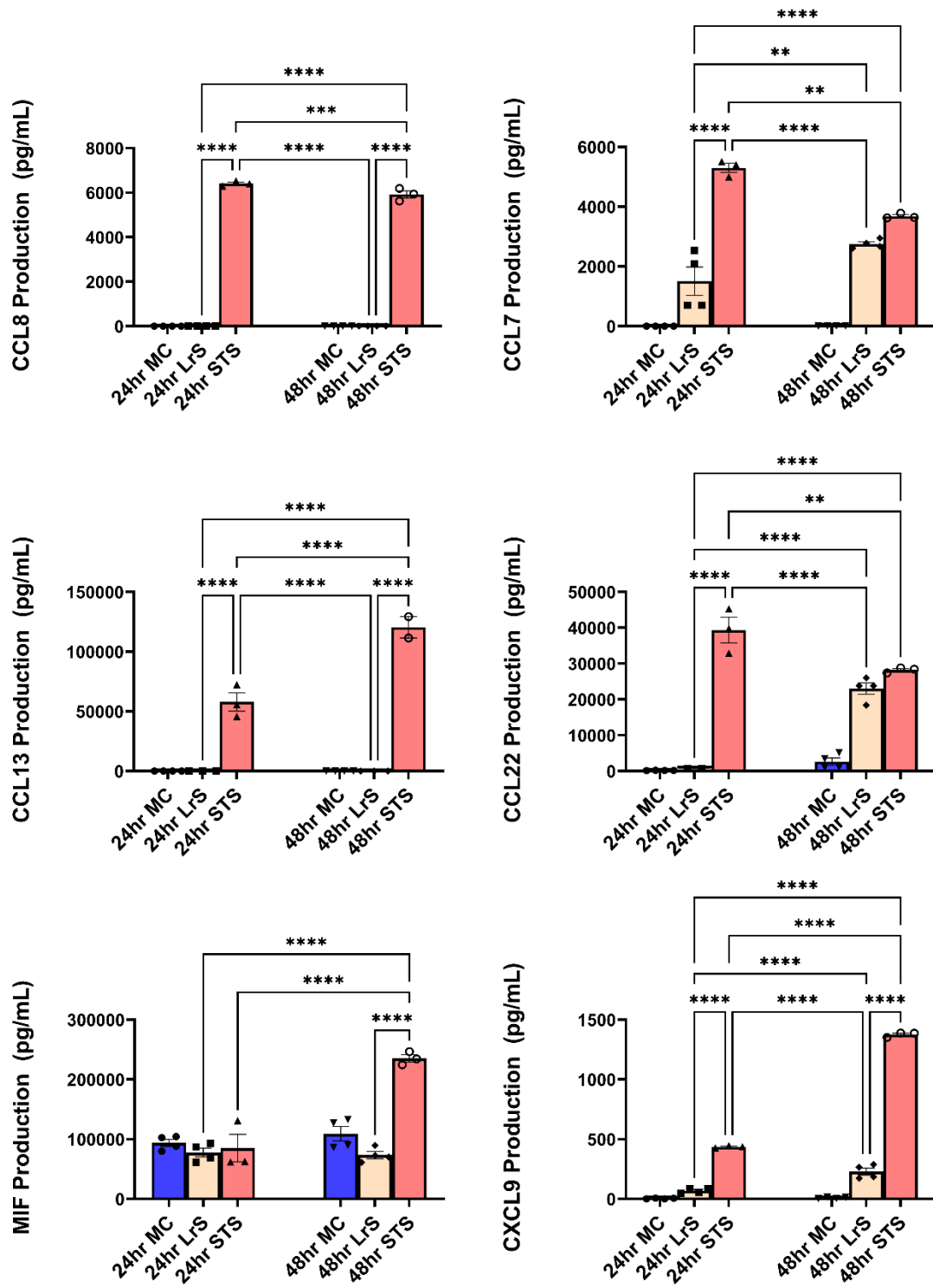
This is a continuation of Figure 2-7.



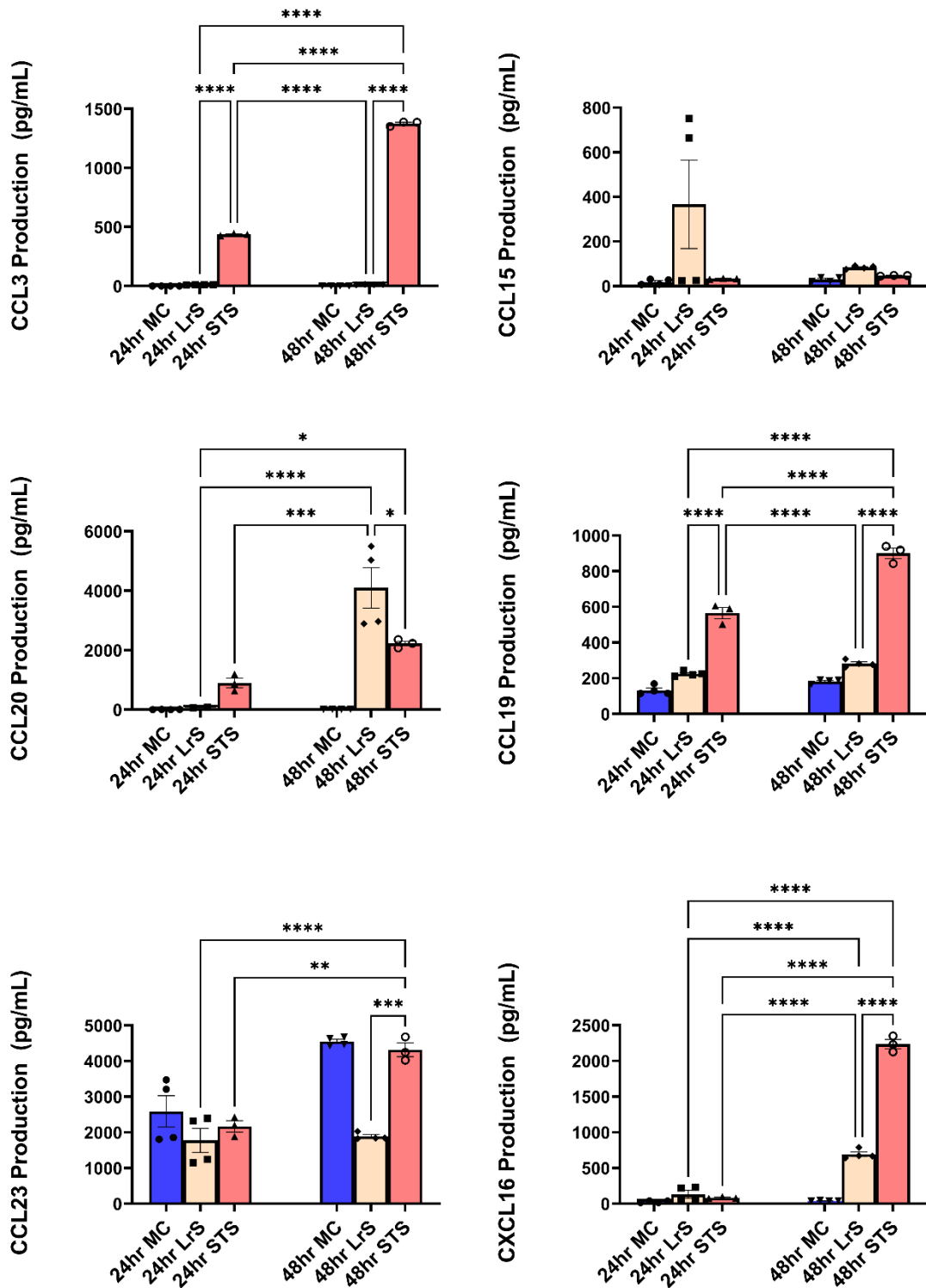
This is a continuation of Figure 2-7.



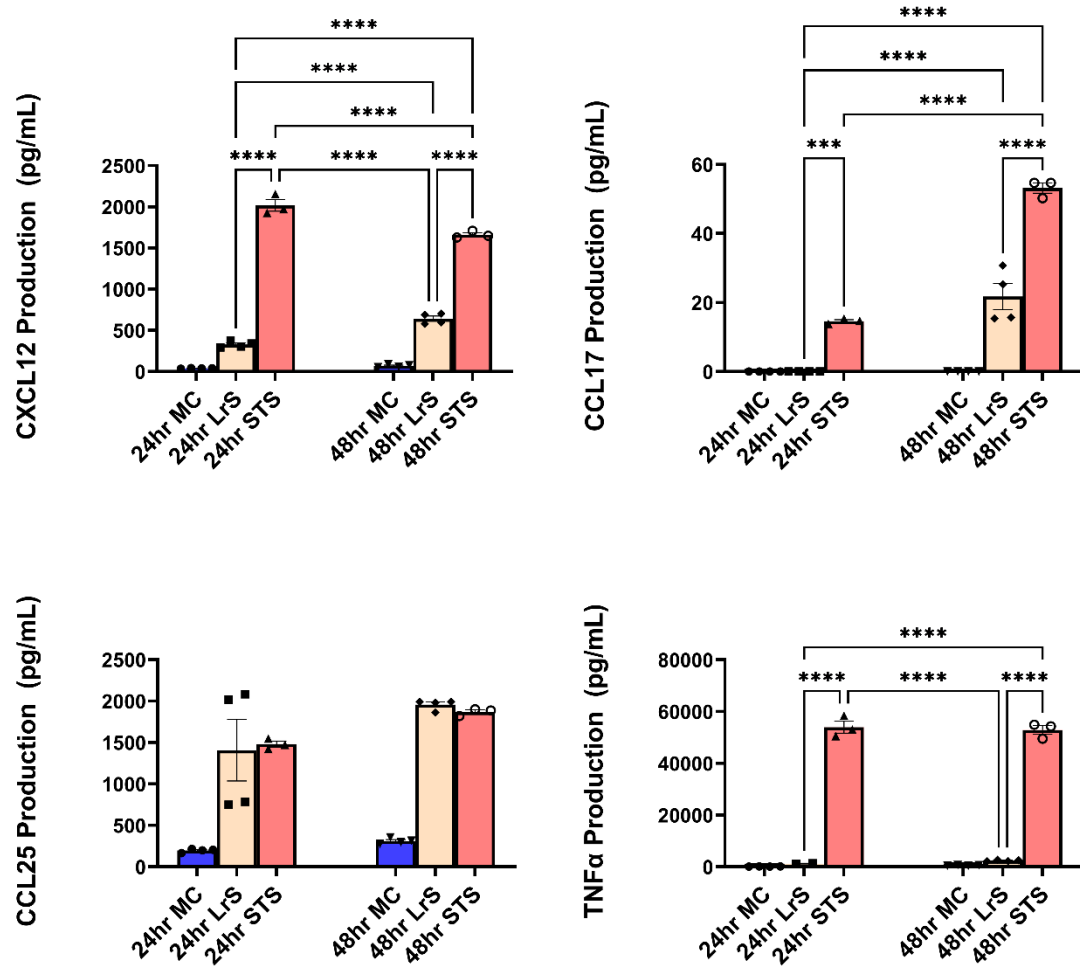
This is a continuation of Figure 2-7.



This is a continuation of Figure 2-7.



This is a continuation of Figure 2-7.



This is a continuation of Figure 2-7.

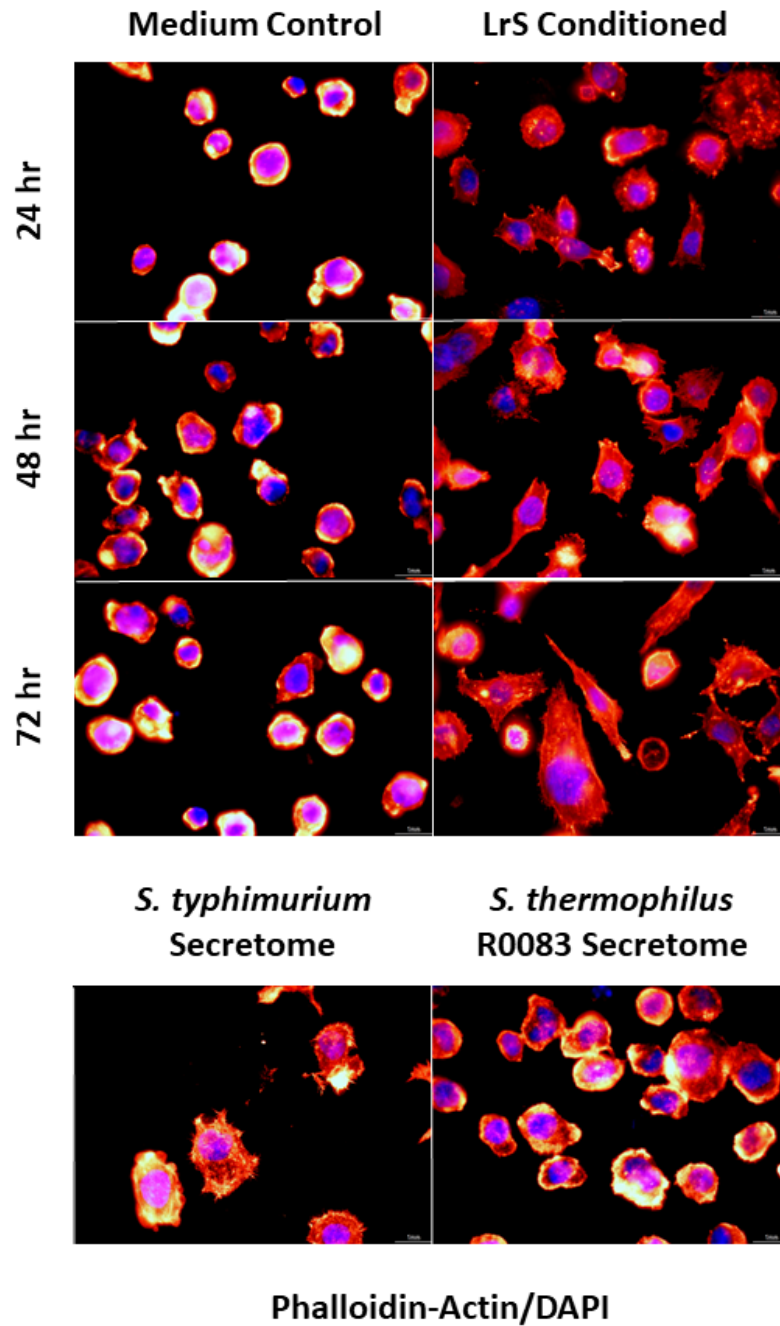


Figure 2-8. Conditioning with the LrS induces distinct morphological changes in THP-1 monocytes indicative of differentiation into a macrophage phenotype when compared to secretomes derived from *S. enterica* serovar Typhimurium and *S. thermophilus* R0083. Cells were stained with phalloidin-CF568 (red) and counterstained with DAPI (blue) and visualized at 100X magnification under oil immersion.

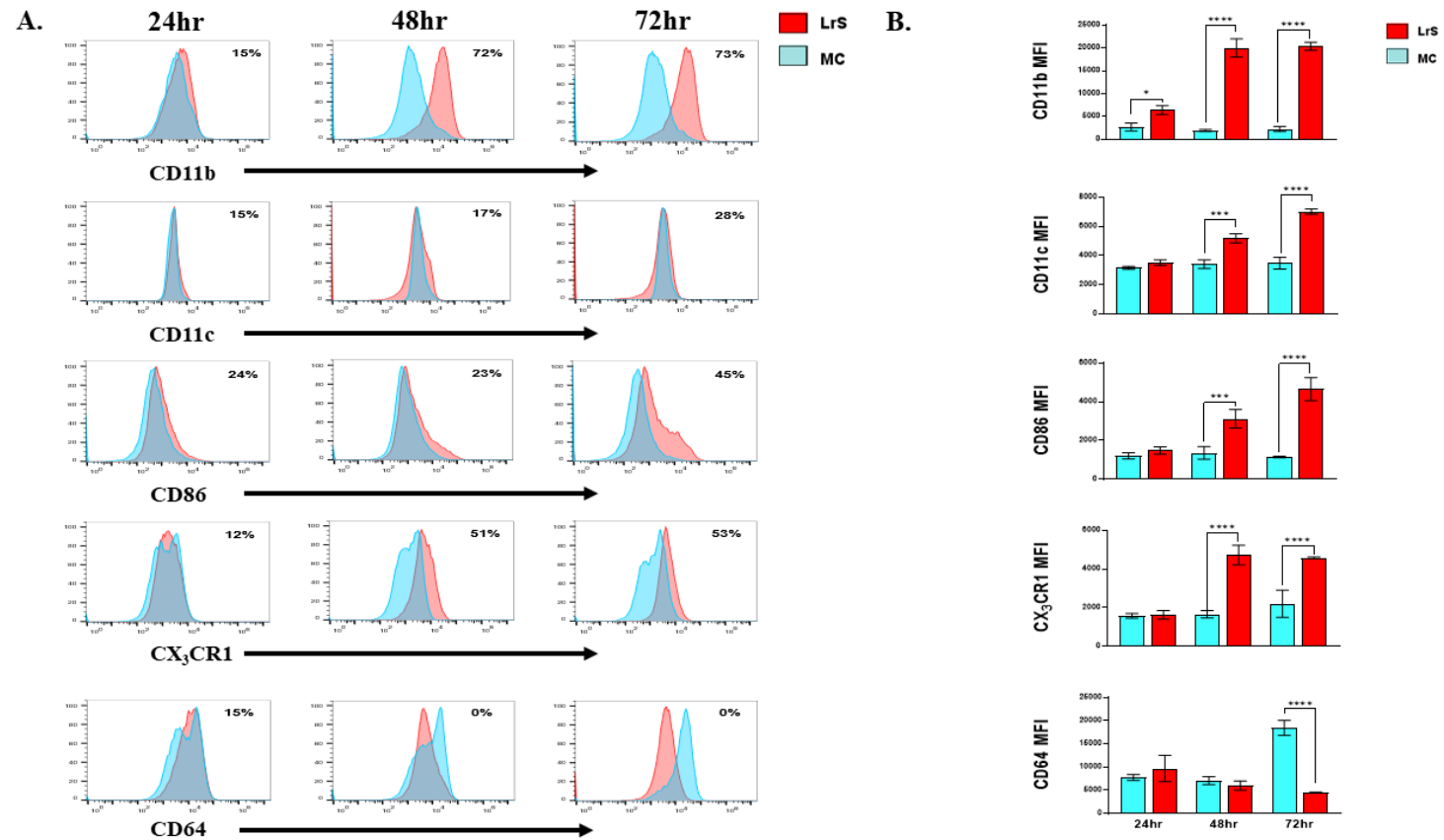
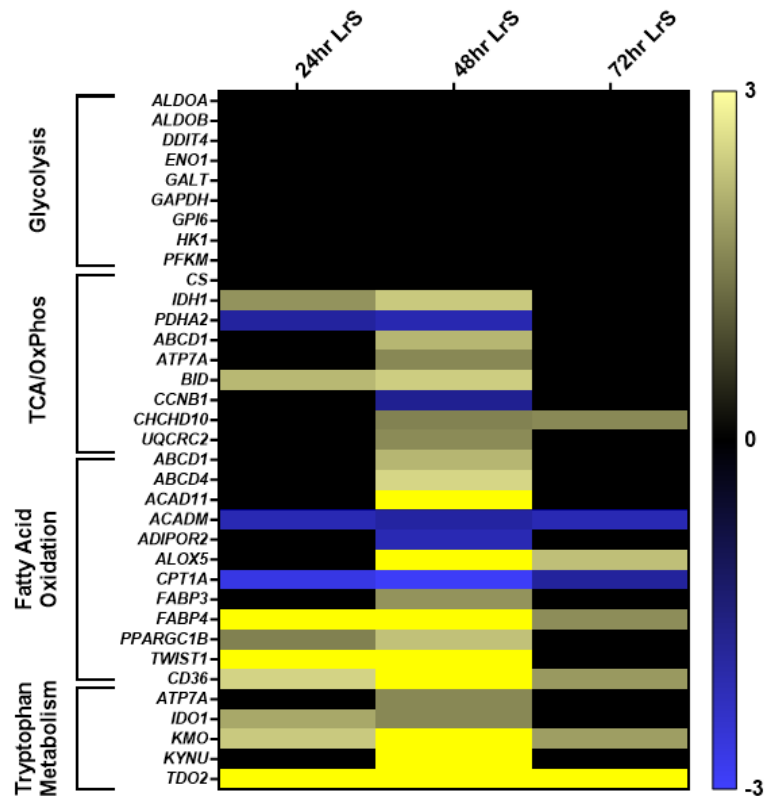


Figure 2-9. Conditioning with the LrS induces distinct morphological changes and increases the cell-surface expression of CD11b, CD11c, CX3CR1 and CD86 in THP-1 human monocytes. **A** Histogram Overton subtraction was used to determine the relative number of cells expressing CD11b, CD11c, CD86, CX3CR1, or CD64 following conditioning with the LrS (red) over untreated medium controls (MC; blue). **B.** Median fluorescence intensity (MFI) of THP-1 cells expressing CD11b, CD11c, CD86, CX3CR1, or CD64 was used to confirm the results of the histogram Overton subtraction. Data shown is the mean of the MFI \pm SEM ($n = 3$). Significance is indicated as * $p < 0.05$, ** $p < 0.01$, *** $p < 0.001$ as determined by one-way ANOVA and Tukey's post-hoc test.

A.



B.

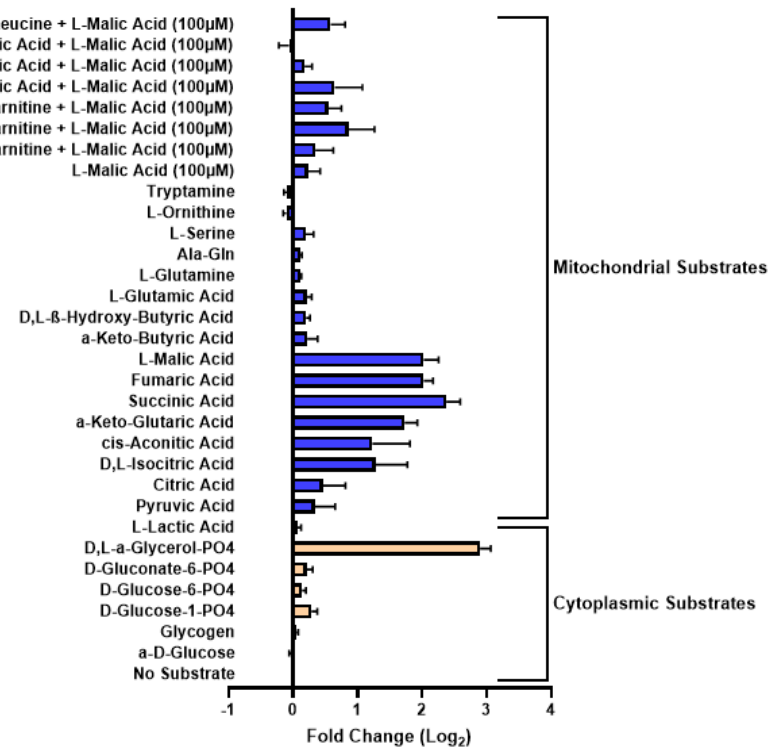


Figure 2-10. The LrS induces metabolic functional changes in THP-1 human monocytes. **A.** Temporal changes in the transcription of genes involved in glycolysis, fatty acid oxidation, oxidative phosphorylation, and tryptophan metabolism. **B.** Conditioning with the LrS results in different metabolic utilization signatures in THP-1 human monocytes. Data shown is the mean of the fold change (log₂) ± SEM of substrate utilization when compared to an untreated control over 24 hours (*n* = 3).

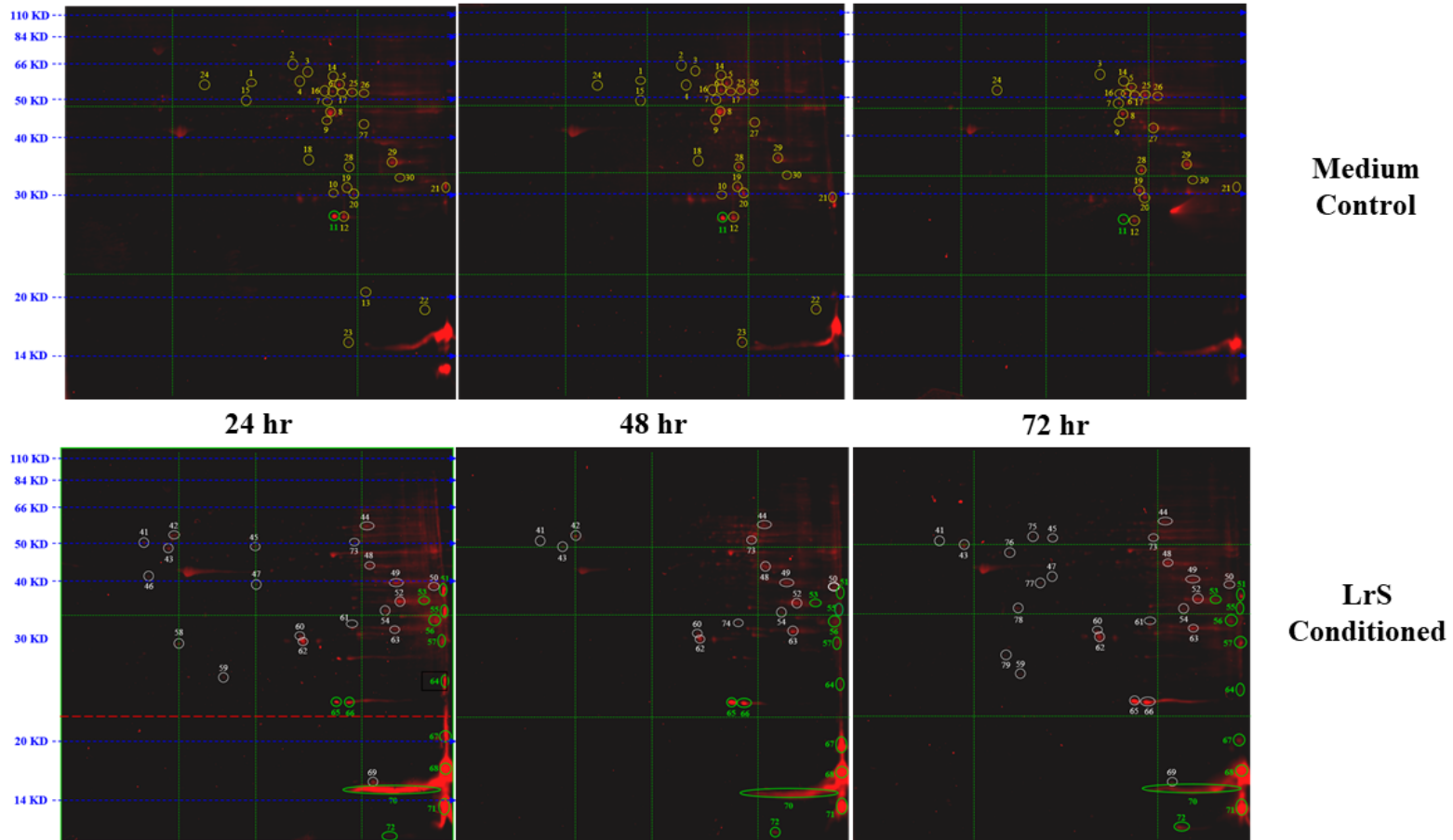


Figure 2-11. The LrS induces unique temporal changes in protein acetylation patterns in THP-1 human monocytes following conditioning for 24-, 48-, and 72-hours. 2-D Western Blots probed for anti-lysine acetylation identified unique protein acetylation patterns following LrS conditioning when compared to controls.

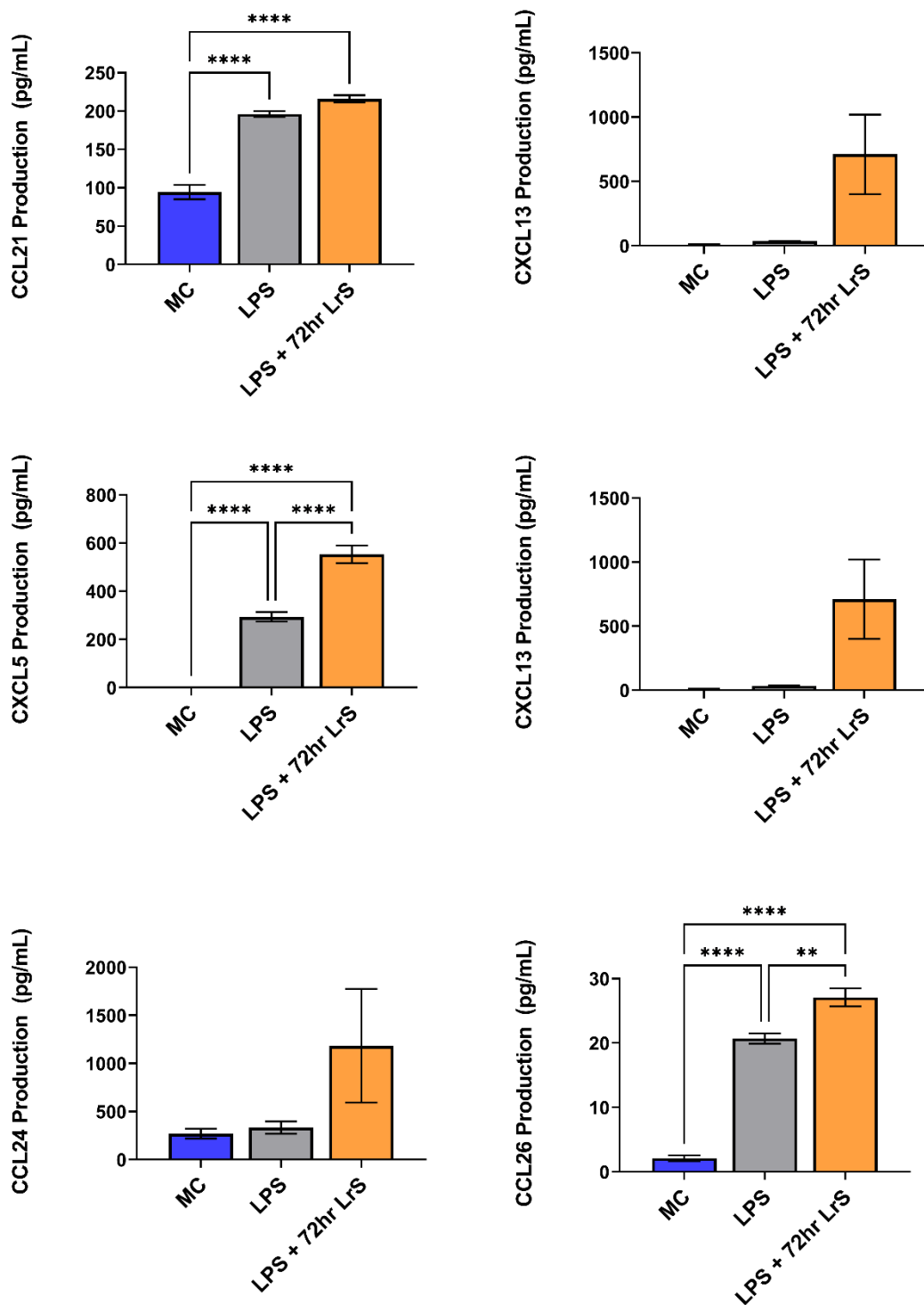
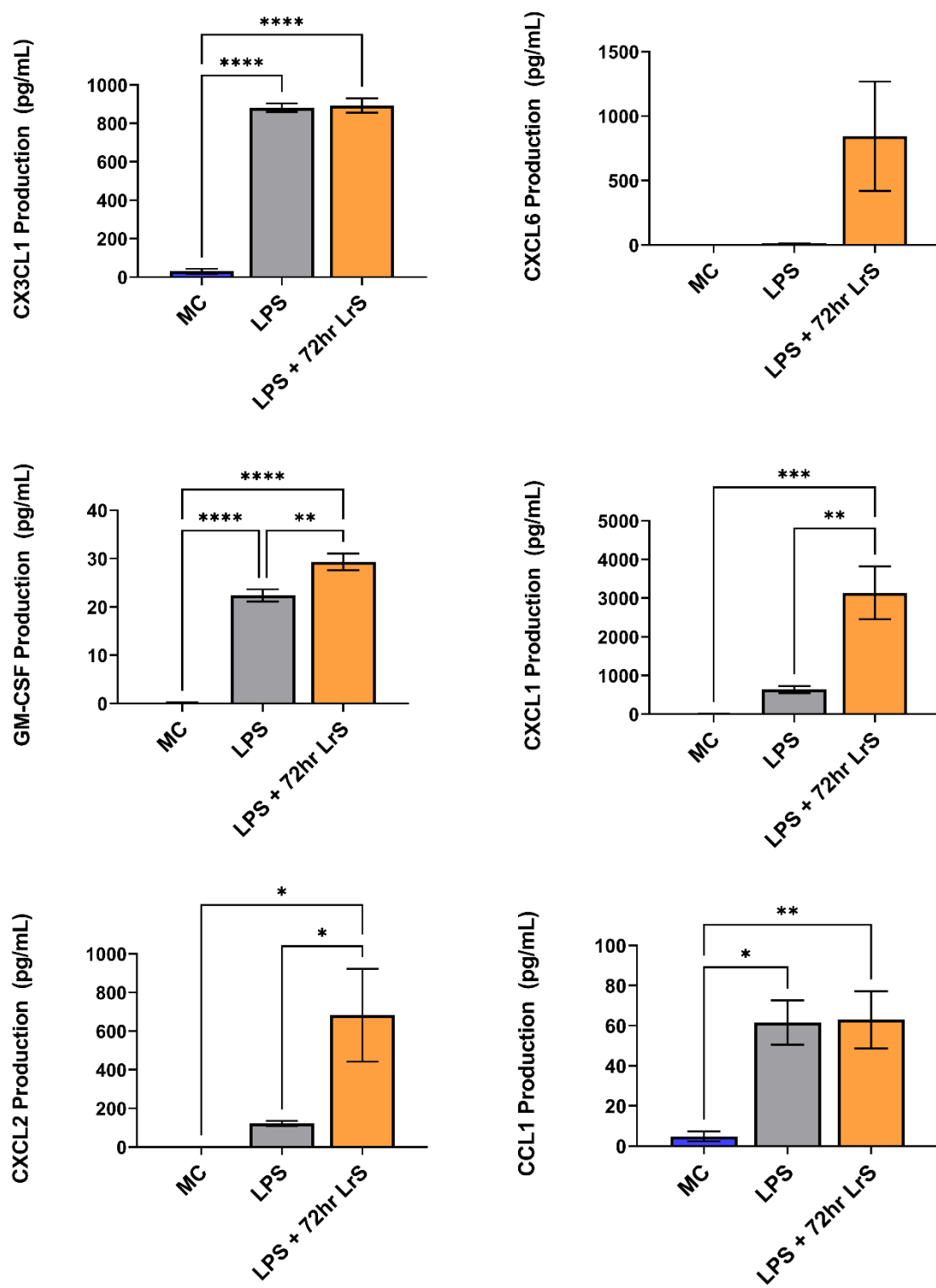
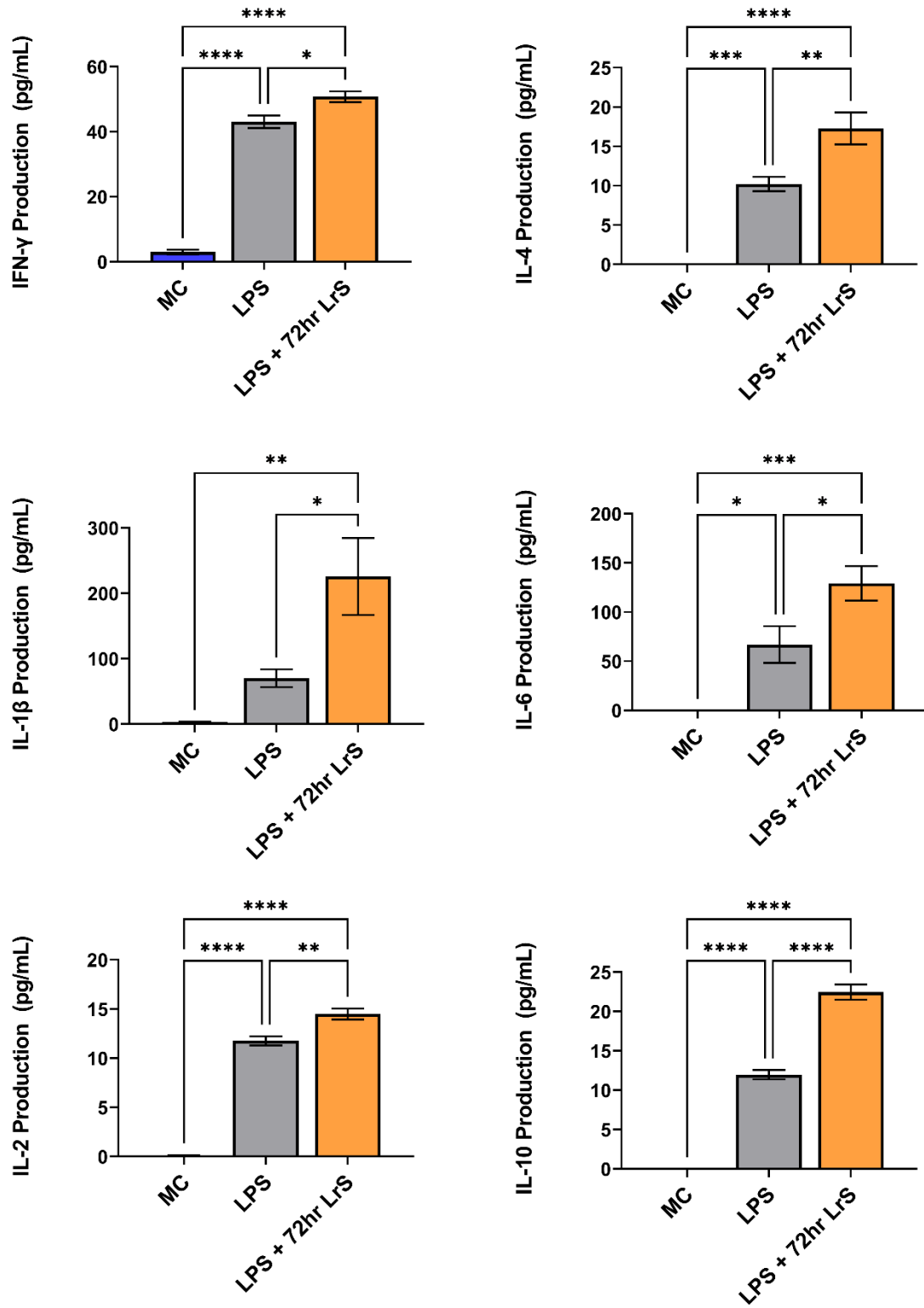


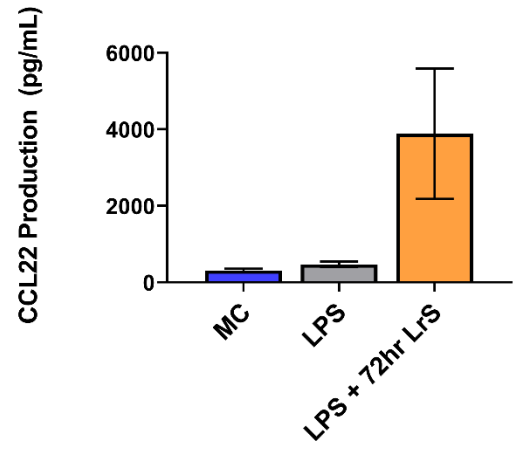
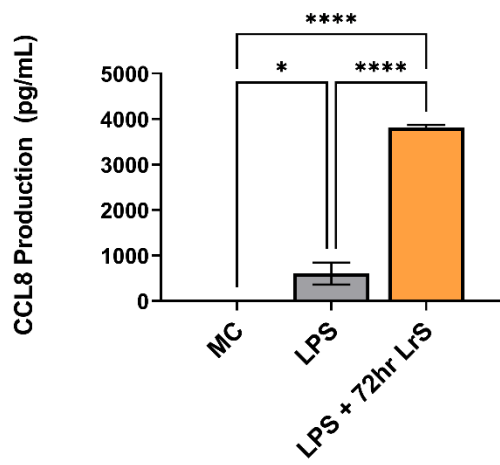
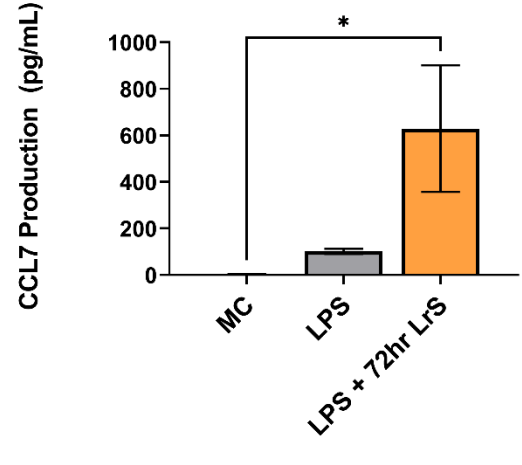
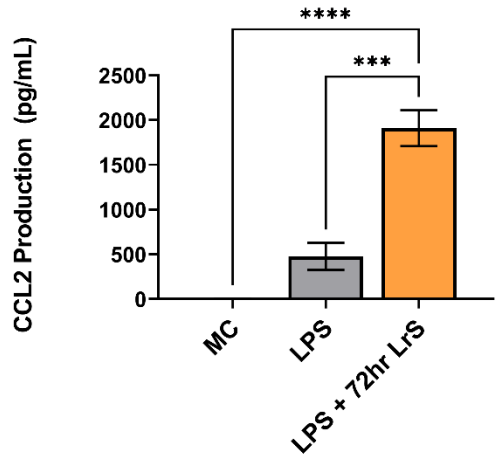
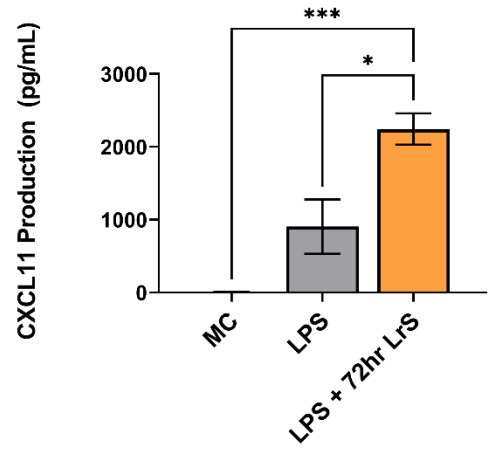
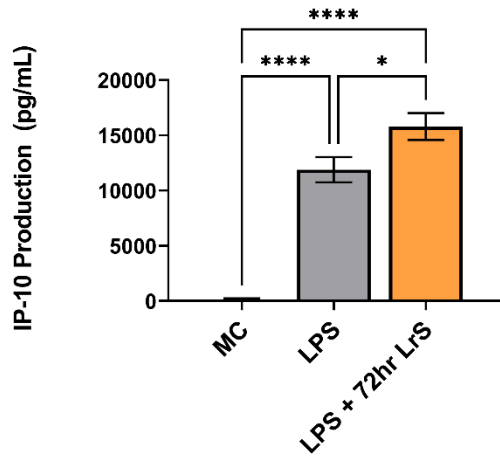
Figure 2-13. Cytokine and chemokine profiles from THP-1s conditioned with the LrS (20% v/v) 72-hours followed by challenge with LPS (125ng/mL) or LPS challenge alone for 6 hours. Data shown is the means cytokine/chemokine production (pg/mL) \pm SEM (n = 4). Significance is indicated as * p < 0.05, ** p < 0.01, *** p < 0.001 as determined by one-way ANOVA and Tukey's post-hoc test.



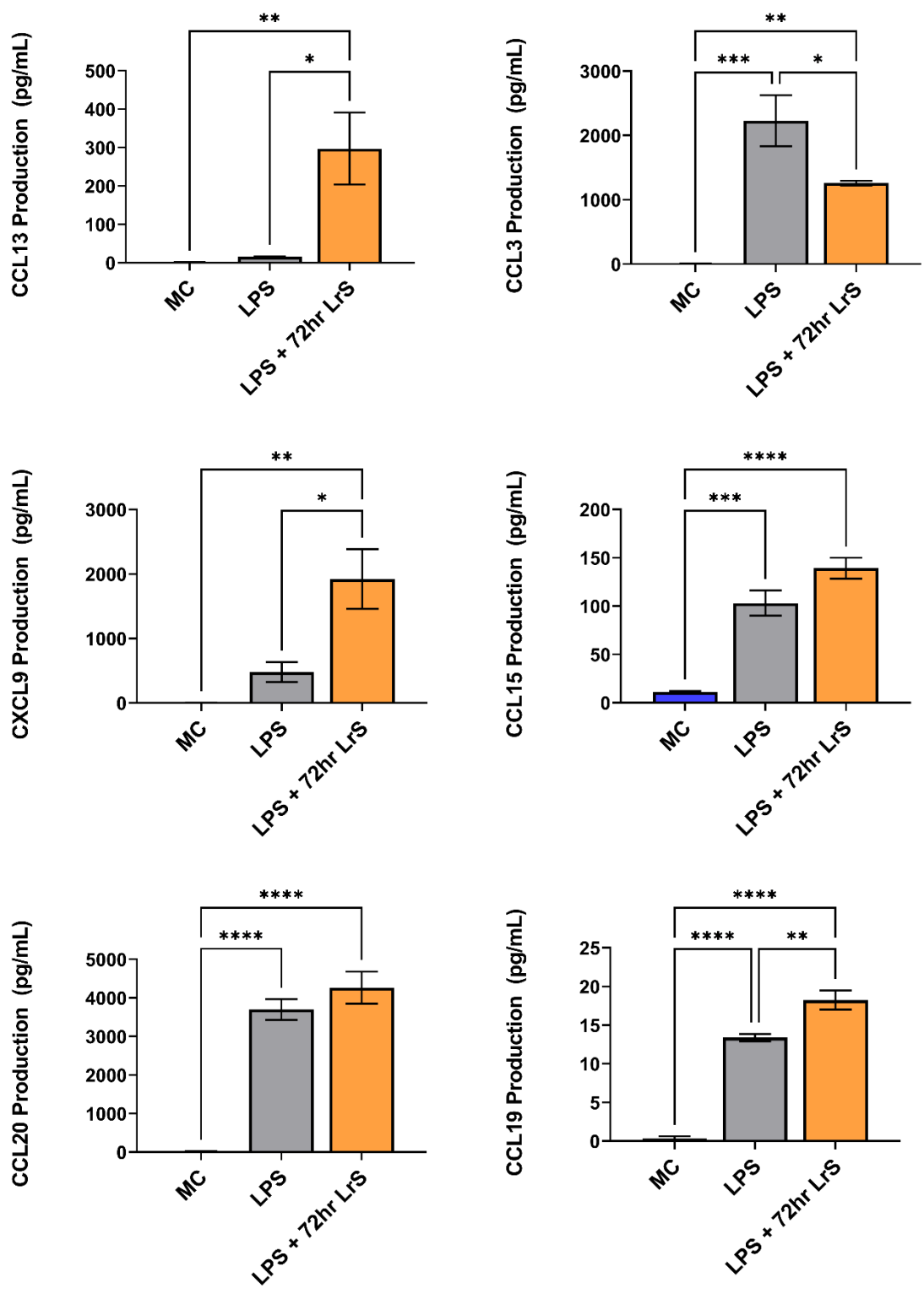
This is a continuation of Figure 2-13



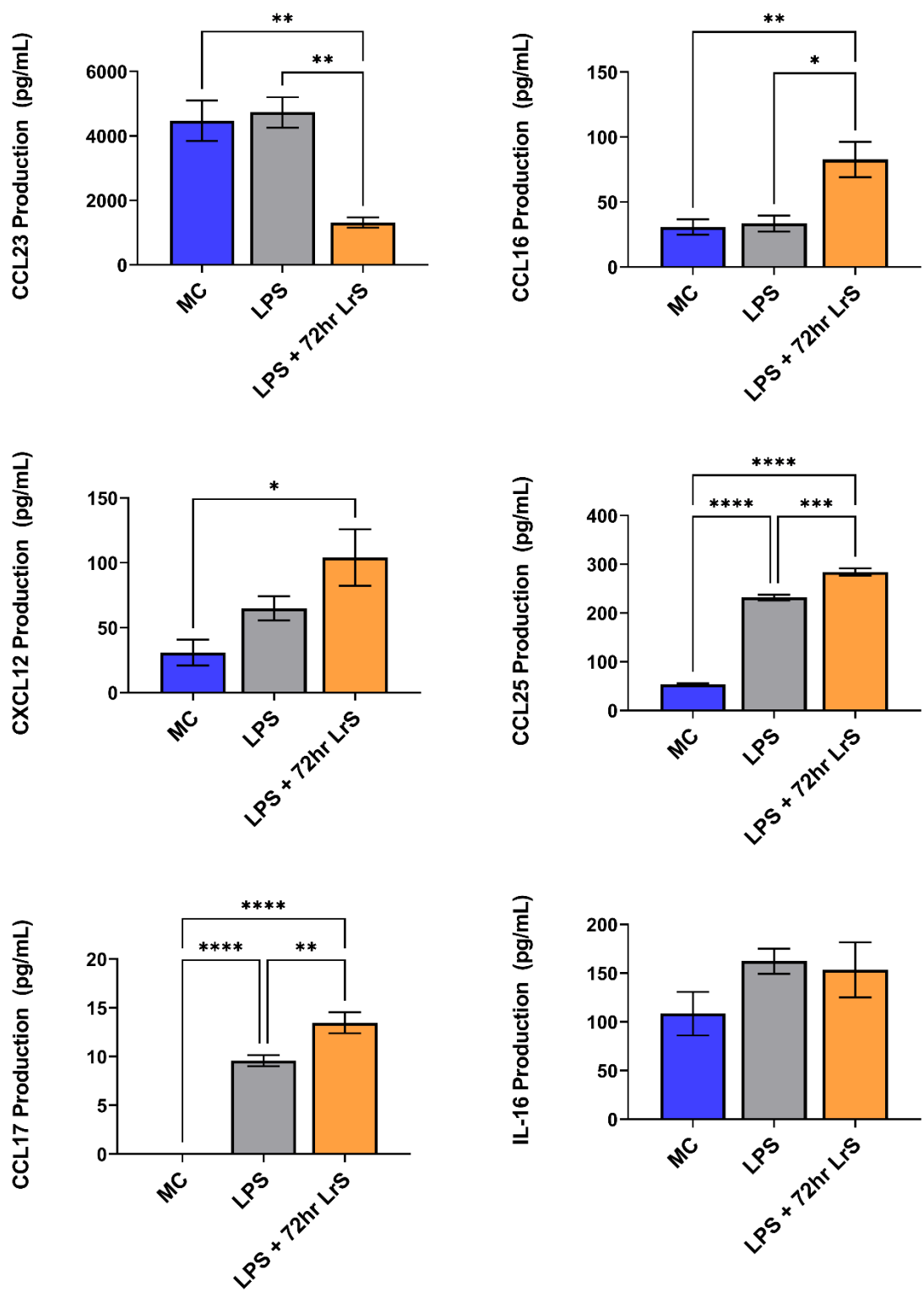
This is a continuation of Figure 2-13



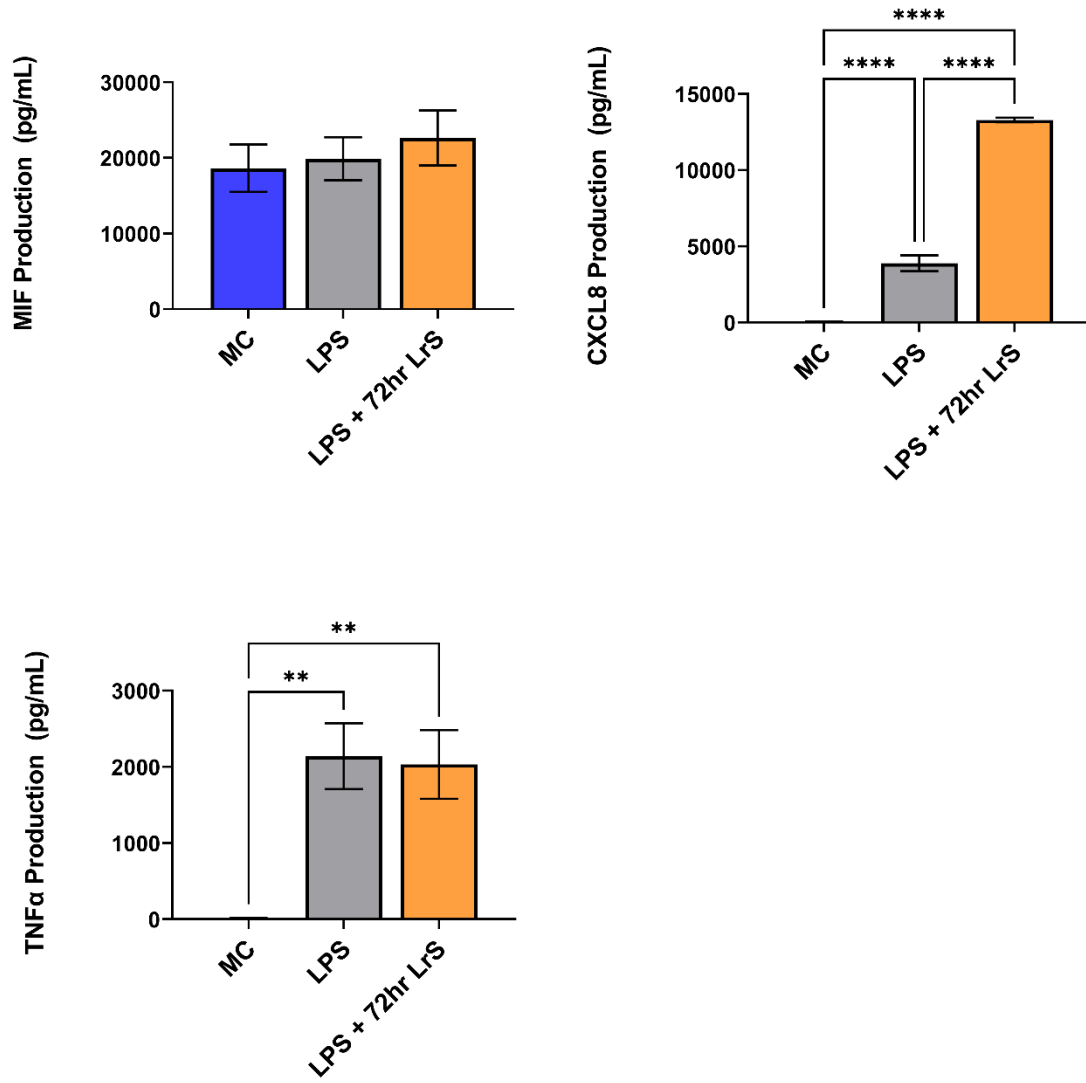
This is a continuation of Figure 2-13



This is a continuation of Figure 2-13



This is a continuation of Figure 2-13



This is a continuation of Figure 2-13

CHAPTER 3: *Lactocaseibacillus rhamnosus* R0011 secretome impact on immune outcomes in intestinal epithelial and antigen-presenting cell interactions using an *in vitro* co-culture system

3.1 Introduction

Interactions between IECs and APCs help to shape the immune outcomes of bidirectional host-microbe communication at the gut mucosal interface. While IECs provide a physical barrier between contents found within the intestinal lumen, they are also important mediators of host-microbe communication by integrating microbial-derived signals to the underlying APC populations (Goto, 2019; Peterson *et al.*, 2014). As the primary sensors of microbial activity within the gut, IECs have the capacity to induce antimicrobial and immunoregulatory activity within underlying APCs via signal transduction events following IEC PRR recognition of microbial components. Due to the constant barrage of microbial signals, IECs must tightly regulate their activation in order to maintain a state of homeostasis and reduce hyperresponsiveness to the normal gut microbiota (Burgueno *et al.*, 2020). For this reason, TLR expression is often limited to the basolateral side of polarized IECs, limiting the number of interactions with microbial components found within the luminal contents of the intestine. For example, TLR5, which is responsible for recognizing bacterial flagella, is typically only expressed on the basolateral side of polarized IECs (Gewirtz *et al.*, 2001). This enables IECs to only respond to flagellated bacteria if there is a breakdown of the epithelial barrier or translocation of the bacterium across the epithelial barrier, necessitating the need for a robust inflammatory response from the surrounding immune cell population to clear out the invading bacteria. The consequences of TLR recognition of microbial contents can also be dependent on

whether the ligand is recognized on the apical or basolateral side of polarized IECs (Abreu, 2010). TLR9, which recognizes unmethylated CpG DNA sequences, is expressed on both the apical and basolateral side of polarized IECs. When TLR9 is activated on the apical surface of IECs, there is a muted response with the activation of genes involved in the regulation of NF- κ B signaling, whereas basolateral recognition of CpG DNA induces the activation of classical NF- κ B signaling (Lee *et al.*, 2006), reinforcing the importance of examining immune outcomes in the context of polarized IECs and spatial compartmentalization of PRR-induced signaling within the gut.

IECs express tight junction proteins including the occludins, claudins, zonula occludens (ZO), and junctional adhesion molecules which work in concert to prevent the paracellular transport of intestinal luminal contents into the basolateral side of the epithelium (Gunzel *et al.*, 2013; Suzuki, 2013). These proteins are tightly regulated and are key cellular players in the maintenance of normal barrier integrity and function (Harhaj *et al.*, 2004; Karczewski *et al.*, 2000; Marchiando *et al.*, 2010). As such, perturbations in their activity can lead to the breakdown of the gut epithelial barrier resulting in the activation of dysregulated immune activity within the underlying APC population and the potential for dissemination of luminal contents and bacteria into systemic circulation. Certain pro-inflammatory cytokines, such as IFN- γ , can act to increase intestinal barrier permeability by reducing ZO-1 expression and localization (Scharl *et al.*, 2009), while some gut-associated pathogens, such as *S. enterica* serovar Typhimurium, can also produce virulence factors which selectively disrupt ZO-1 and other tight junction proteins allowing for their translocation across the intestinal barrier (Boyle *et al.*, 2006; Tafazoli *et al.*, 2003). Commensal microorganisms and LAB have been shown to strengthen epithelial barrier

integrity, a mechanism believed to be used by these bacteria to enhance their capacity for host colonization, and to antagonize the detrimental impacts of certain gut-associated pathogens on the gut epithelium (Madsen, 2012; Ohland *et al.*, 2010). Although most studies examining the impacts of gut-associated bacteria on gut epithelial barrier integrity have focused on direct interactions between live bacteria and IECs, some have suggested a role of microbial-derived metabolites and soluble components in this context. For example, *E. coli* Nissle 1917 conditioned media increased Caco-2 IEC monolayer integrity (Stetinova *et al.*, 2010) and secreted peptides from *Bifidobacterium infantis* reversed TNF- α and IFN- γ -induced IEC barrier damage (Ewaschuk *et al.*, 2008).

In vitro approaches to study the interactions between epithelial cells and APCs have relied on the use of Transwell cell culture inserts. These cell culture inserts allow for the examination of gut barrier integrity and function by measuring the transport of apically delivered ions and other macromolecules across a monolayer of IECs grown on a microporous membrane (Donato *et al.*, 2011). To achieve this, IECs are cultured until a polarized monolayer is formed within the Transwell insert, creating distinct apical and basolateral compartments *in vitro*. IEC barrier function and permeability can then be readily studied following cell challenge by measuring the transepithelial electrical resistance (TER) and the flux of a fluorescently labelled sugar of known molecular weight across the IEC monolayer (Harhaj *et al.*, 2004). T84 human IECs are a widely used cell line for *in vitro* study of IECs, and do not easily differentiate into a heterogenous cell population with altered phenotypic characteristics following polarization into a confluent monolayer, making them an ideal tool for studying IEC barrier function and permeability in response to cell challenge (Dharmasathaphorn *et al.*, 1990; Donato *et al.*, 2011; Hillgren

et al., 1995). To facilitate the study of IEC and APC interactions with bacteria, APCs can be cultured in the basolateral chamber and bacteria and their soluble components can be administered into the apical chamber following IEC monolayer formation to simulate interactions found within the gut-mucosal interface. This presents an ideal *in vitro* system to study the dynamics of microbe-mediated immune communication in the context of IEC and APC interactions.

3.2 Objectives

As discussed in **Chapters I and II**, the LrS has the capacity to modulate immune outcomes in both human IECs and APCs with transcriptional and cytokine/chemokine profiling revealing context-dependant and cell-type specific immunomodulatory activity of the LrS. However, many questions remain about the LrS in regulating host immune outcomes in the context of IEC and APC interactions. To date, most studies examining the effects of LAB and their secreted products have focused on host immune responses using a single cell type (IEC or APC) *in vitro* and therefore do not necessarily reflect the impact these bacteria may have on interactions between these key innate immune cell types within the host. Recent evidence also suggests that the effects of LAB and their secreted factors can be very different when tested in co-cultures of human IECs and APCs (Bermudez-Brito *et al.*, 2015). As such, it is important to examine the immunomodulatory impacts of the LrS using co-cultures of human IECs and APC (**Figure 3-1**). Analysis of the effects of the LrS in Transwell systems using co-cultures of human IECs and APCs provides an appropriate approach to determine the impact of the LrS and its mechanisms of action in a context which more closely mimics that which occurs *in vivo*.

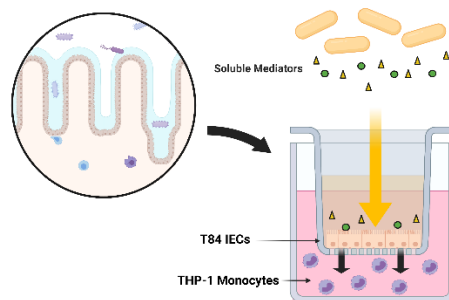


Figure 3-1. Transwell *in vitro* co-culture systems allow for the investigation of interactions between bacteria, IECs, and APCs in an environment which closely mimics the intestinal environment.

3.3 Materials and Methods

Bacterial Culture

Lyophilized *Lactobacillus rhamnosus* R0011 was obtained from RIMAP (Montreal, Quebec, Canada). The LrS was prepared as previously described (Jeffrey *et al.*, 2018). Briefly, bacteria were grown in deMan, Rogosa and Sharpe (MRS) medium (Difco, Canada) at 37°C for 17 hours in a shaking incubator and then diluted in non-supplemented RPMI-1640 medium and allowed to further propagate for an additional 23 hours under the same conditions. Both the bacterial culture and controls were centrifuged at 3000 x g for 20 minutes and filtered through a 0.22 µm filter (Progene, Canada) to remove any bacteria. The filtered supernatant samples were also subjected to size fractionation using < 10 kDa Amicon Ultra – 15 centrifugal filter (EMD Millipore, MA, USA).

For preparation of the STS, bacteria were propagated overnight in tryptone soya broth (Oxoid) in a shaking incubator at 37°C. Overnight cultures were centrifuged at 3000 X g for 20 minutes at 4°C and filtered through a 0.22 µm filter and the secretome was stored at -80°C.

Cell Culture and Challenge Assay and RNA extraction

The T84 human colorectal carcinoma cell line was obtained from the American Type Culture Collection (ATCC, #CCL-248) and was maintained in DMEM/F-12 medium supplemented with 10% bovine calf serum and 0.05 mg/mL gentamicin (Sigma-Aldrich, MO, USA) and were grown in 75 cm² tissue culture flasks (Greiner-Bio-One, NC, USA) at 37°C, 5% CO₂ in a humidified incubator (Thermo Fisher, MA, USA) as described previously (Jeffrey *et al.*, 2018). T84s IECs were enumerated and viability determined

using Trypan Blue following sub-culturing. Cells were then resuspended in complete culture medium (DMEM/F-12 medium supplemented with 10% bovine calf serum and 0.05 mg/mL gentamicin) and 1.0×10^6 cells were seeded into 12-well Millicell hanging cell culture inserts with a pore size of $0.4 \mu\text{m}$ (EMD Millipore, MA, USA). This pore size was selected to allow for direct and indirect cellular communication as mediated by cytokines/chemokines and other small molecules while preventing the movement of cells through the Transwell. To obtain polarized confluent monolayers, seeded T84 IECs were incubated at 37°C , 5% CO_2 in a humidified incubator for 7 days, or until a minimum TER of $1000\Omega\text{cm}^2$ as described previously (Sherman *et al.*, 2005). T84 IEC cell culture medium was aspirated and replaced with fresh non-supplemented (no calf serum) DMEM/F12 medium containing the LrS, the STS (1% v/v), or a combination of these secretome challenges in the apical chamber of the hanging cell culture and THP-1 human monocyte cells were then added to the basolateral chamber at a concentration of 1×10^6 cells/mL for 24 hours. For some challenges, cells were also cultured with an antibody specific for human MIF (AF-289-PB) ($0.05\mu\text{g/mL}$) (R&D Systems) or with goat IgG isotype controls (AB-108-C) ($0.05\mu\text{g/mL}$) (R&D Systems). This anti-MIF antibody has been used successfully to block the activity of MIF produced by IECs (Man *et al.*, 2008) Following challenge, supernatants were collected from both the apical and basolateral sides of the Transwell inserts. TER measurements were done in triplicate using the Millicell ERS-2 Voltohmmeter (Millipore Sigma, MA, USA) to determine changes in epithelial monolayer integrity compared to controls and initial readings. Total RNA was also harvested after exposure to the various challenges from both T84 IECs and THP-1 human monocytes using the phenol-based TRIzol method of RNA extraction (Chomczynski, 1993) following manufacturer's

protocols (ThermoFisher Scientific, MA, USA). Briefly, Transwell inserts were removed from the tissue culture plate, rinsed and transferred into a new 12-well tissue culture plate and 1 mL of TRIzol reagent was added to the Transwell insert to lyse the T84 IECs. THP-1 cells found within the basolateral chamber were collected and 1 mL of TRIzol reagent was added to lyse the cells. Cell culture homogenates were added to Phase Lock Gel-Heavy tubes for phase separation of total RNA. Total extracted RNA was then purified using the RNeasy Plus Mini Kit (Qiagen, Hilden, Germany). The purity and quality of RNA was determined using a BioDrop Duo Spectrophotometer.

Paracellular Flux Measurement

To determine the impact of the LrS or the STS on the permeability of T84 IEC monolayers, the flux of FITC-dextran across the epithelial monolayer was determined. T84 monolayers were washed with Hank's Balanced Salt Solution (HBSS) (Millipore Sigma). Following washing, HBSS was added into the apical and basolateral chambers of the hanging cell culture insert and allowed to equilibrate for 30 minutes in a 37°C, 5% CO₂ humidified incubator. The HBSS in the apical chamber was then replaced with HBSS containing 1mg/mL of 4 kDa FITC-dextran (Millipore Sigma) and allowed to incubate for 1 hour. Following incubation, a sample from the basolateral chamber was taken and placed into a black 96-well plate and fluorescence was quantified using a Synergy HT Microplate Reader (BioTek Instruments) set to 485/20 excitation and a 535/20 emission filter pair and a PMT sensitivity of 55. A FITC-dextran standard was used to quantify the concentration of FITC-dextran crossing the epithelial monolayer. This was repeated every hour for a total of 6 hours and the transepithelial flux was determined by taking the average concentration

of FITC-dextran and dividing by the surface area of the hanging cell culture insert; this was expressed as nM/cm²/h (Sanders *et al.*, 1995).

Comparative RT-qPCR

DNase-treated RNA (1µg) from controls and each challenge were reverse transcribed with Superscript IV following manufacturer's protocols as previously described (Macpherson *et al.*, 2014). Reverse-transcribed cDNA was diluted 1:4 prior to amplification and 2.5 µl of diluted cDNA was used with SsoAdvanced Universal SYBR Green Supermix (Bio-Rad, CA, USA) in RT-qPCR. Gene-specific primers for targets identified as being potentially important in LrS-mediated impacts on IEC and THP-1 monocyte activity as described in **Chapters I and II (Table 3-I)** were used. An initial incubation of 5 min at 95°C was performed, followed by 40 cycles consisting of template denaturation (15 s at 95°C) and one-step annealing and elongation (30 s at 60°C), with a Bio-Rad CFX Connect instrument (Bio-Rad, CA, USA). Four biological replicates were analyzed for each gene tested, and fold change expression levels were normalized to the expression levels of two reference genes for T84 IECs (*RPLPO* and *B2M*) and THP-1 monocytes (*RPL37A* and *ACTB*) and negative controls using Bio-Rad CFX Manager 3.1 software.

Morphological Characterization

Changes in T84 IEC monolayer integrity following challenge with the LrS or the STS was visualized by staining ZO-1 with an anti-ZO-1 monoclonal antibody (ZO1-1A12) conjugated with Alexa Fluor 488 (ThermoFisher), following manufacturing protocols. Briefly, following conditioning, cells were fixed with 3.75% formaldehyde, permeabilized

with 0.5% Triton X-100, and stained with anti-ZO for 2 hours at room temperature. Cells were counter-stained and mounted using ProLong™ Diamond Antifade Mountant with DAPI (ThermoFisher Cat #: P36966).

Cytokine/Chemokine/Inflammatory Marker Analysis

Cell culture supernatants from both the apical and basolateral chambers of the hanging cell culture inserts were collected following 24 hours of challenge in order to allow sufficient time for the production of key inflammatory cytokines and chemokines and to determine directionality of cytokine release. Cytokine and chemokine profiling was performed using the Bio-Plex Pro™ 40-Plex Human Chemokine Panel (Bio-Rad #171ak99mr2) and the Bio-Plex Pro™ Human Inflammation Panel 1, 37-Plex (Bio-Rad #171AL001M). All 40 chemokines (CCL21, BCA-1 / CXCL13, CTACK / CCL27, ENA-78 / CXCL5, Eotaxin / CCL11, Eotaxin-2 / CCL24, Eotaxin-3 / CCL26, Fractalkine / CX3CL1, GCP-2 / CXCL6, GM-CSF, Gro- α / CXCL1, Gro- β / CXCL2, I-309 / CCL1, IFN- γ , IL-1 β , IL-2, IL-4, IL-6, IL-8 / CXCL8, IL-10, IL-16, IP-10 / CXCL10, I-TAC / CXCL11, MCP-1 / CCL2, MCP-2 / CCL8, MCP-3 / CCL7, MCP-4 / CCL13, MDC / CCL22, MIF, MIG / CXCL9, MIP-1 α / CCL3, MIP-1 δ / CCL15, MIP-3 α / CCL20, MIP-3 β / CCL19, MPIF-1 / CCL23, SCYB16 / CXCL16, SDF-1 α + β / CXCL12, TARC / CCL17, TECK / CCL25, TNF- α) or 37 cytokines (APRIL/TNFSF13, BAFF/ TNFSF13B, sCD30/TNFRSF8, sCD163, Chitinase-3-like 1, gp130/sIL-6R β , IFN- α 2, IFN- β , IFN- γ , IL-2, sIL-6R α , IL-8, IL-10, IL-11, IL-12 (p40), IL-12 (p70), IL-19, IL-20, IL-22, IL-26, IL-27 (p28), IL-28A/IFN- λ 2, IL-29/IFN- λ 1, IL-32, IL-34, IL-35, LIGHT/TNFSF14, MMP-1, MMP-2, MMP-3, Osteocalcin, Osteopontin, Pentraxin-3, sTNF-R1, sTNF-R2, TSLP, TWEAK/TNFSF12) were multiplexed on the same 96-well plate. Chemokine/cytokine

standards were serially diluted and chemokine profiling from all cell challenges was done following manufacturer's instructions (Bio-Rad, CA, USA) with 4 biological replicates. Quality controls were also included to ensure the validity of the concentrations that were obtained. The Bio-Plex ManagerTM software was used to determine the concentration of the analytes within each sample using the generated standard curves and concentration was expressed in pg/mL (concentration in range). Statistical analysis was done using GraphPad Prism's (Version 8) one-way analysis of variance (ANOVA) and Tukey's multiple comparison test when the ANOVA indicated significant differences were present. All data are shown as the mean pg/mL \pm standard error of the mean (SEM). Z-scores were determined and visualized using R version 4.0.0 and package Bioconductor to determine the overall impact of each challenge on cytokine and chemokine production from T84 IEC and THP-1 monocyte co-cultures.

3.4 Results

The LrS attenuates STS-induced pro-inflammatory cytokine and chemokine production from T84 IEC and THP-1 APC co-cultures

Cytokine and chemokine profiling of IEC and APC co-cultures was done to determine whether apically delivered LrS and STS could alter functional immune outcomes in co-cultures of T84 IEC monolayers and THP-1 human monocytes. STS-challenge resulted in increased production of CCL1, CCL15, CCL20, CCL21, CCL24, CCL26, CX3CL1, CXCL1, CXCL2, CXCL8, CXCL10, CXCL11, CXCL16, IFN- γ , TNF- α , TNFSF13, TNFSF13B, C3L1, and gp130/sIL-6R β into the apical chamber of the co-culture system when compared to controls ($n = 4$; $p < 0.05$) (**Figures 3-2 and 3-3**). This correlated with increased production of CCL15, CCL21, CCL23, CCL27, CX3CL1, GM-CSF, CXCL1, CXCL8, IFN γ , IL-6RA, IL-16, and C3L1 found within the basolateral chamber of the co-culture system when compared to controls, suggesting that the STS has the capacity to influence immune effector function of cells found beneath an IEC monolayer ($n = 4$; $p < 0.05$) (**Figures 3-2 and 3-3**). In contrast, challenge with the LrS only resulted in increased apical production of CD163, IL-32, IL-34, MIF and TNFR2, with no significant impact on cytokines and chemokines found within the basolateral chamber ($n = 4$; $p < 0.05$) (**Figures 3-2 and 3-3**). Challenge of IEC-APC co-cultures with a combination of the STS and LrS resulted in attenuation of all STS-induced pro-inflammatory mediator production to constitutive levels in both the apical and basolateral chambers of the co-culture system, indicating that apically-delivered LrS can attenuate STS-induced inflammatory mediator production in co-cultures of IECs and APCs ($p < 0.05$; **Figures 3-2 and 3-3**).

The LrS attenuates STS-induced pro-inflammatory gene expression in T84 IECs and THP-1 monocytes

Analysis of changes in gene-expression profiles in co-cultures of T84 IECs and THP-1 monocytes in response to challenge with the LrS or the STS was carried out to interrogate potential mechanism(s) of action behind the immunomodulatory activity of the LrS observed in individual cell populations. Consistent with the results obtained from the cytokine/chemokine profiling, STS-challenge of T84 IECs resulted in increased transcription of *CXCL8* ($n = 3; p < 0.05$) (**Figure 3-4**), an effect also seen in the underlying THP-1 monocyte cell population (**Figure 3-5**). STS-challenge also up-regulated the transcription of *NFκB1*, a key transcription factor in the NF-κB signalling complex, in T84 IECs ($n = 3; p < 0.05$) and THP-1 monocytes ($n = 3; p < 0.05$) (**Figure 3-4** and **3-5**). Interestingly, STS challenge down-regulated the expression of *ZO-1*, a gene encoding a tight-junction associated protein, indicating that the STS may be impacting tight-junctions within T84 IEC monolayers ($n = 3; p < 0.05$) (**Figure 3-4**). Concurrent challenge of co-cultures of T84 IECs and THP-1 monocytes with the LrS and the STS resulted in the attenuation of STS-induced transcription of *CXCL8* and *NFκB1* in both T84 IECs and THP-1 monocytes, coupled with increased transcription of *ZO-1* and of *ATF3* and *DUSP1*, negative regulators of innate immunity, in T84 IECs ($n = 3; p < 0.05$) (**Figures 3-4 and 3-5**). Moreover, concurrent challenge of co-cultures of T84 IECs and THP-1 monocytes with the LrS and the STS up-regulated the expression of *ZFP36L1*, *CD36*, and *ATF3* in the underlying THP-1 monocyte cell population when compared to STS- or LrS-challenge alone ($n = 3; p < 0.05$) (**Figure 3-5**).

The LrS reverses STS-induced damage to T84 IEC monolayer integrity via increased MIF production

To further interrogate potential underlying mechanism(s) of action behind the observed bioactivity of the LrS in the context of STS challenge within a co-culture system, the impact of the LrS and STS on IEC barrier integrity and permeability was determined. The LrS had no significant impact on TER measurements of T84 IEC monolayers, with no significant changes to the paracellular flux of FITC-dextran when compared to controls ($n = 4; p > 0.05$) (**Figure 3-6**), indicating no detrimental impacts on IEC monolayer integrity and permeability. In contrast, T84 IECs challenged with the STS had a significantly lower TER measurement than cells incubated with the LrS ($n = 4; p < 0.05$) (**Figure 3-6A**), confirming the results obtained by RT-qPCR analysis which indicated that the STS reduced the expression of tight junction proteins. This correlated with significantly higher amounts of paracellular flux of FITC-dextran when compared to controls and cells challenged with the LrS ($n = 4; p < 0.05$) (**Figure 3-6**), indicating overall deleterious impacts of the STS on IEC monolayer function and integrity. Co-challenge of STS-challenged T84 monolayers with the LrS resulted in no significant alterations in TER or paracellular flux, suggesting that the LrS can antagonize the negative impacts of STS-challenge on IEC monolayer integrity ($n = 4; p < 0.05$) (**Figure 3-6**). Morphological changes in T84 monolayers confirmed these findings as T84 IECs challenged with the STS displayed broken tight junctions via reduced expression of ZO-1 (**Figure 3-7**). In contrast, T84 IECs challenged with the LrS or co-challenged with both the STS and LrS had intact tight junctions (**Figure 3-7**). The addition of a MIF neutralizing antibody abrogated the observed bioactivity of the LrS on STS-challenged T84 IEC barrier integrity and function (**Figure 3-8**), suggesting

that LrS-induced MIF production may play a protective role in maintaining IEC barrier integrity.

3.5 Discussion

Interactions between IECs and the underlying APC population work in concert to shape immune responses to apically sensed bacteria and their soluble mediators. While evidence suggests that certain LAB and gut-associated pathogenic bacteria or their soluble mediators can influence host immune outcomes in single cell *in vitro* cell cultures, less is known about their impacts on IEC and APC co-cultures. Moreover, the impact of soluble mediators derived from both LAB and gut-associated pathogens on IEC monolayer integrity and subsequent activity on the underlying APC population remains unknown, with recent evidence suggesting that this is an important route of host-microbe immune communication within the GALT. Based on earlier observations described in **Chapters I** and **II**, the ability of the LrS to influence immune outcomes in co-cultures of IECs and APCs was examined to determine if the LrS retains bioactivity in a context which more closely mimics that which occurs *in vivo*.

Cytokine and chemokine profiling revealed that LrS challenge induced a muted response from T84 IEC and THP-1 monocyte co-cultures, with no significant changes in the production of cytokines and chemokines from THP-1 monocytes found within the basolateral chamber of the co-culture system. However, the LrS induced the production of IL-32 into the apical compartment of the co-culture system. Although IL-32 has been associated with the pathophysiology of inflammatory bowel disease (Khawar *et al.*, 2016), evidence suggests that it may also play an immunoregulatory role in the progression of disease. For example, IL-32 can inhibit TNF- α -induced IL-8 production by inhibiting the translation of IL-8 mRNA into functional protein through an unknown mechanism (Imaeda *et al.*, 2011). LrS challenge also induced the production of MIF by T84 IECs into the apical

chamber, a result consistent with that seen previously in HT-29 IECs challenged with the LrS (Jeffrey *et al.*, 2020), indicating that LrS-induced MIF production is not limited to HT-29 IECs. As discussed in **Chapter I**, MIF has pleiotropic roles in regulating immune outcomes in IECs. However, MIF also plays an integral role in initiating inflammatory responses in APCs through NLRP3 inflammasome activation and subsequent release of inflammatory mediators (Lang *et al.*, 2018). Interestingly, LrS challenge did not increase MIF secretion into the basolateral chamber or induce MIF production from THP-1 monocytes, suggesting that LrS-induced MIF production is spatially compartmentalized into the apical chamber, limiting potential activation of the underlying THP-1 monocytes. Limiting the directionality of the release of certain cytokines and chemokines by IECs may serve as a means of muting bidirectional immune communication and subsequent activation of the underlying APC population within the GALT to certain challenges while still allowing for paracrine communication with adjacent IECs.

STS-challenge resulted in increased production of pro-inflammatory cytokines and chemokines found in the apical and basolateral chambers of the co-culture system. Indeed, previous evidence describes a route through which ST can invade the intestinal mucosa by infecting IECs and the underlying APC populations. However, induction of pro-inflammatory mediator production in co-cultures of T84 IECs and THP-1 monocytes in response to STS challenge represents a potential novel route of pathogenicity mediated through soluble mediators derived from gut-associated pathogens. Co-challenge with the LrS attenuated STS-induced pro-inflammatory mediator production from T84 IEC and THP-1 monocyte co-cultures, a result that is in keeping with the observed bioactivity of the LrS in STS-challenged HT-29 IECs (Jeffrey, MacPherson, *et al.*, 2020). In contrast,

Lactobacillus paracasei CNCM-4034 and its secretome was found to induce pro-inflammatory mediator production and enhance pro-inflammatory gene transcription in response to challenge with *Salmonella typhi* in Caco-2 IEC and APC co-cultures, possibly through the up-regulation of genes involved in TLR signaling pathways (Bermudez-Brito *et al.*, 2015).

Challenge with the LrS induced the expression of *ATF3* and *DUSP1*, but not *TRIB3* in T84 IECs. This is in contrast to previous transcriptional profiling of HT-29 IECs following LrS challenge, as induction of these negative regulators of innate immunity was only seen following co-challenge of HT-29 IECs with the LrS and TNF- α or the STS (Jeffrey *et al.*, 2020). THP-1 human monocytes were less responsive to LrS challenge than T84 IECs as there were no significant changes to gene expression profiles in the absence of pro-inflammatory challenge. Co-challenge of STS-challenged co-cultures with the LrS attenuated *NF- κ B1* as well as *CXCL8* gene expression in both T84 IECs and THP-1 monocytes, confirming the results obtained in the cytokine and chemokine profiling. As was seen in HT-29 IECs co-challenged with the LrS and the STS (Jeffrey *et al.*, 2020), there was also increased expression of *ATF3*, *DUSP1*, and *TRIB3* in STS-challenged T84 IECs following concurrent secretome challenge, suggesting conserved immunoregulatory activity of the LrS across different *in vitro* IEC models and in *in vitro* co-culture systems which more closely mimic *in vivo* conditions.

Interestingly, the STS-challenge also reduced the expression of *ZO-1*, a tight-junction protein integral to proper function of the IEC barrier, providing potential insight into STS-induced pro-inflammatory responses in THP-1 monocytes observed in the basolateral chamber of the co-culture system. Deterioration of IEC monolayer integrity

through disruption of tight junction proteins such as ZO-1 is a hallmark of *S. enterica* serovar Typhimurium infection, resulting in enhanced translocation of the bacteria into the lamina propria (Boyle *et al.*, 2006; Kohler *et al.*, 2007). In keeping with these findings, the STS decreased T84 IEC TER and increased the flux of FITC-dextran across T84 IEC monolayers, indicating damage to IEC monolayer integrity and function. These results were further confirmed through visual inspection of ZO-1 expression following STS-challenge. Typically, damage to IEC monolayer integrity caused by *S. enterica* serovar Typhimurium infection is mediated by the direct delivery of virulence factors into host cells via a type III secretion system (Coburn, Grassl, *et al.*, 2007; Coburn, Sekirov, *et al.*, 2007). However, the results presented here suggest that secretome components derived from *S. enterica* serovar Typhimurium grown under normal conditions can also disrupt normal IEC monolayer function. The LrS attenuated STS-induced damage to T84 IEC monolayer integrity and function. Although there have been other reports of LAB-mediated beneficial impacts on IEC monolayer barrier integrity, the results presented here suggest a possible novel route through which soluble mediators derived from LAB can antagonize the activity of certain gut-associated pathogens within the GALT.

Addition of a MIF-neutralizing antibody reversed the ability of the LrS to attenuate STS-induced damage to IEC epithelial monolayer integrity. Recent evidence has suggested that MIF is integral for IEC repair and regeneration as well as for normal barrier function of IECs, as MIF deficient mice have increased intestinal permeability due to impairment of tight junction proteins such as ZO-1 (Vujicic *et al.*, 2020; Vujicic *et al.*, 2018). Mechanistically, MIF binds to CD74 (Leng *et al.*, 2003), typically following pro-inflammatory challenge or perturbations in normal IEC activity (Farr, Ghosh, & Moonah,

2020). The CD74-MIF signaling complex facilitates the activation of PI3K/AkT and ERK cell proliferation and survival cellular pathways (Farr, Ghosh, Jiang, *et al.*, 2020; Lue *et al.*, 2007). However, the precise mechanism(s) involved in the induction of MIF production following LrS challenge remain unknown and warrant further study, especially in the context of polarized IECs which display directionality in the secretion of certain cytokines and chemokines.

While evidence for LAB-mediated attenuation of pathogen-induced inflammatory responses in co-cultures of IECs and APCs remains limited, the results presented here provide additional mechanistic evidence for the ability of the LrS to modulate immune responses to STS-challenge in a context that allows for IEC and APC cell communication. The LrS was able to reverse STS-induced damage to IEC monolayer integrity, an effect potentially mediated through LrS-induced MIF production by IECs. Further experimentation using additional timepoints and secretomes derived from different LAB may reveal species-specific and time-dependant consequences of prolonged exposure to soluble components from LAB in a context which more closely mimics that which occurs *in vivo*. These future studies would provide further potential insights into mechanisms of gut microbe-host immune communication at the gut-mucosal interface.

Table 3-I. List of primers used for relative RT-qPCR for determination of gene expression profiles in T84 IECs and THP-1 monocyte co-cultures.

Gene	GenBank Accession Number	Amplicon Length (bp)	Primer Sequence (5'-3')	Source
<i>B2M</i>	NM_004048	150	F: GTGCTCGCGCTACTCTCTC R: GTCAACTTCAATGTCGGAT	(Dydensborg <i>et al.</i> , 2006)
<i>RPLPO</i>	NM_001002	142	F: GCAATGTTGCCAGTGTCTG R: GCCTTGACCTTTTCAGCAA	(Dydensborg <i>et al.</i> , 2006)
<i>TRIB3</i>	NM_021158.4	184	F: TGGTACCCAGCTCCTCTACG R: GACAAAGCGACACAGCTTGA	(Jousse <i>et al.</i> , 2007)
<i>ATF3</i>	NM_001206484.3	71	F: AAGAACGAGAAGCAGCATTGAT R: TTCTGAGCCCGGACAATACAC	(Bottone <i>et al.</i> , 2005)
<i>DUSP1</i>	NM_004417	80	F: GGCCCCGAGAACAGACAAA R: GTGCCCACTTCCATGACCAT	(Locati <i>et al.</i> , 2002)
<i>NFκB1</i>	NM_003998.3	130	F: GCAGCACTACTTCTTGACCACC R: TCTGCTCCTGAGCATTGACGTC	(Macpherson <i>et al.</i> , 2014)
<i>CLDN1</i>	NM_021101.5	81	F: CCTATGACCCCAGTCAATGC R: TCCCAGAAGGCAGAGAGAAG	(Tisza <i>et al.</i> , 2016)
<i>CLDN3</i>	NM_001306.4	161	F: GTCCGTCCGTCCGTCCG R: GCCCAGCACGGCCAGC	(Rangel <i>et al.</i> , 2003)
<i>ZO-1</i>	NM_001330239.4	102	F: AAGTCACACTGGTGAAATCC R: CTCTTGCTGCCAAACTATCT	(Boeckx <i>et al.</i> , 2015)
<i>IL1R2</i>	NM_004633.4	101	F: TGTGCTGGCCCCACTTTC R: GCACAGTCAGACCATCTGCTTT	(Mar <i>et al.</i> , 2015)
<i>IDO1</i>	NM_002164.6	119	F: GCCTGATCTCATAGAGTCTGGC R: TGCATCCCAGAACTAGACGTGC	(S. Zhou <i>et al.</i> , 2019)
<i>CD36</i>	NM_001001548.3	118	F: CAGGTCAACCTATTGGTCAAGCC R: GCCTTCTCATCACCAATGGTCC	(Chen <i>et al.</i> , 2020)

This is a continuation of Table 3-I.

Gene	GenBank Accession Number	Amplicon Length (bp)	Primer Sequence (5'-3')	Source
<i>TLR1</i>	NM_003263.4	105	F: CAGTGTCTGGTACACGCATGGT R: TTTCAAAAACCGTGTCTGTTAAGAGA	(Lv <i>et al.</i> , 2018)
<i>DC-SIGN</i>	NM_001144893.2	136	F: TCAAGCAGTATTGGAACAGAGGA R: CAGGAGGCTGCGGACTTTTT	(Chanput <i>et al.</i> , 2013)
<i>CD206</i>	NM_002438.4	97	F: CAGCGCTTGTGATCTTCATT R: TACCCCTGCTCCTGGTTTT	(Chanput <i>et al.</i> , 2013)
<i>ZFP36L1</i>	NM_001244698.2	116	F: ATGACCACCACCCTCGTGT R: TTTCTGTCCAGCAGGCAACC	(Chen <i>et al.</i> , 2015)
<i>ACTB</i>	NM_001101.5	150	F: ATTGCCGACAGGATGCAGAA R: GCTGATCCACATCTGCTGGAA	(Maess <i>et al.</i> , 2010)
<i>RPL37A</i>	NM_000998.5	94	F: ATTGAAATCAGCCAGCACGC R: AGGAACCACAGTGCCAGATCC	(Maess <i>et al.</i> , 2010)

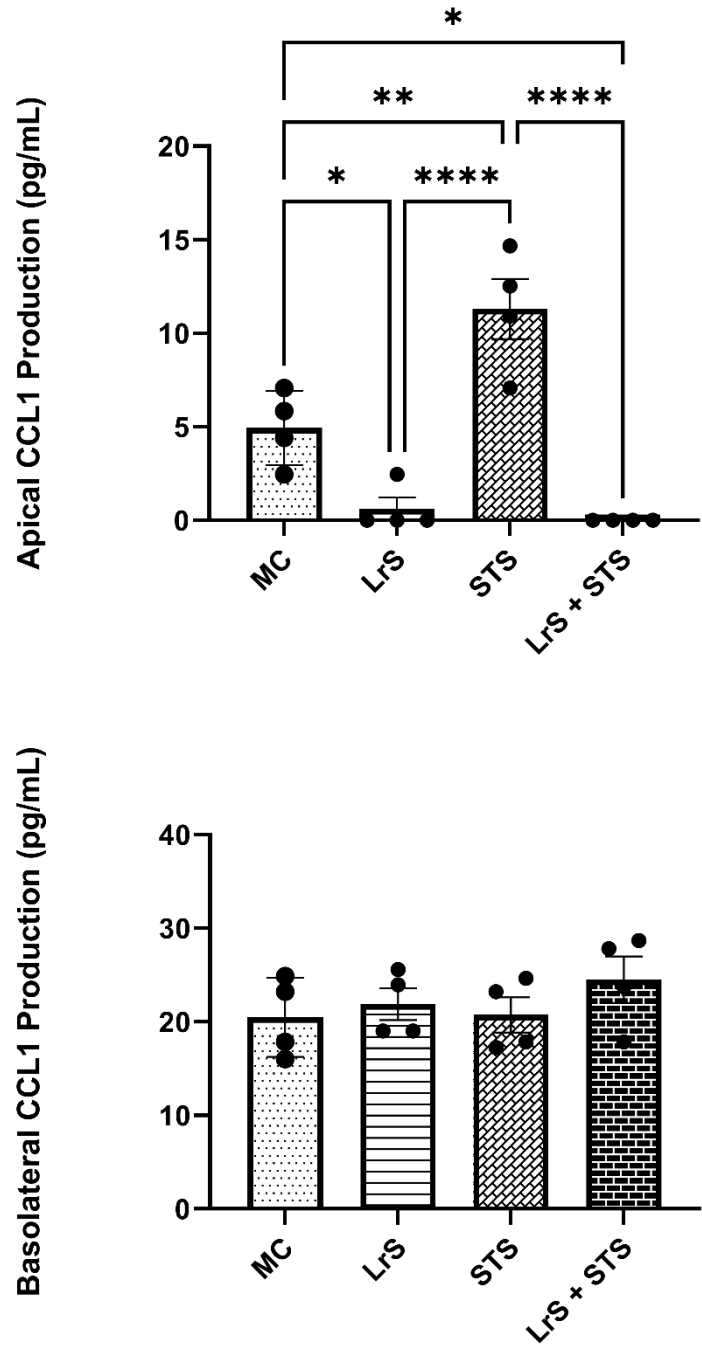


Figure 3-3A. Apical and basolateral production of CCL1 by T84 IEC and THP-1 monocyte cocultures following challenge with the LrS, STS, or a combination of the secretomes for 24 hours. Data shown is the mean cytokine/chemokine production (pg/mL) \pm SEM (n = 4). Significance is indicated as * $p < 0.05$, ** $p < 0.01$, *** $p < 0.001$ as determined by one-way ANOVA and Tukey's post-hoc test.

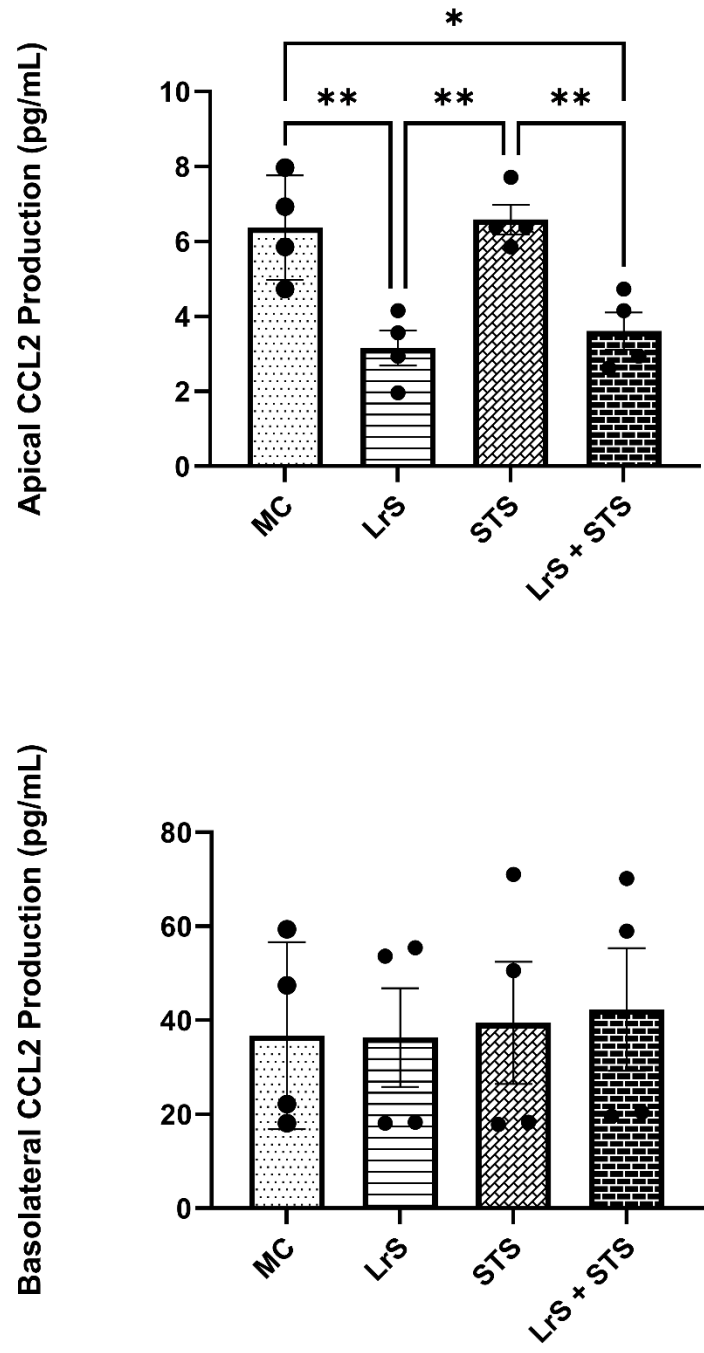


Figure 3-3B. Apical and basolateral production of CCL2 by T84 IEC and THP-1 monocyte co-cultures following challenge with the LrS, STS, or a combination of the secretomes for 24 hours. Data shown is the mean cytokine/chemokine production (pg/mL) \pm SEM (n = 4). Significance is indicated as * $p < 0.05$, ** $p < 0.01$, *** $p < 0.001$ as determined by one-way ANOVA and Tukey's post-hoc test.

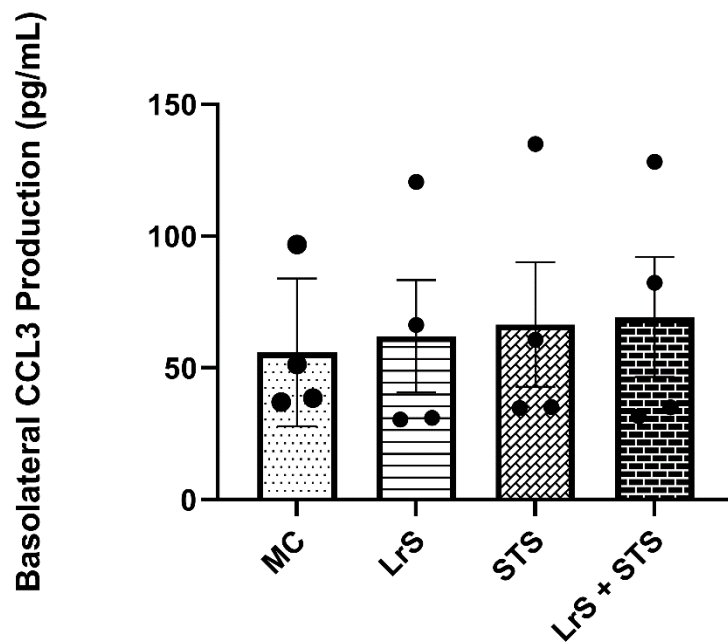
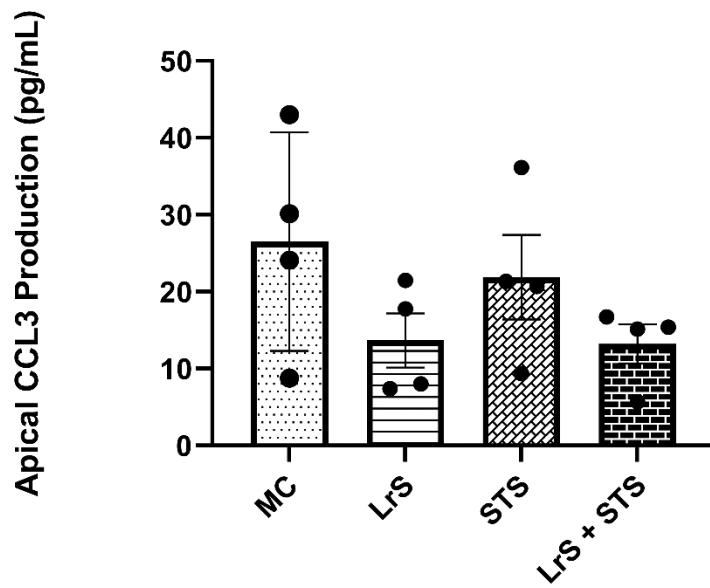


Figure 3-3C. Apical and basolateral production of CCL3 by T84 IEC and THP-1 monocyte co-cultures following challenge with the LrS, STS, or a combination of the secretomes for 24 hours. Data shown is the mean cytokine/chemokine production (pg/mL) \pm SEM (n = 4). Significance is indicated as * $p < 0.05$, ** $p < 0.01$, *** $p < 0.001$ as determined by one-way ANOVA and Tukey's post-hoc test.

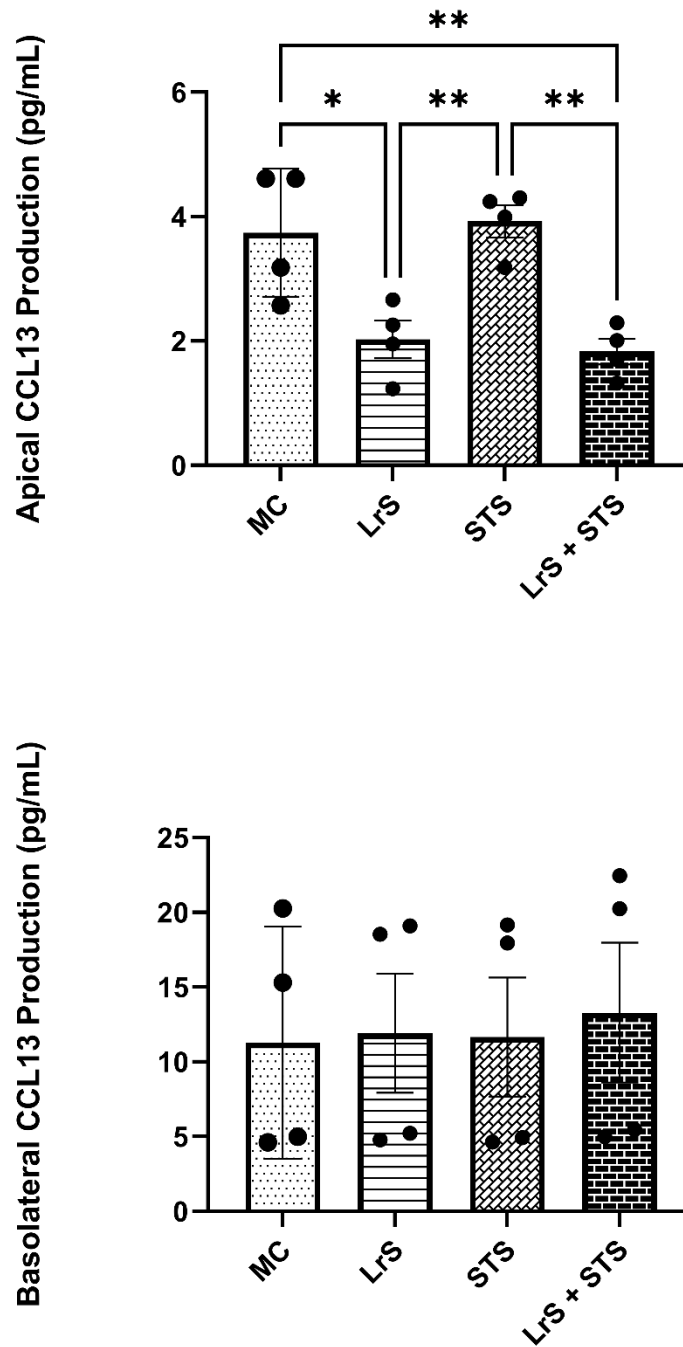


Figure 3-3D. Apical and basolateral production of CCL13 by T84 IEC and THP-1 monocyte co-cultures following challenge with the LrS, STS, or a combination of the secretomes for 24 hours. Data shown is the mean cytokine/chemokine production (pg/mL) \pm SEM (n = 4). Significance is indicated as * $p < 0.05$, ** $p < 0.01$, *** $p < 0.001$ as determined by one-way ANOVA and Tukey's post-hoc test.

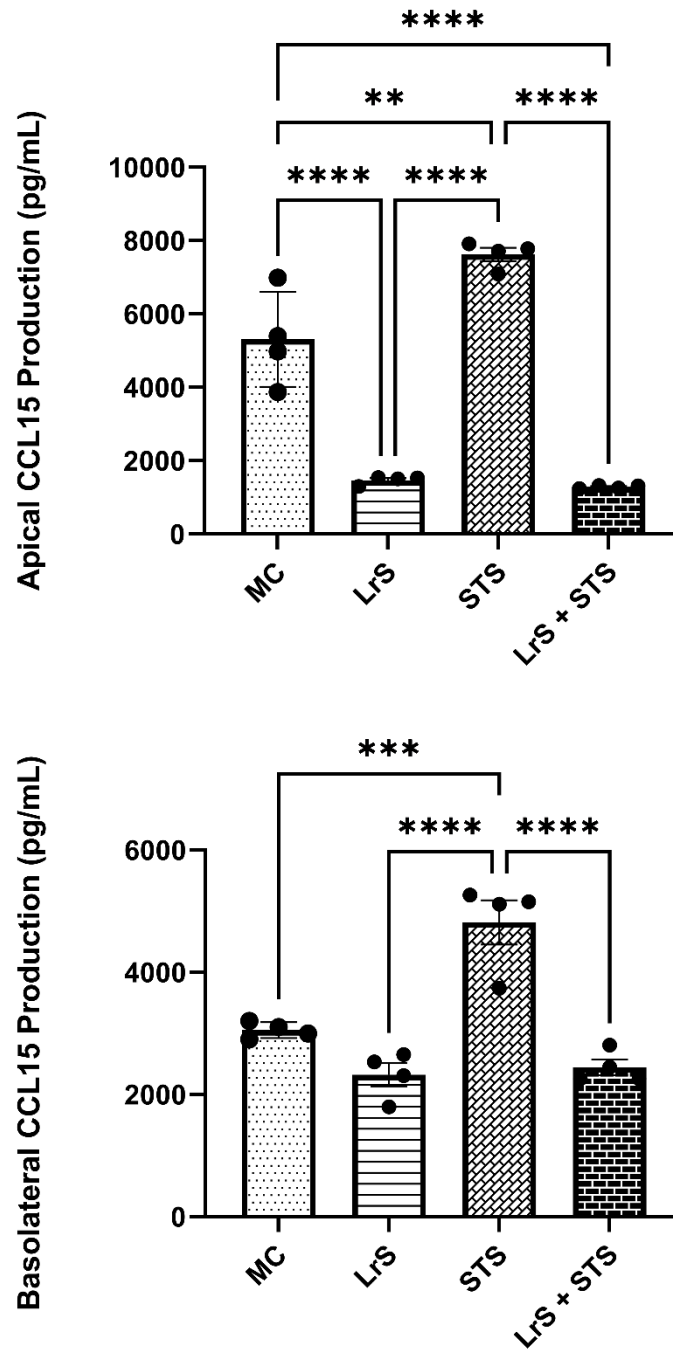


Figure 3-3E. Apical and basolateral production of CCL15 by T84 IEC and THP-1 monocyte co-cultures following challenge with the LrS, STS, or a combination of the secretomes for 24 hours. Data shown is the mean cytokine/chemokine production (pg/mL) \pm SEM (n = 4). Significance is indicated as * $p < 0.05$, ** $p < 0.01$, *** $p < 0.001$ as determined by one-way ANOVA and Tukey's post-hoc test.

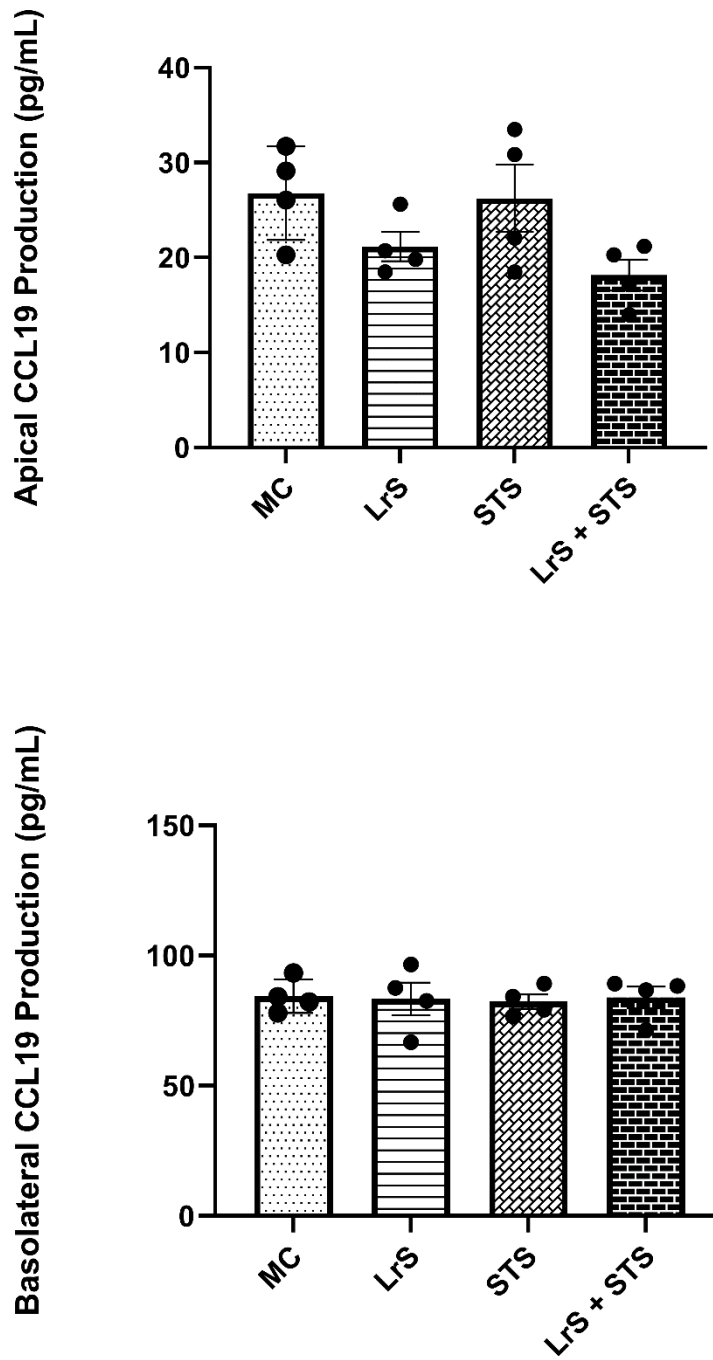


Figure 3-3F. Apical and basolateral production of CCL19 by T84 IEC and THP-1 monocyte co-cultures following challenge with the LrS, STS, or a combination of the secretomes for 24 hours. Data shown is the mean cytokine/chemokine production (pg/mL) \pm SEM (n = 4). Significance is indicated as * $p < 0.05$, ** $p < 0.01$, *** $p < 0.001$ as determined by one-way ANOVA and Tukey's post-hoc test.

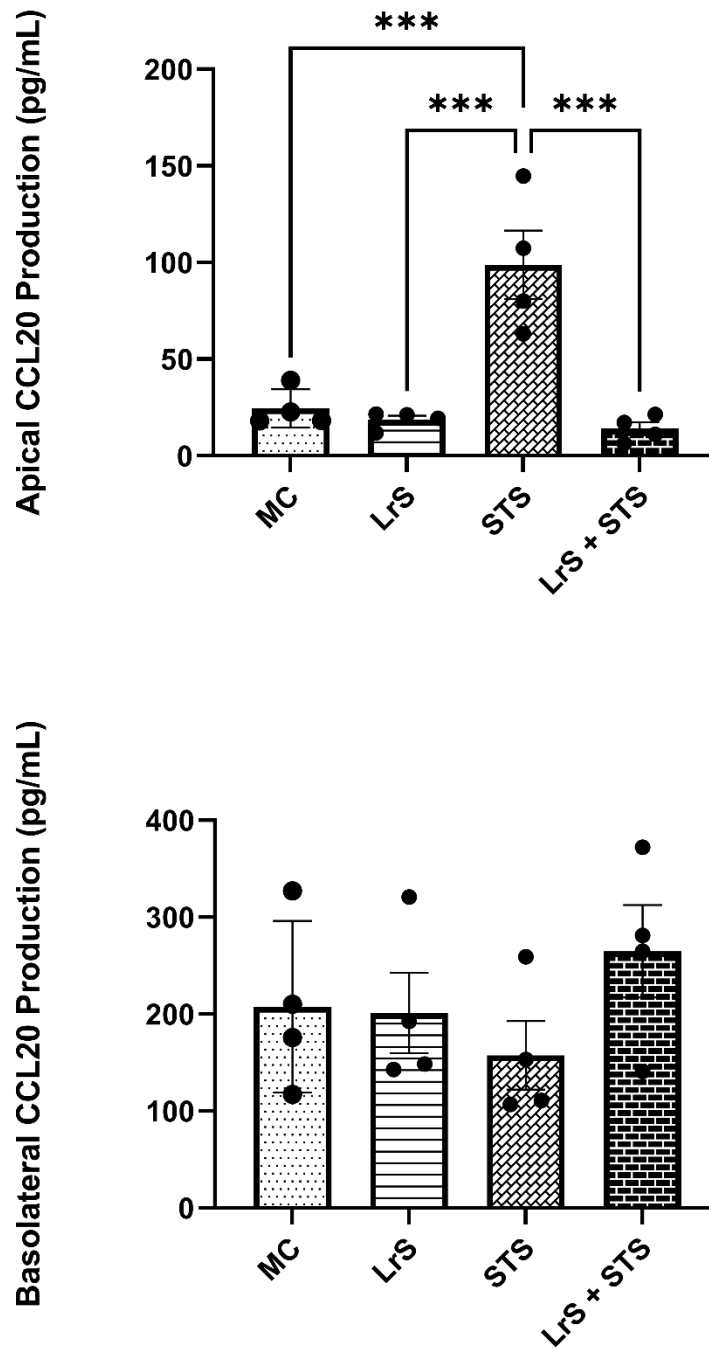


Figure 3-3G. Apical and basolateral production of CCL20 by T84 IEC and THP-1 monocyte co-cultures following challenge with the LrS, STS, or a combination of the secretomes for 24 hours. Data shown is the mean cytokine/chemokine production (pg/mL) \pm SEM (n = 4). Significance is indicated as * $p < 0.05$, ** $p < 0.01$, *** $p < 0.001$ as determined by one-way ANOVA and Tukey's post-hoc test.

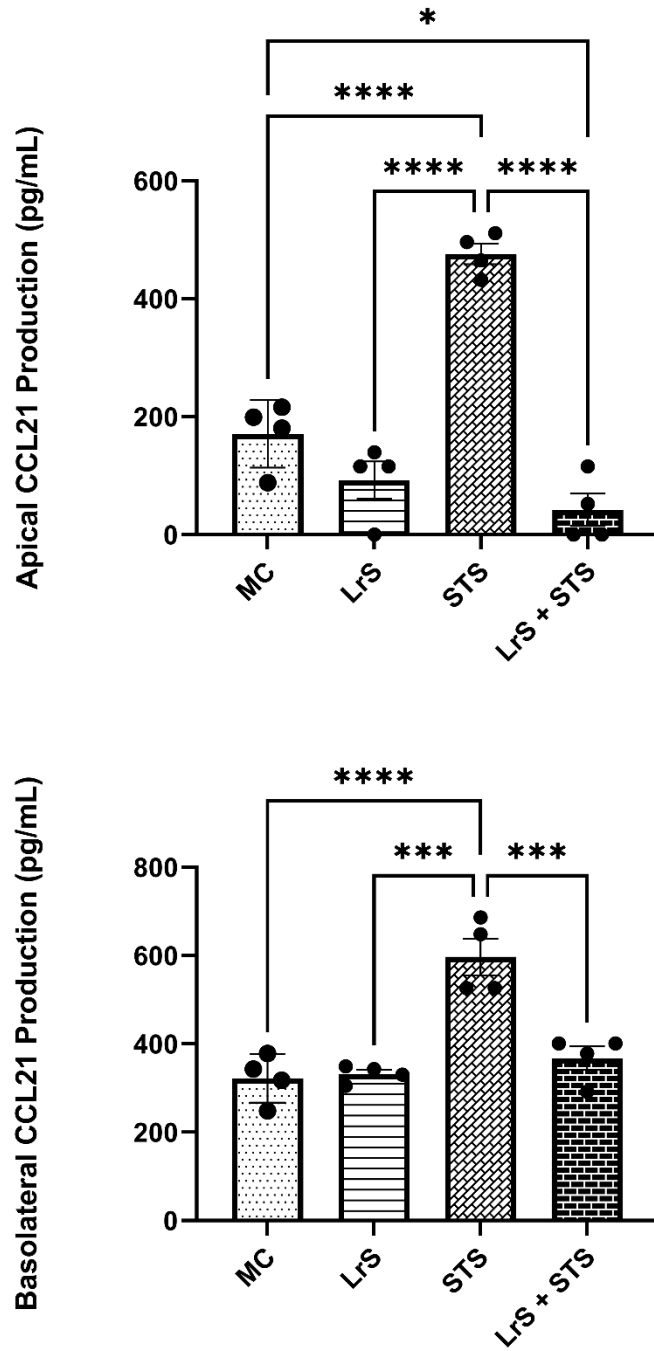


Figure 3-3H. Apical and basolateral production of CCL21 by T84 IEC and THP-1 monocyte co-cultures following challenge with the LrS, STS, or a combination of the secretomes for 24 hours. Data shown is the mean cytokine/chemokine production (pg/mL) \pm SEM (n = 4). Significance is indicated as * $p < 0.05$, ** $p < 0.01$, *** $p < 0.001$ as determined by one-way ANOVA and Tukey's post-hoc test.

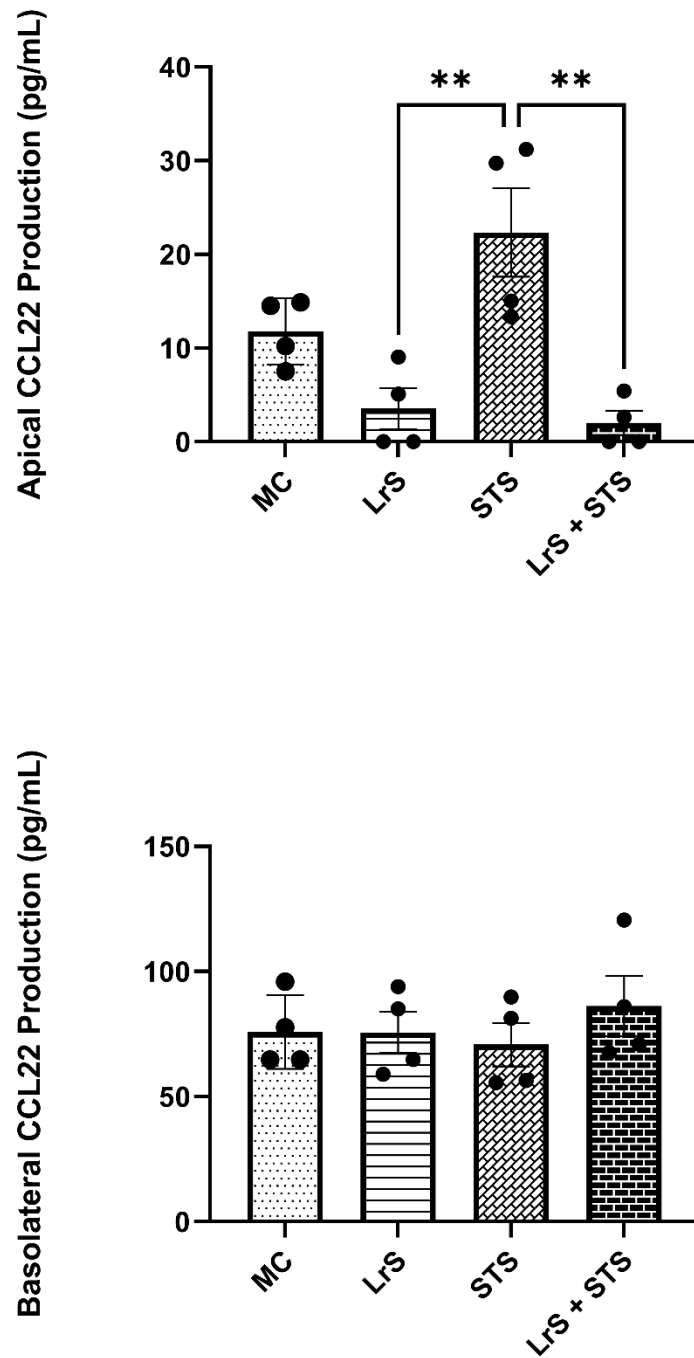


Figure 3-3I. Apical and basolateral production of CCL22 by T84 IEC and THP-1 monocyte co-cultures following challenge with the LrS, STS, or a combination of the secretomes for 24 hours. Data shown is the mean cytokine/chemokine production (pg/mL) \pm SEM (n = 4). Significance is indicated as * $p < 0.05$, ** $p < 0.01$, *** $p < 0.001$ as determined by one-way ANOVA and Tukey's post-hoc test.

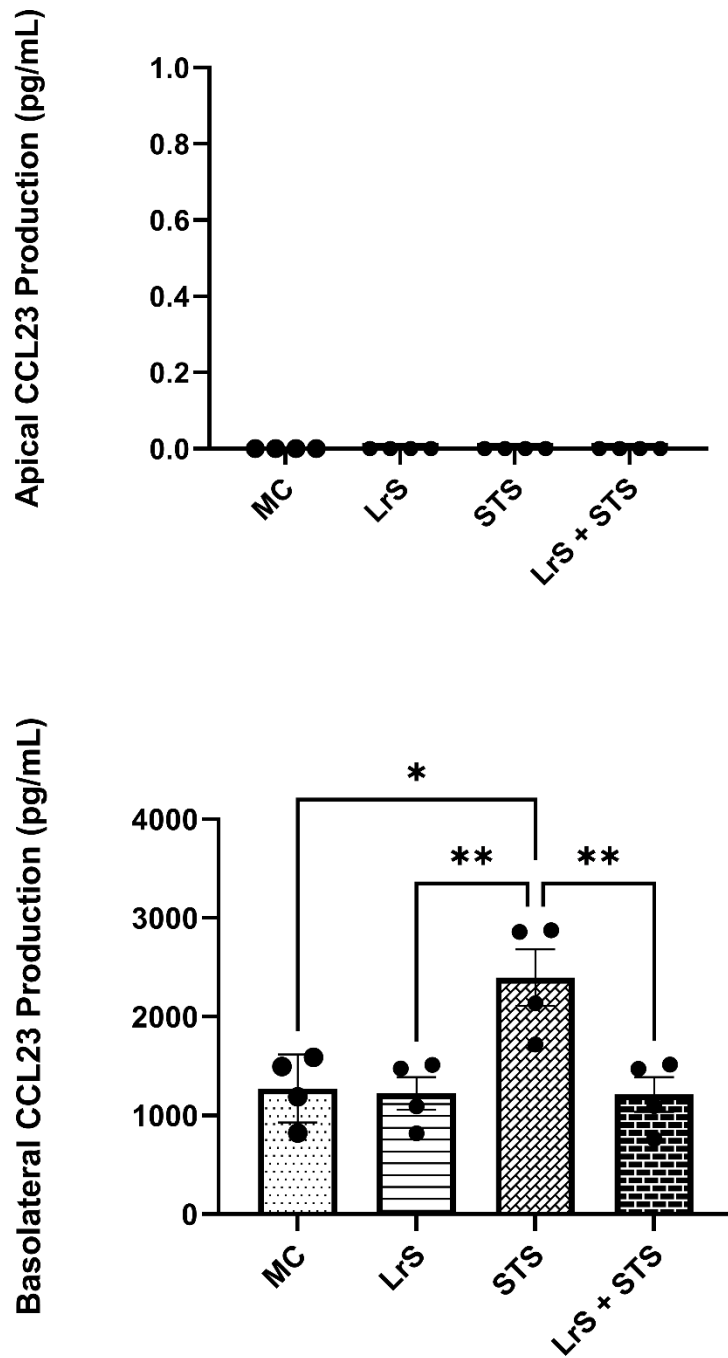


Figure 3-3J. Apical and basolateral production of CCL23 by T84 IEC and THP-1 monocyte co-cultures following challenge with the LrS, STS, or a combination of the secretomes for 24 hours. Data shown is the mean cytokine/chemokine production (pg/mL) \pm SEM (n = 4). Significance is indicated as * $p < 0.05$, ** $p < 0.01$, *** $p < 0.001$ as determined by one-way ANOVA and Tukey's post-hoc test.

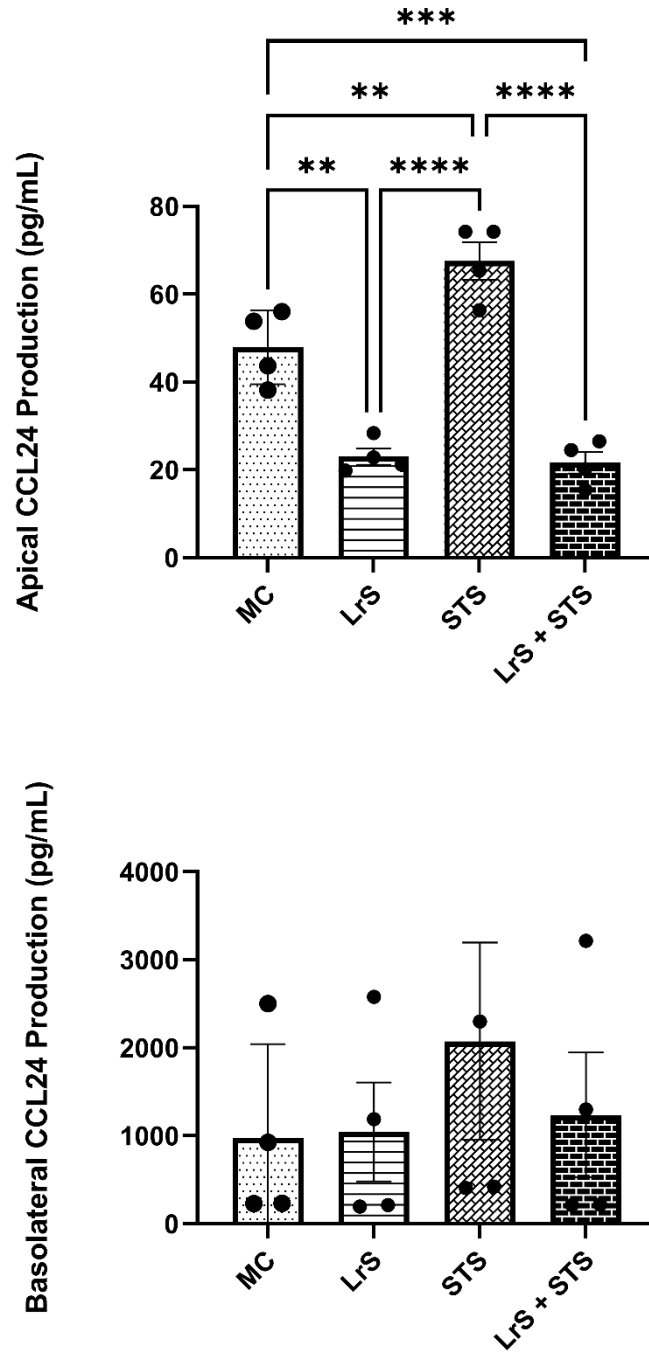


Figure 3-3K. Apical and basolateral production of CCL24 by T84 IEC and THP-1 monocyte co-cultures following challenge with the LrS, STS, or a combination of the secretomes for 24 hours. Data shown is the mean cytokine/chemokine production (pg/mL) \pm SEM (n = 4). Significance is indicated as * $p < 0.05$, ** $p < 0.01$, *** $p < 0.001$ as determined by one-way ANOVA and Tukey's post-hoc test.

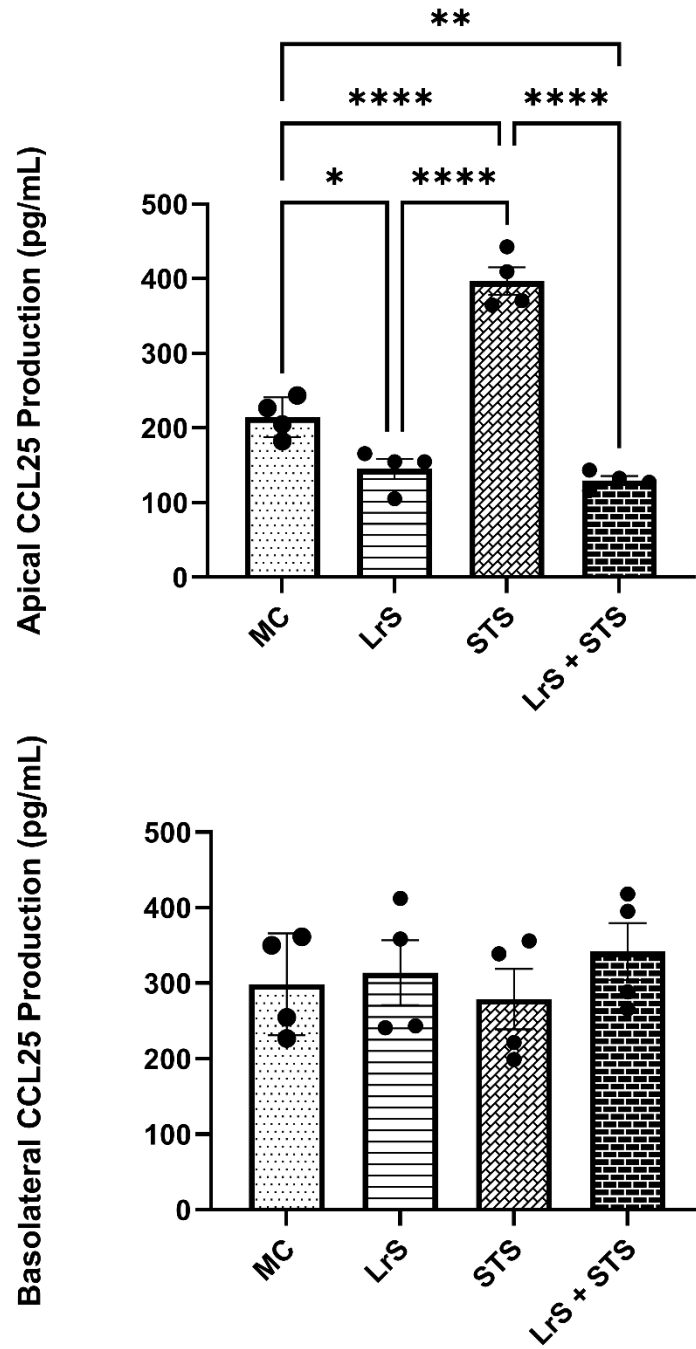


Figure 3-3L. Apical and basolateral production of CCL25 by T84 IEC and THP-1 monocyte co-cultures following challenge with the LrS, STS, or a combination of the secretomes for 24 hours. Data shown is the mean cytokine/chemokine production (pg/mL) \pm SEM (n = 4). Significance is indicated as * $p < 0.05$, ** $p < 0.01$, **** $p < 0.0001$ as determined by one-way ANOVA and Tukey's post-hoc test.

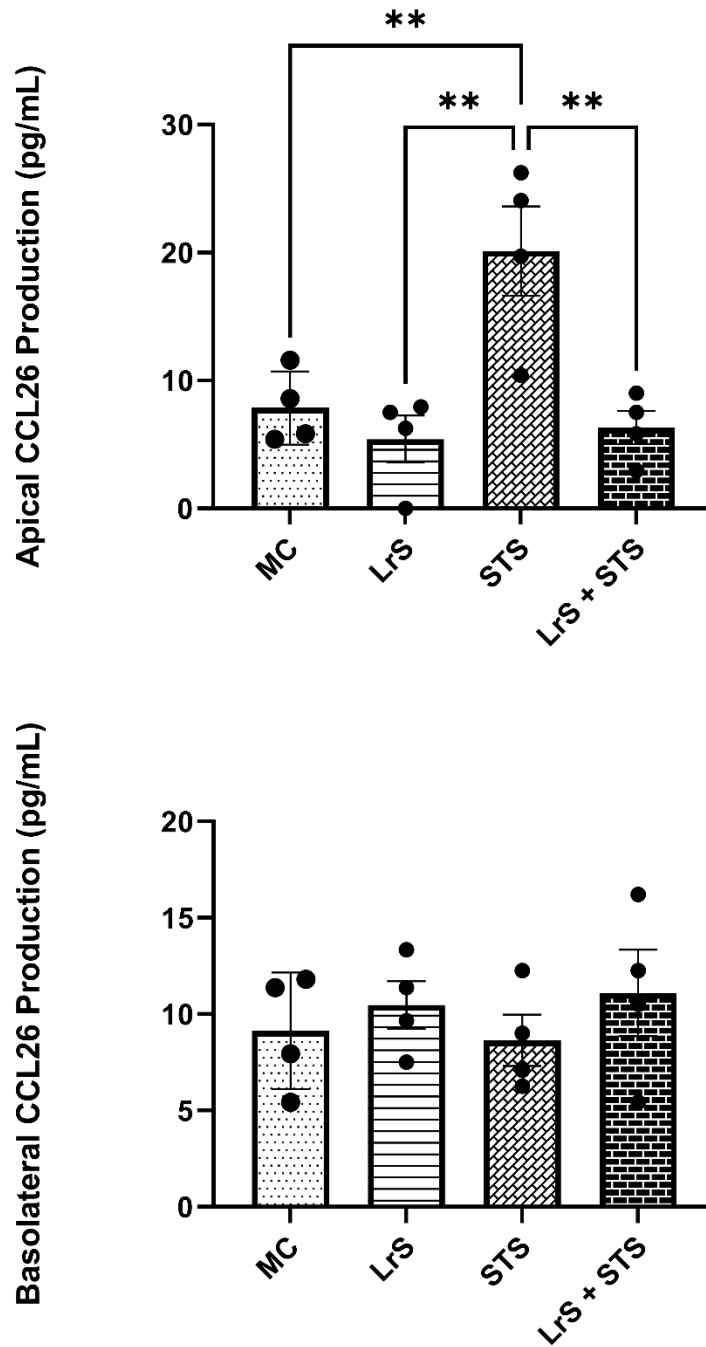


Figure 3-3M. Apical and basolateral production of CCL26 by T84 IEC and THP-1 monocyte co-cultures following challenge with the LrS, STS, or a combination of the secretomes for 24 hours. Data shown is the mean cytokine/chemokine production (pg/mL) \pm SEM (n = 4). Significance is indicated as * $p < 0.05$, ** $p < 0.01$, *** $p < 0.001$ as determined by one-way ANOVA and Tukey's post-hoc test.

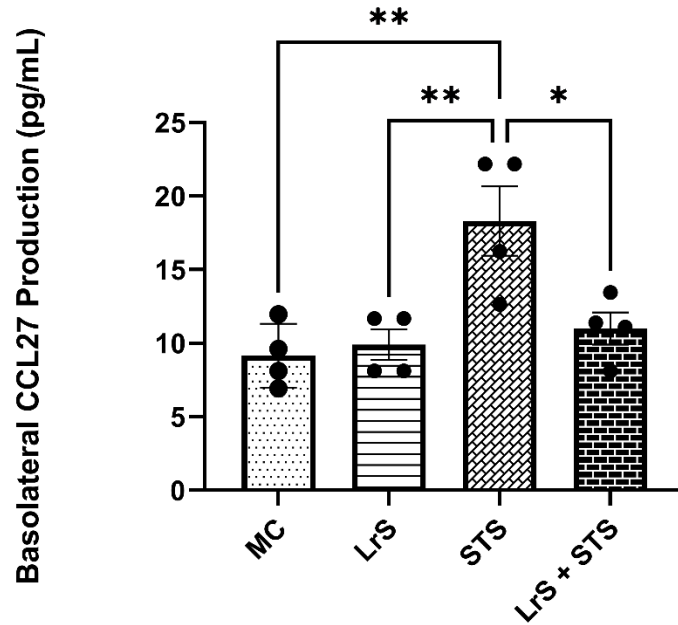
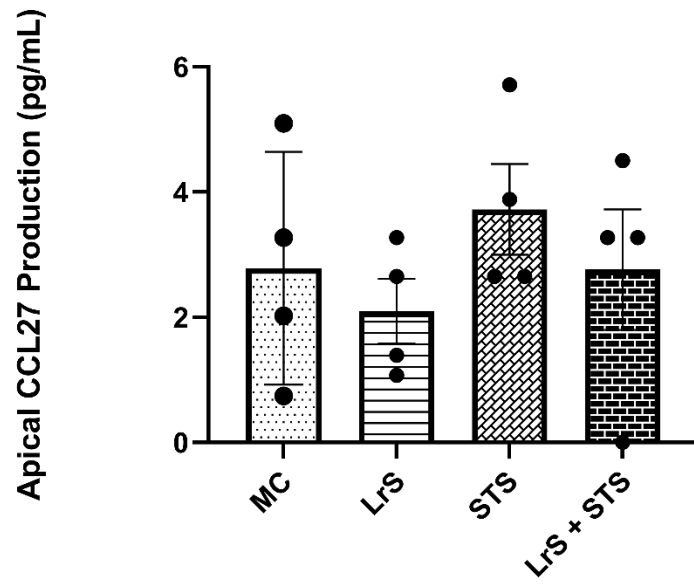


Figure 3-3N. Apical and basolateral production of CCL27 by T84 IEC and THP-1 monocyte co-cultures following challenge with the LrS, STS, or a combination of the secretomes for 24 hours. Data shown is the mean cytokine/chemokine production (pg/mL) \pm SEM (n = 4). Significance is indicated as * $p < 0.05$, ** $p < 0.01$, *** $p < 0.001$ as determined by one-way ANOVA and Tukey's post-hoc test.

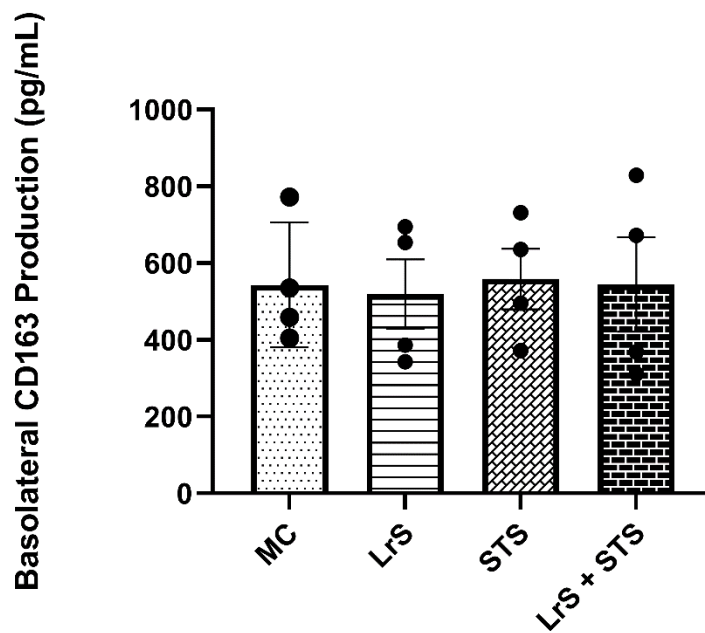
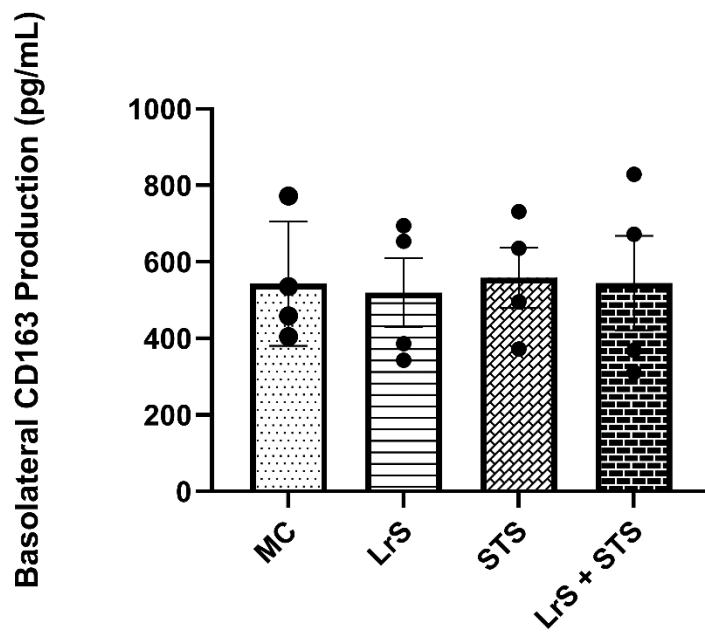


Figure 3-30. Apical and basolateral production of CD163 by T84 IEC and THP-1 monocyte co-cultures following challenge with the LrS, STS, or a combination of the secretomes for 24 hours. Data shown is the mean cytokine/chemokine production (pg/mL) \pm SEM (n = 4). Significance is indicated as * $p < 0.05$, ** $p < 0.01$, *** $p < 0.001$ as determined by one-way ANOVA and Tukey's post-hoc test.

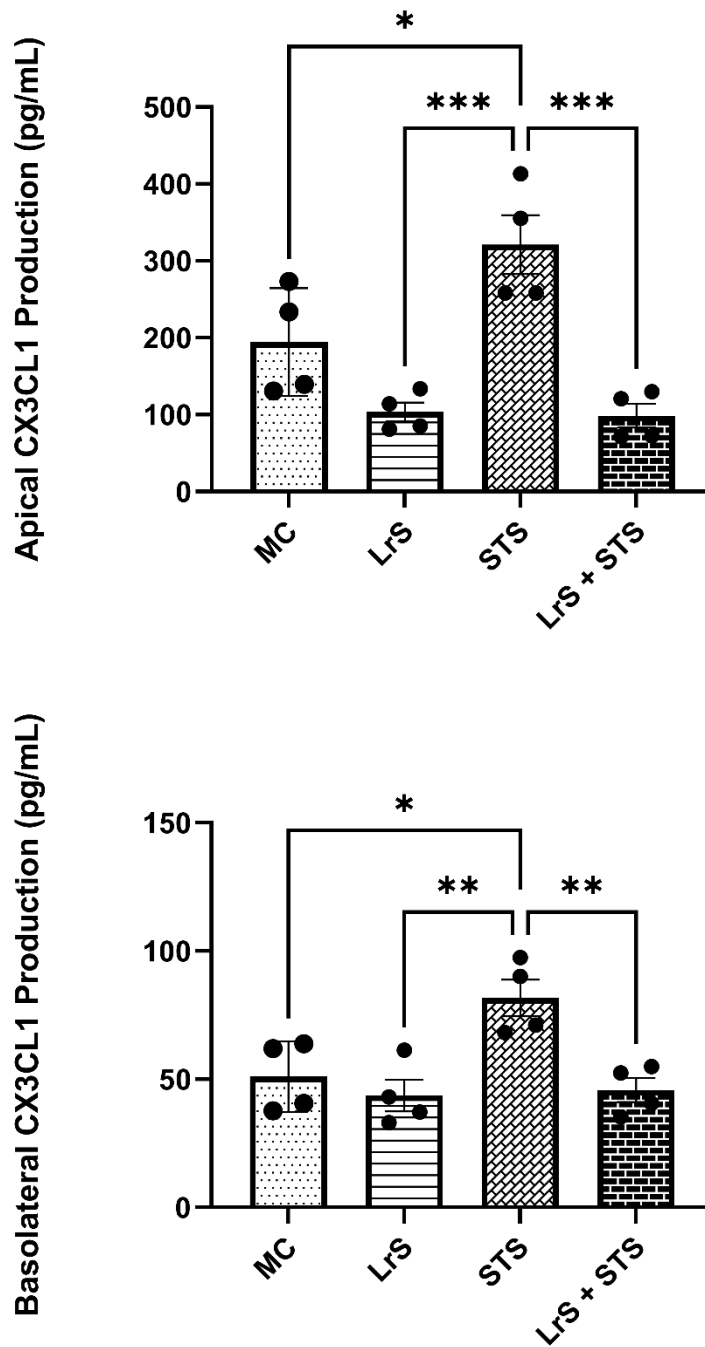


Figure 3-3P. Apical and basolateral production of CX3CL1 by T84 IEC and THP-1 monocyte cocultures following challenge with the LrS, STS, or a combination of the secretomes for 24 hours. Data shown is the mean cytokine/chemokine production (pg/mL) \pm SEM (n = 4). Significance is indicated as * $p < 0.05$, ** $p < 0.01$, *** $p < 0.001$ as determined by one-way ANOVA and Tukey's post-hoc test.

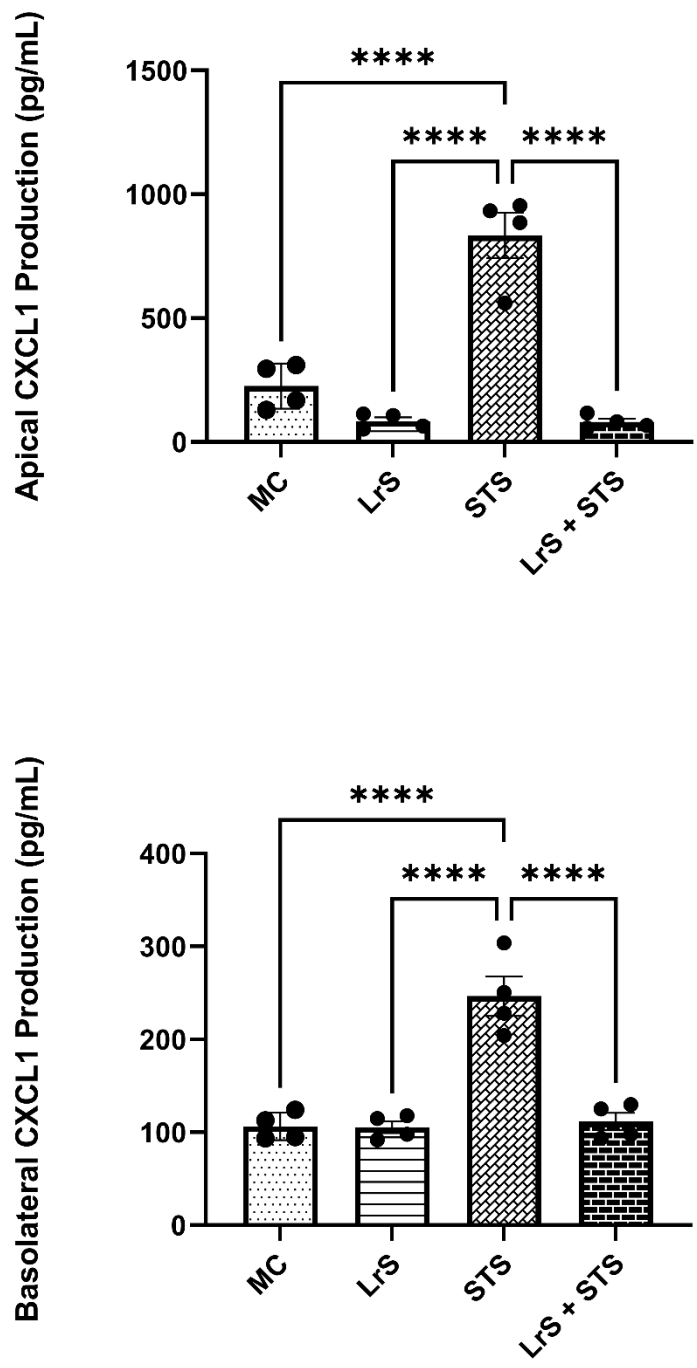


Figure 3-3Q. Apical and basolateral production of CXCL1 by T84 IEC and THP-1 monocyte cocultures following challenge with the LrS, STS, or a combination of the secretomes for 24 hours. Data shown is the mean cytokine/chemokine production (pg/mL) \pm SEM (n = 4). Significance is indicated as * $p < 0.05$, ** $p < 0.01$, *** $p < 0.001$ as determined by one-way ANOVA and Tukey's post-hoc test.

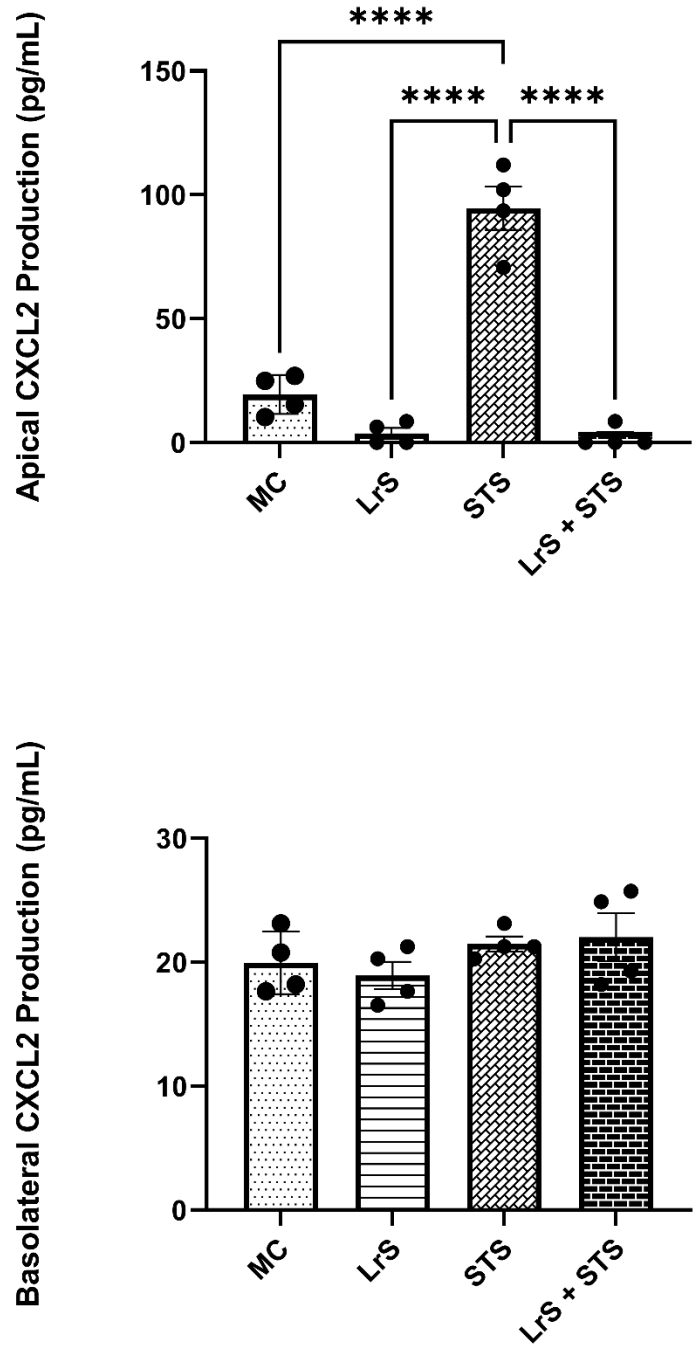


Figure 3-3R. Apical and basolateral production of CXCL2 by T84 IEC and THP-1 monocyte co-cultures following challenge with the LrS, STS, or a combination of the secretomes for 24 hours. Data shown is the mean cytokine/chemokine production (pg/mL) \pm SEM (n = 4). Significance is indicated as * $p < 0.05$, ** $p < 0.01$, *** $p < 0.001$ as determined by one-way ANOVA and Tukey's post-hoc test.

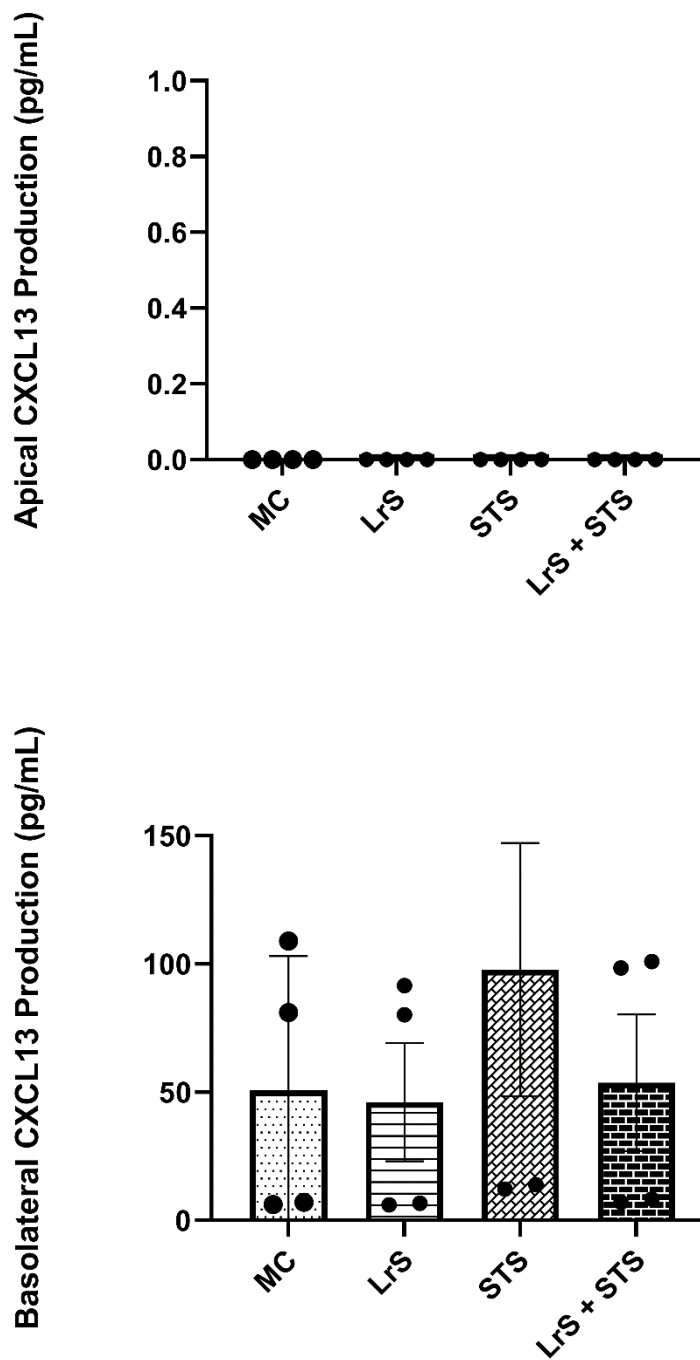


Figure 3-3S. Apical and basolateral production of CXCL3 by T84 IEC and THP-1 monocyte co-cultures following challenge with the LrS, STS, or a combination of the secretomes for 24 hours. Data shown is the mean cytokine/chemokine production (pg/mL) \pm SEM (n = 4). Significance is indicated as * $p < 0.05$, ** $p < 0.01$, *** $p < 0.001$ as determined by one-way ANOVA and Tukey's post-hoc test.

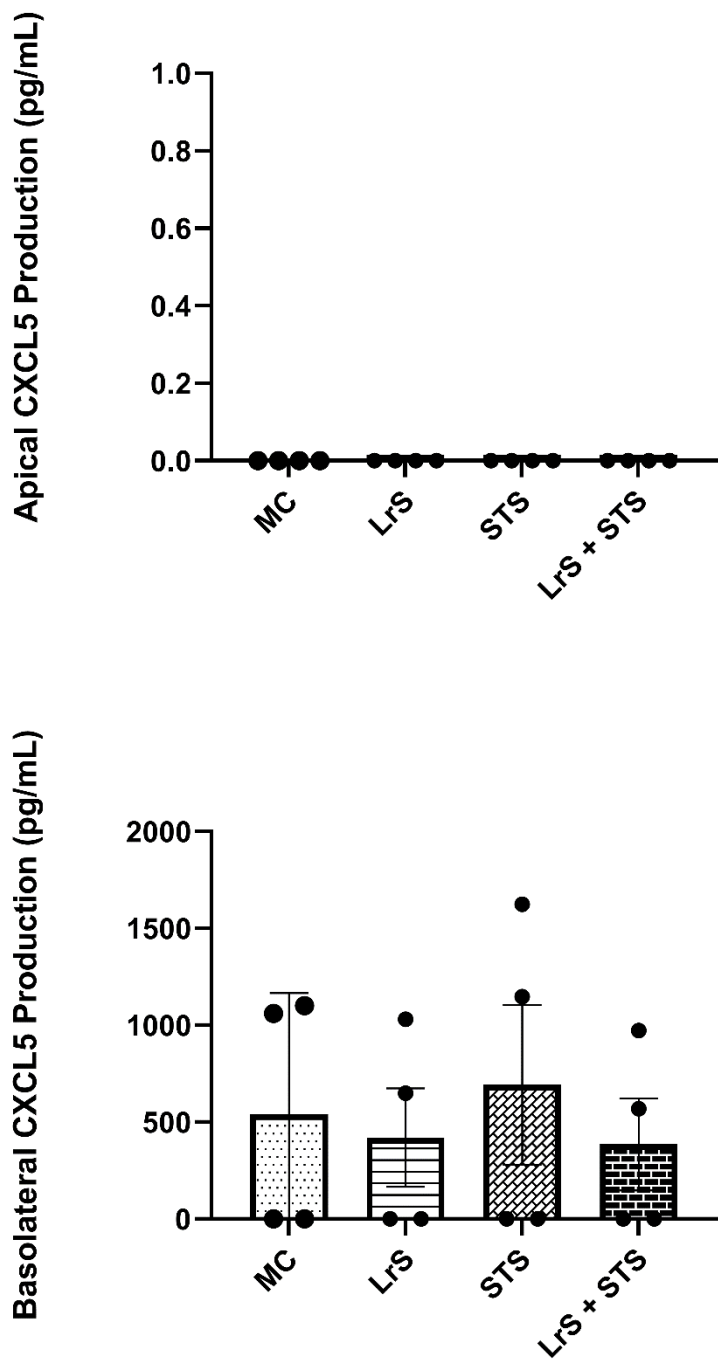


Figure 3-3T. Apical and basolateral production of CXCL5 by T84 IEC and THP-1 monocyte co-cultures following challenge with the LrS, STS, or a combination of the secretomes for 24 hours. Data shown is the mean cytokine/chemokine production (pg/mL) \pm SEM (n = 4). Significance is indicated as * $p < 0.05$, ** $p < 0.01$, *** $p < 0.001$ as determined by one-way ANOVA and Tukey's post-hoc test.

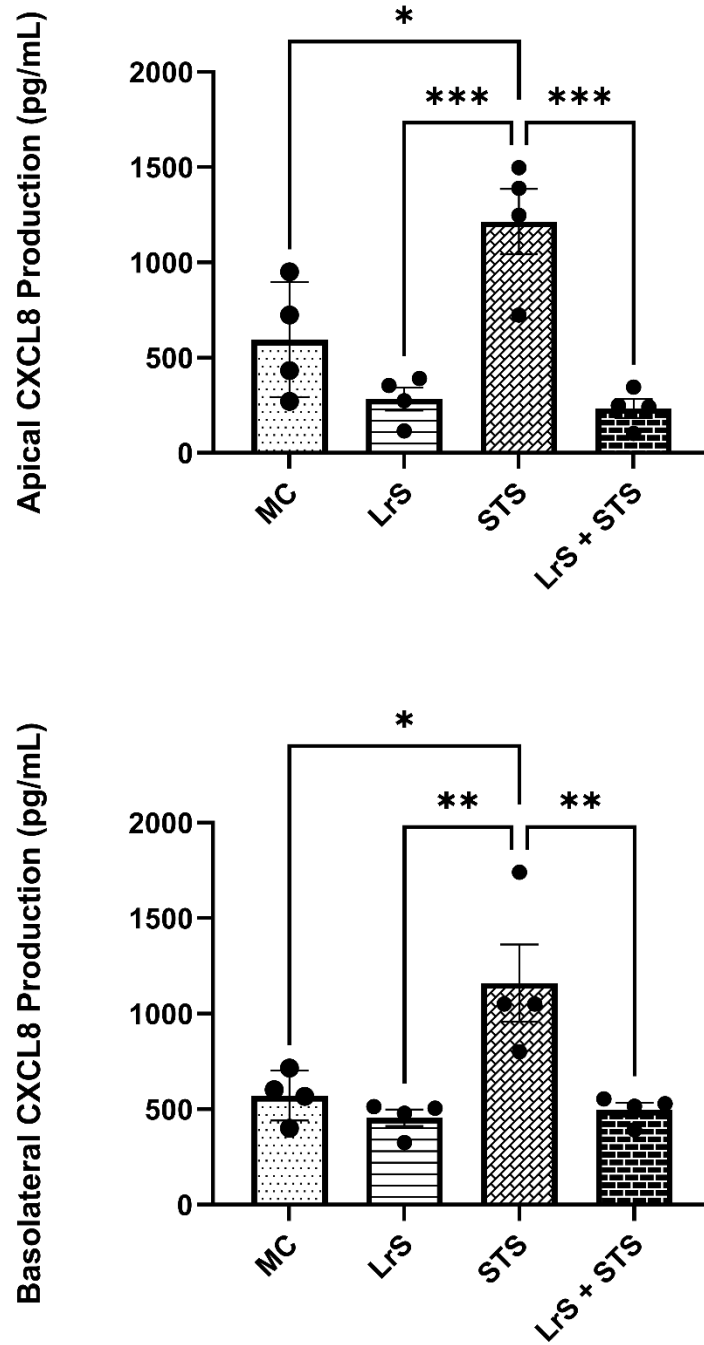


Figure 3-3U. Apical and basolateral production of CXCL8 by T84 IEC and THP-1 monocyte cocultures following challenge with the LrS, STS, or a combination of the secretomes for 24 hours. Data shown is the mean cytokine/chemokine production (pg/mL) \pm SEM (n = 4). Significance is indicated as * $p < 0.05$, ** $p < 0.01$, *** $p < 0.001$ as determined by one-way ANOVA and Tukey's post-hoc test.

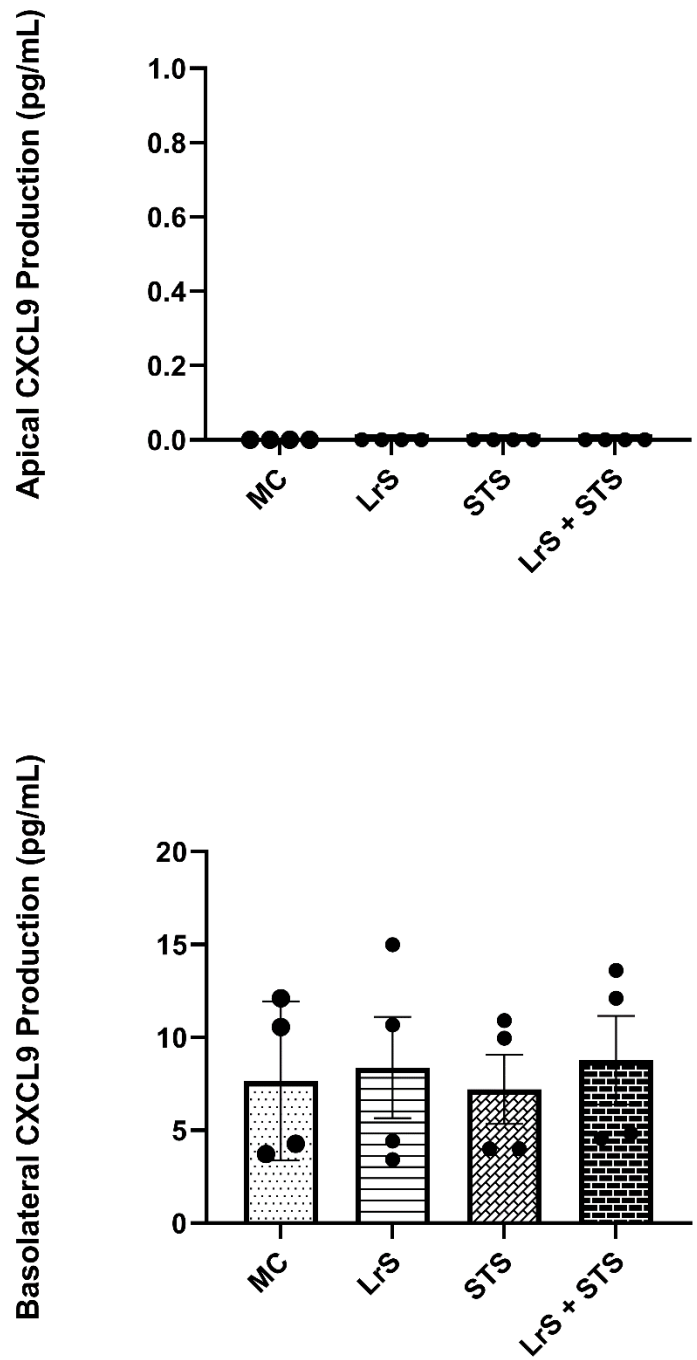


Figure 3-3V. Apical and basolateral production of CXCL9 by T84 IEC and THP-1 monocyte co-cultures following challenge with the LrS, STS, or a combination of the secretomes for 24 hours. Data shown is the mean cytokine/chemokine production (pg/mL) \pm SEM (n = 4). Significance is indicated as * $p < 0.05$, ** $p < 0.01$, *** $p < 0.001$ as determined by one-way ANOVA and Tukey's post-hoc test.

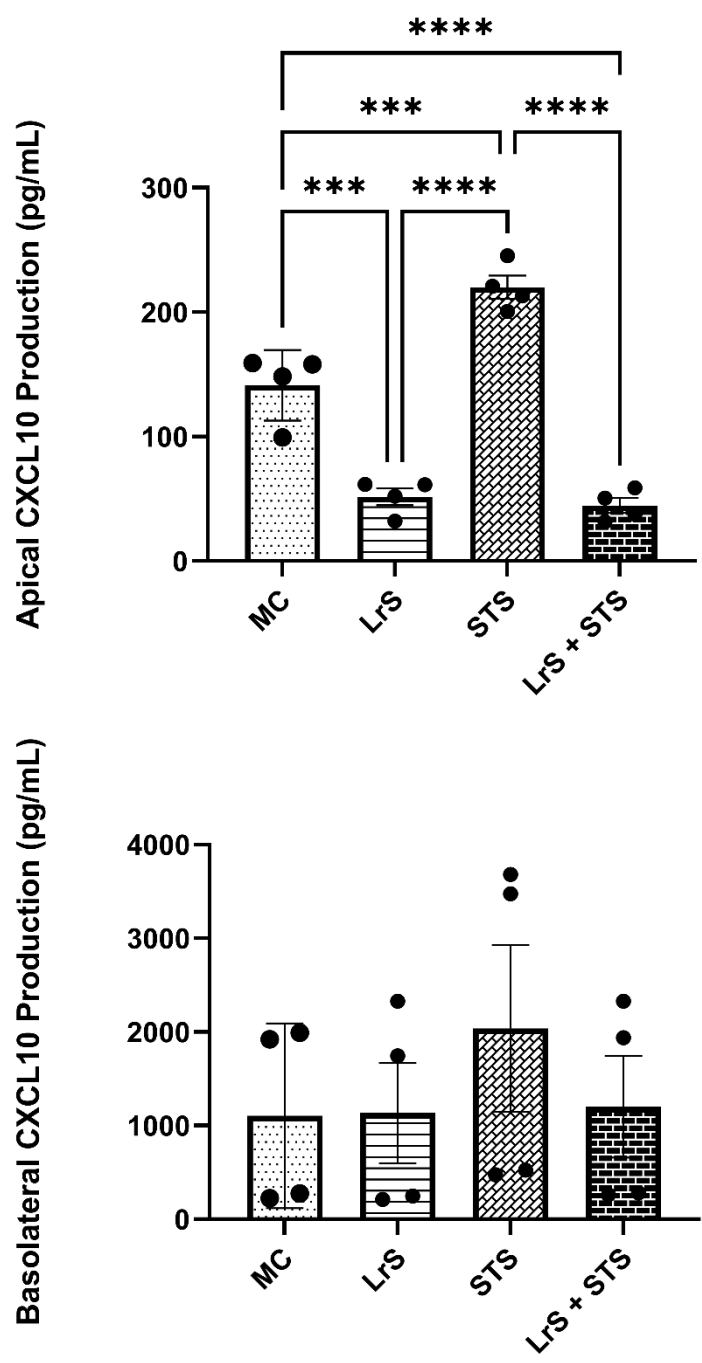


Figure 3-3W. Apical and basolateral production of CXCL10 by T84 IEC and THP-1 monocyte co-cultures following challenge with the LrS, STS, or a combination of the secretomes for 24 hours. Data shown is the mean cytokine/chemokine production (pg/mL) ± SEM (n = 4). Significance is indicated as * $p < 0.05$, ** $p < 0.01$, *** $p < 0.001$ as determined by one-way ANOVA and Tukey's post-hoc test.

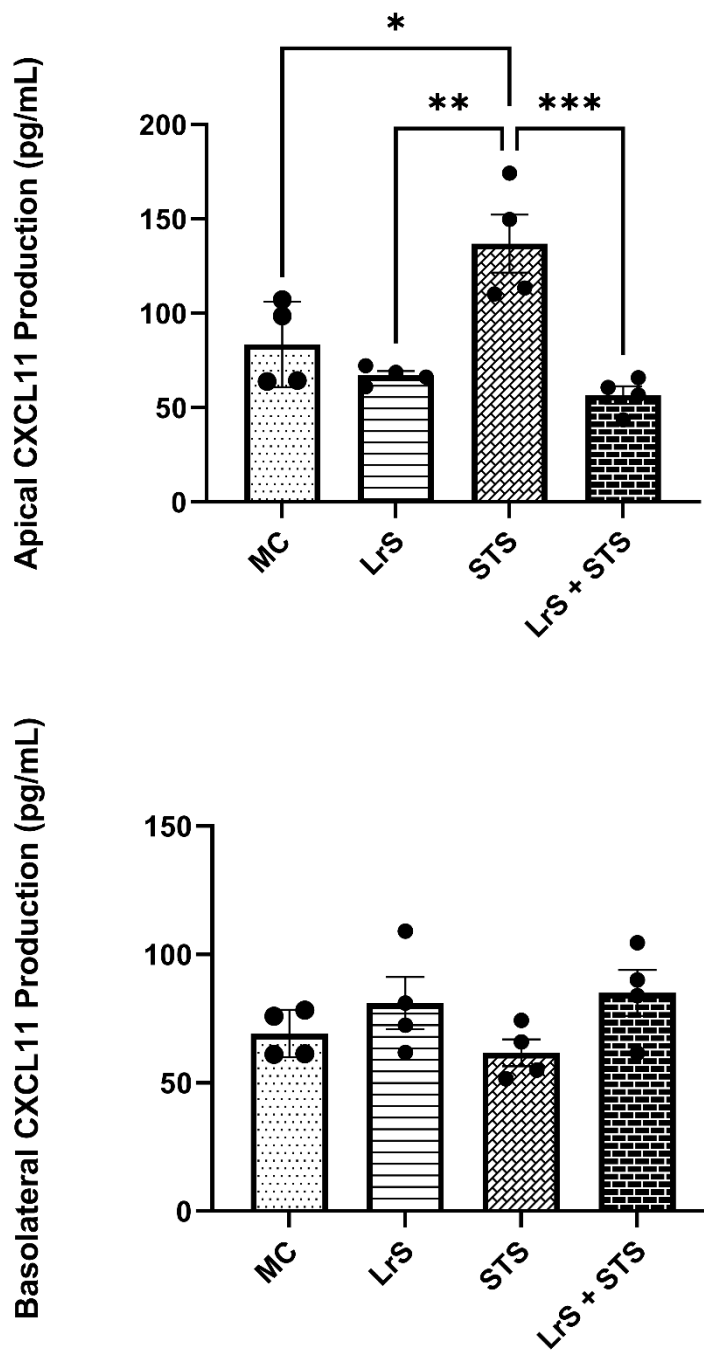


Figure 3-3X. Apical and basolateral production of CXCL11 by T84 IEC and THP-1 monocyte co-cultures following challenge with the LrS, STS, or a combination of the secretomes for 24 hours. Data shown is the mean cytokine/chemokine production (pg/mL) \pm SEM (n = 4). Significance is indicated as * $p < 0.05$, ** $p < 0.01$, *** $p < 0.001$ as determined by one-way ANOVA and Tukey's post-hoc test.

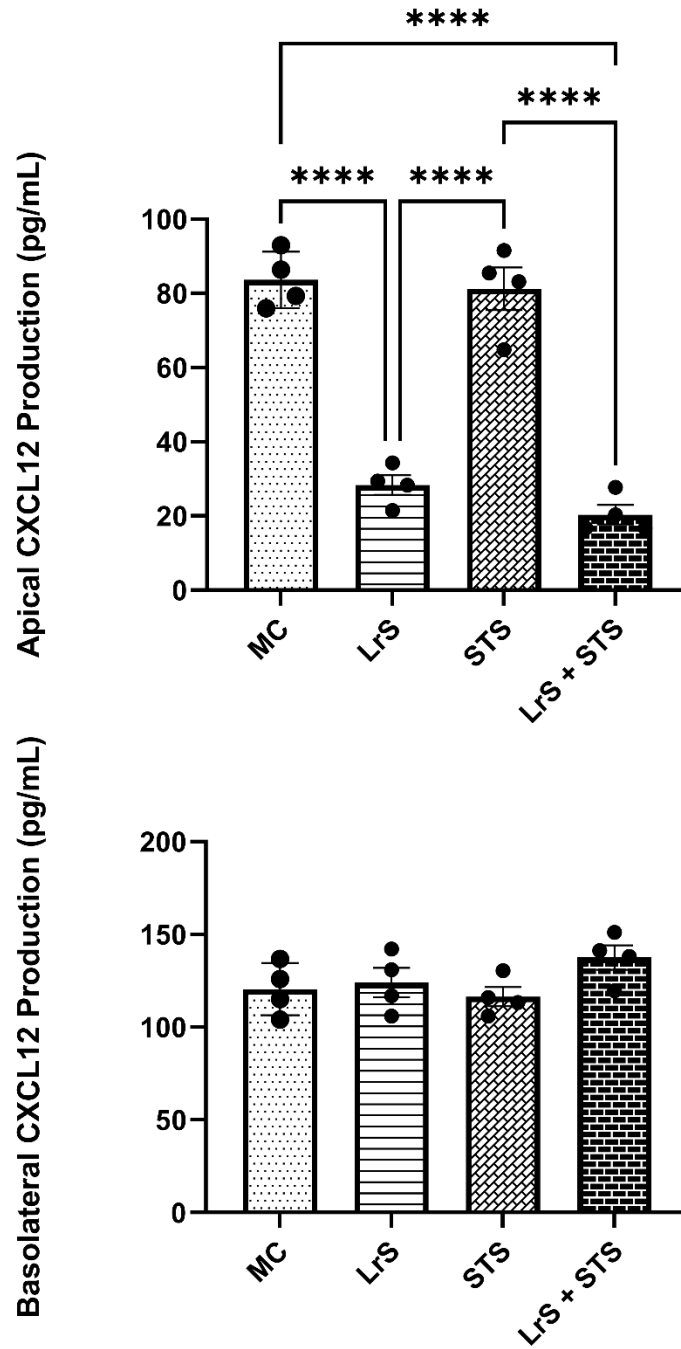


Figure 3-3Y. Apical and basolateral production of CXCL12 by T84 IEC and THP-1 monocyte co-cultures following challenge with the LrS, STS, or a combination of the secretomes for 24 hours. Data shown is the mean cytokine/chemokine production (pg/mL) \pm SEM (n = 4). Significance is indicated as * $p < 0.05$, ** $p < 0.01$, *** $p < 0.001$ as determined by one-way ANOVA and Tukey's post-hoc test.

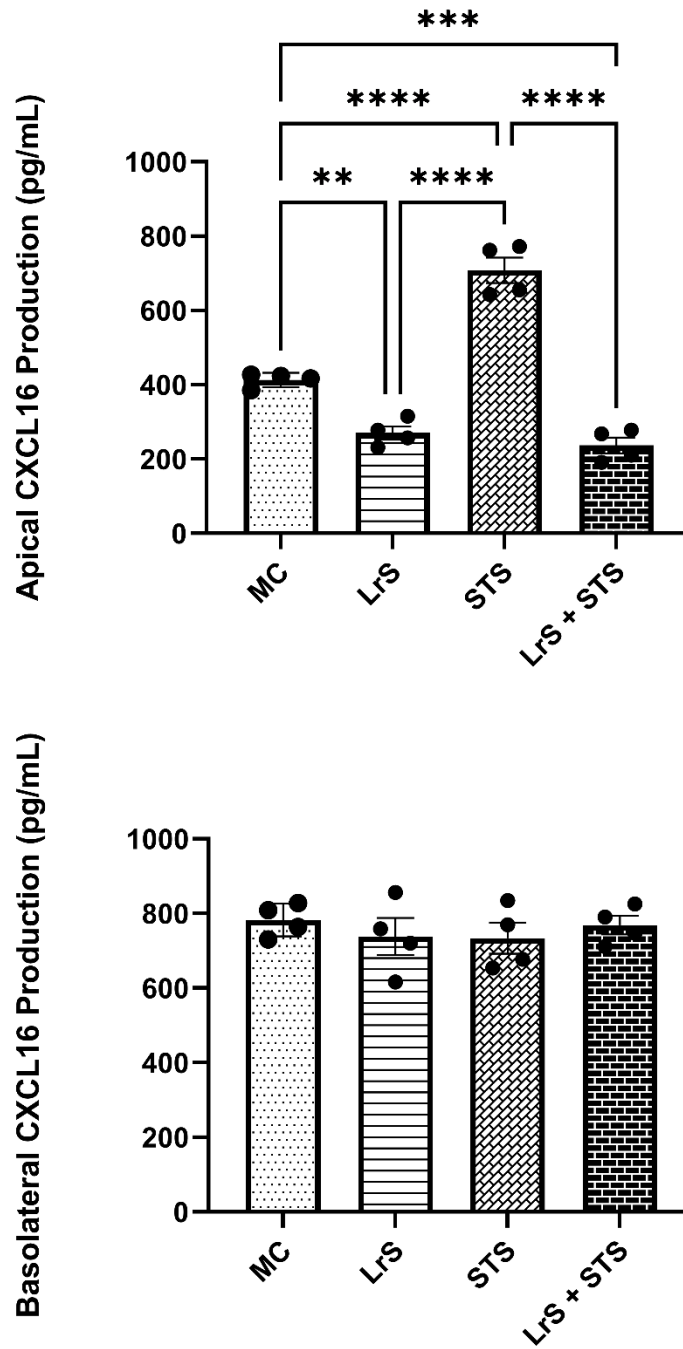


Figure 3-3Z. Apical and basolateral production of CXCL16 by T84 IEC and THP-1 monocyte co-cultures following challenge with the LrS, STS, or a combination of the secretomes for 24 hours. Data shown is the mean cytokine/chemokine production (pg/mL) \pm SEM (n = 4). Significance is indicated as * $p < 0.05$, ** $p < 0.01$, *** $p < 0.001$ as determined by one-way ANOVA and Tukey's post-hoc test.

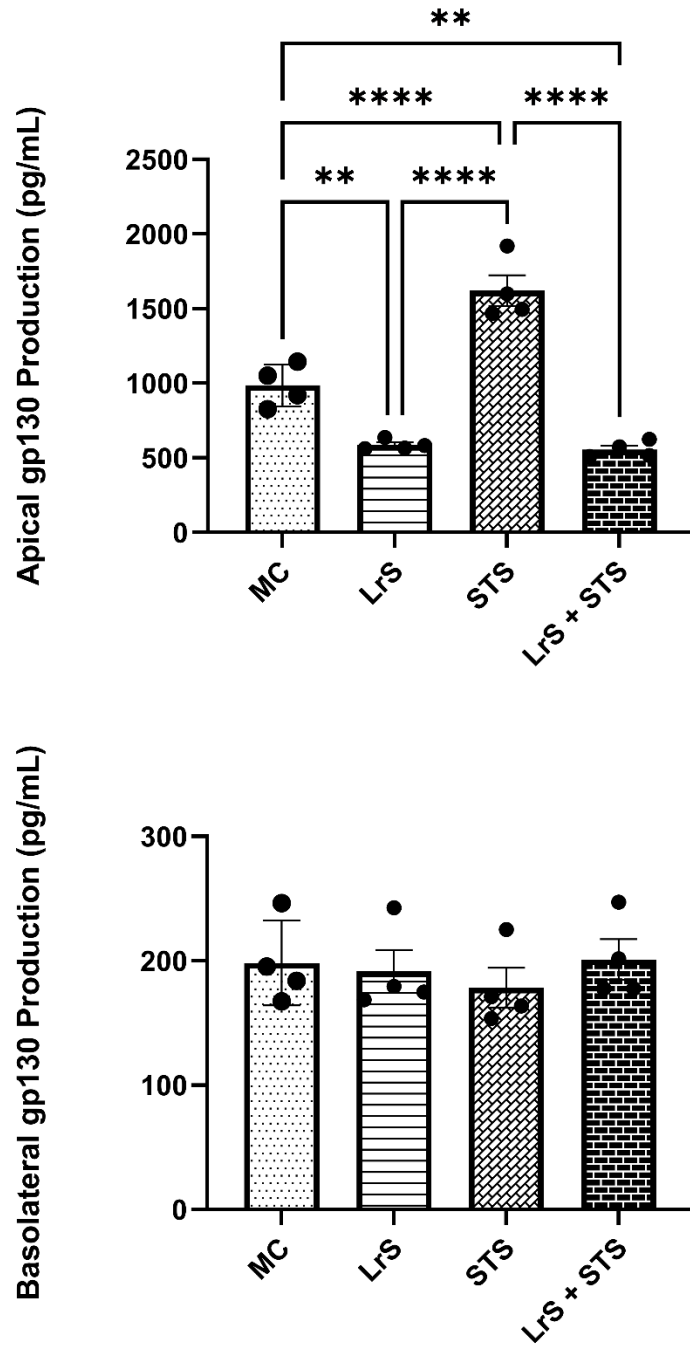


Figure 3-3AA. Apical and basolateral production of gp130 by T84 IEC and THP-1 monocyte co-cultures following challenge with the LrS, STS, or a combination of the secretomes for 24 hours. Data shown is the mean cytokine/chemokine production (pg/mL) \pm SEM (n = 4). Significance is indicated as * $p < 0.05$, ** $p < 0.01$, *** $p < 0.001$ as determined by one-way ANOVA and Tukey's post-hoc test.

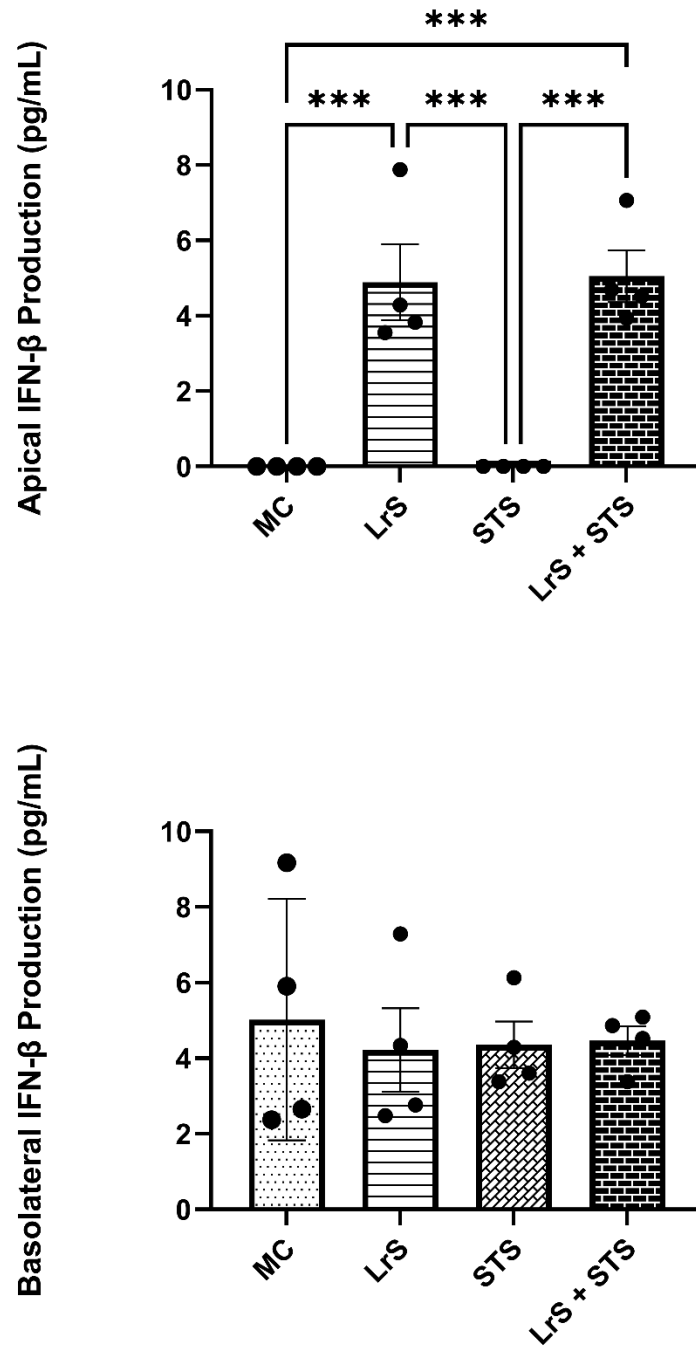


Figure 3-3BB. Apical and basolateral production of IFN- β by T84 IEC and THP-1 monocyte co-cultures following challenge with the LrS, STS, or a combination of the secretomes for 24 hours. Data shown is the mean cytokine/chemokine production (pg/mL) \pm SEM (n = 4). Significance is indicated as * $p < 0.05$, ** $p < 0.01$, *** $p < 0.001$ as determined by one-way ANOVA and Tukey's post-hoc test.

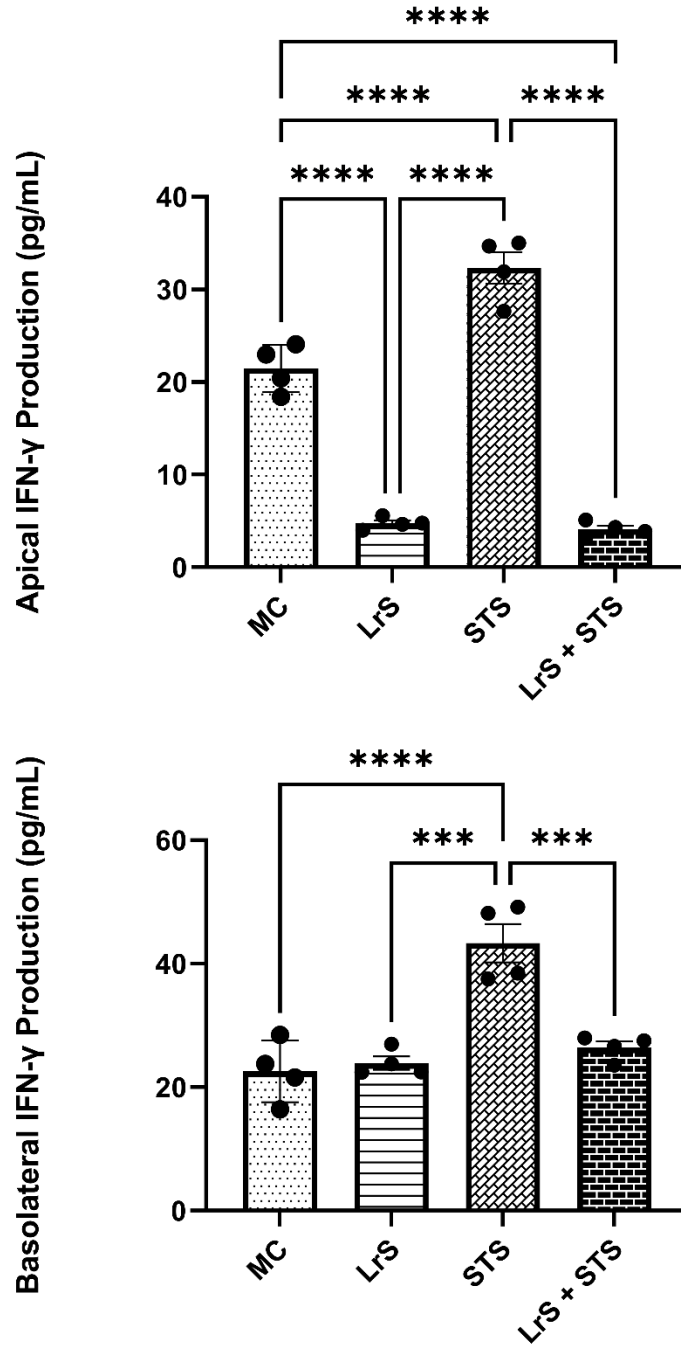


Figure 3-3CC. Apical and basolateral production of IFN- γ by T84 IEC and THP-1 monocyte co-cultures following challenge with the LrS, STS, or a combination of the secretomes for 24 hours. Data shown is the mean cytokine/chemokine production (pg/mL) \pm SEM (n = 4). Significance is indicated as * $p < 0.05$, ** $p < 0.01$, *** $p < 0.001$ as determined by one-way ANOVA and Tukey's post-hoc test.

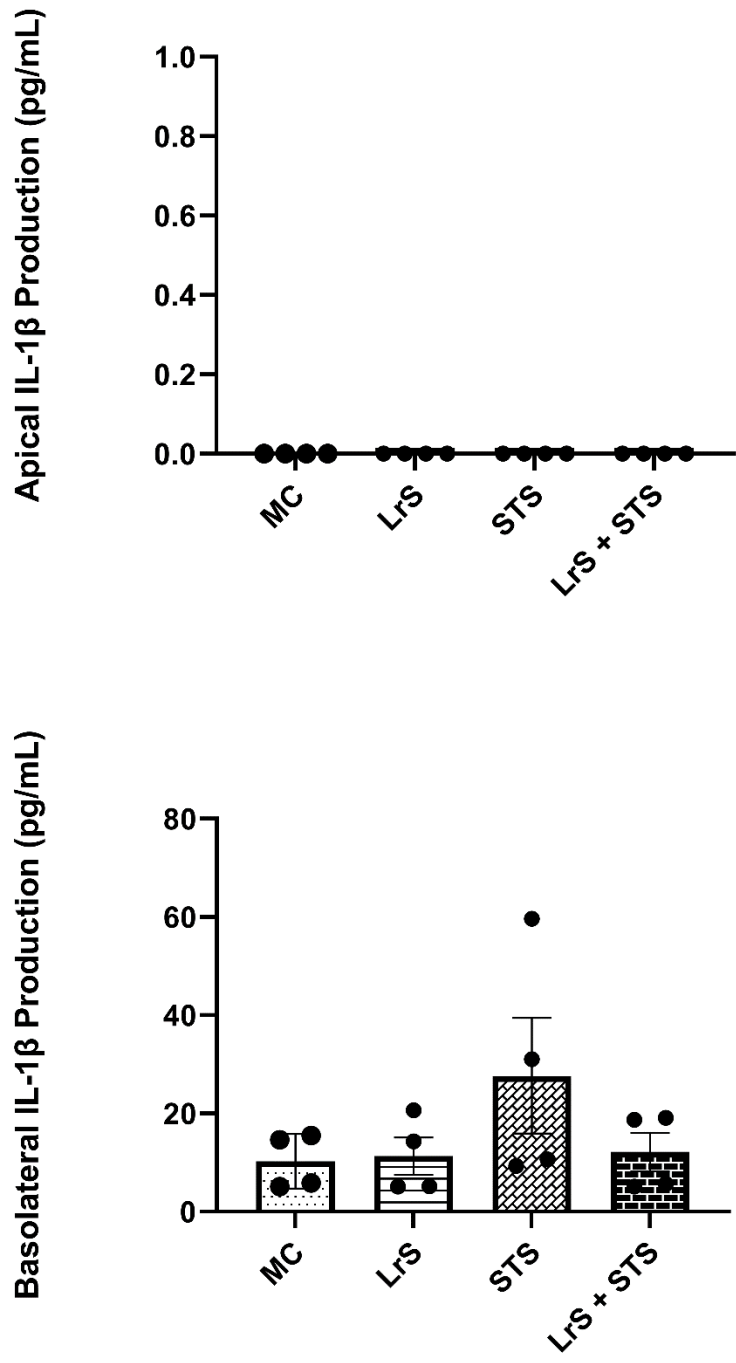


Figure 3-3DD. Apical and basolateral production of IL-1 β by T84 IEC and THP-1 monocyte co-cultures following challenge with the LrS, STS, or a combination of the secretomes for 24 hours. Data shown is the mean cytokine/chemokine production (pg/mL) \pm SEM (n = 4). Significance is indicated as * $p < 0.05$, ** $p < 0.01$, *** $p < 0.001$ as determined by one-way ANOVA and Tukey's post-hoc test.

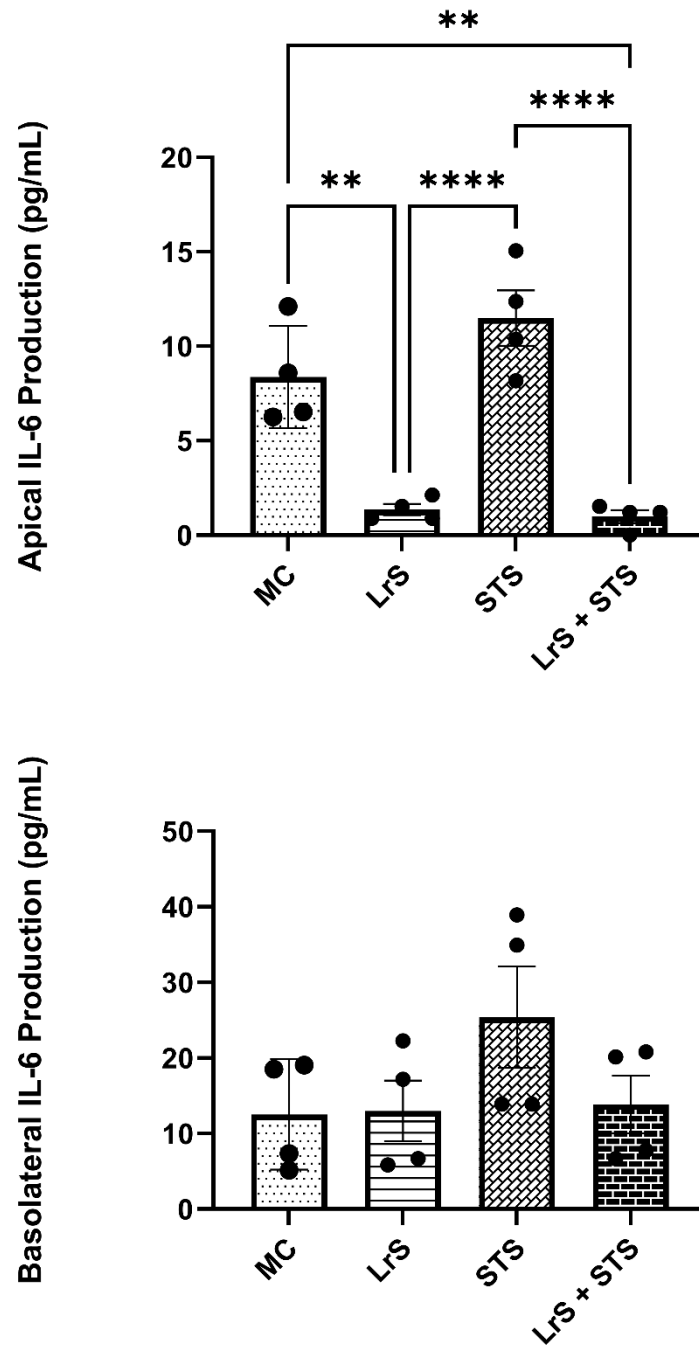


Figure 3-3EE. Apical and basolateral production of IL-6 by T84 IEC and THP-1 monocyte co-cultures following challenge with the LrS, STS, or a combination of the secretomes for 24 hours. Data shown is the mean cytokine/chemokine production (pg/mL) \pm SEM (n = 4). Significance is indicated as * $p < 0.05$, ** $p < 0.01$, *** $p < 0.001$ as determined by one-way ANOVA and Tukey's post-hoc test.

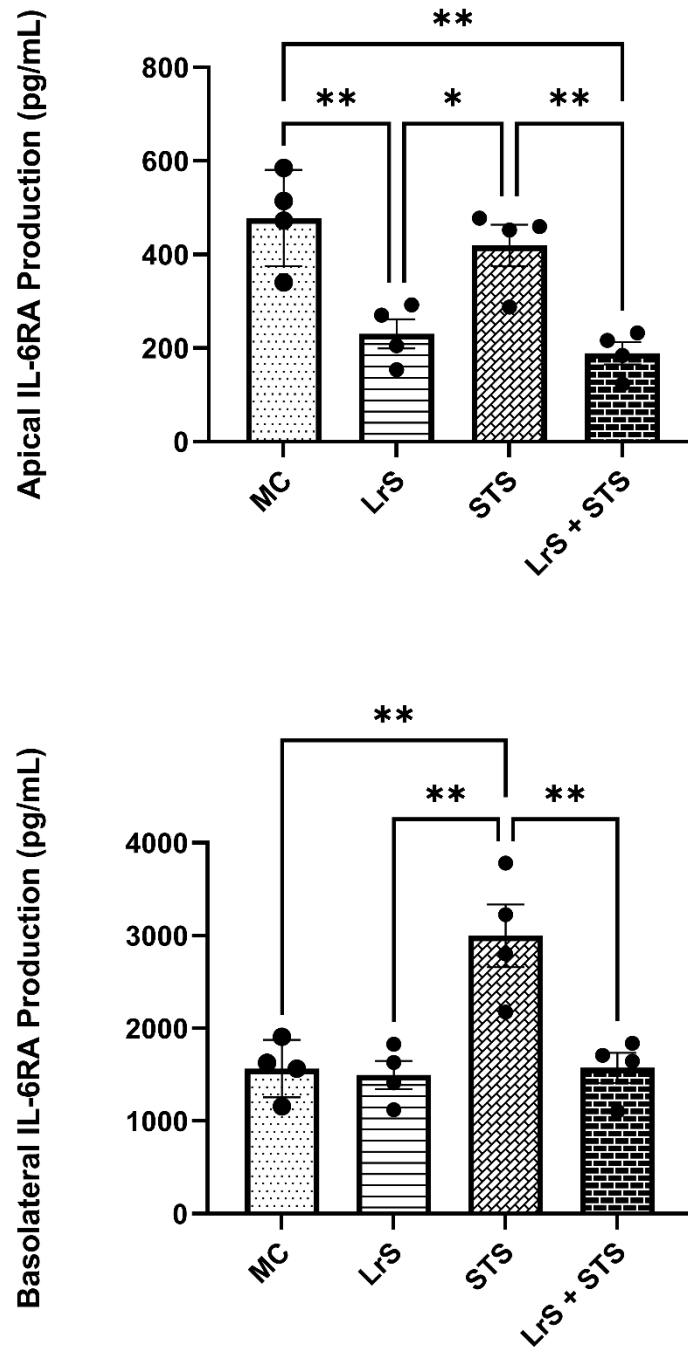


Figure 3-3FF. Apical and basolateral production of IL-6RA by T84 IEC and THP-1 monocyte co-cultures following challenge with the LrS, STS, or a combination of the secretomes for 24 hours. Data shown is the mean cytokine/chemokine production (pg/mL) \pm SEM (n = 4). Significance is indicated as * $p < 0.05$, ** $p < 0.01$, *** $p < 0.001$ as determined by one-way ANOVA and Tukey's post-hoc test.

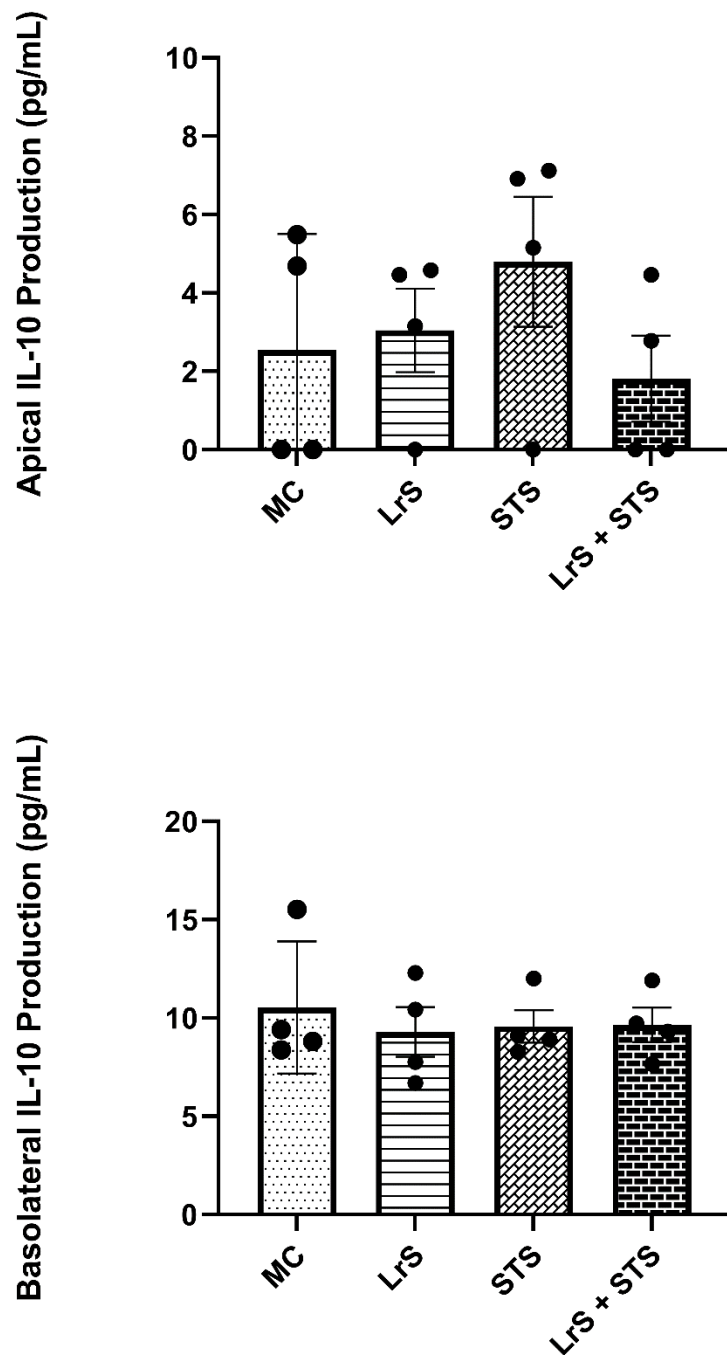


Figure 3-3GG. Apical and basolateral production of IL-10 by T84 IEC and THP-1 monocyte co-cultures following challenge with the LrS, STS, or a combination of the secretomes for 24 hours. Data shown is the mean cytokine/chemokine production (pg/mL) \pm SEM (n = 4). Significance is indicated as * $p < 0.05$, ** $p < 0.01$, *** $p < 0.001$ as determined by one-way ANOVA and Tukey's post-hoc test.

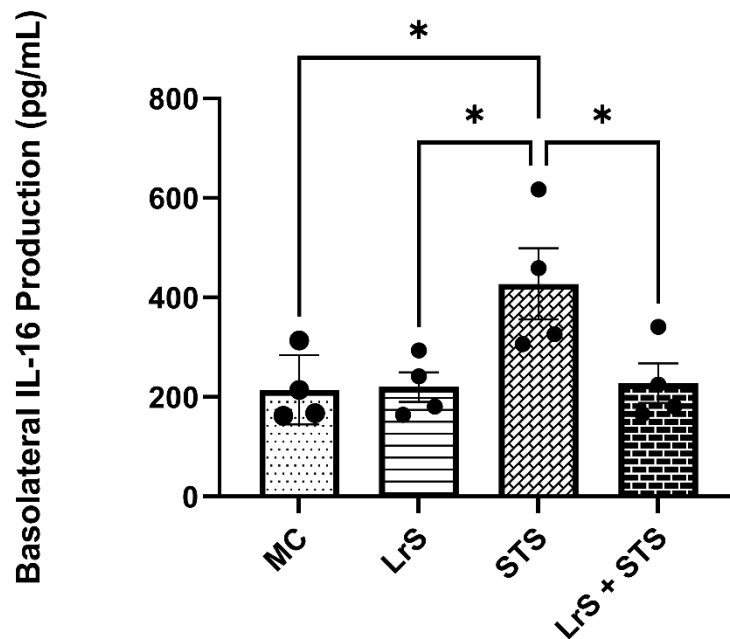
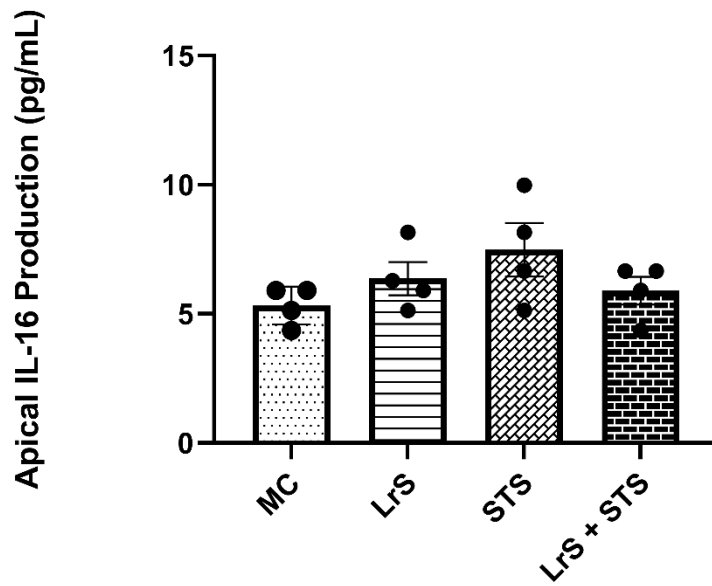


Figure 3-3HH. Apical and basolateral production of IL-16 by T84 IEC and THP-1 monocyte co-cultures following challenge with the LrS, STS, or a combination of the secretomes for 24 hours. Data shown is the mean cytokine/chemokine production (pg/mL) \pm SEM (n = 4). Significance is indicated as * $p < 0.05$, ** $p < 0.01$, *** $p < 0.001$ as determined by one-way ANOVA and Tukey's post-hoc test.

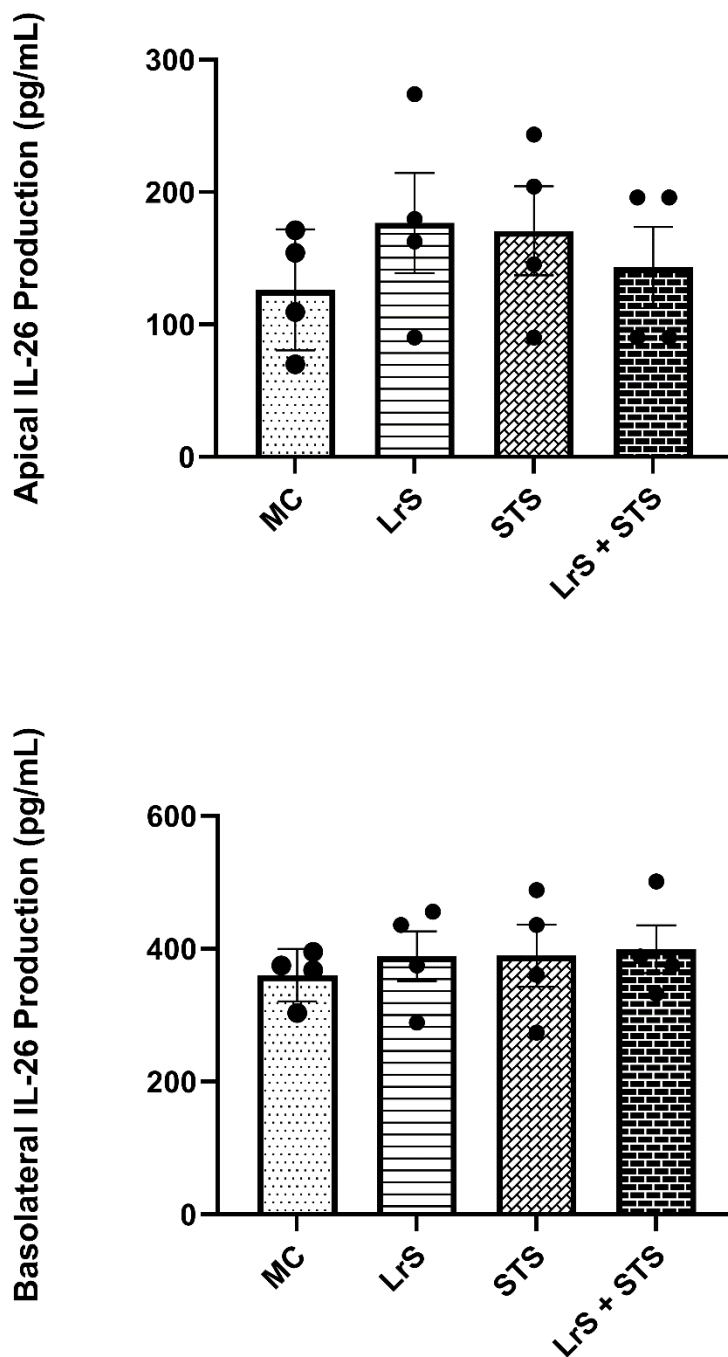


Figure 3-3II. Apical and basolateral production of IL-26 by T84 IEC and THP-1 monocyte co-cultures following challenge with the LrS, STS, or a combination of the secretomes for 24 hours. Data shown is the mean cytokine/chemokine production (pg/mL) \pm SEM (n = 4). Significance is indicated as * $p < 0.05$, ** $p < 0.01$, *** $p < 0.001$ as determined by one-way ANOVA and Tukey's post-hoc test.

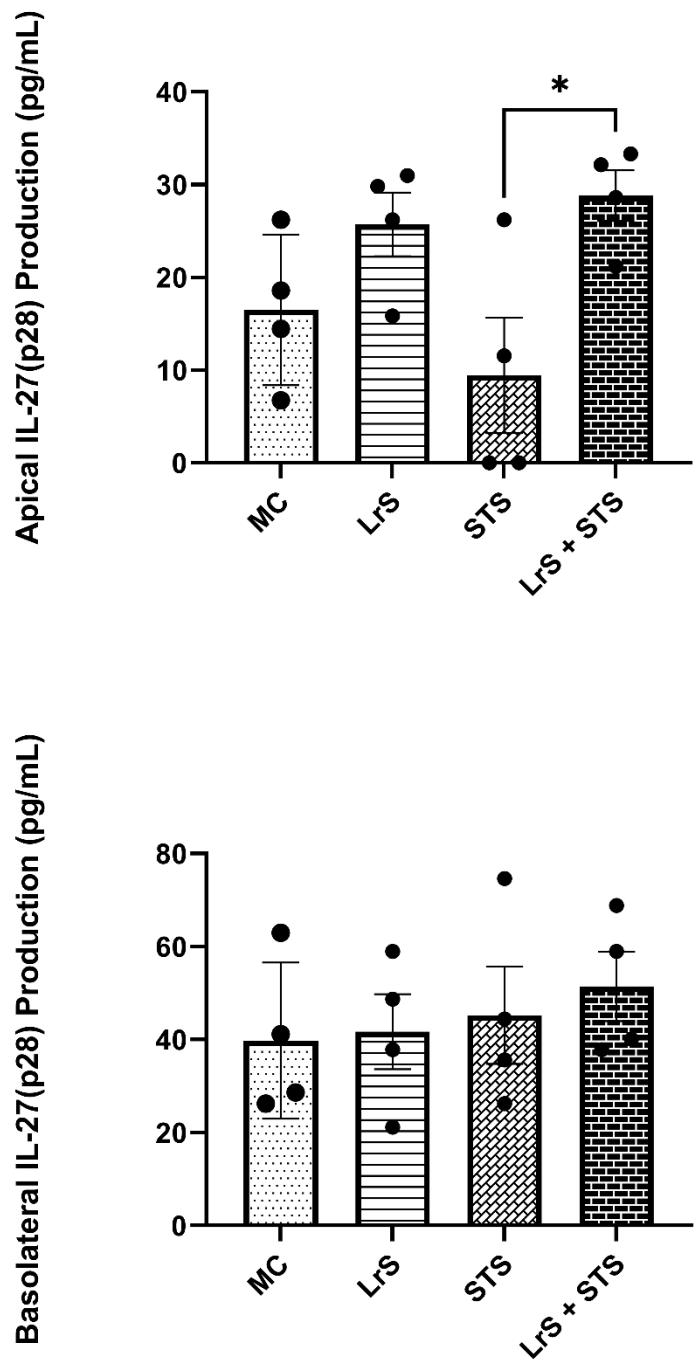


Figure 3-3JJ. Apical and basolateral production of IL-27(p28) by T84 IEC and THP-1 monocyte co-cultures following challenge with the LrS, STS, or a combination of the secretomes for 24 hours. Data shown is the mean cytokine/chemokine production (pg/mL) \pm SEM (n = 4). Significance is indicated as * $p < 0.05$, ** $p < 0.01$, *** $p < 0.001$ as determined by one-way ANOVA and Tukey's post-hoc test.

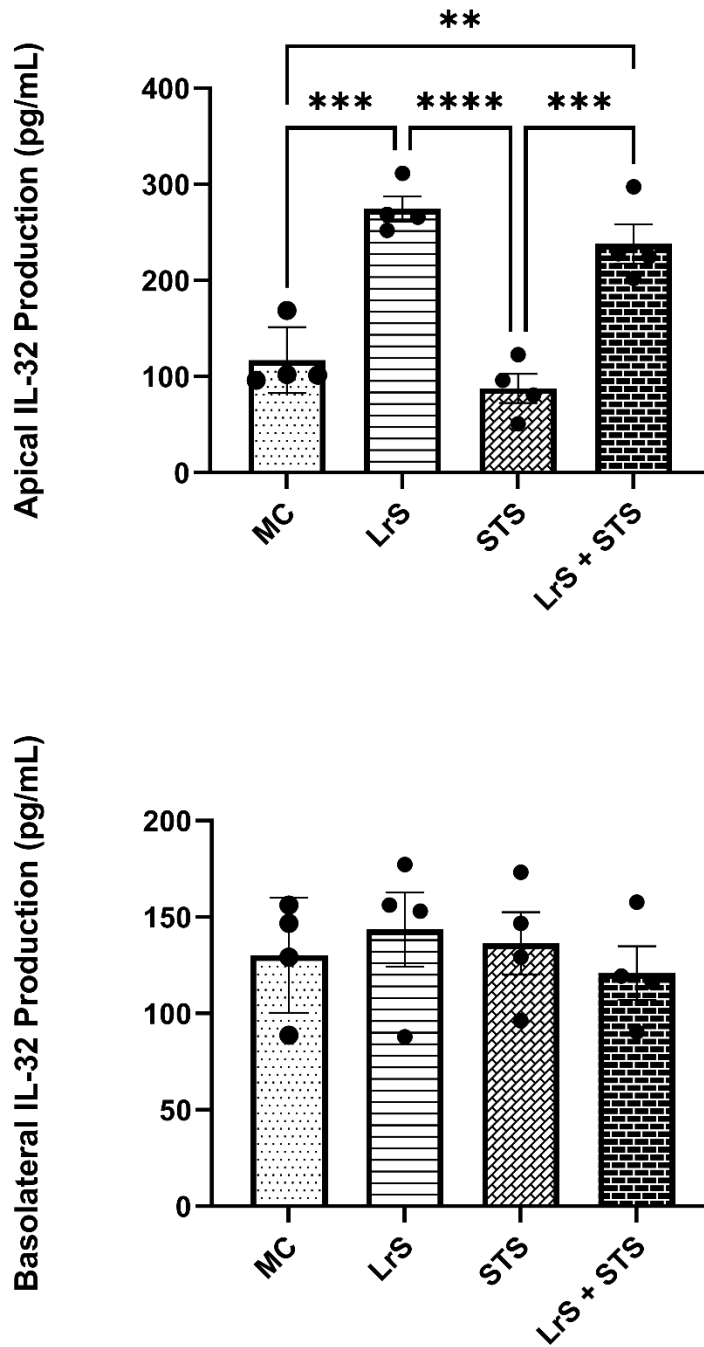


Figure 3-3KK. Apical and basolateral production of IL-32 by T84 IEC and THP-1 monocyte co-cultures following challenge with the LrS, STS, or a combination of the secretomes for 24 hours. Data shown is the mean cytokine/chemokine production (pg/mL) \pm SEM (n = 4). Significance is indicated as * $p < 0.05$, ** $p < 0.01$, *** $p < 0.001$ as determined by one-way ANOVA and Tukey's post-hoc test.

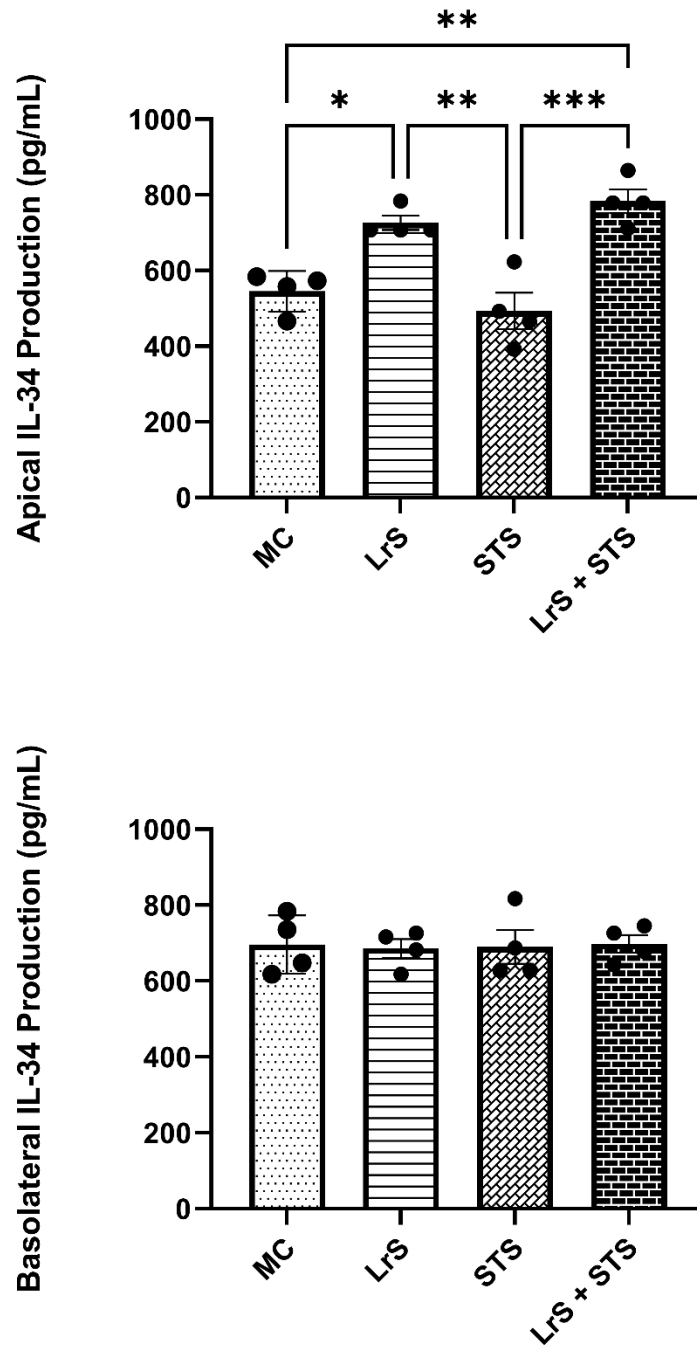


Figure 3-3LL. Apical and basolateral production of IL-34 by T84 IEC and THP-1 monocyte co-cultures following challenge with the LrS, STS, or a combination of the secretomes for 24 hours. Data shown is the mean cytokine/chemokine production (pg/mL) \pm SEM (n = 4). Significance is indicated as * $p < 0.05$, ** $p < 0.01$, *** $p < 0.001$ as determined by one-way ANOVA and Tukey's post-hoc test.

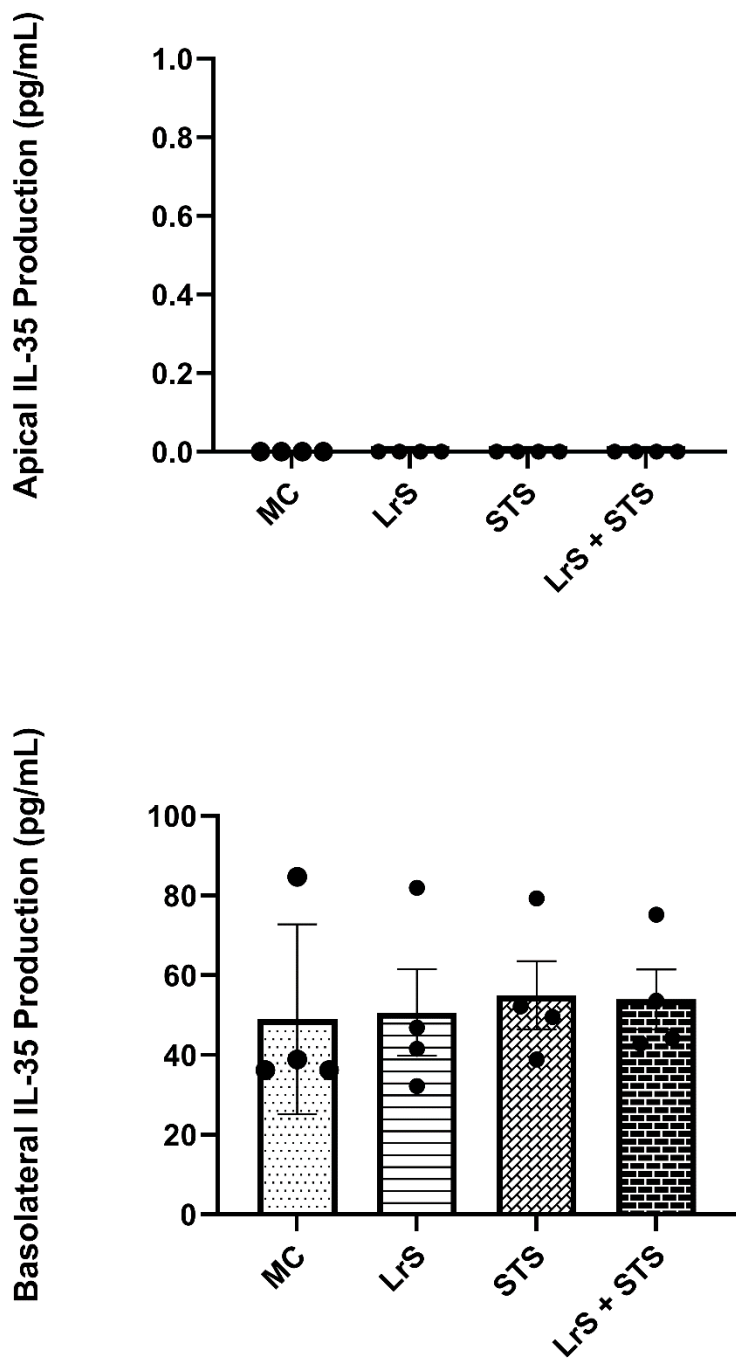


Figure 3-3MM. Apical and basolateral production of IL-35 by T84 IEC and THP-1 monocyte co-cultures following challenge with the LrS, STS, or a combination of the secretomes for 24 hours. Data shown is the mean cytokine/chemokine production (pg/mL) \pm SEM (n = 4). Significance is indicated as * $p < 0.05$, ** $p < 0.01$, *** $p < 0.001$ as determined by one-way ANOVA and Tukey's post-hoc test.

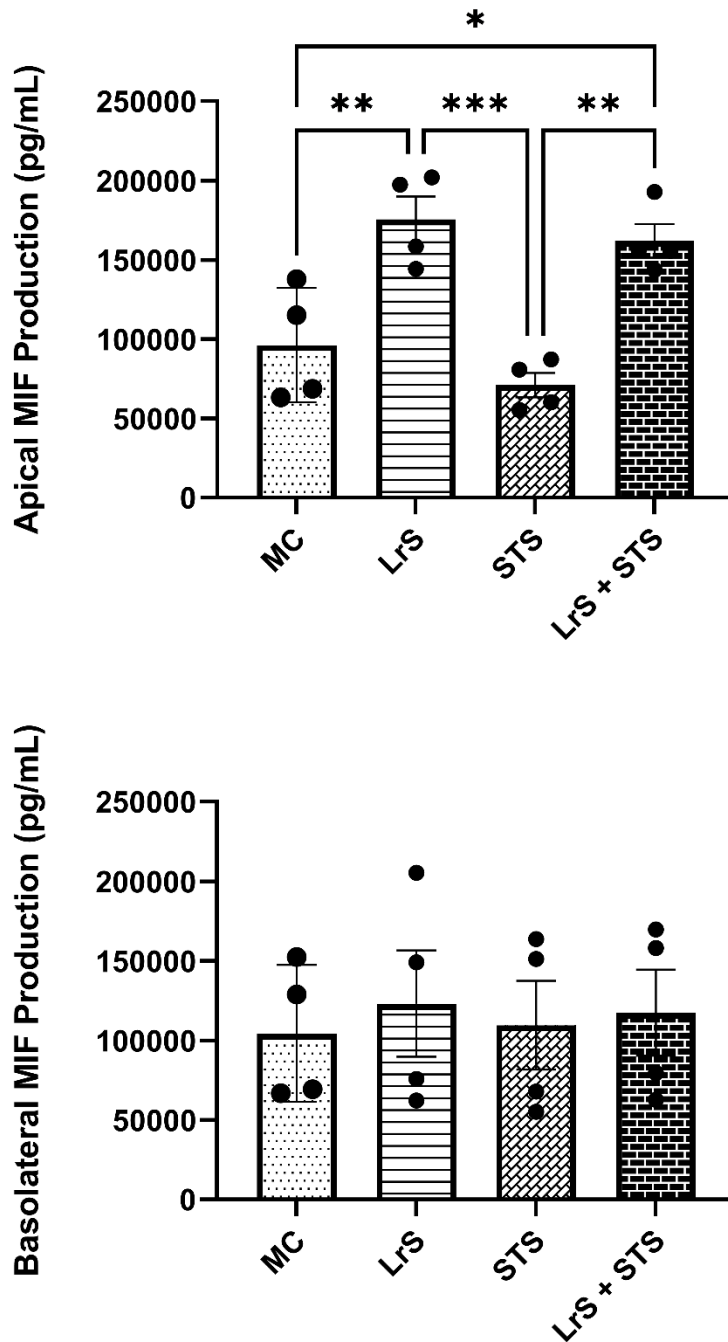


Figure 3-3NN. Apical and basolateral production of MIF by T84 IEC and THP-1 monocyte co-cultures following challenge with the LrS, STS, or a combination of the secretomes for 24 hours. Data shown is the mean cytokine/chemokine production (pg/mL) \pm SEM (n = 4). Significance is indicated as * $p < 0.05$, ** $p < 0.01$, *** $p < 0.001$ as determined by one-way ANOVA and Tukey's post-hoc test.

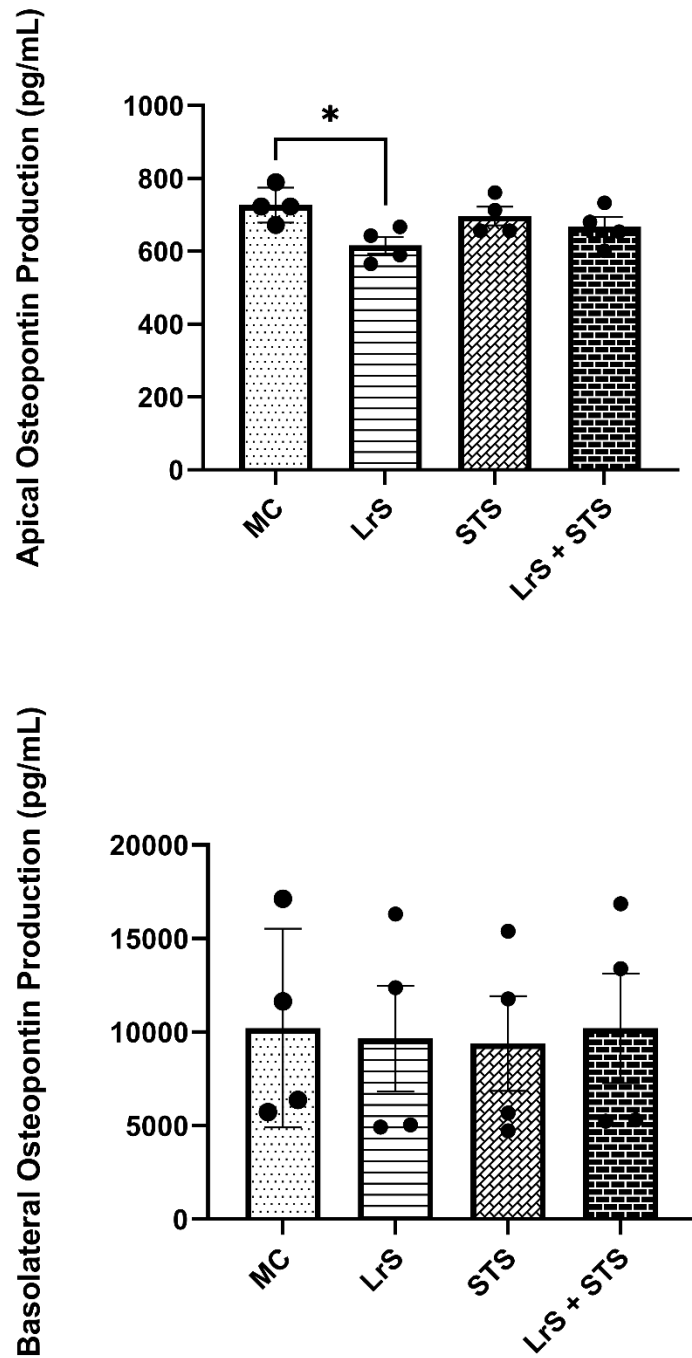


Figure 3-300. Apical and basolateral production of Osteopontin by T84 IEC and THP-1 monocyte co-cultures following challenge with the LrS, STS, or a combination of the secretomes for 24 hours. Data shown is the mean cytokine/chemokine production (pg/mL) \pm SEM (n = 4). Significance is indicated as * $p < 0.05$, ** $p < 0.01$, *** $p < 0.001$ as determined by one-way ANOVA and Tukey's post-hoc test.

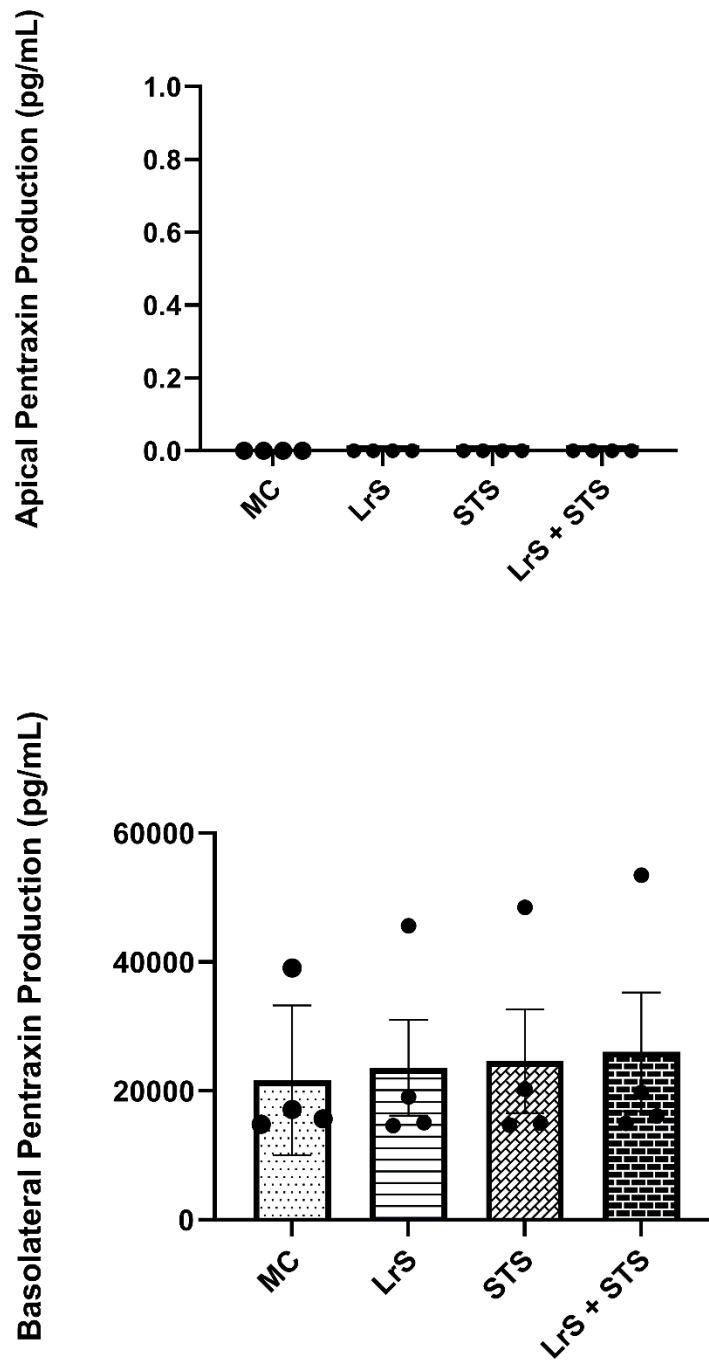


Figure 3-3P. Apical and basolateral production of Pentraxin by T84 IEC and THP-1 monocyte co-cultures following challenge with the LrS, STS, or a combination of the secretomes for 24 hours. Data shown is the mean cytokine/chemokine production (pg/mL) \pm SEM (n = 4). Significance is indicated as * $p < 0.05$, ** $p < 0.01$, *** $p < 0.001$ as determined by one-way ANOVA and Tukey's post-hoc test.

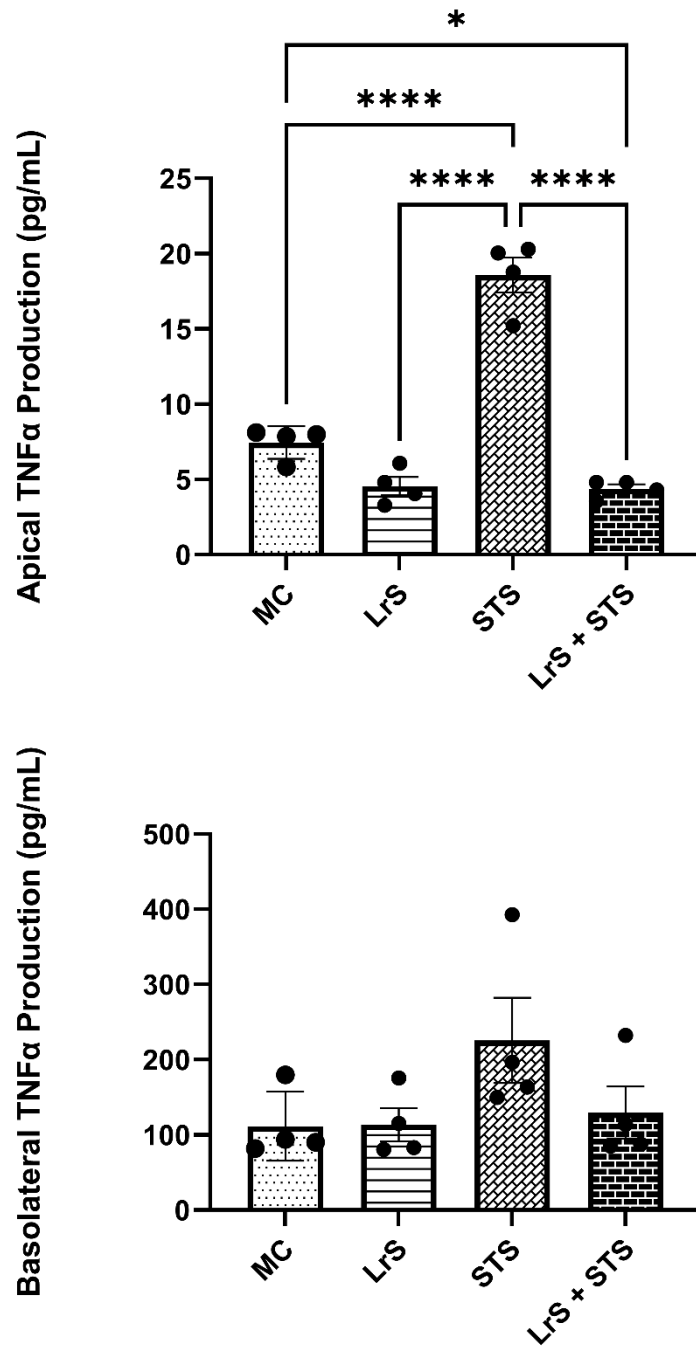


Figure 3-3QQ. Apical and basolateral production of TNF- α by T84 IEC and THP-1 monocyte co-cultures following challenge with the LrS, STS, or a combination of the secretomes for 24 hours. Data shown is the mean cytokine/chemokine production (pg/mL) \pm SEM (n = 4). Significance is indicated as * $p < 0.05$, ** $p < 0.01$, *** $p < 0.001$ as determined by one-way ANOVA and Tukey's post-hoc test.

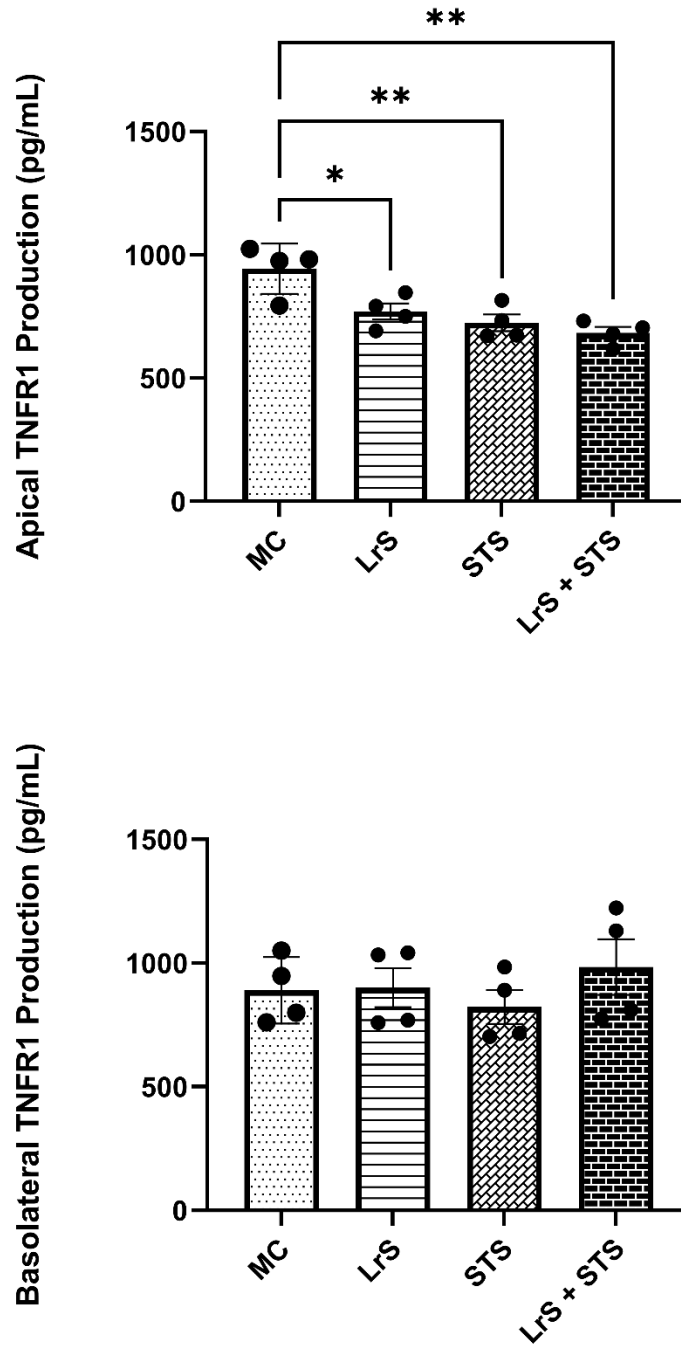


Figure 3-3RR. Apical and basolateral production of TNFR1 by T84 IEC and THP-1 monocyte co-cultures following challenge with the LrS, STS, or a combination of the secretomes for 24 hours. Data shown is the mean cytokine/chemokine production (pg/mL) \pm SEM (n = 4). Significance is indicated as * $p < 0.05$, ** $p < 0.01$, *** $p < 0.001$ as determined by one-way ANOVA and Tukey's post-hoc test.

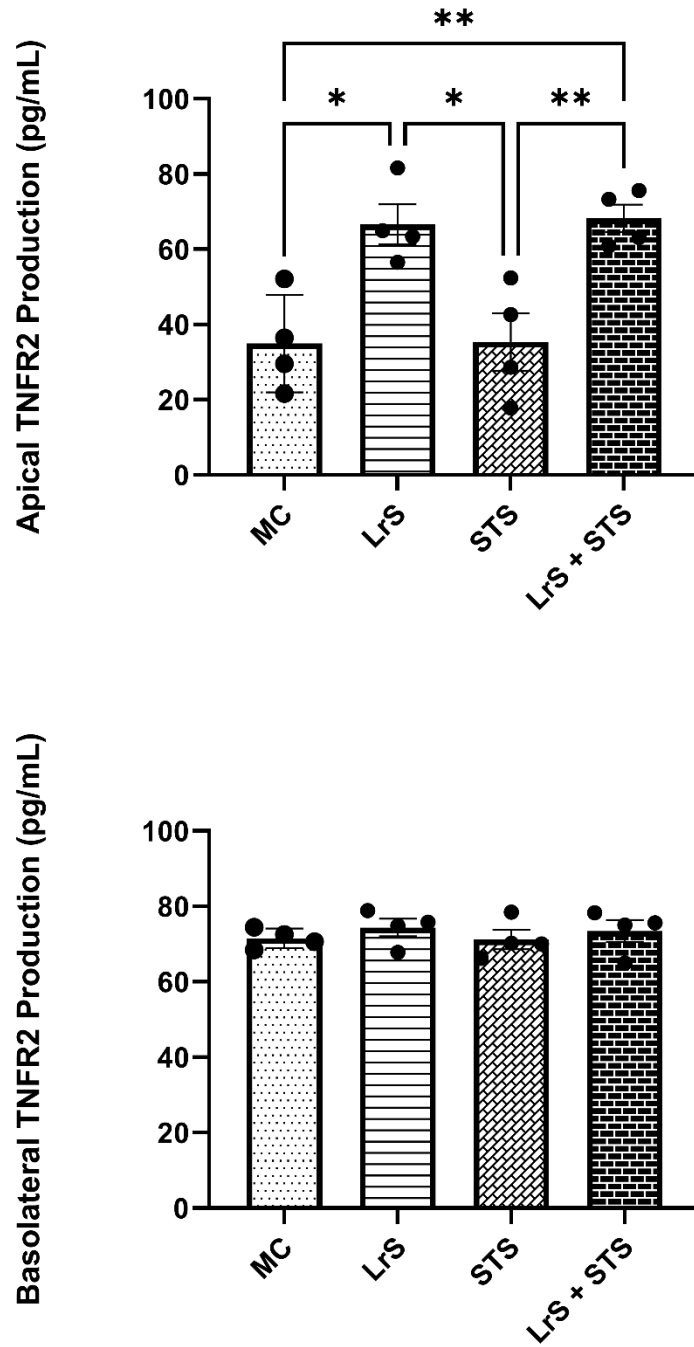


Figure 3-3SS. Apical and basolateral production of TNFR2 by T84 IEC and THP-1 monocyte co-cultures following challenge with the LrS, STS, or a combination of the secretomes for 24 hours. Data shown is the mean cytokine/chemokine production (pg/mL) \pm SEM (n = 4). Significance is indicated as * $p < 0.05$, ** $p < 0.01$, *** $p < 0.001$ as determined by one-way ANOVA and Tukey's post-hoc test.

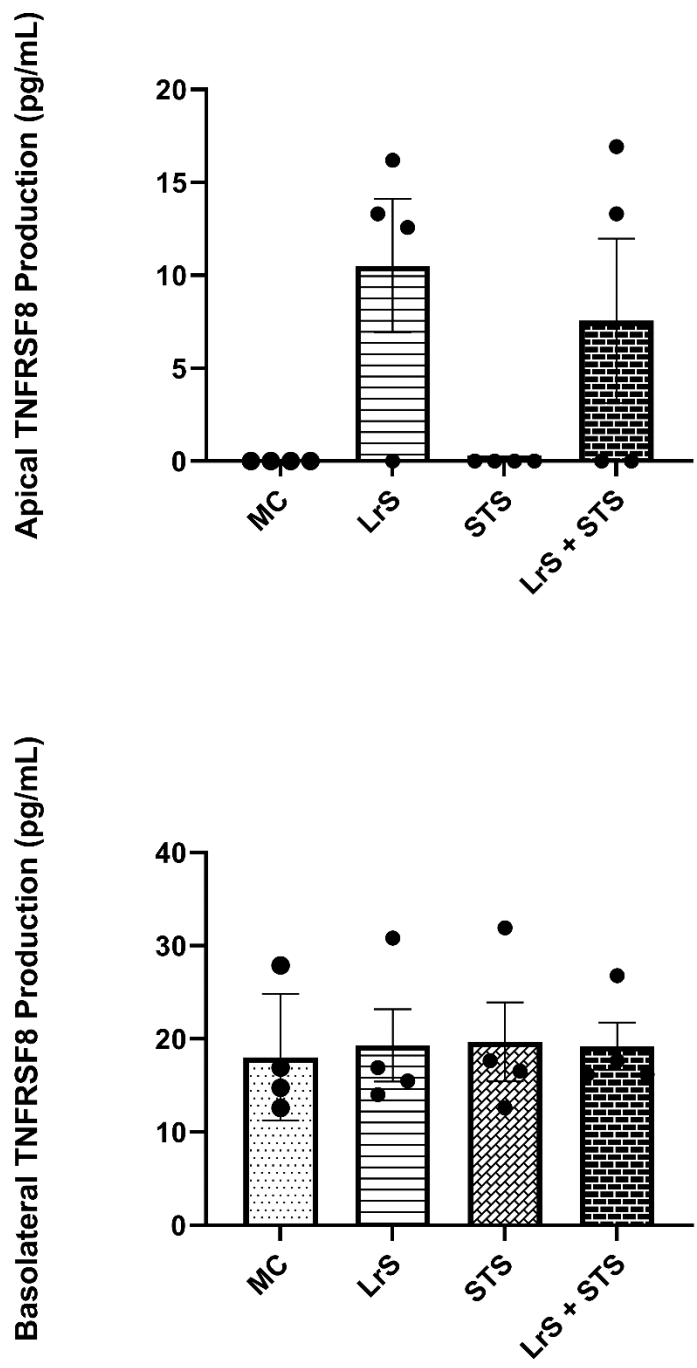


Figure 3-3TT. Apical and basolateral production of TNFRSF8 by T84 IEC and THP-1 monocyte co-cultures following challenge with the LrS, STS, or a combination of the secretomes for 24 hours. Data shown is the mean cytokine/chemokine production (pg/mL) \pm SEM (n = 4). Significance is indicated as * $p < 0.05$, ** $p < 0.01$, *** $p < 0.001$ as determined by one-way ANOVA and Tukey's post-hoc test.

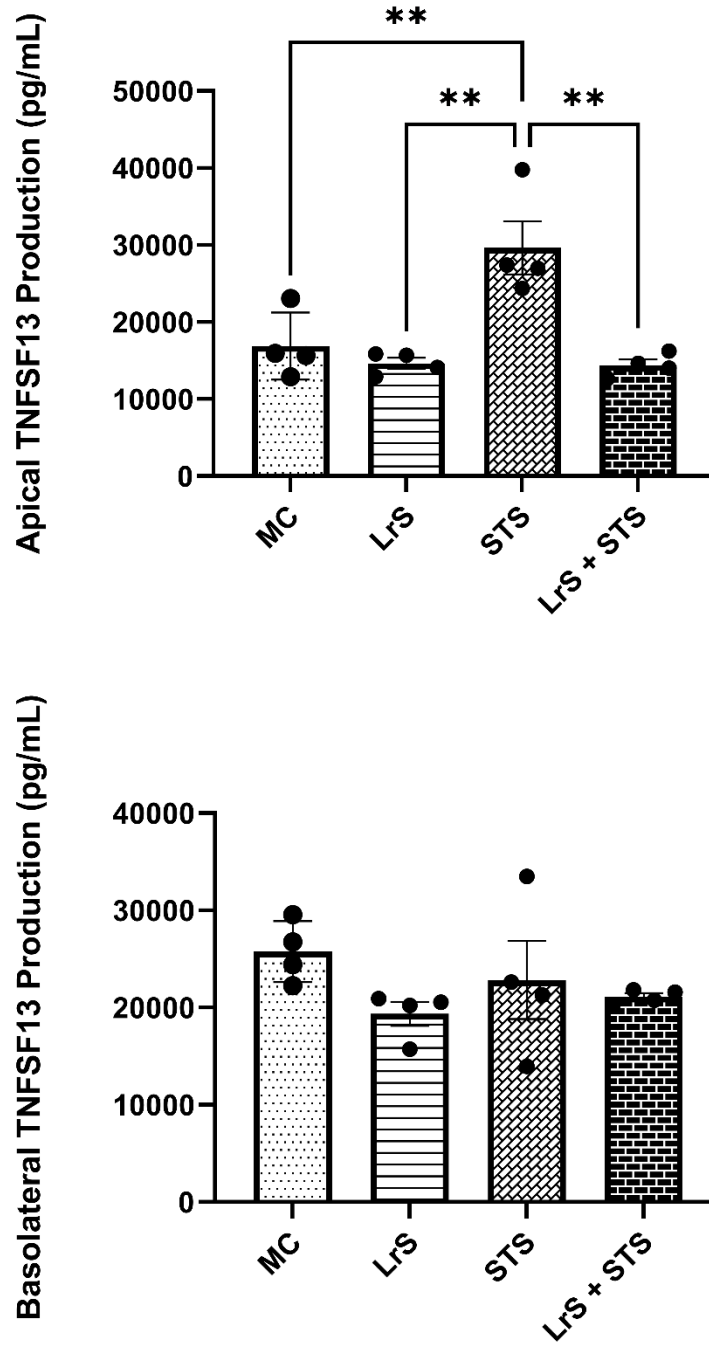


Figure 3-3UU. Apical and basolateral production of TNFSF13 by T84 IEC and THP-1 monocyte co-cultures following challenge with the LrS, STS, or a combination of the secretomes for 24 hours. Data shown is the mean cytokine/chemokine production (pg/mL) \pm SEM (n = 4). Significance is indicated as * $p < 0.05$, ** $p < 0.01$, *** $p < 0.001$ as determined by one-way ANOVA and Tukey's post-hoc test.

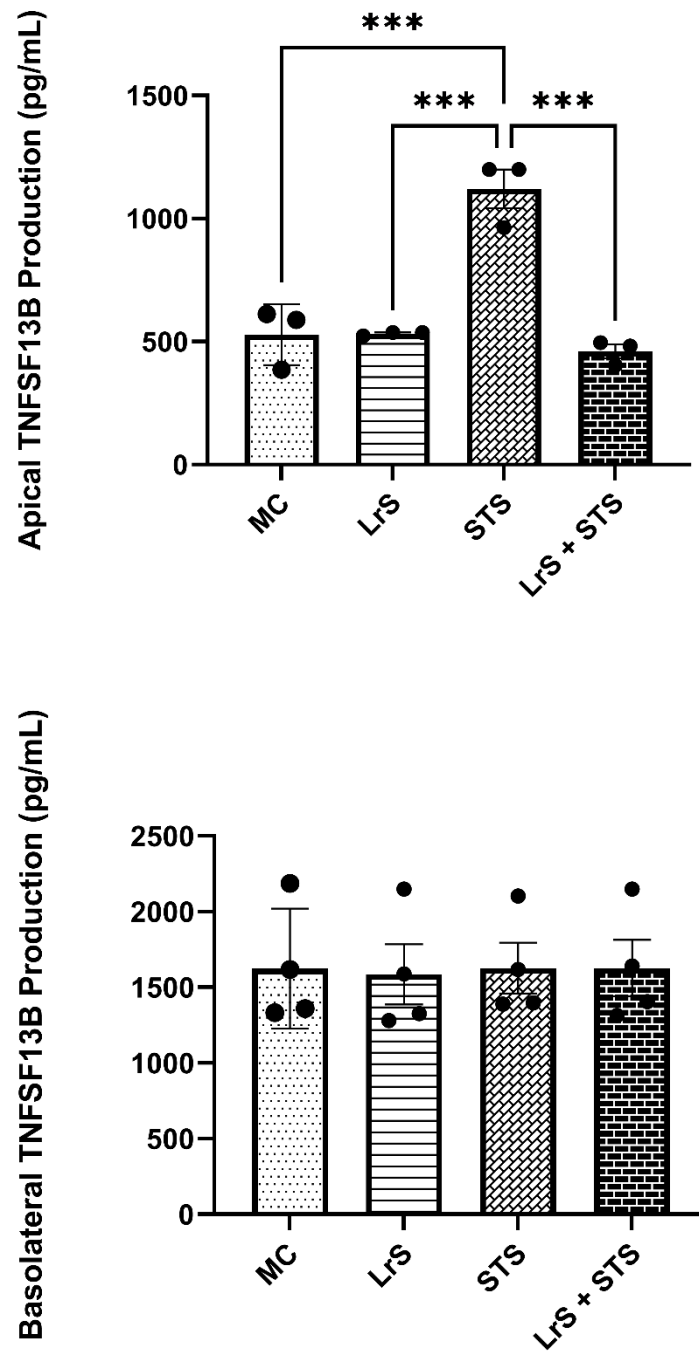


Figure 3-3VV. Apical and basolateral production of TNFSF13B by T84 IEC and THP-1 monocyte co-cultures following challenge with the LrS, STS, or a combination of the secretomes for 24 hours. Data shown is the mean cytokine/chemokine production (pg/mL) \pm SEM (n = 4). Significance is indicated as * $p < 0.05$, ** $p < 0.01$, *** $p < 0.001$ as determined by one-way ANOVA and Tukey's post-hoc test.

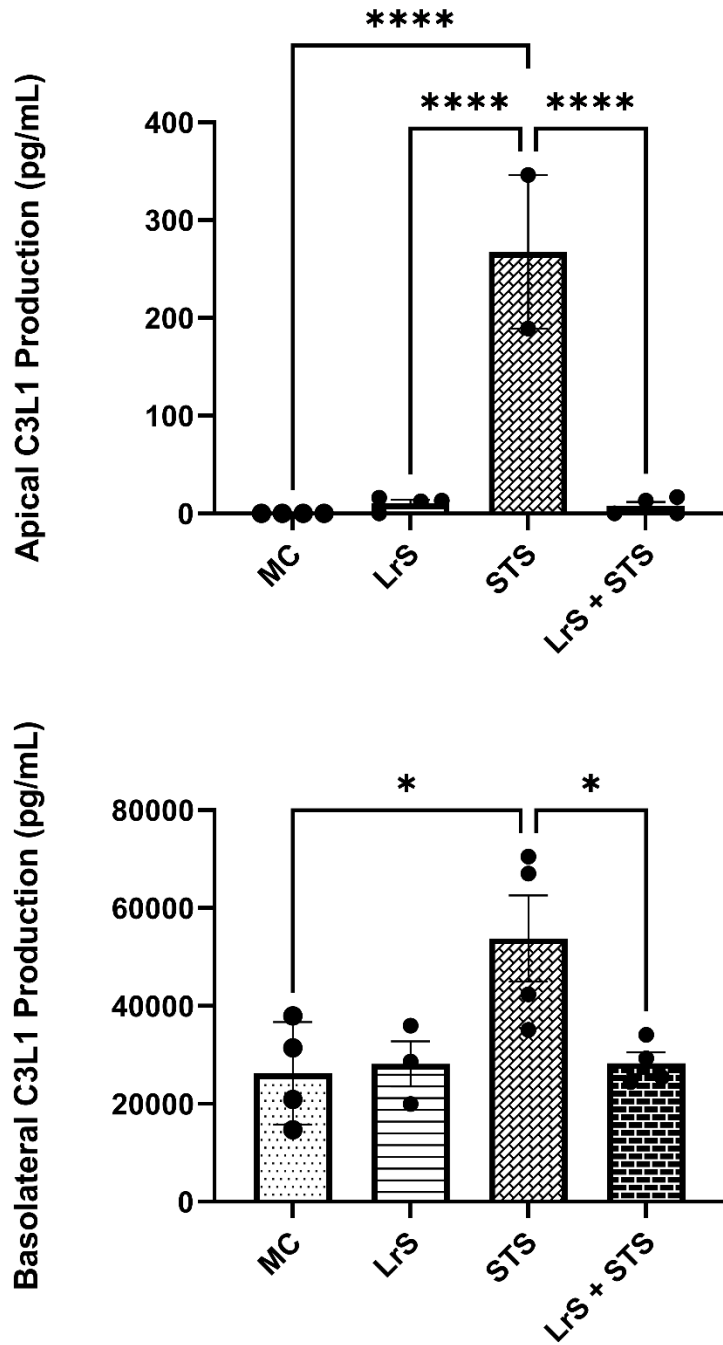


Figure 3-3WW. Apical and basolateral production of C3L1 by T84 IEC and THP-1 monocyte co-cultures following challenge with the LrS, STS, or a combination of the secretomes for 24 hours. Data shown is the mean cytokine/chemokine production (pg/mL) \pm SEM (n = 4). Significance is indicated as * $p < 0.05$, ** $p < 0.01$, *** $p < 0.001$ as determined by one-way ANOVA and Tukey's post-hoc test.

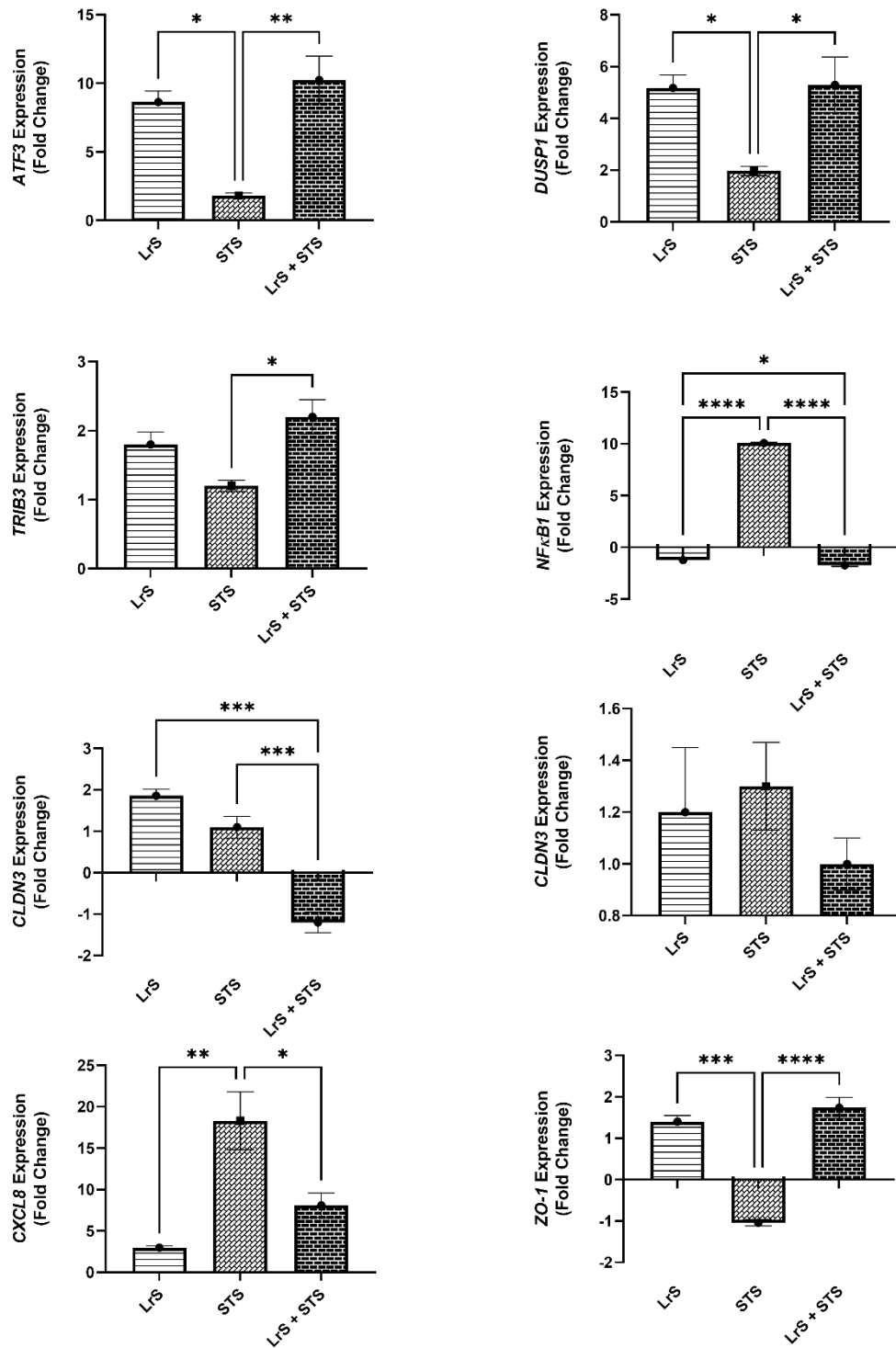


Figure 3-4. Gene expression profiles of T84 IECs in T84 IEC/THP-1 monocyte co-cultures challenged with the LrS, STS, or a combination of the challenges. Data shown is the mean fold-change relative to untreated controls \pm SEM (n = 4). Significance is indicated as * $p < 0.05$, ** $p < 0.01$, *** $p < 0.001$ as determined by one-way ANOVA and Tukey's post-hoc test.

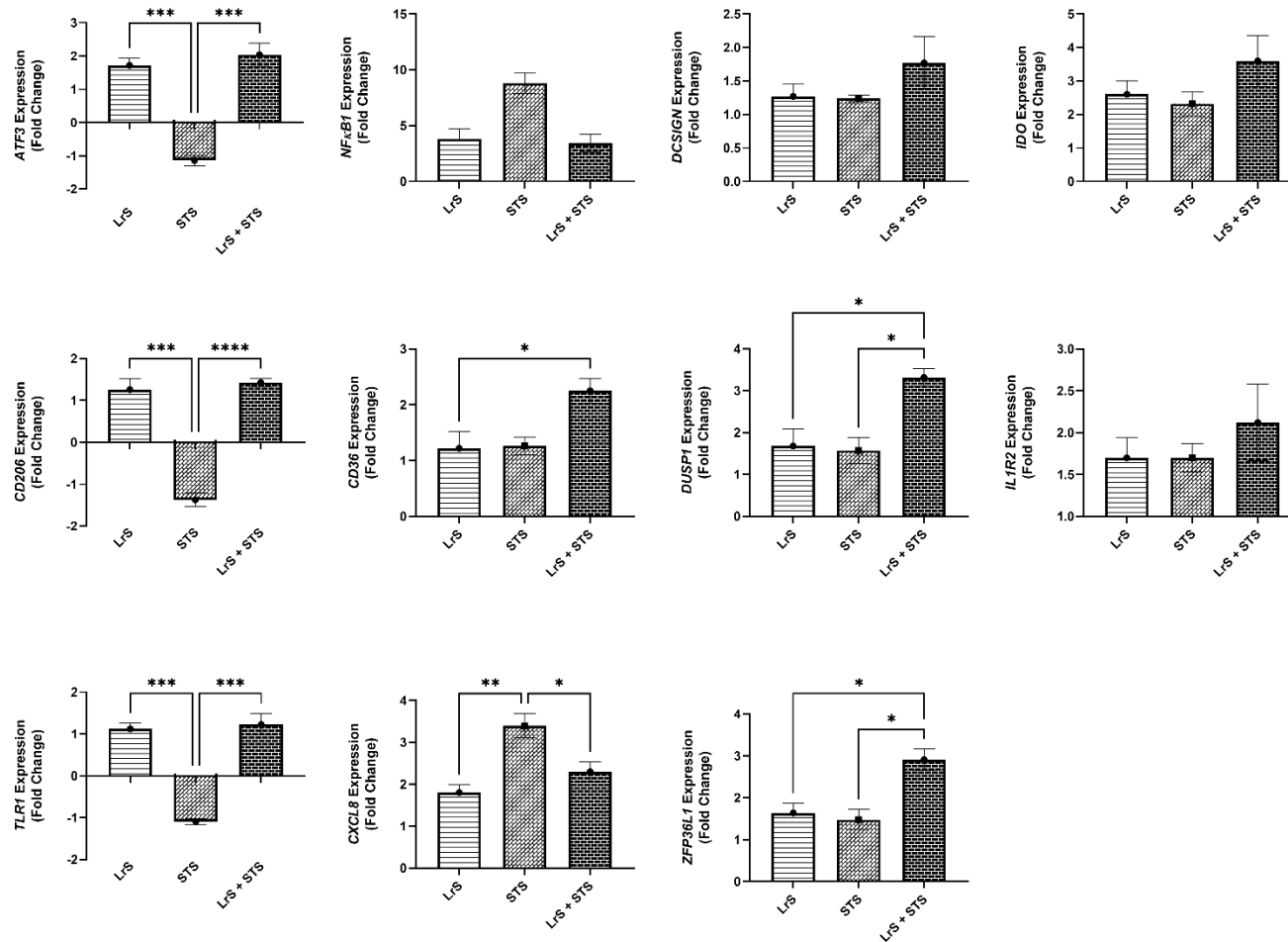


Figure 3-5. Gene expression profiles of THP-1 monocytes in T84 IEC/THP-1 monocyte co-cultures challenged with the LrS, STS, or a combination of the challenges. Data shown is the mean fold-change relative to untreated controls \pm SEM (n = 4). Significance is indicated as * $p < 0.05$, ** $p < 0.01$, *** $p < 0.001$ as determined by one-way ANOVA and Tukey's post-hoc test.

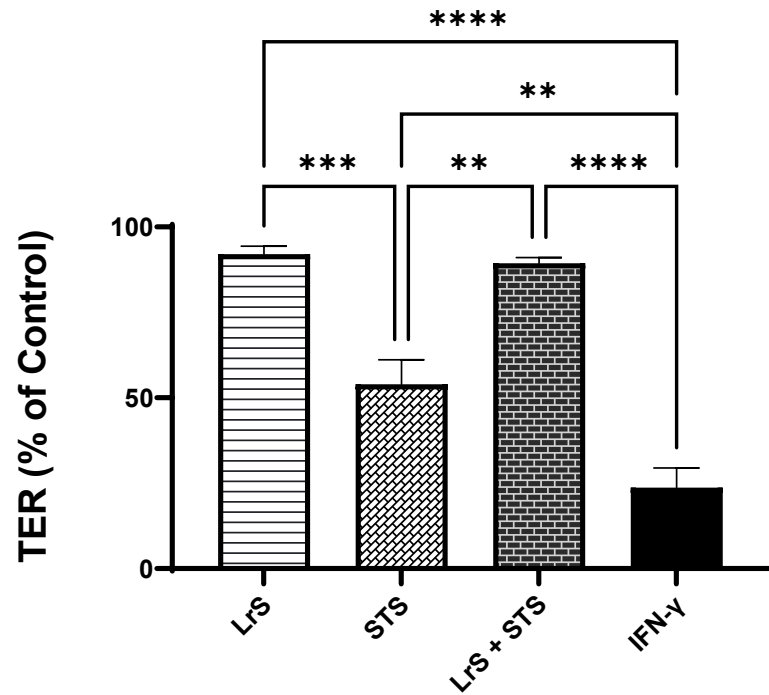
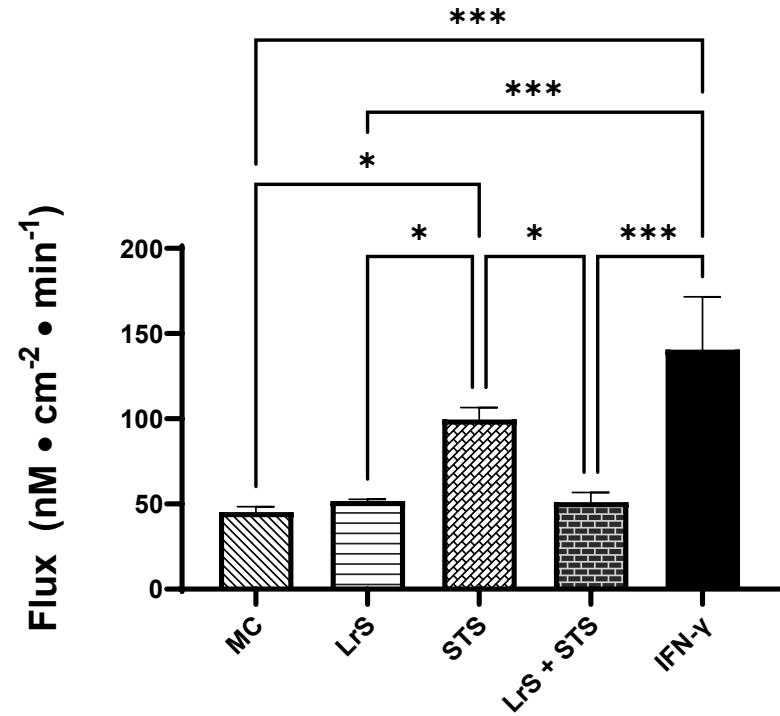
A.**B.**

Figure 3-6. The LrS attenuates STS-induced damage to T84 IEC monolayer integrity and permeability. **A.** Transepithelial resistance (TER) was measured following challenge of T84 IECs with the LrS, STS, or combined secretome challenges for 24 hours (n = 3). **B.** T84 IEC monolayer permeability was determined by measuring the amount of flux of FITC-dextran following challenge (n = 3). Significance is indicated as * $p < 0.05$, ** $p < 0.01$, *** $p < 0.001$ as determined by one-way ANOVA and Tukey's post-hoc test.

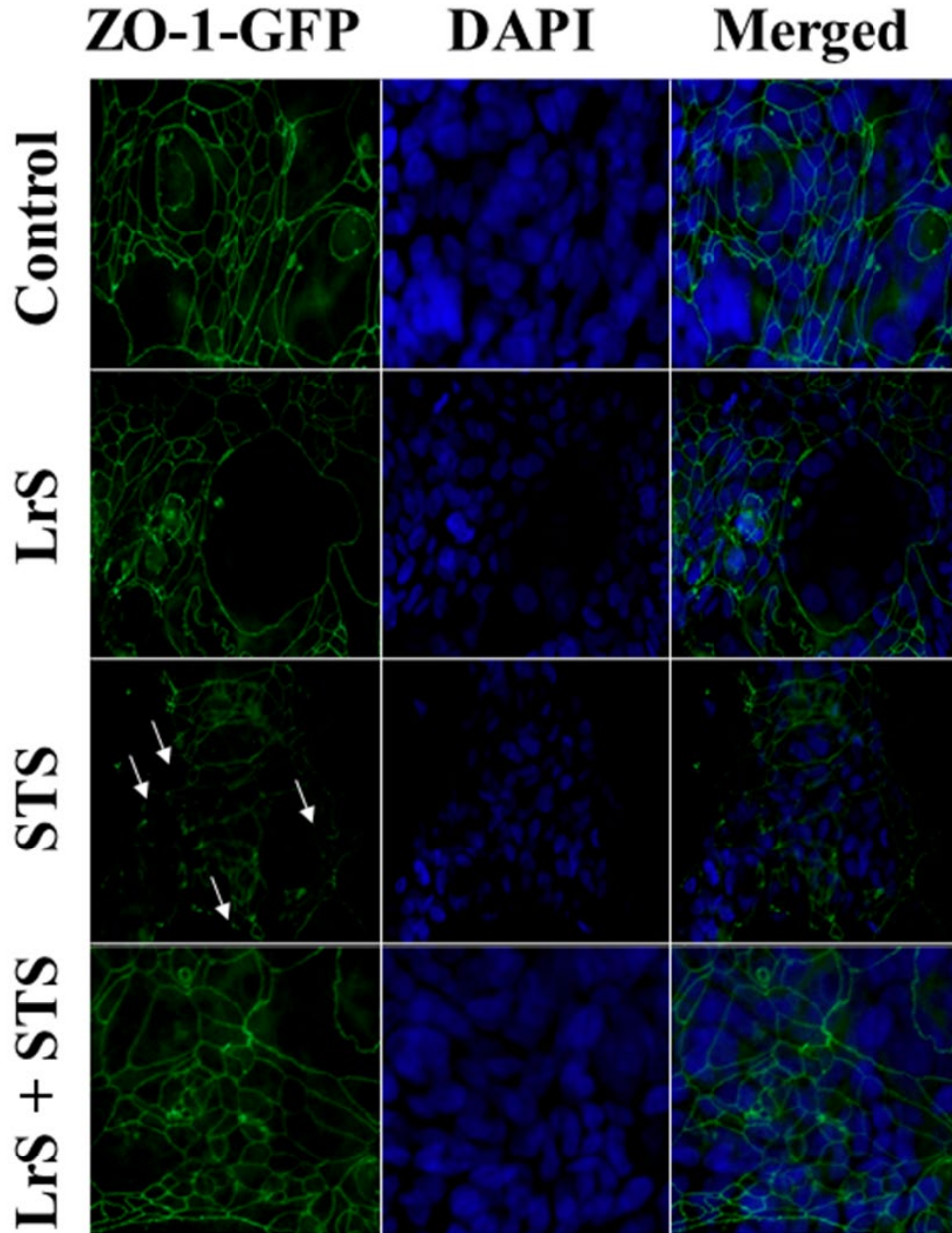
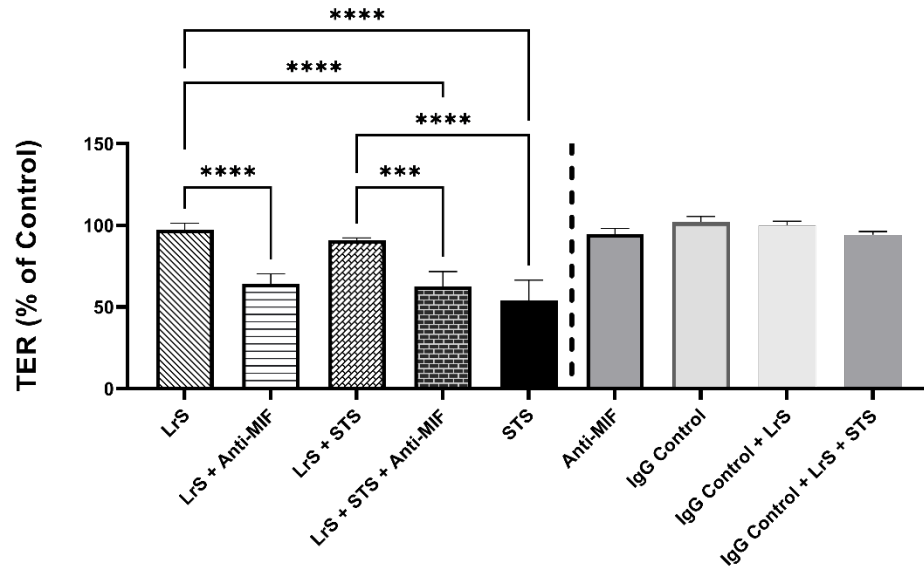


Figure 3-7. The LrS attenuates STS-induced damage to T84 IEC monolayer and integrity by antagonizing STS damage to ZO-1. Confluent T84 IECs were stained with anti-ZO-1-GFP and counterstained with DAPI following 24 hours of challenge with the LrS, STS, LrS + STS, or medium controls and visualized at 100X under oil immersion. Arrows indicate a reduction in ZO-1 expression

A.



B.

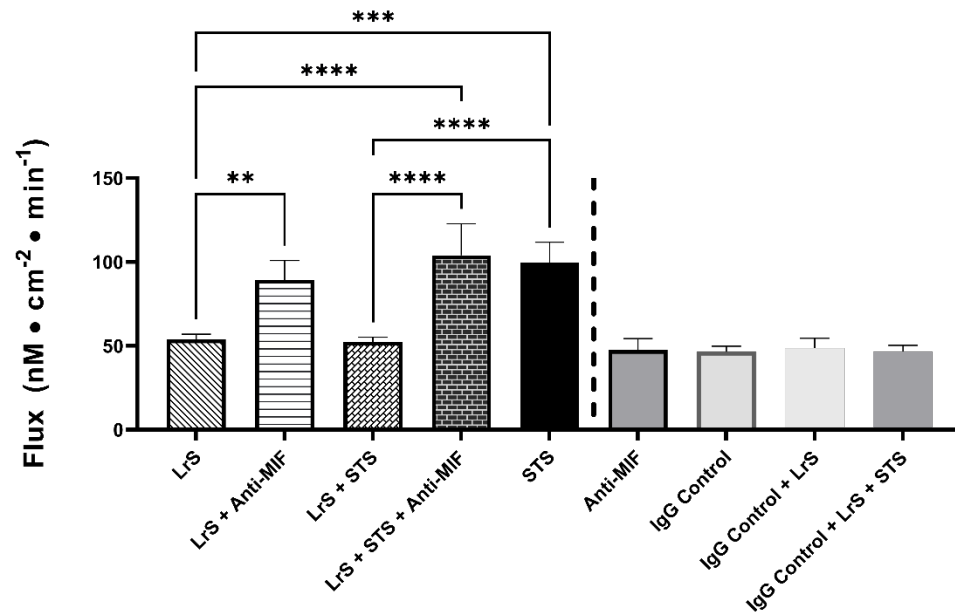


Figure 3-8. The impact of the LrS on T84 IEC barrier function and integrity is abrogated by the addition of a MIF blocking antibody. **A.** Transepithelial resistance (TER) was measured following challenge of T84 IECs with the LrS, STS, or a combination of the challenges with an anti-MIF antibody or isotype controls (0.5 μ g/mL) for 24 hours ($n = 3$). **B.** T84 IEC monolayer permeability was determined by measuring the amount of flux of FITC-dextran following challenge ($n = 3$). Significance is indicated as * $p < 0.05$, ** $p < 0.01$, *** $p < 0.001$ as determined by one-way ANOVA and Tukey's post-hoc test.

CHAPTER 4: Biochemical characterization and identification of components of the *Lactocaseibacillus rhamnosus* R0011 secretome

4.1 Introduction

Gut bacteria-derived soluble mediators and metabolites serve as important messengers which facilitate complex bidirectional host-microbiota communication (Blacher *et al.*, 2017; Levy *et al.*, 2017; Levy *et al.*, 2016). Evidence for systemic dissemination of these metabolites has indicated that these secreted metabolites can also influence and shape host physiology and metabolism outside of the gut (Donia *et al.*, 2015; Yadav *et al.*, 2018). Gut bacteria metabolite and soluble mediator driven immunological changes at the gut mucosal interface suggest multifaceted and strain and species-dependent impacts on host gut immune homeostasis. For example, secretome components derived from *Salmonella enterica* serovar Typhimurium can drive inflammatory mediator production by intestinal epithelial cells, while *Lactocaseibacillus rhamnosus* R0011 produces soluble mediators capable of attenuating ST-driven intestinal inflammatory mediator production (Jeffrey *et al.*, 2020). Impacts of soluble mediators derived from gut-associated bacteria and LAB on other cell types involved in innate immunity as described in **Chapter II** suggest context- and species-dependant regulation of immune outcomes.

Proteins, peptides, and other large macromolecules typically found on the bacterial cell surface were among the first LAB-derived soluble mediators to be identified as important mediators of host-microbe immune communication. Exopolysaccharides, large biopolymers produced by LAB to counter acidic and osmotic stress in their microenvironments, have been shown to have species- and strain-specific immunomodulatory activity via attenuation of pro-inflammatory cytokine and chemokine

production (Murofushi *et al.*, 2015; Nguyen *et al.*, 2020; Patten *et al.*, 2014). Similarly, LTA that is shed and liberated by certain LAB during bacterial cell turnover can also alter immune outcomes following cellular recognition via a TLR-2 dependent mechanism. Structural differences in the lipid moieties found within different LTA molecules points to strain- and species-dependent immunoregulatory capacities of certain LAB (Lebeer *et al.*, 2012). Lactocepin, a biologically active serine protease that is secreted into the extracellular milieu by some LAB, has been shown to selectively degrade CXCL10, CXCL11, CXCL12, CX3CL1, and CCL11 *in vitro* as well as CXCL10 in an *in vivo* model of murine colitis (Hormannsperger *et al.*, 2013; von Schillde *et al.*, 2012; Vong *et al.*, 2014).

Characterization of potential immunomodulatory impacts of gut microbiota-metabolites also indicates a role for gut-derived aromatic amino acid metabolites. Tryptophan metabolites activate the aryl-hydrocarbon receptor leading to alterations in host physiology and immune outcomes at the gut-mucosal interface (Zelante *et al.*, 2013). Moreover, these indole-containing metabolites can be detected in serum, and their presence depends solely on the presence of a resident gut microbiota (Wikoff *et al.*, 2009). Tryptophan metabolites produced by residents of the gut microbiota can also function as neurotransmitters with the capacity of modulating the gut-brain axis (Kaur *et al.*, 2019). Moreover, certain amino acids produced by the resident gut microbiota are sensed by the host and can contribute to intestinal epithelial maintenance; some are used by the host to activate inflammasome activity to maintain a stable colonization state through the production of anti-microbial compounds (Levy *et al.*, 2016).

Metabolite-driven competition between constituents of the gut microbiota has also revealed intricate and complex strategies for developing niches within the gut ecosystem. For example, species belonging to the Lactobacillaceae and Bifidobacteriaceae families produce bacteriocins which can prevent the growth of certain bacterial species (Hammami *et al.*, 2013), while others produce quorum-sensing (QS) molecules which can orchestrate transcriptional changes within bacterial populations to influence growth of different populations of microbes (Kleerebezem, 2004). Moreover, a soluble factor produced by *Escherichia coli* (strain MG1655) can inhibit the growth of *Candida albicans* (Cabral *et al.*, 2018), while Msp1, a soluble mediator produced by several Lactobacillaceae species, reduces hyphal formation by *C. albicans* (Allonsius *et al.*, 2019), highlighting the potential role of soluble-mediator driven changes to the makeup and activity of the gut microbiota and mycobiota. Some metabolites produced by the gut microbiota, such as AMP, can also instruct the underlying intestinal epithelial cells to produce antimicrobial compounds that target certain bacterial species (Eckmann, 2005), indicative of soluble-mediator derived communication between the host and the resident gut microbiota in driving changes to the gut microbiota composition.

4.2 Objectives

To date, effective approaches to decipher the roles of soluble mediator-driven immunological changes mediated by LAB and commensal microorganisms in the context of host-microbe immune communication remain difficult. As such, utilizing high-resolution and global amino acid, proteomic, and metabolomic profiling approaches to interrogate the impact/effects of LAB-derived secretomes presents a useful strategy to determine strain-specific production of potential bioactive molecules, and to characterize potential soluble mediator-driven interactions between the host and LAB. *L. rhamnosus* R0011, *Lactobacillus helveticus* R0052, and *Lactobacillus helveticus* R0389 have been shown to alter host immune outcomes to pro-inflammatory challenge through direct and indirect interactions as mediated by soluble bioactive mediators (Jeffrey *et al.*, 2020; Jeffrey *et al.*, 2018; Macpherson *et al.*, 2014; MacPherson *et al.*, 2017). Previous analyses have indicated that the bioactive constituent(s) of these bacterially derived secretomes is found within the secretome of stationary-phase cultures, suggesting these biomolecules are absent or produced at low concentrations in the exponential phase. For this reason, secretomes from cultures grown to exponential phase were included for useful comparisons to help facilitate identification of potential bioactive constituent(s) with capacity for immunomodulation.

4.3 Materials and Methods

Bacterial Culture

Lyophilized *Lactocaseibacillus rhamnosus* R0011, *Lactobacillus helveticus* R0052, and *Lactobacillus helveticus* R0389 was obtained from RIMAP (Montreal, Quebec, Canada). Secretomes were prepared as previously described (Jeffrey *et al.*, 2018). Briefly, bacteria were grown in deMan, Rogosa and Sharpe (MRS) medium (Difco, Canada) at 37°C for 17 hours in a shaking incubator and then diluted in non-supplemented RPMI-1640 medium and allowed to further propagate for an additional 23 hours under the same conditions. A medium control consisting of MRS diluted in RPMI-1640 medium was included and subjected to the same culture conditions. Both the bacterial culture and controls were centrifuged at 3000 x g for 20 minutes and filtered through a 0.22 µm filter (Progene, Canada) to remove any bacteria. Optical density measurements and viable bacterial cell counts were recorded to ensure consistencies between the number of bacteria contributing to biomolecule production within each secretome prior to filtration and downstream analyses.

Amino acid analyses

Total free amino acid profiling was done at the SickKids Proteomics, Analytics, Robotics & Chemical Biology Centre (SPARC Biocentre, Toronto, ON, CA). Briefly, frozen secretome samples were analyzed using a Waters ACQUITY UPLC which utilizes a C-18 based column. Free amino acid concentrations within the secretomes were averaged and corrected by subtracting the corresponding value of each amino acid found in the medium controls. Resulting background-corrected amino acid profiles were plotted in a

heat map using the Mutli-experiment Viewer (MeV) software with hierarchical clustering using Euclidean distance to order the treatments by similarities ($n = 3$).

Two-dimensional difference gel electrophoresis (2D-DIGE) and protein identification via mass spectrometry

MRS or RPMI-1640 grown exponential and stationary-phase derived *L. rhamnosus* R0011 secretomes were sent to Applied Biomics (California, USA) for protein analysis using 2D Difference Gel Electrophoresis (DIGE) and DeCyder In-gel Analysis (DIA). Briefly, equal amounts of protein found within the secretome samples (Cy3 for proteins found within stationary phase-derived and Cy5 for proteins found within exponential phase-derived secretomes) or medium controls (Cy2) were fluorescently labelled and multiplexed on a single 2D-gel (isoelectric focusing in the first dimension and SDS-PAGE in the second dimension) for direct comparison. Following electrophoresis, the gel was scanned using a Typhoon image scanner to detect signals from each of the CyDye signals. ImageQuant and DeCyder In-gel analysis software was used to determine protein expression ratios between the different samples. Proteins were selected for identification via mass spectrometry based on their relative abundance and size and whether they were found exclusively within the exponential or stationary phases of growth. Protein identification was done using the *L. rhamnosus* R0011 protein database. A BLASTp search was carried out using the *Lactobacillus rhamnosus* database to assign putative identification of proteins which have not yet been annotated in the *L. rhamnosus* R0011 database.

Metabolomic profiling

Metabolomic and small molecule profiling of RPMI-1640 grown exponential and stationary-phase derived *L. rhamnosus* R0011, *L. helveticus* R0052, and *L. helveticus* R0389 secretomes was performed by Metabolon (Morrisville, NC, USA). Briefly, samples were prepared using the automated MicroLab STAR system (Hamilton Company) and several recovery standards were added prior to the first step in the extraction process for quality control purposes. Small molecules and metabolites were extracted with methanol to precipitate any protein and dissociate small molecules bound to protein or media components. The resulting extracts were then analysed using a Waters ACQUITY ultra-performance liquid chromatography (UPLC) and a Thermo Scientific Q-Exactive high resolution/accurate mass spectrometer interfaced with a heated electrospray ionization (HESI-II) source and Orbitrap mass analyzer operated at 35,000 mass resolution. Data extraction and subsequent small molecule identification and quantification, statistical analyses, and data visualization was done using Metabolon's proprietary Laboratory Information Management system, using a curated library of standards to facilitate biochemical identification. Matched pairs *t*-test, Two-way ANOVA, and Principal Component Analysis (PCA) were used to analyze the data and were performed on natural log-transformed data.

4.4 Results

The LrS has unique amino acid profiles when compared to secretomes derived from L. helveticus R0052 and R0389

Amino acid profiling of the secretomes from *L. rhamnosus* R0011, *L. helveticus* R0389, and *L. helveticus* R0052 revealed a high degree of strain specificity in amino acid metabolism (**Figure 4-1**). Hierarchical clustering revealed similarities between the amino acid composition of the secretomes of *L. rhamnosus* R0011 and *L. helveticus* R0052, while *L. helveticus* R0389 clustered separately. In general, the secretomes of all three strains had higher concentrations of arginine, glutamine, and glutamate (**Figure 4-1**). Asparagine was consumed by both *L. rhamnosus* R0011 and *L. helveticus* R0052, but not *L. helveticus* R0389 (**Figure 4-1**). Interestingly, the secretomes of *L. helveticus* R0052 and *L. helveticus* R0389 contain an appreciably higher concentration of γ -amino butyric acid (GABA) (**Figure 4-1**).

Protein profiling identified unique proteins in the secretomes of exponential and stationary grown cultures

2D DIGE protein profiling was done to interrogate the differential protein expression patterns of proteins found within the LrS harvested in exponentially- or stationary-grown MRS or RPMI-1640 cultures. A total of 19 and 16 differentially expressed proteins were detected in the secretomes derived from cultures grown in MRS or RPMI-1640 medium, respectively (**Figure 4-2**). Since the immunomodulatory activity detected previously (Jeffrey *et al.*, 2020; Jeffrey *et al.*, 2018) is observed when the secretome is collected during the stationary phase of growth, protein identification focused primarily on proteins that were expressed predominantly in the stationary phase. Although

the number and types of proteins found in the LrS showed some degree of growth-medium dependence, GAPDH and cell wall-associated glycoside hydrolases were found to be present in secretome grown to the stationary phase (**Table 4-I and 4-II**). Multiple species alignment of *L. rhamnosus* R0011-derived GAPDH using NCBI BLASTp revealed that this strain potentially secretes a relatively unique isoform of GAPDH. Two biological replicates were run to ensure reproducibility of the results (**Figure 4-3**).

Metabolite composition of the three lactobacilli secretomes is species- and growth-phase-dependent

Principle component analysis of global metabolic profiles of the three different lactobacilli-derived secretomes revealed divergent species- and growth-phase dependant clusters, suggesting that the three individual bacterial strains produce distinct metabolite-rich secretomes (**Figure 4-4**). Compared to the medium control, between 38 and 50% of all metabolites were altered during the exponential phase and between 62 and 68% were altered during the stationary phase. During the exponential phase, *L. rhamnosus* R0011, *L. helveticus* R0052, and *L. helveticus* R0389 secreted 85, 113, and 194 biochemicals, respectively, while during the stationary phase, *L. rhamnosus* R0011, *L. helveticus* R0052, and *L. helveticus* R0389 secreted 219, 242, and 262 biochemicals, respectively. During the stationary phase, *L. rhamnosus* R0011, *L. helveticus* R0052, and *L. helveticus* R0389 secreted 34, 37, and 40 distinct metabolites, respectively. Lactate, indicative of metabolically active cultures, was found in the stationary secretomes of each species tested, with each strain secreting approximately the same amount of lactate.

Tryptophan-derived AhR ligands and phenylalanine-derived metabolites were secreted by all strains

During stationary phase, indole-3-carboxylate was consumed by all strains and indolelactate was secreted by all strains. However, during the exponential phase, only *L. rhamnosus* R0011 consumed indole-3-carboxylate, while *L. helveticus* R0052 and *L. helveticus* R0389 secreted indolelactate (**Figure 4-5**). Interestingly, *L. helveticus* R0052 was the only strain to secrete indoleacetate. During both the exponential and stationary phases all strains secreted the phenylalanine-derived metabolites phenethylamine and phenyllactate (**Figure 4-6**). Similar to the pattern observed for indolelactate production, the strain that secreted the most phenyllactate was *L. helveticus* R0389 (**Figure 4-6**).

Methionine metabolism was altered between all bacterial strains

Methionine was consumed by *L. helveticus* R0052 and *L. helveticus* R0389 in both exponential and stationary phases but was not consumed by *L. rhamnosus* R0011 (**Figure 4-7**), confirming previous amino acid analyses (**Figure 4-1**). In contrast, *L. rhamnosus* R0011 and *L. helveticus* R0389 secreted the methionine-derived metabolites homocysteine and cysteine, especially during the stationary phase. Secretion of homocysteine may indicate an increase in LuxS enzyme activity and the production of autoinducer-2 (AI-2) (**Figure 4-7**).

4.5 Discussion

Gut bacteria-derived metabolites serve as messengers which facilitate dynamic and complex host-microbiota immune communication. These metabolites play an integral role in the development and maintenance of host immune and physiological outcomes, with recent advances in host-microbiome research indicating a causal relationship between some gut microbiota-derived metabolites and host immune activity. As such, global metabolic profiling of LAB secretomes provides an effective strategy for identifying strain-specific production of potential bioactive metabolites. Free amino acid profiling of the secretomes from *L. rhamnosus* R0011, *L. helveticus* R0389, and *L. helveticus* R0052 when grown to stationary phase revealed that secretomes from all three strains contained high concentrations of arginine and glutamine. Glutamine has been reported to influence gut physiology and gut inflammation by influencing many signaling pathways involved in cell cycle regulation and proliferation, as well as by inhibiting NF- κ B pathway activation (Kim *et al.*, 2017). More specifically, glutamine has been shown to activate dual specificity phosphatase 1 (DUSP1), a key regulator of the mitogen-activated protein kinase signaling pathway. Treatment of challenged HT-29 human and T84 IECs with the LrS up-regulates the expression of DUSP1 (Jeffrey *et al.*, 2020) suggesting a possible link between the glutamine found within the LrS and the observed immunomodulatory activity of the secretome. Arginine, also present at high concentrations in the LrS, has been shown to reduce intestinal inflammation in response to pathogen challenge (Fritz, 2013), suggesting this amino acid could also participate in the immunomodulatory activity of this strain in the gut environment.

In stationary phase-derived secretomes collected from RPMI-1640 grown *L. rhamnosus* R0011 cultures, there were a total of six proteins identified as the same cell wall-associated glycoside hydrolase, each with a unique size and isoelectric point, indicating that this particular protein has undergone differential post-translational modification. Cell wall-associated hydrolases have been attributed with having peptidoglycan and lipoteichoic acid (LTA) modifying ability (Xu *et al.*, 2015). Analysis of by-products of bacterial cell turnover as a result of the activity of these enzymes may provide some insight into the immunomodulatory activity of the *L. rhamnosus* R0011 secretome, as LTA and peptidoglycan derivatives have been attributed with immunomodulatory capacities (Lebeer *et al.*, 2012; Lebeer *et al.*, 2008, 2010). Moreover, glyceraldehyde-3-phosphate (GAPDH) was found to be secreted into the extracellular milieu by *L. rhamnosus* R0011 during the stationary phase of growth. This is in keeping with findings suggesting that GAPDH is secreted by some bacteria in response to stress. In fact, stationary phase cultures of *L. plantarum* 299v show an increase in GAPDH presence and activity on the bacterial cell wall when compared to exponential phase cultures (Saad *et al.*, 2009). GAPDH is associated with multiple moonlighting functions including playing a pivotal role in adhesion of lactobacilli to epithelial cells, with strain-specific effects observed (Kainulainen *et al.*, 2014). For example, the GAPDH isolated from *L. plantarum* LA 318 binds human colonic mucin (Kinoshita *et al.*, 2008) while GAPDH isolated from *L. crispatus* binds human plasminogen (Hurmala *et al.*, 2007). GAPDH has also been shown to exert effects on host immune outcomes. More recently, Nakano *et al.*, (2017) have shown that exogenously supplied GAPDH can influence macrophage phenotype and activity by changing the glycolytic flux within the cell. LPS-stimulated macrophages

treated with GAPDH show a reduction in TNF α production with a simultaneous increase in the production of the regulatory cytokine IL-10. This immunomodulatory activity was associated with an increase in intracellular NADH concentration, which skewed macrophage polarization to a M2 immunoregulatory phenotype (Nakano *et al.*, 2018). However, the exact mechanisms by which these proteins are translocated across the cell membrane into the extracellular environment remain largely unknown. Future experiments examining the effects of *L. rhamnosus* R0011-derived GAPDH should be done to ascertain if this secreted protein is responsible for the observed immunomodulatory activity observed with THP-1 human monocytes as described in **Chapter II**.

Tryptophan is metabolized by gut bacteria to produce metabolites such as indoles. In fact, most indoles can be linked directly to microbial metabolism since mammalian cells lack the enzymes necessary to produce these molecules. Indolelactate (ILA), indoleacetate, and indole-3-carboxylate are tryptophan metabolites that are exclusively contributed by bacterial metabolism and are thought to play key roles in shaping immune outcomes within the gastrointestinal environment through AhR activation. For example, ILA produced by *Bifidobacterium longum* subsp. *infantis* has been shown to reduce CXCL8 production in immature intestinal enterocytes following interleukin-1 β challenge through AhR activation (Meng *et al.*, 2020). Furthermore, ILA has also been shown to enhance neurite outgrowth and acetylcholinesterase activity through AhR activation of rat adrenal pheochromocytoma cells, suggesting a possible link between gut bacteria-derived AhR ligands and neuronal differentiation (Wong *et al.*, 2020).

Secretion of homocysteine may indicate an increase in LuxS enzyme activity and the production of autoinducer-2 (AI-2). AI-2 is proposed to be a universal signal for inter-

species cell-to-cell communication. The synthesis of AI-2 is linked to the methionine cycle whereby the metabolism of S-adenosylmethionine can be recycled via sequential metabolic reactions of intermediates. In bacteria, metabolism of S-adenosylmethionine to S-adenosylhomocysteine is followed by hydrolysis by the Pfs nucleosidase to produce S-ribosylhomocysteine. Subsequently, S-ribosylhomocysteine is cleaved by LuxS to generate homocysteine and 4,5-dihydroxy 2,3-pentanedione, which spontaneously cyclizes to form pro-AI-2 molecules (Jimenez *et al.*, 2014). Although we could not conclusively determine whether these lactobacilli secretomes contained the other LuxS-dependent metabolites, the higher levels of homocysteine secretion and metabolism by *L. rhamnosus* R0011 and *L. helveticus* R0389 may suggest increased LuxS activity and AI-2-like molecule secretion. Furthermore, phenyllactate, the major phenylalanine catabolite produced by the three lactobacilli strains, has been shown to inhibit radial growth and sporulation of filamentous fungi (Svanstrom *et al.*, 2013), indicating that these strains produce an array of metabolites capable of shaping the gut microbiota.

To date, comprehensive profiling of secretomes derived from LAB has remained difficult. Using a combinatorial approach using amino acid, proteomic, and metabolomic profiling, species- and growth phase-dependent production and consumption of a large range of bioactive molecules was identified. Although some of the soluble mediators identified have been associated with altering host physiology and immune function, insights into specific activities behind most of the soluble mediators identified remain unknown. As such, future experimentation should focus on ascertaining the roles that these soluble mediators may play in the observed immunomodulatory activity of the LrS and more broadly in complex host-microbe immune communication.

Table 4-I. Protein identification via mass spectrometry of proteins found in the LrS from MRS-grown cultures.

Spot Number ¹	Top Ranked Protein Name [Species]	Accession Number	Protein MW	Protein Score (Confidence %)
Stationary Phase-derived <i>L. rhamnosus</i> R0011 Secretome				
2	Hsp20 family small heat shock protein [<i>Lactobacillus rhamnosus</i> R0011]	gi 357538804	16,616	0
4	cell wall-associated glycoside hydrolase (NLP/P60 protein) [<i>Lactobacillus rhamnosus</i> MTCC 5462]	gi 357537998	49,709	100
6	transcriptional regulator LysR family protein [<i>Lactobacillus rhamnosus</i> R0011]	gi 357538675	33,127	0
13	glyceraldehyde-3-phosphate dehydrogenase [<i>Lactobacillus rhamnosus</i> R0011]	gi 357538940	42,560	100
18	ATP-dependent protease ATP-binding subunit HslU [<i>Lactobacillus rhamnosus</i> R0011]	gi 357540050	52,157	0
Exponential Phase-derived <i>L. rhamnosus</i> R0011 Secretome				
9	surface antigen [<i>Lactobacillus rhamnosus</i> R0011]	gi 357538940	42,560	100
15	Hsp20 family small heat shock protein [<i>Lactobacillus rhamnosus</i> R0011]	gi 357538804	16,616	0
17	Xre-like DNA-binding protein [<i>Lactobacillus rhamnosus</i> R0011]	gi 357539596	32,981	0

Table 4-II. Protein identification via mass spectrometry of proteins found in the LrS when grown in RPMI-1640 medium.

Spot Number ¹	Top Ranked Protein Name [Species]	Accession Number	Protein MW	Protein Score (Confidence %)
Stationary Phase-derived <i>L. rhamnosus</i> R0011 Secretome				
1	ATP-dependent protease ATP-binding subunit HslU [<i>Lactobacillus rhamnosus</i> R0011]	gi 357540050	52,157	-
2	cell wall-associated glycoside hydrolase (NLP/P60 protein) [<i>Lactobacillus rhamnosus</i> R0011]	gi 357537998	49,709	100
3	cell wall-associated glycoside hydrolase (NLP/P60 protein) [<i>Lactobacillus rhamnosus</i> R0011]	gi 357537998	49,709	100
4	cell wall-associated glycoside hydrolase (NLP/P60 protein) [<i>Lactobacillus rhamnosus</i> R0011]	gi 357537998	49,709	-
5	cell wall-associated glycoside hydrolase (NLP/P60 protein) [<i>Lactobacillus rhamnosus</i> R0011]	gi 357537998	49,709	100
6	cell wall-associated glycoside hydrolase (NLP/P60 protein) [<i>Lactobacillus rhamnosus</i> R0011]	gi 357537998	49,709	100
8	hypothetical protein R0011_12960 [<i>Lactobacillus rhamnosus</i> R0011]	gi 357537076	34,135	100
9	hypothetical protein R0011_12960 [<i>Lactobacillus rhamnosus</i> R0011]	gi 357537076	34,135	100
14	glyceraldehyde-3-phosphate dehydrogenase [<i>Lactobacillus rhamnosus</i> R0011]	gi 357539641	36,701	100
15	ribonucleotide-diphosphate reductase subunit alpha [<i>Lactobacillus rhamnosus</i> R0011]	gi 357540106	82,112	-
16	peptide chain release factor 1 [<i>Lactobacillus rhamnosus</i> R0011]	gi 357539812	40,954	-
Exponential Phase-derived <i>L. rhamnosus</i> R0011 Secretome				
7	cell wall-associated glycoside hydrolase (NLP/P60 protein) [<i>Lactobacillus rhamnosus</i> R0011]	gi 357537998	49,709	100
10	Hsp20 family small heat shock protein [<i>Lactobacillus rhamnosus</i> R0011]	gi 357538804	16,616	5
11	surface antigen [<i>Lactobacillus rhamnosus</i> R0011]	gi 357538940	42,560	100
12	surface antigen [<i>Lactobacillus rhamnosus</i> R0011]	gi 357538940	42,560	100
13	anaerobic ribonucleoside triphosphate reductase [<i>Lactobacillus rhamnosus</i> R0011]	gi 357539043	82,511	-

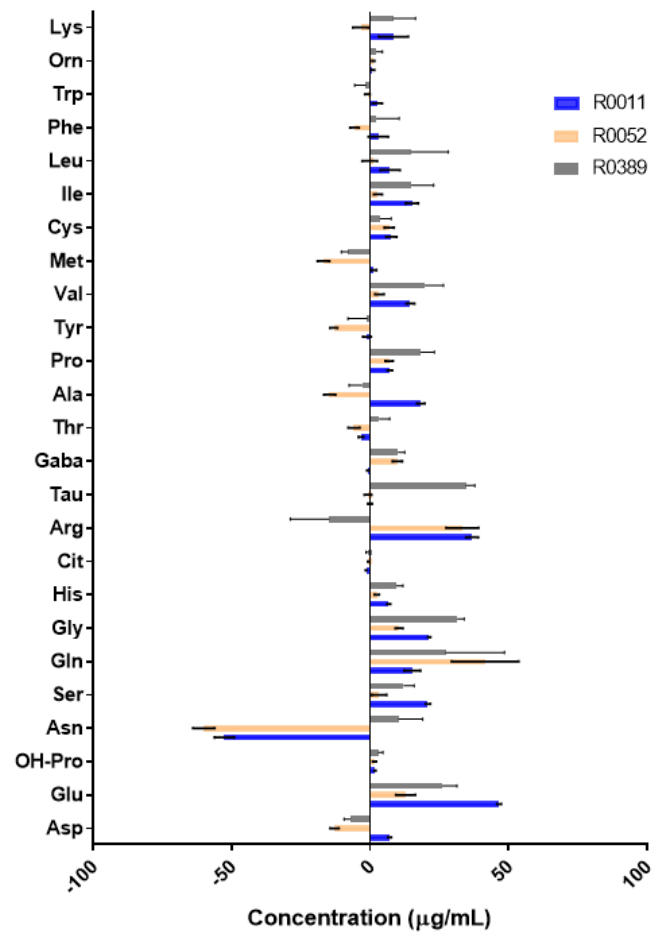
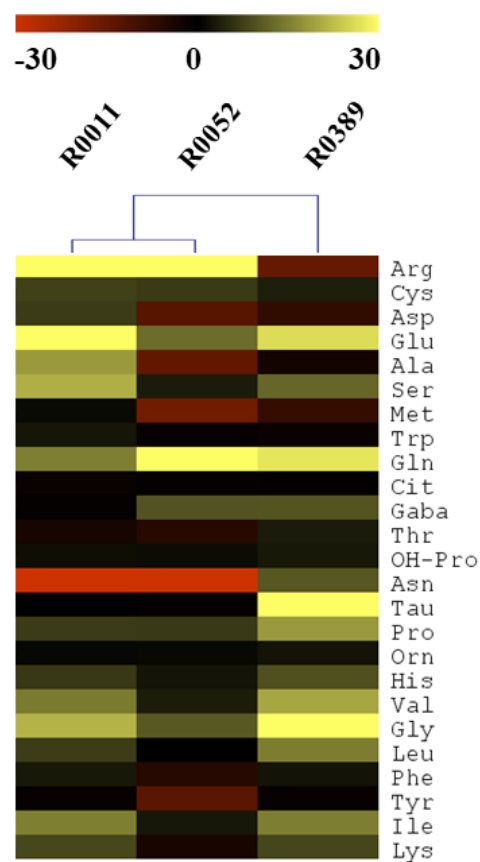


Figure 4-1. Free amino acid profiling of the secretomes of *L. rhamnosus* R0011, *L. helveticus* R0052, and *L. helveticus* R0389 when grown to stationary phase in RPMI-1640 medium. Data shown is the background corrected average of three biological replicates ($\mu\text{g/mL} \pm \text{SEM}$) ($n = 3$).

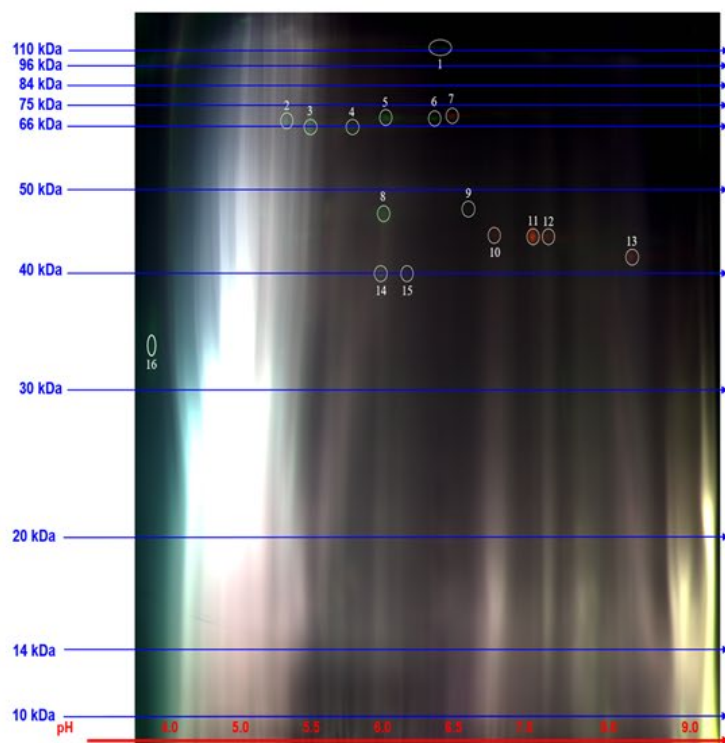
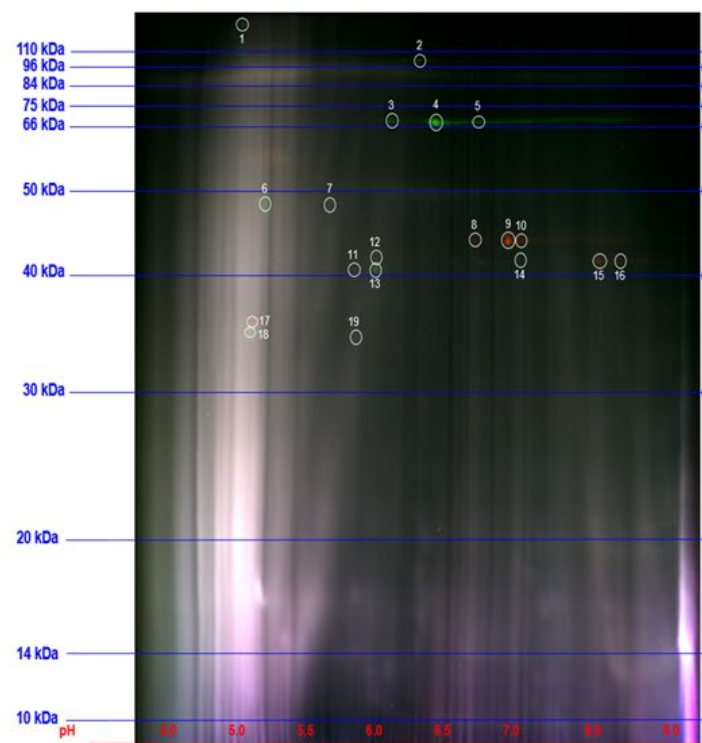
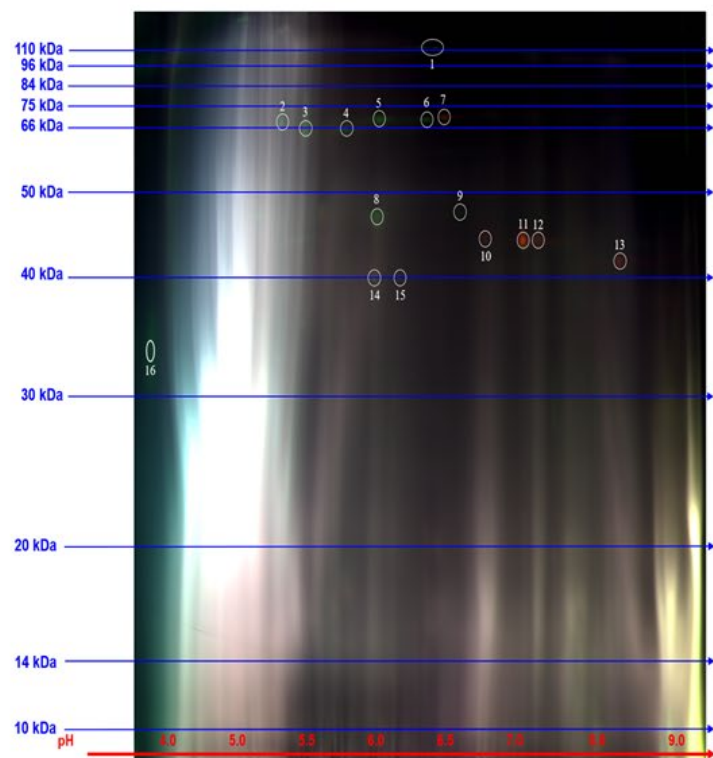
A.**B.**

Figure 4-2. 2D DIGE analysis of differentially expressed proteins found within A. RPMI-1640 grown stationary-phase and exponential-phase *L. rhamnosus* R0011 secretomes and B. MRS grown stationary-phase and exponential-phase *L. rhamnosus* R0011 secretomes. Green spots indicate those proteins found within the stationary-phase LrS while red spots indicate proteins found within the exponential-phase secretome.

A.



B.

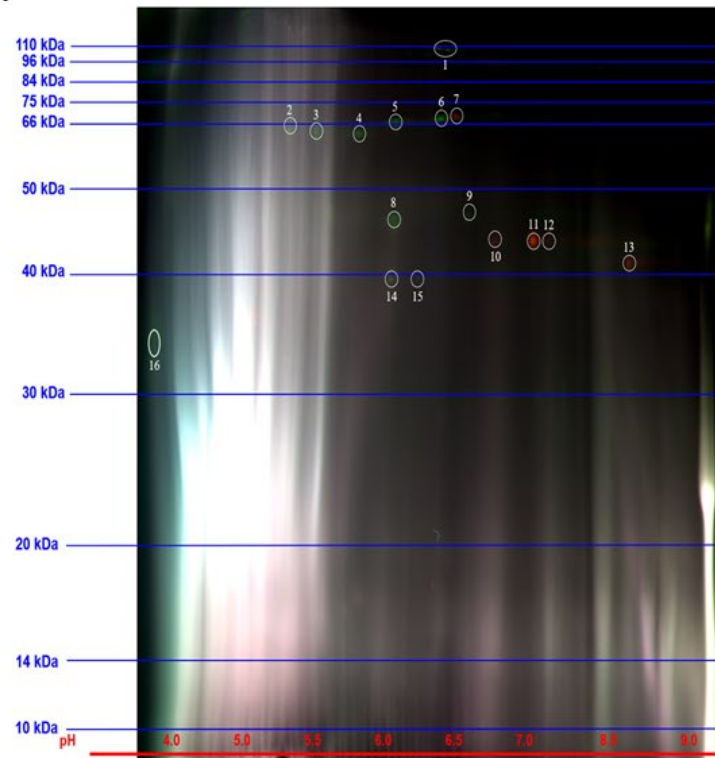


Figure 4-3. 2D DIGE analysis of differentially expressed proteins found within RPMI-1640 grown stationary-phase and exponential-phase LrS of two biological replicates (A and B). Green spots indicate proteins detected in the stationary-phase LrS while red spots indicate proteins detected in the exponential-phase secretome.

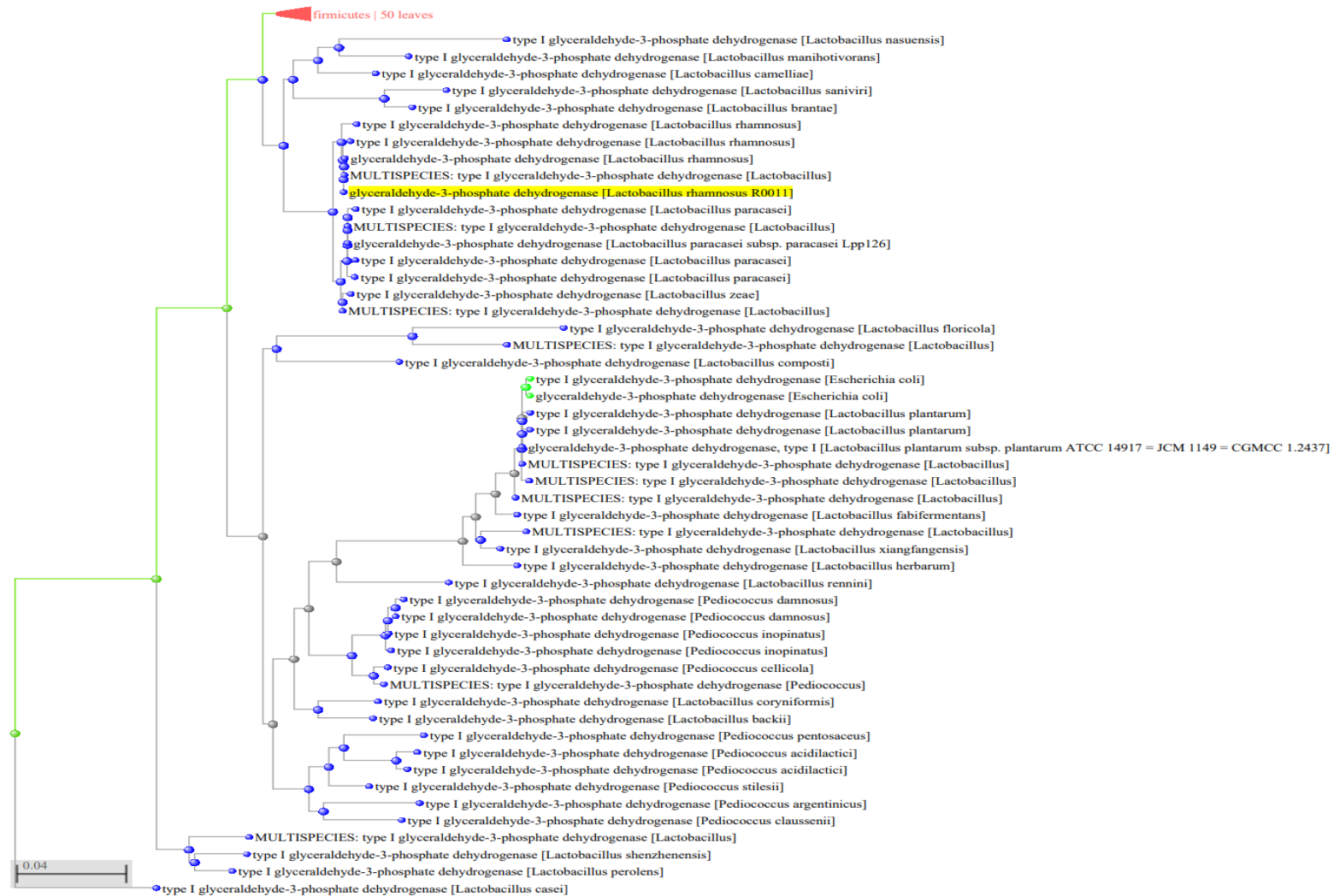


Figure 4-4. BLAST Tree View of the multiple species alignment of NCBI BLASTp results using the *L. rhamnosus* R0011 GAPDH as the query search.

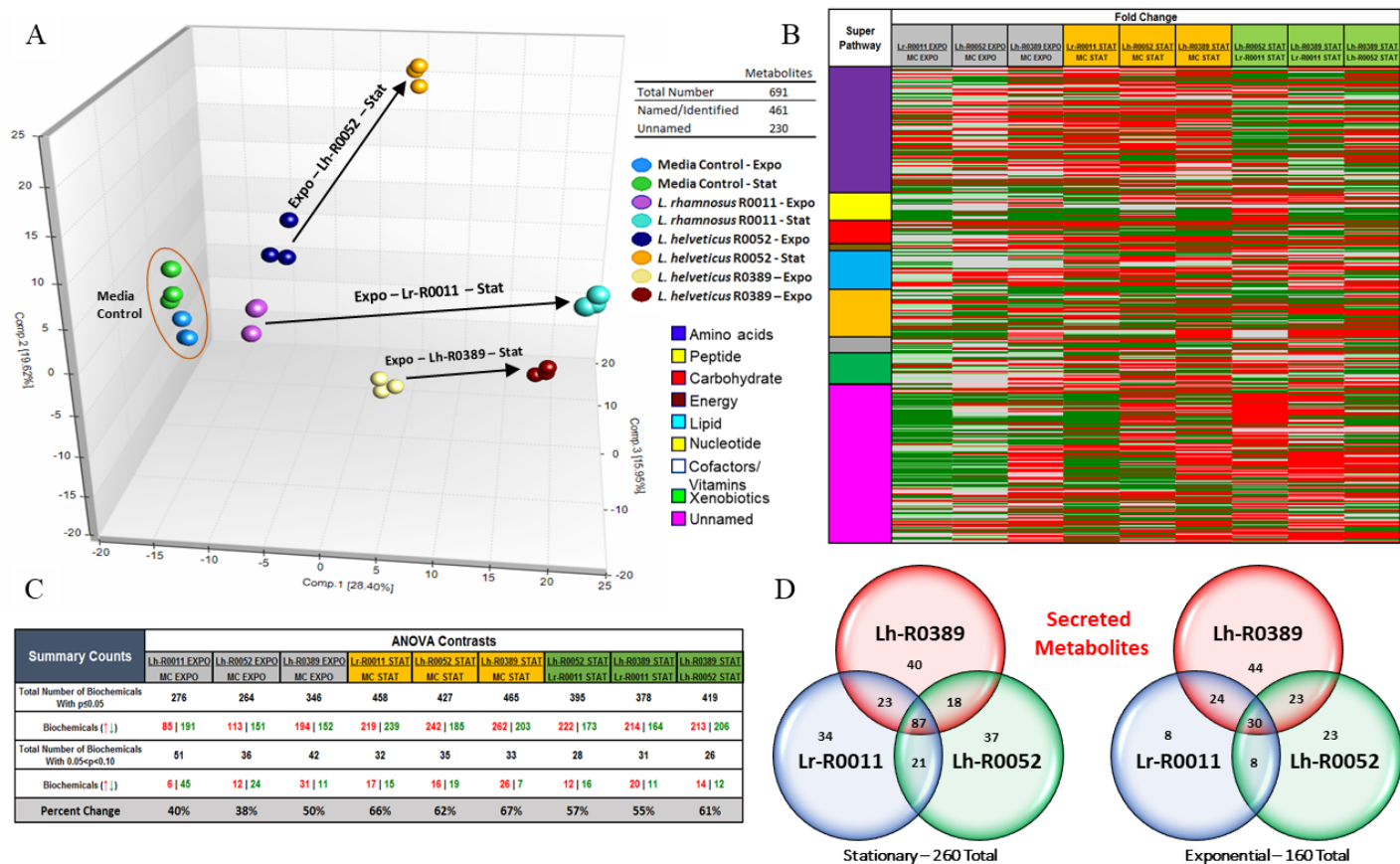


Figure 4-5. PCA analysis, overview heat map representation, and summary counts of statistically significant metabolites in secretomes from exponential and stationary phase cultures of *L. rhamnosus* R0011 (Lr-R0011), *L. helveticus* R0052 (Lh-R0052), and *L. helveticus* R0389 (Lh-R0389) ($n = 3$). **B.** All named and unnamed metabolites were grouped according to super pathway and trending ($0.05 < p < 0.10$) and significant ($p \leq 0.05$) elevations are indicated by pink and red shading, respectively, while trending and significant reductions are represented by light green and dark green shading, respectively. Grey boxes indicate metabolites that are not significantly different. **C.** Number of significantly altered compounds ($p \leq 0.05$) between each comparison is indicated in the table. **D.** Venn Diagram analysis showing similarities and differences between the total number of metabolites identified in exponential and stationary phase secretomes.

Biochemical Name	Fold Change					
	Lr-R0011	Lh-R0052	Lh-R0389	Lr-R0011	Lh-R0052	Lh-R0389
	MC EXPO	MC EXPO	MC EXPO	MC STAT	MC STAT	MC STAT
tryptophan	0.94	1.03	1.02	1.11	0.94	0.75
N-acetyltryptophan	1.41	0.99	1.62	4.24	1.42	2.12
kynurenine	0.92	0.92	1.03	1.51	1.36	1.12
kynurenate	0.85	0.76	0.77	2.80	1.47	1.03
tryptamine	1.04	1.50	1.32	1.24	1.24	1.12
indolelactate	1.05	2.68	13.11	22.78	10.36	91.53
indoleacetate	0.87	1.57	0.80	0.90	1.39	1.20
indole-3-carboxylate	0.85	0.98	0.90	0.68	0.87	0.68

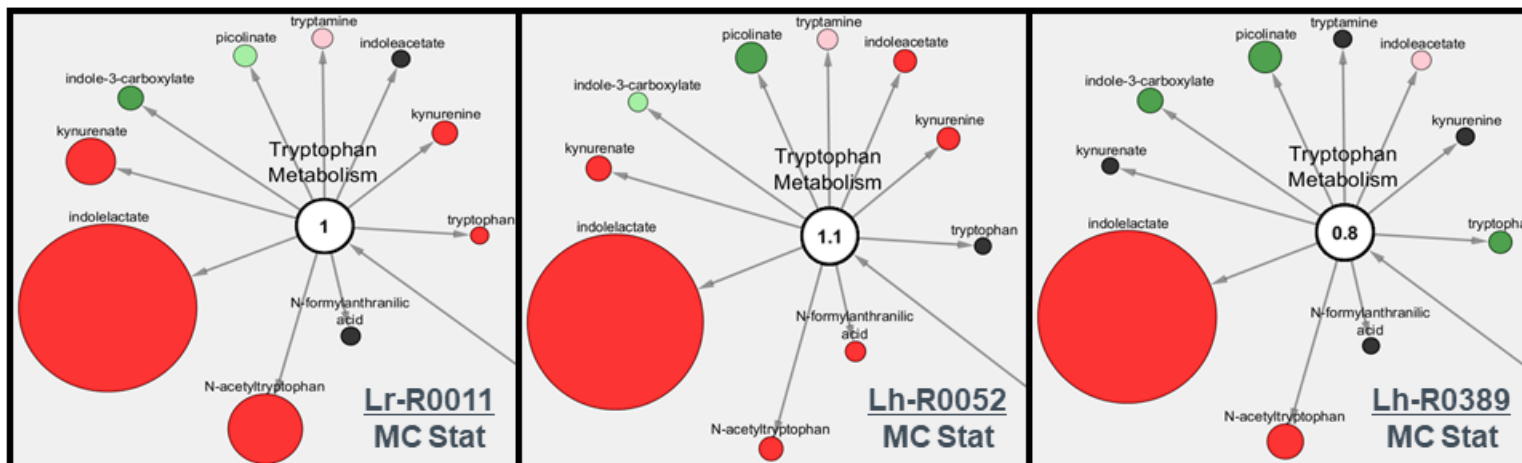
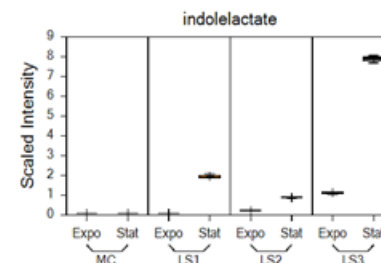
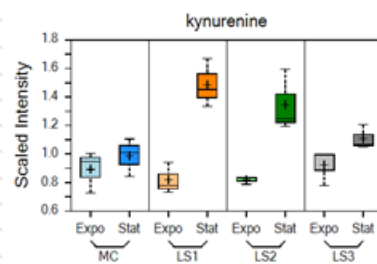


Figure 4-6. Heat map, boxplots, and Cytoscape visualizations of tryptophan metabolites found within the Lr-R0011, Lh-R0052, and the Lh-R0389 secretomes. Trending ($0.05 < p < 0.10$) and significant ($p \leq 0.05$) elevations are indicated by pink and red shading, respectively, while trending and significant reductions are represented by light green and dark green shading, respectively ($n = 3$).

Biochemical Name	Fold Change					
	Lr-R0011 MC EXPO	Lh-R0052 MC EXPO	Lh-R0389 MC EXPO	Lr-R0011 MC STAT	Lh-R0052 MC STAT	Lh-R0389 MC STAT
phenylalanine	0.98	0.96	0.90	0.99	0.87	0.71
N-acetylphenylalanine	1.30	0.96	1.26	2.50	1.13	1.47
1-carboxyethylphenylalanine	2.35	1.29	3.55	16.21	4.69	24.45
phenylpyruvate	0.86	1.00	3.34	0.30	1.13	0.51
phenyllactate (PLA)	29.82	41.72	261.46	226.56	145.62	453.07
phenethylamine	2.01	2.20	3.25	2.76	2.79	2.88
phenylacetate	0.81	1.10	0.73	0.52	0.63	0.53

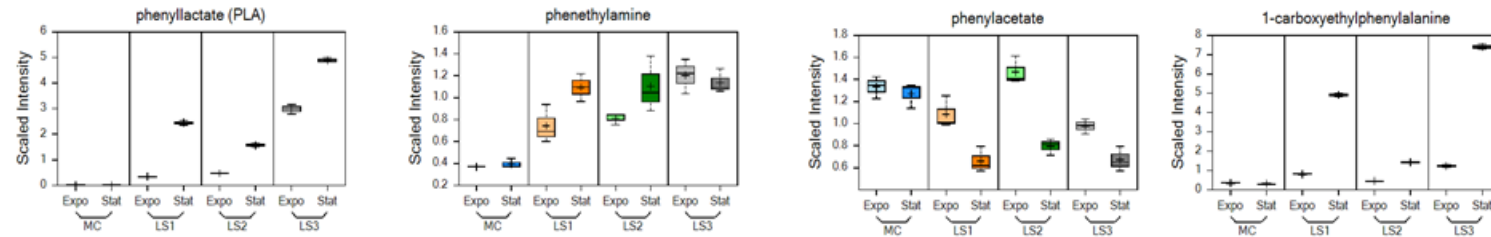
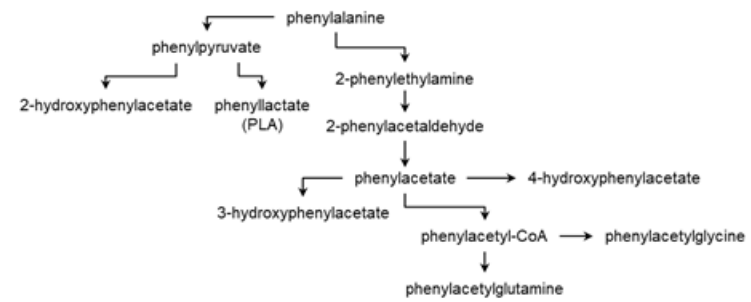


Figure 4-7. Heat map, boxplots, and Cytoscape visualizations of phenylalanine metabolites found within the Lr-R0011, Lh-R0052, and the Lh-R0389 secretomes. Trending ($0.05 < p < 0.10$) and significant ($p \leq 0.05$) elevations are indicated by pink and red shading, respectively, while trending and significant reductions are represented by light green and dark green shading, respectively ($n = 3$).

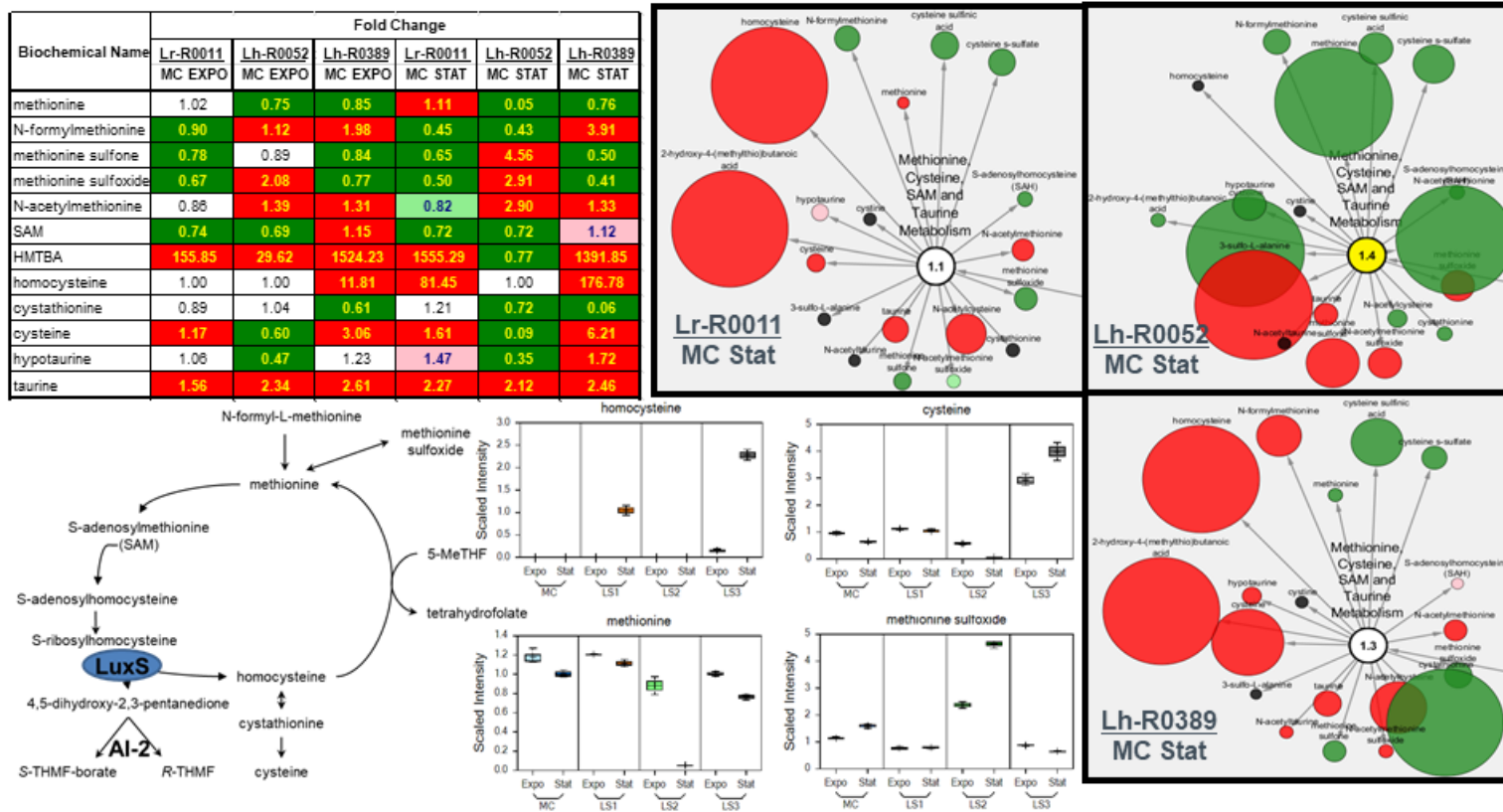


Figure 4-8. Heat map, boxplots, and Cytoscape visualizations of methionine metabolites found within the Lr-R0011, Lh-R0052, and the Lh-R0389 secretomes. Trending ($0.05 < p < 0.10$) and significant ($p \leq 0.05$) elevations are indicated by pink and red shading, respectively, while trending and significant reductions are represented by light green and dark green shading, respectively ($n = 3$).

GENERAL DISCUSSION AND CONCLUSIONS

Host-microbe immune communication plays an integral role in shaping host immune responses within the gut as well as within other mucosal and potentially systemic locations. Certain LAB, such as *L. rhamnosus* R0011, have been associated with a range of host-immune modulatory activities including down-regulation of pro-inflammatory gene transcription and expression in IECs following pro-inflammatory challenge. While host IECs and APCs can interact directly with both pathogenic and commensal bacteria through innate immune pattern recognition receptors, recent evidence indicates indirect communication through secreted molecules as an important route for facilitating host-microbe immune communication within the gut. This communication route may be especially important in the context of IEC and APC interactions, key cell types in immune activity at the intestinal mucosal interface, as the effects of LAB and their secreted factors can be very different when tested in co-cultures of human IECs and APCs. However, many questions remain about the interactions of these bacteria with cells of the innate immune system as mediated through secreted components, and the resulting host immune outcomes in the context of IEC and APC interactions. To begin to address these gaps in knowledge, the ability of soluble components derived from *L. rhamnosus* R0011 to influence immune outcomes in IECs, APCs, and co-cultures of IECs and APCs was examined.

In the initial study, the LrS was found to attenuate pro-inflammatory gene expression from TNF- α - and STS-challenged HT-29 IECs, including genes involved in NF- κ B activation (**Figure D-1**). This decrease in pro-inflammatory gene expression was accompanied with concurrent increases in the transcription of *DUSP1*, *TRIB3*, and *ATF3*, central regulators of innate immune activity (Gilchrist *et al.*, 2006; Hammer *et al.*, 2006;

Kwon *et al.*, 2015; Lang *et al.*, 2006; Li *et al.*, 2010; Smith *et al.*, 2011; Whitmore *et al.*, 2007), as well as a reduction in TNF- α - and STS-induced histone acetylation. Interestingly, up-regulation of these negative regulators of innate immunity was only observed when HT-29 IECs were also responding to either TNF- α or the STS challenge, but not to the LrS alone, suggesting context-dependent mechanism(s) of action behind the immunoregulatory activity of the LrS. In fact, challenge with the LrS alone resulted in a muted response, with little change in the overall transcriptional profile of HT-29 IECs when compared to medium controls, and in marked contrast to challenge with TNF- α or the STS. In keeping with these findings, the LrS also attenuated the production of pro-inflammatory cytokines, chemokines, and other mediators from TNF- α - and STS-challenged HT-29 IECs.

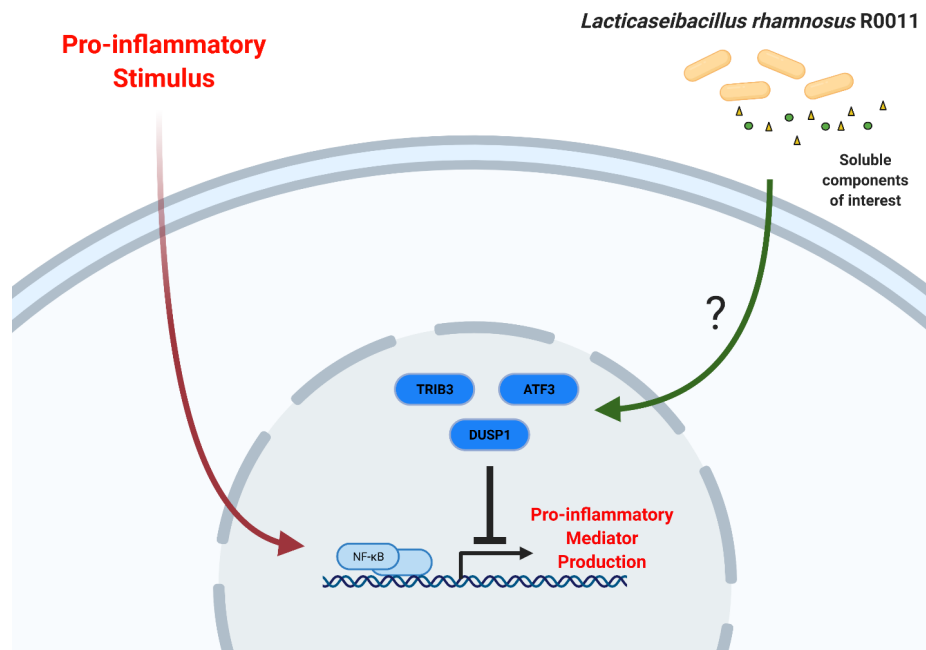


Figure D-1. Proposed mechanism of action behind the observed immunomodulatory activity of the LrS on HT-29 IECs challenged with the STS or TNF- α . When challenged HT-29 IECs are co-challenged with the LrS, there is increased expression of *ATF3*, *TRIB3*, and *DUSP1*, which work in concert to decrease NF- κ B activity and subsequent pro-inflammatory mediator production. Image created with BioRender.

Expanding upon this work, the ability of the LrS to influence immune outcomes in monocytes, another key cellular player in innate immunity, was examined. THP-1 monocytes conditioned with the LrS displayed temporal transcriptional, metabolic, and functional reprogramming and immune signatures consistent with differentiation into immunoregulatory M2 macrophages. In contrast with the results obtained from HT-29 IECs, the LrS heavily influenced the transcriptional landscape of THP-1 monocytes, providing further evidence of context- and cell-dependent mechanism(s) of action behind this secretome-mediated immunoregulatory activity. Further interrogation of the signaling pathways influenced by LrS conditioning revealed changes in the differential expression of genes associated with immune, metabolic, cytoskeletal rearrangement, and myeloid leukocyte differentiation related pathways. Morphological, flow cytometric, and functional analyses confirmed these findings, as LrS-conditioned THP-1 monocytes differentiated into a macrophage phenotype with increased production of immunoregulatory cytokines and reduced reliance on glycolysis for energy production, characteristics shared with immunoregulatory M2 macrophages. Although LrS-conditioned macrophages displayed an overall M2 immunoregulatory phenotype, LPS challenge of LrS-conditioned THP-1 monocytes revealed heightened responsiveness, indicative of innate immune priming (**Figure D-2**). The ability to still respond robustly to pathogen challenge is an important effector function of macrophages, especially within the gut where macrophages are required to respond rapidly to mount an appropriate immune response to bacteria breaching the IEC barrier. Future work should aim to characterize the impact of the LrS and other LAB-derived secretomes on dendritic cells (DC), as they also play an integral role in shaping host immune responses within the gut. DC can also differentiate into different

functional phenotypes in response to microbial products and can be conditioned to regulatory and pro-inflammatory phenotypes through PRR activation and IEC interactions (Campeau *et al.*, 2012; Hoarau *et al.*, 2008; Iwasaki, 2007). DC activation by lactic acid bacteria has been reported (Bermudez-Brito *et al.*, 2015), but many questions surround the mechanisms involved. Further work is needed to investigate the role of LAB and their secreted molecules in the transcriptional and immunometabolic reprogramming of both macrophages and DC, and the ability to confer innate immune tolerance and innate immune training within the context of host-microbe immune communication in the GALT.

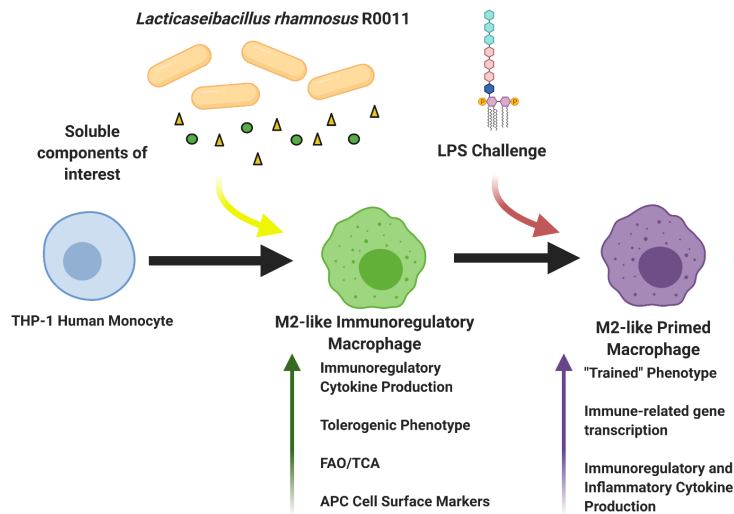


Figure D-2. The LrS differentiates THP-1 human monocytes into macrophages which display functional similarities to M2-like macrophages. Image created with BioRender.

Surprisingly, the LrS altered the acetylation of lysine residues in several proteins in THP-1 monocytes, including those involved in metabolism, redox signaling, and cytoskeletal organization. In particular, the LrS deacetylated PGAM1 and GAPDH, two key enzymes involved in glycolysis. When these enzymes are deacetylated, they have reduced activity, providing potential insights into how the LrS is able to instruct immunometabolic reprogramming of THP-1 monocytes towards increased reliance on the

TCA cycle and oxidative phosphorylation for energy production, a hallmark of M2 immunoregulatory macrophage activity (**Figure D-3**). Other proteins were also identified which had differential lysine acetylation patterns following LrS conditioning, but the function of these post-translational modifications remain unknown. Moreover, the specific lysine residues acetylated within the identified proteins were not determined, which makes subsequent extrapolation about the functional consequences of these post-translational modifications difficult. Although these results suggest a novel means of host-microbe communication through which soluble LAB-derived components regulate the activity of many important cellular processes, more research is needed to ascertain the diverse functional outcomes of these post-translational modifications, especially in the context of host-microbe interactions.

Next, the impact of the LrS on co-cultures of human IECs and APCs was examined in order to gain a better understanding of the immunomodulatory capacity of the LrS in a context which more closely mimics *in vivo* conditions. The LrS did not negatively impact T84 IEC monolayer integrity or function as determined by TER measurements and the paracellular flux of FITC-dextran. Moreover, the LrS did not induce the production of pro-inflammatory mediators from the underlying THP-1 monocyte population, indicating an overall homeostatic response to the LrS. In contrast, challenge with the STS resulted in damage to T84 IEC monolayer integrity, with increases in the production of pro-inflammatory mediators into the apical and basolateral chambers of the co-culture system. The LrS attenuated STS-induced deterioration of T84 monolayer integrity, as well as the production of pro-inflammatory mediators, a result consistent with the observed immunomodulatory activity of the LrS on STS-challenged HT-29 IECs (**Figure D-4**).

Moreover, the LrS attenuated STS-induced *NF-κB1* expression, and increased the expression of *ATF3*, *DUSP1*, and *TRIB3* in T84 IECs challenged with the STS, suggesting that the induction of these negative regulators of innate immune activity is not limited to HT-29 IECs.

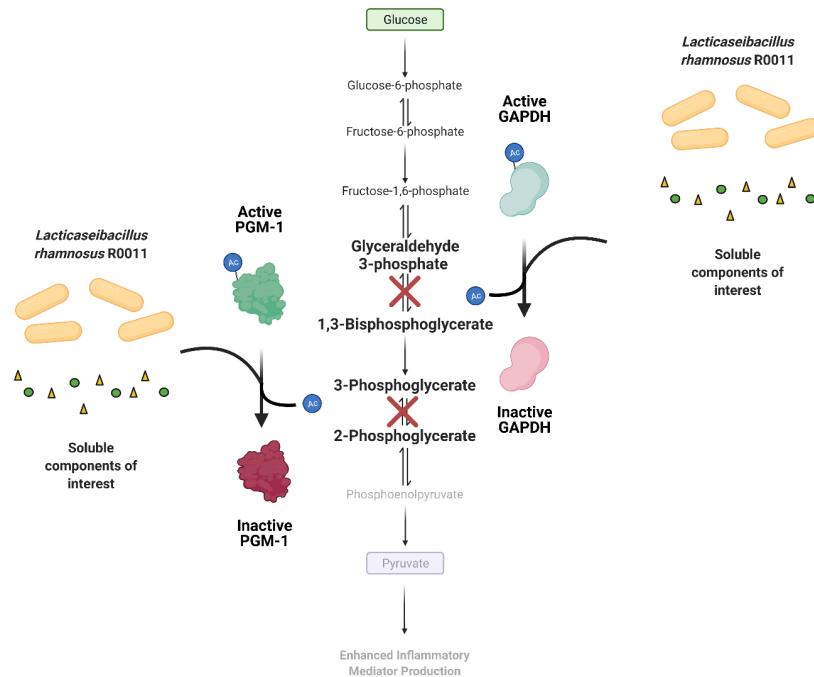


Figure D-3. Post-translational modifications by the LrS to key enzymes involved in glycolysis may reveal mechanism(s) of action behind the observed immunometabolic shift towards an M2-like phenotype in LrS-conditioned macrophages. Image created with BioRender.

Interestingly, LrS challenge also induced the production of MIF by T84 IECs into the apical chamber of the co-culture *in vitro* system. This result is consistent with that seen in LrS-challenged HT-29 IECs, providing further evidence that the observed immunoregulatory activity of the LrS is not limited to HT-29 IECs. Since recent evidence has implicated a role for MIF in maintaining IEC barrier function through MIF/CD74 signaling (Farr, Ghosh, Jiang, *et al.*, 2020; Farr, Ghosh, & Moonah, 2020; Man *et al.*, 2008;

Vujcic *et al.*, 2020; Vujcic *et al.*, 2018), the functional consequences of LrS-induced MIF production were examined in the context of T84 IEC monolayer integrity. The addition of a MIF-neutralizing antibody abrogated the ability of the LrS to reverse STS-induced damage to T84 IEC monolayer integrity, suggesting a novel role for MIF in maintaining IEC barrier function and integrity in response to soluble components derived from LAB. However, the precise mechanism through which the LrS induces the production of MIF remains unknown and warrants further study as does the potential role of MIF/CD74 signaling in shaping host responses to LAB. These results also highlight the importance of utilizing *in vitro* models which allow for vectorial secretion of cytokines and chemokines, in order to gain a better understanding of the functional immune outcomes of bidirectional host-microbe communication.

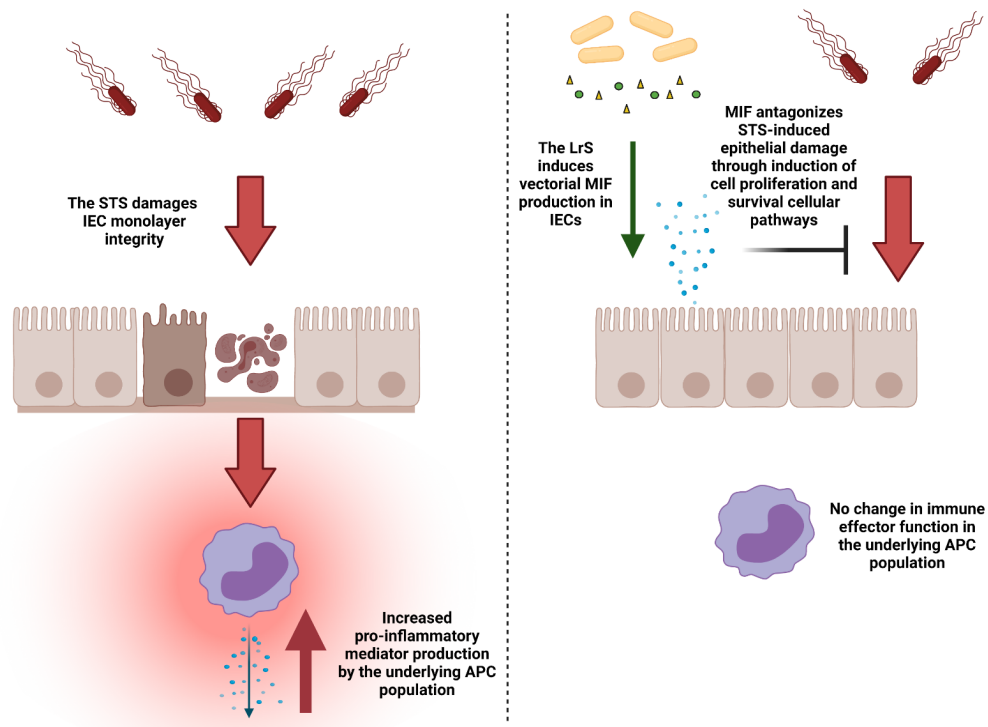


Figure D-4. LrS-induced MIF production by T84 IECs antagonizes STS-induced damage to IEC monolayer integrity and subsequent inflammatory activity by the underlying APC population. Image created with BioRender.

Recent evidence points to secretory proteins and small molecules as important modulators of host-pathogen interactions (Jeffrey *et al.*, 2020; Tommassen *et al.*, 2017; Vivek-Ananth *et al.*, 2018; Zargar *et al.*, 2015). However, less is known about the roles of secretome components derived from gut-associated pathogens in host immune responses within the gut. Throughout these studies, the STS was found to induce robust pro-inflammatory gene expression and mediator production from both HT-29 and T84 human IECs, as well as THP-1 human monocytes, providing evidence for indirect host-pathogen immune communication. While the mechanisms through which the STS induced pro-inflammatory mediator production from IECs and APCs was not determined, this work reinforces the need to consider the roles of soluble mediators derived from pathogens in the context of host-microbe interactions.

Although not one of the primary research goals of this project, biochemical characterization of the soluble components found within the LrS was done to begin preliminary identification of potential bioactive molecules. By applying a combinatorial approach using amino acid, proteomic, and metabolomic profiling, species- and growth phase-dependent production and consumption of a large range of bioactive molecules was characterized. Indeed, the LrS was found to contain several soluble mediators identified as being associated with altering host physiology and immune function. However, the specific activities behind these and most of the soluble mediators identified remain unknown and warrant further study to elucidate their roles in host-microbe communication.

Taken together, the results presented here provide new insights into the role of soluble bioactive molecules derived from both pathogenic bacteria and LAB in facilitating

host-microbe immune communication with host IECs and APCs. LAB secretome-mediated effects on IEC signaling pathways through the induction of *ATF3*, *TRIB3*, *DUSP1*, negative regulators of the NF- κ B and MAPK signaling pathways, present a novel means of LAB regulation of innate immune activity within the gut. The LrS also conditioned THP-1 human monocytes into immunoregulatory M2 macrophages through transcriptional, metabolic, and functional reprogramming, an effect which may be partially mediated through LrS-induced post-translational modifications of key proteins involved in distinct and diverse cellular pathways. Moreover, LrS-conditioning of THP-1 monocytes did not impair responses to subsequent LPS challenge, despite their overall homeostatic M2 phenotype, suggesting context- and cell-dependent mechanism(s) of action behind the observed bioactivity of the LrS. The LrS was also able influence immune outcomes in co-cultures of IECs and APCs, suggesting that the LrS retains bioactivity in a context which more closely mimics that which occurs *in vivo*. The LrS antagonized STS-induced damage to IEC monolayer integrity, potentially through the induction of MIF, a cytokine that has been implicated in maintaining IEC barrier integrity and function. Overall, these findings give novel insight into the complex mechanisms of action behind LAB and pathogen-associated secretome-mediated interdomain communication at the gut-mucosal interface and suggest new directions for approaches to delineate the activities of gut-associated bacteria and LAB *in vivo*.

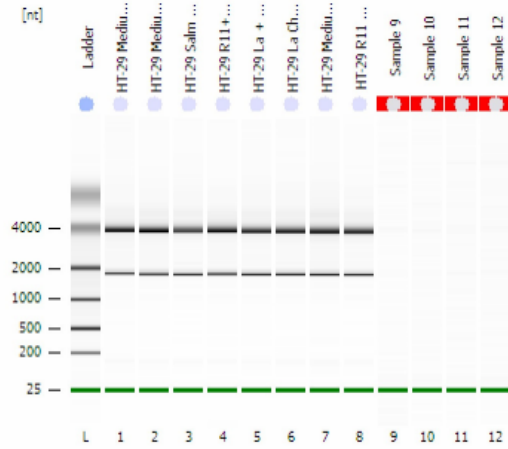
APPENDIX

MJHT-29Chip3_Eukaryote Total RNA Nano_DE72905011_2017-05-29_13-19-12.xad

Page 1 of 13

Assay Class: Eukaryote Total RNA Nano
 Data Path: C:\...Eukaryote Total RNA Nano_DE72905011_2017-05-29_13-19-12.xad
 Created: 5/29/2017 1:19:11 PM
 Modified: 5/29/2017 1:56:28 PM

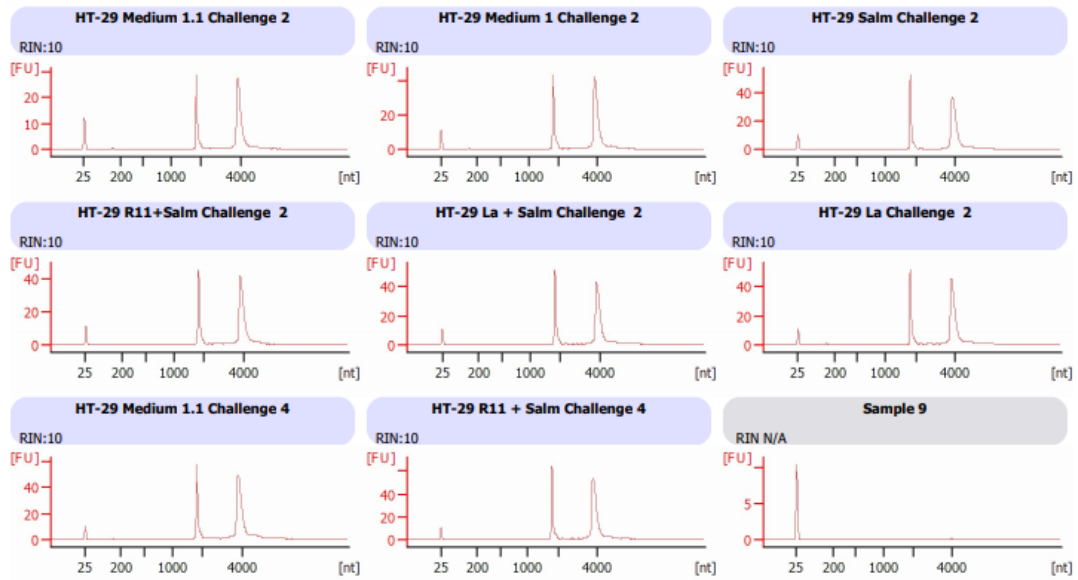
Electrophoresis File Run Summary



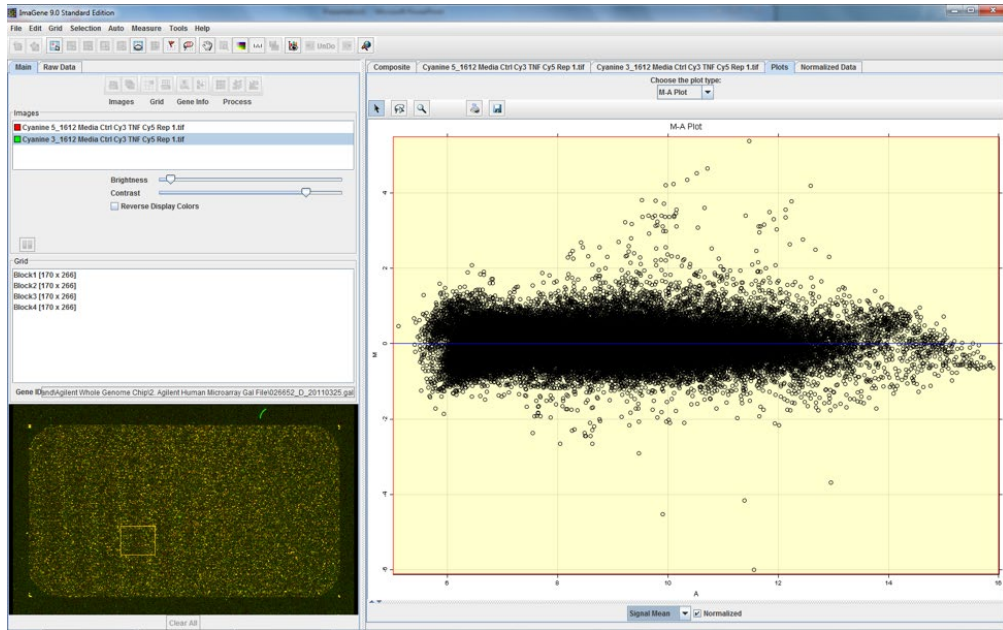
Instrument Information:
 Instrument Name: DE72905011 Firmware: C.01.069
 Serial#: DE72905011 Type: G2938C

Assay Information:
 Assay Origin Path: C:\Program Files\Agilent\2100 bioanalyzer\2100 expert\assays\RNA\Eukaryote Total RNA Nano Series II.xsy
 Assay Class: Eukaryote Total RNA Nano
 Version: 2.6
 Assay Comments: Total RNA Analysis ng sensitivity (Eukaryote)
 © Copyright 2003 - 2009 Agilent Technologies, Inc.

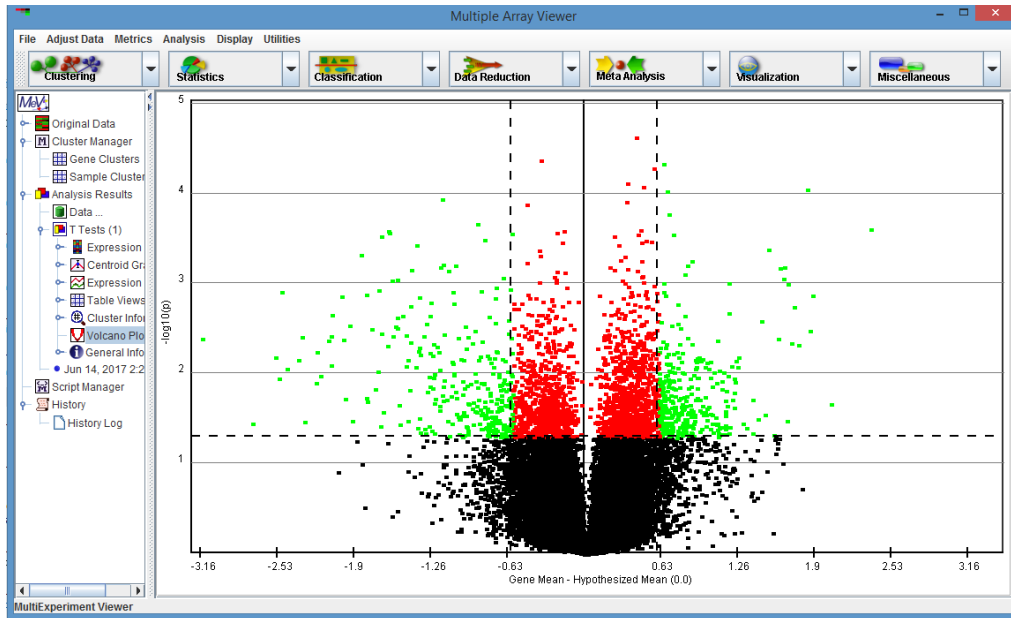
Chip Information:
 Chip Lot #:
 Reagent Kit Lot #:
 Chip Comments:



Appendix A1. Sample readout obtained from the Agilent 2000 Bioanalyzer to determine RNA quality prior to cDNA synthesis for qRT-PCR and microarray experiments.



Appendix A2. Sample MA plot with LOWESS normalization of microarray gene expression data taken from HT-29 IECs challenged with TNF- α .



Appendix A3. Volcano plot analysis of gene expression data taken from HT-29 IECs conditioned with the LrS, conducted using MeV software. Gene selection sliders (dashed lines) were chosen with a cut-off of ± 1.5 -fold change difference. Those spots highlighted in green are genes which have a fold change of ± 1.5 and have been statistically significantly modified by the treatment ($p < 0.05$).

Appendix A4. Cytokines/chemokines examined and their associated functions.

Analyte	Pro-Inflammatory/Regulatory	Function ¹
6Ckine / CCL21	Pro-inflammatory	Chemotactic protein for thymocytes and activated T cells
BCA-1 / CXCL13	Pro-inflammatory	B-cell chemoattractant
CTACK / CCL27	Pro-inflammatory	Memory T cell chemoattractant
ENA-78 / CXCL5	Pro-inflammatory	Neutrophil chemoattractant
Eotaxin / CCL11	Pro-inflammatory	Eosinophil chemoattractant
Eotaxin-2 / CCL24	Pro-inflammatory	Resting T cell and eosinophil chemoattractant
Eotaxin-3 / CCL26	Pro-inflammatory	Eosinophil and basophil chemoattractant
Fractalkine / CX3CL1	Pro-inflammatory	Activated T cell, monocyte, neutrophil, natural killer cell, immature dendritic cell chemoattractant
GCP-2 / CXCL6	Pro-inflammatory	Neutrophil chemoattractant
GM-CSF	Pleiotropic	Stimulates growth and differentiation of granulocytes and macrophages as well as differentiation of dendritic cells into a tolerogenic phenotype
Gro- α / CXCL1	Pro-inflammatory	Neutrophil chemoattractant
Gro- β / CXCL2	Pro-inflammatory	Neutrophil chemoattractant
I-309 / CCL1	Pro-inflammatory	Neutrophil and monocyte chemoattractant
IFN- γ	Pro-inflammatory	Potent activator of macrophages and involved in the cellular response to viral and microbial infections
IL-1 β	Pro-inflammatory	T cell and macrophage activation
IL-2	Pro-inflammatory	Involved in T cell proliferation
IL-4	Regulatory	B cell activation and class switching from IgE and induces differentiation of T cells into T _H 2 cells
IL-6	Pleiotropic	T and B cell growth and differentiation
IL-8 / CXCL8	Pro-inflammatory	Potent neutrophil chemoattractant
IL-10	Regulatory	Potent suppressor of NF- κ B activity and down-regulates the expression of many pro-inflammatory cytokines
IL-16	Pro-inflammatory	CD4 T cell, monocyte, and eosinophil chemoattractant
IP-10 / CXCL10	Pro-inflammatory	Promotes adhesion and serves as a chemoattractant for monocytes, natural killer and T cells
I-TAC / CXCL11	Pro-inflammatory	Natural killer, B, and T cell chemoattractant
MCP-1 / CCL2	Pro-inflammatory	Monocyte and basophil chemoattractant
IL-34	Pro-inflammatory	Promotes release of proinflammatory chemokines
IL-35	Regulatory	Suppresses inflammatory responses
LIGHT / TNFSF14	Pro-inflammatory	Stimulates proliferation of T cells and triggers apoptosis in tumor cells
MMP-1	Pleiotropic	Breakdown of extracellular matrices; cleaves collagen
MMP-2	Pleiotropic	Breakdown of extracellular matrices
MMP-3	Pleiotropic	Breakdown of extracellular matrices; cleaves fibronectin, laminin, gelatin, and collagen
Osteocalcin	Pleiotropic	Regulates bone remodeling and energy metabolism
Osteopontin	Pro-inflammatory	Induces production of IFN γ and IL-12
Pentraxin-3	Pro-inflammatory	Complement activation
sTNF-R1	Pleiotropic	Can interact with free TNF α to inhibit inflammation
sTNF-R2	Pro-inflammatory	Can interact with free TNF α to inhibit inflammation
TSLP	Pro-inflammatory	Induces the release of T-cell-attracting chemokines from monocytes
TWEAK/TNFSF12	Pro-inflammatory	Induces apoptosis

¹Summary of function taken from the GeneCards Human Gene Database entry (Stelzer *et al.*, 2016)

Appendix A4 Continued. Cytokines/chemokines examined and their associated functions.

Analyte	Pro-Inflammatory/Regulatory	Function ¹
MCP-2 / CCL8	Pro-inflammatory	Monocyte, lymphocyte, basophil, and eosinophil chemoattractant
MCP-3 / CCL7	Pro-inflammatory	Macrophage chemoattractant
MCP-4 / CCL13	Pro-inflammatory	Monocyte, lymphocyte, basophil and eosinophil chemoattractant
MDC / CCL22	Pro-inflammatory	Monocyte, dendritic cell, natural killer and T cell chemoattractant
MIF	Pleiotropic	Inhibits macrophage migration, promotes macrophage activation, helps in the maintenance of the epithelial barrier
MIG / CXCL9	Pro-inflammatory	Activated T cell chemoattractant
MIP-1 α / CCL3	Pro-inflammatory	Macrophage, neutrophil, and monocyte chemoattractant
MIP-1 δ / CCL15	Pro-inflammatory	T cell and monocyte chemoattractant
MIP-3 α / CCL20	Pro-inflammatory	Lymphocyte and dendritic cell chemoattractant
MIP-3 β / CCL19	Pro-inflammatory	Lymphocyte chemoattractant; lymphocyte homing and recirculation
MPIF-1 / CCL23	Pro-inflammatory	Resting lymphocyte and monocyte chemoattractant
SCYB16 / CXCL16	Pro-inflammatory	Activated T and natural killer cell chemoattractant
SDF-1 α + β / CXCL12	Pro-inflammatory	T cell and monocyte chemoattractant
TARC / CCL17	Pro-inflammatory	T cell chemoattractant
TECK / CCL25	Pro-inflammatory	Macrophage and intraepithelial lymphocyte chemoattractant
TNF- α	Pro-inflammatory	Promotes production of pro-inflammatory chemokines/cytokines, pyrogen, impairs regulatory T cell function
APRIL/TNFSF13	Pro-inflammatory	Member of the TNF family; induces apoptosis
BAFF/TNFSF13B	Pro-inflammatory	Member of the TNF family; potent B cell activator
sCD30/TNFRSF8	Pro-inflammatory	Member of the TNF family; activates NF- κ B and induces apoptosis
sCD163	Pro-inflammatory	Induces local inflammation upon bacterial challenge
Chitinase-3-like 1	Pro-inflammatory	Inflammation and tissue remodelling
Gp130/sIL-6R β	Pro-inflammatory	Involved in apoptosis and inflammatory responses
IFN- α 2	Pro-inflammatory	Defense against viral infections
IFN- β	Pro-inflammatory	Defense against viral infections; cell differentiation
IFN- γ	Pro-inflammatory	Cellular responses to viral and microbial infections
IL-2	Pleiotropic	Proliferation of T and B lymphocytes
sIL-6R α	Pro-inflammatory	Activator of JAK/STAT pathways
IL-8	Pro-inflammatory	Potent neutrophil chemoattractant
IL-10	Regulatory	Immunoregulation; blocks NF- κ B activation
IL-11	Pro-inflammatory	Stimulates proliferation of hematopoietic stem cells
IL-12p40	Pro-inflammatory	Inactive form of IL-12; activator of T and natural killer cells
IL-12p70	Pro-inflammatory	Bioactive and functional IL-12; activator of T and natural killer cells
IL-19	Pro-inflammatory	Induces IL-6 and TNF α production
IL-20	Pro-inflammatory	Pro-inflammatory and angiogenic responses
IL-22	Pro-inflammatory	Antimicrobial defense
IL-26	Pro-inflammatory	Induces IL-8, TNF α , and ICAM1; decreases proliferation of IECs
IL-27p28	Pleiotropic	Promotes T-helper cell development; stimulates cytotoxic T cell activity
IL-28A/ IFN- λ 2	Pro-inflammatory	Antiviral defense in epithelial tissues
IL-29/ IFN- λ 1	Pro-inflammatory	Antiviral defense in epithelial tissues
IL-32	Pro-inflammatory	Induces TNF α production

¹Summary of function taken from the GeneCards Human Gene Database entry (Stelzer *et al.*, 2016)

REFERENCES

- Abreu, M. T. (2010). Toll-like receptor signalling in the intestinal epithelium: how bacterial recognition shapes intestinal function. *Nat Rev Immunol*, *10*(2), 131-144. doi:10.1038/nri2707
- Akinrinmade, O. A., Chetty, S., Daramola, A. K., Islam, M. U., Thepen, T., & Barth, S. (2017). CD64: An Attractive Immunotherapeutic Target for M1-type Macrophage Mediated Chronic Inflammatory Diseases. *Biomedicines*, *5*(3). doi:10.3390/biomedicines5030056
- Alemka, A., Clyne, M., Shanahan, F., Tompkins, T., Corcionivoschi, N., & Bourke, B. (2010). Probiotic colonization of the adherent mucus layer of HT29MTXE12 cells attenuates *Campylobacter jejuni* virulence properties. *Infect Immun*, *78*(6), 2812-2822. doi:10.1128/IAI.01249-09
- Allonsius, C. N., Vandenheuvell, D., Oerlemans, E. F. M., Petrova, M. I., Donders, G. G. G., Cos, P., Delputte, P., & Lebeer, S. (2019). Inhibition of *Candida albicans* morphogenesis by chitinase from *Lactobacillus rhamnosus* GG. *Sci Rep*, *9*(1), 2900. doi:10.1038/s41598-019-39625-0
- Ambarus, C. A., Krausz, S., van Eijk, M., Hamann, J., Radstake, T. R., Reedquist, K. A., Tak, P. P., & Baeten, D. L. (2012). Systematic validation of specific phenotypic markers for in vitro polarized human macrophages. *J Immunol Methods*, *375*(1-2), 196-206. doi:10.1016/j.jim.2011.10.013
- Arthur, J. S., & Ley, S. C. (2013). Mitogen-activated protein kinases in innate immunity. *Nat Rev Immunol*, *13*(9), 679-692. doi:10.1038/nri3495
- Artis, D. (2008). Epithelial-cell recognition of commensal bacteria and maintenance of immune homeostasis in the gut. *Nat Rev Immunol*, *8*(6), 411-420. doi:10.1038/nri2316
- Audy, J., Mathieu, O., Belvis, J., & Tompkins, T. A. (2012). Transcriptomic response of immune signalling pathways in intestinal epithelial cells exposed to lipopolysaccharides, Gram-negative bacteria or potentially probiotic microbes. *Benef Microbes*, *3*(4), 273-286. doi:10.3920/BM2012.0027
- Ayres, J. S. (2016). Cooperative Microbial Tolerance Behaviors in Host-Microbiota Mutualism. *Cell*, *165*(6), 1323-1331. doi:<https://doi.org/10.1016/j.cell.2016.05.049>
- Baeza, J., Smallegan, M. J., & Denu, J. M. (2016). Mechanisms and Dynamics of Protein Acetylation in Mitochondria. *Trends Biochem Sci*, *41*(3), 231-244. doi:10.1016/j.tibs.2015.12.006
- Bai, A. P., Ouyang, Q., Zhang, W., Wang, C. H., & Li, S. F. (2004). Probiotics inhibit TNF-alpha-induced interleukin-8 secretion of HT29 cells. *World J Gastroenterol*, *10*(3), 455-457. Retrieved from <https://www.ncbi.nlm.nih.gov/pubmed/14760780>
- Balzaretti, S., Taverniti, V., Guglielmetti, S., Fiore, W., Minuzzo, M., Ngo, H. N., Ngere, J. B., Sadiq, S., Humphreys, P. N., & Laws, A. P. (2017). A Novel Rhamnose-Rich Hetero-exopolysaccharide Isolated from *Lactobacillus paracasei* DG Activates THP-1 Human Monocytic Cells. *Appl Environ Microbiol*, *83*(3). doi:10.1128/AEM.02702-16
- Barman, M., Unold, D., Shifley, K., Amir, E., Hung, K., Bos, N., & Salzman, N. (2008). Enteric salmonellosis disrupts the microbial ecology of the murine gastrointestinal tract. *Infect Immun*, *76*(3), 907-915. doi:10.1128/IAI.01432-07

- Bauer, H., Horowitz, R. E., Levenson, S. M., & Popper, H. (1963). The response of the lymphatic tissue to the microbial flora. Studies on germfree mice. *The American journal of pathology*, 42(4), 471-483. Retrieved from <https://pubmed.ncbi.nlm.nih.gov/13966929>
- <https://www.ncbi.nlm.nih.gov/pmc/articles/PMC1949649/>
- Berger, J. A., Hautaniemi, S., Jarvinen, A. K., Edgren, H., Mitra, S. K., & Astola, J. (2004). Optimized LOWESS normalization parameter selection for DNA microarray data. *BMC Bioinformatics*, 5, 194. doi:10.1186/1471-2105-5-194
- Bermudez-Brito, M., Munoz-Quezada, S., Gomez-Llorente, C., Matencio, E., Romero, F., & Gil, A. (2015). *Lactobacillus paracasei* CNCM I-4034 and its culture supernatant modulate Salmonella-induced inflammation in a novel transwell co-culture of human intestinal-like dendritic and Caco-2 cells. *BMC Microbiol*, 15(1), 79. doi:10.1186/s12866-015-0408-6
- Bhat, M. I., Kumari, A., Kapila, S., & Kapila, R. (2019). Probiotic lactobacilli mediated changes in global epigenetic signatures of human intestinal epithelial cells during Escherichia coli challenge. *Annals of Microbiology*, 69(6), 603-612. doi:10.1007/s13213-019-01451-0
- Blacher, E., Levy, M., Tatirovsky, E., & Elinav, E. (2017). Microbiome-Modulated Metabolites at the Interface of Host Immunity. *J Immunol*, 198(2), 572-580. doi:10.4049/jimmunol.1601247
- Boeckx, C., Blockx, L., de Beek, K. O., Limame, R., Camp, G. V., Peeters, M., Vermorken, J. B., Specenier, P., Wouters, A., Baay, M., & Lardon, F. (2015). Establishment and characterization of cetuximab resistant head and neck squamous cell carcinoma cell lines: focus on the contribution of the AP-1 transcription factor. *Am J Cancer Res*, 5(6), 1921-1938. Retrieved from <https://www.ncbi.nlm.nih.gov/pubmed/26269754>
- Bottone, F. G., Jr., Moon, Y., Kim, J. S., Alston-Mills, B., Ishibashi, M., & Eling, T. E. (2005). The anti-invasive activity of cyclooxygenase inhibitors is regulated by the transcription factor ATF3 (activating transcription factor 3). *Mol Cancer Ther*, 4(5), 693-703. doi:10.1158/1535-7163.MCT-04-0337
- Boyle, E. C., Brown, N. F., & Finlay, B. B. (2006). *Salmonella enterica* serovar Typhimurium effectors SopB, SopE, SopE2 and SipA disrupt tight junction structure and function. *Cell Microbiol*, 8(12), 1946-1957. doi:10.1111/j.1462-5822.2006.00762.x
- Broekaert, I. J., Nanthakumar, N. N., & Walker, W. A. (2007). Secreted probiotic factors ameliorate enteropathogenic infection in zinc-deficient human Caco-2 and T84 cell lines. *Pediatr Res*, 62(2), 139-144. doi:10.1203/PDR.0b013e31809fd85e
- Bujko, A., Atlasy, N., Landsverk, O. J. B., Richter, L., Yaqub, S., Horneland, R., Oyen, O., Aandahl, E. M., Aabakken, L., Stunnenberg, H. G., Baekkevold, E. S., & Jahnsen, F. L. (2018). Transcriptional and functional profiling defines human small intestinal macrophage subsets. *J Exp Med*, 215(2), 441-458. doi:10.1084/jem.20170057
- Burgueno, J. F., & Abreu, M. T. (2020). Epithelial Toll-like receptors and their role in gut homeostasis and disease. *Nat Rev Gastroenterol Hepatol*, 17(5), 263-278. doi:10.1038/s41575-019-0261-4

- Campeau, J. L., Salim, S. Y., Albert, E. J., Hotte, N., & Madsen, K. L. (2012). Intestinal epithelial cells modulate antigen-presenting cell responses to bacterial DNA. *Infect Immun*, *80*(8), 2632-2644. doi:10.1128/IAI.00288-12
- Campeato, L. F., Budhu, S., Tchaicha, J., Weng, C. H., Gigoux, M., Cohen, I. J., Redmond, D., Mangarin, L., Pourpe, S., Liu, C., Zappasodi, R., Zamarin, D., Cavanaugh, J., Castro, A. C., Manfredi, M. G., McGovern, K., Merghoub, T., & Wolchok, J. D. (2020). Blockade of the AHR restricts a Treg-macrophage suppressive axis induced by L-Kynurenine. *Nat Commun*, *11*(1), 4011. doi:10.1038/s41467-020-17750-z
- Cerovic, V., Bain, C. C., Mowat, A. M., & Milling, S. W. (2014). Intestinal macrophages and dendritic cells: what's the difference? *Trends Immunol*, *35*(6), 270-277. doi:10.1016/j.it.2014.04.003
- Chang, C. H., Curtis, J. D., Maggi, L. B., Jr., Faubert, B., Villarino, A. V., O'Sullivan, D., Huang, S. C., van der Windt, G. J., Blagih, J., Qiu, J., Weber, J. D., Pearce, E. J., Jones, R. G., & Pearce, E. L. (2013). Posttranscriptional control of T cell effector function by aerobic glycolysis. *Cell*, *153*(6), 1239-1251. doi:10.1016/j.cell.2013.05.016
- Chanput, W., Mes, J. J., Savelkoul, H. F., & Wichers, H. J. (2013). Characterization of polarized THP-1 macrophages and polarizing ability of LPS and food compounds. *Food Funct*, *4*(2), 266-276. doi:10.1039/c2fo30156c
- Chanput, W., Mes, J. J., & Wichers, H. J. (2014). THP-1 cell line: an in vitro cell model for immune modulation approach. *Int Immunopharmacol*, *23*(1), 37-45. doi:10.1016/j.intimp.2014.08.002
- Chen, F., Wu, X., Niculite, C., Gilca, M., Petrusca, D., Rogozea, A., Rice, S., Guo, B., Griffin, S., Calin, G. A., Boswell, H. S., & Konig, H. (2020). Classic and targeted anti-leukaemic agents interfere with the cholesterol biogenesis metagene in acute myeloid leukaemia: Therapeutic implications. *J Cell Mol Med*, *24*(13), 7378-7392. doi:10.1111/jcmm.15339
- Chen, M. T., Dong, L., Zhang, X. H., Yin, X. L., Ning, H. M., Shen, C., Su, R., Li, F., Song, L., Ma, Y. N., Wang, F., Zhao, H. L., Yu, J., & Zhang, J. W. (2015). ZFP36L1 promotes monocyte/macrophage differentiation by repressing CDK6. *Sci Rep*, *5*, 16229. doi:10.1038/srep16229
- Cheng, H.-Y., Ning, M.-X., Chen, D.-K., & Ma, W.-T. (2019). Interactions Between the Gut Microbiota and the Host Innate Immune Response Against Pathogens. *Frontiers in Immunology*, *10*(607). doi:10.3389/fimmu.2019.00607
- Chi, H., Barry, S. P., Roth, R. J., Wu, J. J., Jones, E. A., Bennett, A. M., & Flavell, R. A. (2006). Dynamic regulation of pro- and anti-inflammatory cytokines by MAPK phosphatase 1 (MKP-1) in innate immune responses. *Proc Natl Acad Sci U S A*, *103*(7), 2274-2279. doi:10.1073/pnas.0510965103
- Cho, M. L., Moon, Y. M., Heo, Y. J., Woo, Y. J., Ju, J. H., Park, K. S., Kim, S. I., Park, S. H., Kim, H. Y., & Min, J. K. (2009). NF-kappaB inhibition leads to increased synthesis and secretion of MIF in human CD4+ T cells. *Immunol Lett*, *123*(1), 21-30. doi:10.1016/j.imlet.2009.01.010
- Chomczynski, P. (1993). A reagent for the single-step simultaneous isolation of RNA, DNA and proteins from cell and tissue samples. *Biotechniques*, *15*(3), 532-534, 536-537. Retrieved from <https://www.ncbi.nlm.nih.gov/pubmed/7692896>

- Christoffersen, T. E., Hult, L. T., Kuczkowska, K., Moe, K. M., Skeie, S., Lea, T., & Kleiveland, C. R. (2014). *In vitro* comparison of the effects of probiotic, commensal and pathogenic strains on macrophage polarization. *Probiotics Antimicrob Proteins*, 6(1), 1-10. doi:10.1007/s12602-013-9152-0
- Cipriani, G., Gibbons, S. J., Kashyap, P. C., & Farrugia, G. (2016). Intrinsic Gastrointestinal Macrophages: Their Phenotype and Role in Gastrointestinal Motility. *Cell Mol Gastroenterol Hepatol*, 2(2), 120-130 e121. doi:10.1016/j.jcmgh.2016.01.003
- Clarke, T. B., Davis, K. M., Lysenko, E. S., Zhou, A. Y., Yu, Y., & Weiser, J. N. (2010). Recognition of peptidoglycan from the microbiota by Nod1 enhances systemic innate immunity. *Nat Med*, 16(2), 228-231. doi:10.1038/nm.2087
- Coburn, B., Grassl, G. A., & Finlay, B. B. (2007). Salmonella, the host and disease: a brief review. *Immunol Cell Biol*, 85(2), 112-118. doi:10.1038/sj.icb.7100007
- Coburn, B., Sekirov, I., & Finlay, B. B. (2007). Type III secretion systems and disease. *Clin Microbiol Rev*, 20(4), 535-549. doi:10.1128/CMR.00013-07
- Colin, S., Chinetti-Gbaguidi, G., & Staels, B. (2014). Macrophage phenotypes in atherosclerosis. *Immunol Rev*, 262(1), 153-166. doi:10.1111/imr.12218
- Couper, K. N., Blount, D. G., & Riley, E. M. (2008). IL-10: the master regulator of immunity to infection. *J Immunol*, 180(9), 5771-5777. doi:10.4049/jimmunol.180.9.5771
- Das, R., LaRose, M. I., Hergott, C. B., Leng, L., Bucala, R., & Weiser, J. N. (2014). Macrophage migration inhibitory factor promotes clearance of pneumococcal colonization. *J Immunol*, 193(2), 764-772. doi:10.4049/jimmunol.1400133
- De Schepper, S., Verheijden, S., Aguilera-Lizarraga, J., Viola, M. F., Boesmans, W., Stakenborg, N., Voytyuk, I., Schmidt, I., Boeckx, B., Dierckx de Casterle, I., Baekelandt, V., Gonzalez Dominguez, E., Mack, M., Depoortere, I., De Strooper, B., Sprangers, B., Himmelreich, U., Soenen, S., Guilliams, M., Vanden Berghe, P., Jones, E., Lambrechts, D., & Boeckxstaens, G. (2018). Self-Maintaining Gut Macrophages Are Essential for Intestinal Homeostasis. *Cell*, 175(2), 400-415 e413. doi:10.1016/j.cell.2018.07.048
- Dharmasathaphorn, K., & Madara, J. L. (1990). Established intestinal cell lines as model systems for electrolyte transport studies. *Methods Enzymol*, 192, 354-389. doi:10.1016/0076-6879(90)92082-o
- Dietl, K., Renner, K., Dettmer, K., Timischl, B., Eberhart, K., Dorn, C., Hellerbrand, C., Kastenberger, M., Kunz-Schughart, L. A., Oefner, P. J., Andreesen, R., Gottfried, E., & Kreutz, M. P. (2010). Lactic acid and acidification inhibit TNF secretion and glycolysis of human monocytes. *J Immunol*, 184(3), 1200-1209. doi:10.4049/jimmunol.0902584
- Diskin, C., & Palsson-McDermott, E. M. (2018). Metabolic Modulation in Macrophage Effector Function. *Front Immunol*, 9, 270. doi:10.3389/fimmu.2018.00270
- Donato, R. P., El-Merhibi, A., Gundsambuu, B., Mak, K. Y., Formosa, E. R., Wang, X., Abbott, C. A., & Powell, B. C. (2011). Studying permeability in a commonly used epithelial cell line: T84 intestinal epithelial cells. *Methods Mol Biol*, 763, 115-137. doi:10.1007/978-1-61779-191-8_8
- Donia, M. S., & Fischbach, M. A. (2015). HUMAN MICROBIOTA. Small molecules from the human microbiota. *Science*, 349(6246), 1254766. doi:10.1126/science.1254766

- Dydensborg, A. B., Herring, E., Auclair, J., Tremblay, E., & Beaulieu, J. F. (2006). Normalizing genes for quantitative RT-PCR in differentiating human intestinal epithelial cells and adenocarcinomas of the colon. *Am J Physiol Gastrointest Liver Physiol*, *290*(5), G1067-1074. doi:10.1152/ajpgi.00234.2005
- Eckmann, L. (2005). Defence molecules in intestinal innate immunity against bacterial infections. *Curr Opin Gastroenterol*, *21*(2), 147-151. doi:10.1097/01.mog.0000153311.97832.8c
- Ewaschuk, J. B., Diaz, H., Meddings, L., Diederichs, B., Dmytrash, A., Backer, J., Looijer-van Langen, M., & Madsen, K. L. (2008). Secreted bioactive factors from *Bifidobacterium infantis* enhance epithelial cell barrier function. *Am J Physiol Gastrointest Liver Physiol*, *295*(5), G1025-1034. doi:10.1152/ajpgi.90227.2008
- Farr, L., Ghosh, S., Jiang, N., Watanabe, K., Parlak, M., Bucala, R., & Moonah, S. (2020). CD74 Signaling Links Inflammation to Intestinal Epithelial Cell Regeneration and Promotes Mucosal Healing. *Cell Mol Gastroenterol Hepatol*, *10*(1), 101-112. doi:10.1016/j.jcmgh.2020.01.009
- Farr, L., Ghosh, S., & Moonah, S. (2020). Role of MIF Cytokine/CD74 Receptor Pathway in Protecting Against Injury and Promoting Repair. *Front Immunol*, *11*, 1273. doi:10.3389/fimmu.2020.01273
- Fayol-Messaoudi, D., Berger, C. N., Coconnier-Polter, M. H., Lievin-Le Moal, V., & Servin, A. L. (2005). pH-, Lactic acid-, and non-lactic acid-dependent activities of probiotic Lactobacilli against *Salmonella enterica* Serovar Typhimurium. *Appl Environ Microbiol*, *71*(10), 6008-6013. doi:10.1128/AEM.71.10.6008-6013.2005
- Fenton, M. J., Buras, J. A., & Donnelly, R. P. (1992). IL-4 reciprocally regulates IL-1 and IL-1 receptor antagonist expression in human monocytes. *J Immunol*, *149*(4), 1283-1288. Retrieved from <https://www.ncbi.nlm.nih.gov/pubmed/1386862>
- Fritz, J. H. (2013). Arginine cools the inflamed gut. *Infect Immun*, *81*(10), 3500-3502. doi:10.1128/IAI.00789-13
- Gaisawat, M. B., Iskandar, M. M., MacPherson, C. W., Tompkins, T. A., & Kubow, S. (2019). Probiotic Supplementation is Associated with Increased Antioxidant Capacity and Copper Chelation in *C. difficile*-Infected Fecal Water. *Nutrients*, *11*(9). doi:10.3390/nu11092007
- Ganguli, K., Meng, D., Rautava, S., Lu, L., Walker, W. A., & Nanthakumar, N. (2013). Probiotics prevent necrotizing enterocolitis by modulating enterocyte genes that regulate innate immune-mediated inflammation. *Am J Physiol Gastrointest Liver Physiol*, *304*(2), G132-141. doi:10.1152/ajpgi.00142.2012
- Gao, K., Wang, C., Liu, L., Dou, X., Liu, J., Yuan, L., Zhang, W., & Wang, H. (2017). Immunomodulation and signaling mechanism of *Lactobacillus rhamnosus* GG and its components on porcine intestinal epithelial cells stimulated by lipopolysaccharide. *J Microbiol Immunol Infect*, *50*(5), 700-713. doi:10.1016/j.jmii.2015.05.002
- Garrote, G. L., Abraham, A. G., & Rumbo, M. (2015). Is lactate an undervalued functional component of fermented food products? *Front Microbiol*, *6*, 629. doi:10.3389/fmicb.2015.00629
- Geeraerts, X., Bolli, E., Fendt, S. M., & Van Ginderachter, J. A. (2017). Macrophage Metabolism As Therapeutic Target for Cancer, Atherosclerosis, and Obesity. *Front Immunol*, *8*, 289. doi:10.3389/fimmu.2017.00289

- Gensollen, T., Iyer, S. S., Kasper, D. L., & Blumberg, R. S. (2016). How colonization by microbiota in early life shapes the immune system. *Science*, *352*(6285), 539-544. doi:10.1126/science.aad9378
- Gewirtz, A. T., Navas, T. A., Lyons, S., Godowski, P. J., & Madara, J. L. (2001). Cutting edge: bacterial flagellin activates basolaterally expressed TLR5 to induce epithelial proinflammatory gene expression. *J Immunol*, *167*(4), 1882-1885. doi:10.4049/jimmunol.167.4.1882
- Ghadimi, D., Helwig, U., Schrezenmeir, J., Heller, K. J., & de Vrese, M. (2012). Epigenetic imprinting by commensal probiotics inhibits the IL-23/IL-17 axis in an in vitro model of the intestinal mucosal immune system. *J Leukoc Biol*, *92*(4), 895-911. doi:10.1189/jlb.0611286
- Gilchrist, M., Thorsson, V., Li, B., Rust, A. G., Korb, M., Roach, J. C., Kennedy, K., Hai, T., Bolouri, H., & Aderem, A. (2006). Systems biology approaches identify ATF3 as a negative regulator of Toll-like receptor 4. *Nature*, *441*(7090), 173-178. doi:10.1038/nature04768
- Girardin, S. E., Travassos, L. H., Herve, M., Blanot, D., Boneca, I. G., Philpott, D. J., Sansonetti, P. J., & Mengin-Lecreulx, D. (2003). Peptidoglycan molecular requirements allowing detection by Nod1 and Nod2. *J Biol Chem*, *278*(43), 41702-41708. doi:10.1074/jbc.M307198200
- Goto, Y. (2019). Epithelial Cells as a Transmitter of Signals From Commensal Bacteria and Host Immune Cells. *Front Immunol*, *10*, 2057. doi:10.3389/fimmu.2019.02057
- Griess, B., Mir, S., Datta, K., & Teoh-Fitzgerald, M. (2020). Scavenging reactive oxygen species selectively inhibits M2 macrophage polarization and their pro-tumorigenic function in part, via Stat3 suppression. *Free Radic Biol Med*, *147*, 48-60. doi:10.1016/j.freeradbiomed.2019.12.018
- Gross, M., Salame, T. M., & Jung, S. (2015). Guardians of the Gut - Murine Intestinal Macrophages and Dendritic Cells. *Front Immunol*, *6*, 254. doi:10.3389/fimmu.2015.00254
- Guilliams, M., Mildner, A., & Yona, S. (2018). Developmental and Functional Heterogeneity of Monocytes. *Immunity*, *49*(4), 595-613. doi:10.1016/j.immuni.2018.10.005
- Gunzel, D., & Yu, A. S. (2013). Claudins and the modulation of tight junction permeability. *Physiol Rev*, *93*(2), 525-569. doi:10.1152/physrev.00019.2012
- Guo, H., Callaway, J. B., & Ting, J. P. (2015). Inflammasomes: mechanism of action, role in disease, and therapeutics. *Nat Med*, *21*(7), 677-687. doi:10.1038/nm.3893
- Haas, R., Smith, J., Rocher-Ros, V., Nadkarni, S., Montero-Melendez, T., D'Acquisto, F., Bland, E. J., Bombardieri, M., Pitzalis, C., Perretti, M., Marelli-Berg, F. M., & Mauro, C. (2015). Lactate Regulates Metabolic and Pro-inflammatory Circuits in Control of T Cell Migration and Effector Functions. *PLoS Biol*, *13*(7), e1002202. doi:10.1371/journal.pbio.1002202
- Hadis, U., Wahl, B., Schulz, O., Hardtke-Wolenski, M., Schippers, A., Wagner, N., Muller, W., Sparwasser, T., Forster, R., & Pabst, O. (2011). Intestinal tolerance requires gut homing and expansion of FoxP3+ regulatory T cells in the lamina propria. *Immunity*, *34*(2), 237-246. doi:10.1016/j.immuni.2011.01.016

- Hallows, W. C., Yu, W., & Denu, J. M. (2012). Regulation of glycolytic enzyme phosphoglycerate mutase-1 by Sirt1 protein-mediated deacetylation. *J Biol Chem*, 287(6), 3850-3858. doi:10.1074/jbc.M111.317404
- Hammami, R., Fernandez, B., Lacroix, C., & Fliss, I. (2013). Anti-infective properties of bacteriocins: an update. *Cell Mol Life Sci*, 70(16), 2947-2967. doi:10.1007/s00018-012-1202-3
- Hammer, M., Mages, J., Dietrich, H., Servatius, A., Howells, N., Cato, A. C., & Lang, R. (2006). Dual specificity phosphatase 1 (DUSP1) regulates a subset of LPS-induced genes and protects mice from lethal endotoxin shock. *J Exp Med*, 203(1), 15-20. doi:10.1084/jem.20051753
- Harhaj, N. S., & Antonetti, D. A. (2004). Regulation of tight junctions and loss of barrier function in pathophysiology. *Int J Biochem Cell Biol*, 36(7), 1206-1237. doi:10.1016/j.biocel.2003.08.007
- Harris, J., VanPatten, S., Deen, N. S., Al-Abed, Y., & Morand, E. F. (2019). Rediscovering MIF: New Tricks for an Old Cytokine. *Trends Immunol*, 40(5), 447-462. doi:10.1016/j.it.2019.03.002
- Hart, P. H., Vitti, G. F., Burgess, D. R., Whitty, G. A., Piccoli, D. S., & Hamilton, J. A. (1989). Potential antiinflammatory effects of interleukin 4: suppression of human monocyte tumor necrosis factor alpha, interleukin 1, and prostaglandin E2. *Proc Natl Acad Sci U S A*, 86(10), 3803-3807. doi:10.1073/pnas.86.10.3803
- He, C., Danes, J. M., Hart, P. C., Zhu, Y., Huang, Y., de Abreu, A. L., O'Brien, J., Mathison, A. J., Tang, B., Frasar, J. M., Wakefield, L. M., Ganini, D., Stauder, E., Zielonka, J., Gantner, B. N., Urrutia, R. A., Gius, D., & Bonini, M. G. (2019). SOD2 acetylation on lysine 68 promotes stem cell reprogramming in breast cancer. *Proc Natl Acad Sci U S A*, 116(47), 23534-23541. doi:10.1073/pnas.1902308116
- Herb, M., Gluschko, A., Wiegmann, K., Farid, A., Wolf, A., Utermohlen, O., Krut, O., Kronke, M., & Schramm, M. (2019). Mitochondrial reactive oxygen species enable proinflammatory signaling through disulfide linkage of NEMO. *Sci Signal*, 12(568). doi:10.1126/scisignal.aar5926
- Hillgren, K. M., Kato, A., & Borchardt, R. T. (1995). In vitro systems for studying intestinal drug absorption. *Med Res Rev*, 15(2), 83-109. doi:10.1002/med.2610150202
- Hjelmeland, A. B., & Patel, R. P. (2019). SOD2 acetylation and deacetylation: Another tale of Jekyll and Hyde in cancer. *Proc Natl Acad Sci U S A*, 116(47), 23376-23378. doi:10.1073/pnas.1916214116
- Hoarau, C., Martin, L., Faugaret, D., Baron, C., Dauba, A., Aubert-Jacquin, C., Velge-Roussel, F., & Lebranchu, Y. (2008). Supernatant from bifidobacterium differentially modulates transduction signaling pathways for biological functions of human dendritic cells. *PLoS One*, 3(7), e2753. doi:10.1371/journal.pone.0002753
- Hoetzenecker, W., Echtenacher, B., Guenova, E., Hoetzenecker, K., Woelbing, F., Bruck, J., Teske, A., Valtcheva, N., Fuchs, K., Kneilling, M., Park, J. H., Kim, K. H., Kim, K. W., Hoffmann, P., Krenn, C., Hai, T., Ghoreschi, K., Biedermann, T., & Rocken, M. (2011). ROS-induced ATF3 causes susceptibility to secondary infections during sepsis-associated immunosuppression. *Nat Med*, 18(1), 128-134. doi:10.1038/nm.2557

- Honko, A. N., Sriranganathan, N., Lees, C. J., & Mizel, S. B. (2006). Flagellin is an effective adjuvant for immunization against lethal respiratory challenge with *Yersinia pestis*. *Infect Immun*, *74*(2), 1113-1120. doi:10.1128/IAI.74.2.1113-1120.2006
- Hormansperger, G., von Schillde, M. A., & Haller, D. (2013). Lactocepilin as a protective microbial structure in the context of IBD. *Gut Microbes*, *4*(2), 152-157. doi:10.4161/gmic.23444
- Hotamisligil, G. S. (2017). Inflammation, metaflammation and immunometabolic disorders. *Nature*, *542*(7640), 177-185. doi:10.1038/nature21363
- Hristodorov, D., Mladenov, R., von Felbert, V., Huhn, M., Fischer, R., Barth, S., & Thepen, T. (2015). Targeting CD64 mediates elimination of M1 but not M2 macrophages in vitro and in cutaneous inflammation in mice and patient biopsies. *MAbs*, *7*(5), 853-862. doi:10.1080/19420862.2015.1066950
- Hurmalainen, V., Edelman, S., Antikainen, J., Baumann, M., Lahteenmaki, K., & Korhonen, T. K. (2007). Extracellular proteins of *Lactobacillus crispatus* enhance activation of human plasminogen. *Microbiology (Reading)*, *153*(Pt 4), 1112-1122. doi:10.1099/mic.0.2006/000901-0
- Imaeda, H., Andoh, A., Aomatsu, T., Osaki, R., Bamba, S., Inatomi, O., Shimizu, T., & Fujiyama, Y. (2011). A new isoform of interleukin-32 suppresses IL-8 mRNA expression in the intestinal epithelial cell line HT-29. *Mol Med Rep*, *4*(3), 483-487. doi:10.3892/mmr.2011.442
- Iwasaki, A. (2007). Mucosal dendritic cells. *Annu Rev Immunol*, *25*, 381-418. doi:10.1146/annurev.immunol.25.022106.141634
- Jakubzick, C. V., Randolph, G. J., & Henson, P. M. (2017). Monocyte differentiation and antigen-presenting functions. *Nat Rev Immunol*, *17*(6), 349-362. doi:10.1038/nri.2017.28
- Janes, K. A., Gaudet, S., Albeck, J. G., Nielsen, U. B., Lauffenburger, D. A., & Sorger, P. K. (2006). The response of human epithelial cells to TNF involves an inducible autocrine cascade. *Cell*, *124*(6), 1225-1239. doi:10.1016/j.cell.2006.01.041
- Janeway, C. A., Jr., & Medzhitov, R. (2002). Innate immune recognition. *Annu Rev Immunol*, *20*, 197-216. doi:10.1146/annurev.immunol.20.083001.084359
- Jeffrey, M. P., Jones Taggart, H., Strap, J. L., Edun, G., & Green-Johnson, J. M. (2020). Milk fermented with *Lactobacillus rhamnosus* R0011 induces a regulatory cytokine profile in LPS-challenged U937 and THP-1 macrophages. *Curr Res Food Sci*, *3*, 51-58. doi:10.1016/j.crfs.2020.02.002
- Jeffrey, M. P., MacPherson, C. W., Mathieu, O., Tompkins, T. A., & Green-Johnson, J. M. (2020). Secretome-Mediated Interactions with Intestinal Epithelial Cells: A Role for Secretome Components from *Lactobacillus rhamnosus* R0011 in the Attenuation of *Salmonella enterica* Serovar Typhimurium Secretome and TNF- α -Induced Proinflammatory Responses. *J Immunol*, *204*(9), 2523-2534. doi:10.4049/jimmunol.1901440
- Jeffrey, M. P., Strap, J. L., Jones Taggart, H., & Green-Johnson, J. M. (2018). Suppression of Intestinal Epithelial Cell Chemokine Production by *Lactobacillus rhamnosus* R0011 and *Lactobacillus helveticus* R0389 Is Mediated by Secreted Bioactive Molecules. *Front Immunol*, *9*, 2639. doi:10.3389/fimmu.2018.02639

- Jha, A. K., Huang, S. C., Sergushichev, A., Lampropoulou, V., Ivanova, Y., Loginicheva, E., Chmielewski, K., Stewart, K. M., Ashall, J., Everts, B., Pearce, E. J., Driggers, E. M., & Artyomov, M. N. (2015). Network integration of parallel metabolic and transcriptional data reveals metabolic modules that regulate macrophage polarization. *Immunity*, *42*(3), 419-430. doi:10.1016/j.immuni.2015.02.005
- Jiang, W., Wang, X., Zeng, B., Liu, L., Tardivel, A., Wei, H., Han, J., MacDonald, H. R., Tschopp, J., Tian, Z., & Zhou, R. (2013). Recognition of gut microbiota by NOD2 is essential for the homeostasis of intestinal intraepithelial lymphocytes. *J Exp Med*, *210*(11), 2465-2476. doi:10.1084/jem.20122490
- Jie, W., Andrade, K. C., Lin, X., Yang, X., Yue, X., & Chang, J. (2015). Pathophysiological Functions of Rnd3/RhoE. *Compr Physiol*, *6*(1), 169-186. doi:10.1002/cphy.c150018
- Jimenez, J. C., & Federle, M. J. (2014). Quorum sensing in group A Streptococcus. *Front Cell Infect Microbiol*, *4*, 127. doi:10.3389/fcimb.2014.00127
- Johnson-Henry, K. C., Mitchell, D. J., Avitzur, Y., Galindo-Mata, E., Jones, N. L., & Sherman, P. M. (2004). Probiotics reduce bacterial colonization and gastric inflammation in *H. pylori*-infected mice. *Dig Dis Sci*, *49*(7-8), 1095-1102. doi:10.1023/b:ddas.0000037794.02040.c2
- Jones, R. M., Luo, L., Ardita, C. S., Richardson, A. N., Kwon, Y. M., Mercante, J. W., Alam, A., Gates, C. L., Wu, H., Swanson, P. A., Lambeth, J. D., Denning, P. W., & Neish, A. S. (2013). Symbiotic lactobacilli stimulate gut epithelial proliferation via Nox-mediated generation of reactive oxygen species. *EMBO J*, *32*(23), 3017-3028. doi:10.1038/emboj.2013.224
- Jousse, C., Deval, C., Maurin, A. C., Parry, L., Cherasse, Y., Chaveroux, C., Lefloch, R., Lenormand, P., Bruhat, A., & Fournoux, P. (2007). TRB3 inhibits the transcriptional activation of stress-regulated genes by a negative feedback on the ATF4 pathway. *J Biol Chem*, *282*(21), 15851-15861. doi:10.1074/jbc.M611723200
- Jung, H. C., Eckmann, L., Yang, S. K., Panja, A., Fierer, J., Morzycka-Wroblewska, E., & Kagnoff, M. F. (1995). A distinct array of proinflammatory cytokines is expressed in human colon epithelial cells in response to bacterial invasion. *J Clin Invest*, *95*(1), 55-65. doi:10.1172/JCI117676
- Kainulainen, V., & Korhonen, T. K. (2014). Dancing to another tune-adhesive moonlighting proteins in bacteria. *Biology (Basel)*, *3*(1), 178-204. doi:10.3390/biology3010178
- Kang, B., Alvarado, L. J., Kim, T., Lehmann, M. L., Cho, H., He, J., Li, P., Kim, B. H., Larochelle, A., & Kelsall, B. L. (2020). Commensal microbiota drive the functional diversification of colon macrophages. *Mucosal Immunol*, *13*(2), 216-229. doi:10.1038/s41385-019-0228-3
- Kanwar, Y. S. (2010). TRB3: an oxidant stress-induced pseudokinase with a potential to negatively modulate MCP-1 cytokine in diabetic nephropathy. *Am J Physiol Renal Physiol*, *299*(5), F963-964. doi:10.1152/ajprenal.00479.2010
- Karczewski, J., & Groot, J. (2000). Molecular physiology and pathophysiology of tight junctions III. Tight junction regulation by intracellular messengers: differences in response within and between epithelia. *Am J Physiol Gastrointest Liver Physiol*, *279*(4), G660-665. doi:10.1152/ajpgi.2000.279.4.G660

- Kaur, H., Bose, C., & Mande, S. S. (2019). Tryptophan Metabolism by Gut Microbiome and Gut-Brain-Axis: An in silico Analysis. *Front Neurosci*, *13*, 1365. doi:10.3389/fnins.2019.01365
- Keestra-Gounder, A. M., Tsohis, R. M., & Baumler, A. J. (2015). Now you see me, now you don't: the interaction of Salmonella with innate immune receptors. *Nat Rev Microbiol*, *13*(4), 206-216. doi:10.1038/nrmicro3428
- Khawar, M. B., Abbasi, M. H., & Sheikh, N. (2016). IL-32: A Novel Pluripotent Inflammatory Interleukin, towards Gastric Inflammation, Gastric Cancer, and Chronic Rhino Sinusitis. *Mediators Inflamm*, *2016*, 8413768. doi:10.1155/2016/8413768
- Kim, C. H. (2018). Immune regulation by microbiome metabolites. *Immunology*, *154*(2), 220-229. doi:10.1111/imm.12930
- Kim, H., Jung, B. J., Jung, J. H., Kim, J. Y., Chung, S. K., & Chung, D. K. (2012). Lactobacillus plantarum lipoteichoic acid alleviates TNF-alpha-induced inflammation in the HT-29 intestinal epithelial cell line. *Mol Cells*, *33*(5), 479-486. doi:10.1007/s10059-012-2266-5
- Kim, M., Galan, C., Hill, A. A., Wu, W. J., Fehlner-Peach, H., Song, H. W., Schady, D., Bettini, M. L., Simpson, K. W., Longman, R. S., Littman, D. R., & Diehl, G. E. (2018). Critical Role for the Microbiota in CX3CR1(+) Intestinal Mononuclear Phagocyte Regulation of Intestinal T Cell Responses. *Immunity*, *49*(1), 151-163 e155. doi:10.1016/j.immuni.2018.05.009
- Kim, M. H., & Kim, H. (2017). The Roles of Glutamine in the Intestine and Its Implication in Intestinal Diseases. *Int J Mol Sci*, *18*(5). doi:10.3390/ijms18051051
- Kim, S. I., Kim, S., Kim, E., Hwang, S. Y., & Yoon, H. (2018). Secretion of Salmonella Pathogenicity Island 1-Encoded Type III Secretion System Effectors by Outer Membrane Vesicles in Salmonella enterica Serovar Typhimurium. *Front Microbiol*, *9*, 2810. doi:10.3389/fmicb.2018.02810
- Kinoshita, H., Uchida, H., Kawai, Y., Kawasaki, T., Wakahara, N., Matsuo, H., Watanabe, M., Kitazawa, H., Ohnuma, S., Miura, K., Horii, A., & Saito, T. (2008). Cell surface Lactobacillus plantarum LA 318 glyceraldehyde-3-phosphate dehydrogenase (GAPDH) adheres to human colonic mucin. *J Appl Microbiol*, *104*(6), 1667-1674. doi:10.1111/j.1365-2672.2007.03679.x
- Kleemann, R., Hausser, A., Geiger, G., Mischke, R., Burger-Kentischer, A., Flieger, O., Johannes, F. J., Roger, T., Calandra, T., Kapurniotu, A., Grell, M., Finkelmeier, D., Brunner, H., & Bernhagen, J. (2000). Intracellular action of the cytokine MIF to modulate AP-1 activity and the cell cycle through Jab1. *Nature*, *408*(6809), 211-216. doi:10.1038/35041591
- Kleerebezem, M. (2004). Quorum sensing control of lantibiotic production; nisin and subtilin autoregulate their own biosynthesis. *Peptides*, *25*(9), 1405-1414. doi:10.1016/j.peptides.2003.10.021
- Ko, H. M., Oh, S. H., Bang, H. S., Kang, N. I., Cho, B. H., Im, S. Y., & Lee, H. K. (2009). Glutamine protects mice from lethal endotoxic shock via a rapid induction of MAPK phosphatase-1. *J Immunol*, *182*(12), 7957-7962. doi:10.4049/jimmunol.0900043
- Kohler, H., Sakaguchi, T., Hurley, B. P., Kase, B. A., Reinecker, H. C., & McCormick, B. A. (2007). Salmonella enterica serovar Typhimurium regulates intercellular

- junction proteins and facilitates transepithelial neutrophil and bacterial passage. *Am J Physiol Gastrointest Liver Physiol*, 293(1), G178-187. doi:10.1152/ajpgi.00535.2006
- Kramer, A., Green, J., Pollard, J., Jr., & Tugendreich, S. (2014). Causal analysis approaches in Ingenuity Pathway Analysis. *Bioinformatics*, 30(4), 523-530. doi:10.1093/bioinformatics/btt703
- Kumar, A., Wu, H., Collier-Hyams, L. S., Hansen, J. M., Li, T., Yamoah, K., Pan, Z. Q., Jones, D. P., & Neish, A. S. (2007). Commensal bacteria modulate cullin-dependent signaling via generation of reactive oxygen species. *EMBO J*, 26(21), 4457-4466. doi:10.1038/sj.emboj.7601867
- Kwon, J. W., Kwon, H. K., Shin, H. J., Choi, Y. M., Anwar, M. A., & Choi, S. (2015). Activating transcription factor 3 represses inflammatory responses by binding to the p65 subunit of NF-kappaB. *Sci Rep*, 5, 14470. doi:10.1038/srep14470
- Lachmandas, E., Boutens, L., Ratter, J. M., Hijmans, A., Hooiveld, G. J., Joosten, L. A., Rodenburg, R. J., Franssen, J. A., Houtkooper, R. H., van Crevel, R., Netea, M. G., & Stienstra, R. (2016). Microbial stimulation of different Toll-like receptor signalling pathways induces diverse metabolic programmes in human monocytes. *Nat Microbiol*, 2, 16246. doi:10.1038/nmicrobiol.2016.246
- Lang, R., Hammer, M., & Mages, J. (2006). DUSP meet immunology: dual specificity MAPK phosphatases in control of the inflammatory response. *J Immunol*, 177(11), 7497-7504. doi:10.4049/jimmunol.177.11.7497
- Lang, T., Lee, J. P. W., Elgass, K., Pinar, A. A., Tate, M. D., Aitken, E. H., Fan, H., Creed, S. J., Deen, N. S., Traore, D. A. K., Mueller, I., Stanisic, D., Baiwog, F. S., Skene, C., Wilce, M. C. J., Mansell, A., Morand, E. F., & Harris, J. (2018). Macrophage migration inhibitory factor is required for NLRP3 inflammasome activation. *Nat Commun*, 9(1), 2223. doi:10.1038/s41467-018-04581-2
- LaRock, D. L., Chaudhary, A., & Miller, S. I. (2015). Salmonellae interactions with host processes. *Nat Rev Microbiol*, 13(4), 191-205. doi:10.1038/nrmicro3420
- Latham, T., Mackay, L., Sproul, D., Karim, M., Culley, J., Harrison, D. J., Hayward, L., Langridge-Smith, P., Gilbert, N., & Ramsahoye, B. H. (2012). Lactate, a product of glycolytic metabolism, inhibits histone deacetylase activity and promotes changes in gene expression. *Nucleic Acids Res*, 40(11), 4794-4803. doi:10.1093/nar/gks066
- Lauterbach, M. A., Hanke, J. E., Serefidou, M., Mangan, M. S. J., Kolbe, C. C., Hess, T., Rothe, M., Kaiser, R., Hoss, F., Gehlen, J., Engels, G., Kreutzenbeck, M., Schmidt, S. V., Christ, A., Imhof, A., Hiller, K., & Latz, E. (2019). Toll-like Receptor Signaling Rewires Macrophage Metabolism and Promotes Histone Acetylation via ATP-Citrate Lyase. *Immunity*, 51(6), 997-1011 e1017. doi:10.1016/j.immuni.2019.11.009
- Lawrence, T., & Natoli, G. (2011). Transcriptional regulation of macrophage polarization: enabling diversity with identity. *Nat Rev Immunol*, 11(11), 750-761. doi:10.1038/nri3088
- Lebeer, S., Claes, I. J., & Vanderleyden, J. (2012). Anti-inflammatory potential of probiotics: lipoteichoic acid makes a difference. *Trends Microbiol*, 20(1), 5-10. doi:10.1016/j.tim.2011.09.004

- Lebeer, S., Vanderleyden, J., & De Keersmaecker, S. C. (2008). Genes and molecules of lactobacilli supporting probiotic action. *Microbiol Mol Biol Rev*, 72(4), 728-764, Table of Contents. doi:10.1128/MMBR.00017-08
- Lebeer, S., Vanderleyden, J., & De Keersmaecker, S. C. (2010). Host interactions of probiotic bacterial surface molecules: comparison with commensals and pathogens. *Nat Rev Microbiol*, 8(3), 171-184. doi:10.1038/nrmicro2297
- Lee, J., Mo, J. H., Katakura, K., Alkalay, I., Rucker, A. N., Liu, Y. T., Lee, H. K., Shen, C., Cojocaru, G., Shenouda, S., Kagnoff, M., Eckmann, L., Ben-Neriah, Y., & Raz, E. (2006). Maintenance of colonic homeostasis by distinctive apical TLR9 signalling in intestinal epithelial cells. *Nat Cell Biol*, 8(12), 1327-1336. doi:10.1038/ncb1500
- Lee, S., Kim, G. L., Kim, N. Y., Kim, S. J., Ghosh, P., & Rhee, D. K. (2018). ATF3 Stimulates IL-17A by Regulating Intracellular Ca(2+)/ROS-Dependent IL-1beta Activation During Streptococcus pneumoniae Infection. *Front Immunol*, 9, 1954. doi:10.3389/fimmu.2018.01954
- Leng, L., Metz, C. N., Fang, Y., Xu, J., Donnelly, S., Baugh, J., Delohery, T., Chen, Y., Mitchell, R. A., & Bucala, R. (2003). MIF signal transduction initiated by binding to CD74. *J Exp Med*, 197(11), 1467-1476. doi:10.1084/jem.20030286
- Leppkes, M., Roulis, M., Neurath, M. F., Kollias, G., & Becker, C. (2014). Pleiotropic functions of TNF-alpha in the regulation of the intestinal epithelial response to inflammation. *Int Immunol*, 26(9), 509-515. doi:10.1093/intimm/dxu051
- Levy, M., Blacher, E., & Elinav, E. (2017). Microbiome, metabolites and host immunity. *Curr Opin Microbiol*, 35, 8-15. doi:10.1016/j.mib.2016.10.003
- Levy, M., Thaïss, C. A., & Elinav, E. (2016). Metabolites: messengers between the microbiota and the immune system. *Genes Dev*, 30(14), 1589-1597. doi:10.1101/gad.284091.116
- Li, H. F., Cheng, C. F., Liao, W. J., Lin, H., & Yang, R. B. (2010). ATF3-mediated epigenetic regulation protects against acute kidney injury. *J Am Soc Nephrol*, 21(6), 1003-1013. doi:10.1681/ASN.2009070690
- Li, T., Liu, M., Feng, X., Wang, Z., Das, I., Xu, Y., Zhou, X., Sun, Y., Guan, K. L., Xiong, Y., & Lei, Q. Y. (2014). Glyceraldehyde-3-phosphate dehydrogenase is activated by lysine 254 acetylation in response to glucose signal. *J Biol Chem*, 289(6), 3775-3785. doi:10.1074/jbc.M113.531640
- Li, X., Yu, Y., Gorshkov, B., Haigh, S., Bordan, Z., Weintraub, D., Rudic, R. D., Chakraborty, T., Barman, S. A., Verin, A. D., Su, Y., Lucas, R., Stepp, D. W., Chen, F., & Fulton, D. J. R. (2018). Hsp70 Suppresses Mitochondrial Reactive Oxygen Species and Preserves Pulmonary Microvascular Barrier Integrity Following Exposure to Bacterial Toxins. *Front Immunol*, 9, 1309. doi:10.3389/fimmu.2018.01309
- Lin, Q. Y., Mathieu, O., Tompkins, T. A., Buckley, N. D., & Green-Johnson, J. M. (2016). Modulation of the TNF alpha-induced gene expression profile of intestinal epithelial cells by soy fermented with lactic acid bacteria. *Journal of Functional Foods*, 23, 400-411. doi:10.1016/j.jff.2016.02.047
- Locati, M., Deuschle, U., Massardi, M. L., Martinez, F. O., Sironi, M., Sozzani, S., Bartfai, T., & Mantovani, A. (2002). Analysis of the gene expression profile activated by

- the CC chemokine ligand 5/RANTES and by lipopolysaccharide in human monocytes. *J Immunol*, *168*(7), 3557-3562. doi:10.4049/jimmunol.168.7.3557
- Lue, H., Thiele, M., Franz, J., Dahl, E., Speckgens, S., Leng, L., Fingerle-Rowson, G., Bucala, R., Luscher, B., & Bernhagen, J. (2007). Macrophage migration inhibitory factor (MIF) promotes cell survival by activation of the Akt pathway and role for CSN5/JAB1 in the control of autocrine MIF activity. *Oncogene*, *26*(35), 5046-5059. doi:10.1038/sj.onc.1210318
- Lund, J., Olsen, O. H., Sorensen, E. S., Stennicke, H. R., Petersen, H. H., & Overgaard, M. T. (2013). ADAMDEC1 is a metzincin metalloprotease with dampened proteolytic activity. *J Biol Chem*, *288*(29), 21367-21375. doi:10.1074/jbc.M113.474536
- Lv, X., Wang, H., Su, A., Xu, S., & Chu, Y. (2018). Herpes simplex virus type 2 infection triggers AP-1 transcription activity through TLR4 signaling in genital epithelial cells. *Virology Journal*, *15*(1), 173. doi:10.1186/s12985-018-1087-3
- Maaser, C., Eckmann, L., Paesold, G., Kim, H. S., & Kagnoff, M. F. (2002). Ubiquitous production of macrophage migration inhibitory factor by human gastric and intestinal epithelium. *Gastroenterology*, *122*(3), 667-680. doi:10.1053/gast.2002.31891
- MacMicking, J., Xie, Q. W., & Nathan, C. (1997). Nitric oxide and macrophage function. *Annu Rev Immunol*, *15*, 323-350. doi:10.1146/annurev.immunol.15.1.323
- Macpherson, C., Audy, J., Mathieu, O., & Tompkins, T. A. (2014). Multistrain probiotic modulation of intestinal epithelial cells' immune response to a double-stranded RNA ligand, poly(i.c). *Appl Environ Microbiol*, *80*(5), 1692-1700. doi:10.1128/AEM.03411-13
- MacPherson, C. W., Shastri, P., Mathieu, O., Tompkins, T. A., & Burguiere, P. (2017). Genome-Wide Immune Modulation of TLR3-Mediated Inflammation in Intestinal Epithelial Cells Differs between Single and Multi-Strain Probiotic Combination. *PLoS One*, *12*(1), e0169847. doi:10.1371/journal.pone.0169847
- Madej, M. P., Topfer, E., Boraschi, D., & Italiani, P. (2017). Different Regulation of Interleukin-1 Production and Activity in Monocytes and Macrophages: Innate Memory as an Endogenous Mechanism of IL-1 Inhibition. *Front Pharmacol*, *8*, 335. doi:10.3389/fphar.2017.00335
- Madsen, K. L. (2012). Enhancement of Epithelial Barrier Function by Probiotics. *Journal of Epithelial Biology and Pharmacology*, *5*, 55-59. doi:10.2174/1875044301205010055
- Maess, M. B., Sendelbach, S., & Lorkowski, S. (2010). Selection of reliable reference genes during THP-1 monocyte differentiation into macrophages. *BMC molecular biology*, *11*, 90-90. doi:10.1186/1471-2199-11-90
- Man, A. L., Lodi, F., Bertelli, E., Regoli, M., Pin, C., Mulholland, F., Satoskar, A. R., Taussig, M. J., & Nicoletti, C. (2008). Macrophage migration inhibitory factor plays a role in the regulation of microfold (M) cell-mediated transport in the gut. *J Immunol*, *181*(8), 5673-5680. doi:10.4049/jimmunol.181.8.5673
- Mantovani, A., Sica, A., Sozzani, S., Allavena, P., Vecchi, A., & Locati, M. (2004). The chemokine system in diverse forms of macrophage activation and polarization. *Trends Immunol*, *25*(12), 677-686. doi:10.1016/j.it.2004.09.015
- Mar, A. C., Chu, C. H., Lee, H. J., Chien, C. W., Cheng, J. J., Yang, S. H., Jiang, J. K., & Lee, T. C. (2015). Interleukin-1 Receptor Type 2 Acts with c-Fos to Enhance the

- Expression of Interleukin-6 and Vascular Endothelial Growth Factor A in Colon Cancer Cells and Induce Angiogenesis. *J Biol Chem*, 290(36), 22212-22224. doi:10.1074/jbc.M115.644823
- Marchiando, A. M., Graham, W. V., & Turner, J. R. (2010). Epithelial barriers in homeostasis and disease. *Annu Rev Pathol*, 5, 119-144. doi:10.1146/annurev.pathol.4.110807.092135
- Martinez, F. O., & Gordon, S. (2014). The M1 and M2 paradigm of macrophage activation: time for reassessment. *F1000Prime Rep*, 6, 13. doi:10.12703/P6-13
- Martinez, F. O., Gordon, S., Locati, M., & Mantovani, A. (2006). Transcriptional profiling of the human monocyte-to-macrophage differentiation and polarization: new molecules and patterns of gene expression. *J Immunol*, 177(10), 7303-7311. doi:10.4049/jimmunol.177.10.7303
- Mata Forsberg, M., Bjorkander, S., Pang, Y., Lundqvist, L., Ndi, M., Ott, M., Escriba, I. B., Jaeger, M. C., Roos, S., & Sverremark-Ekstrom, E. (2019). Extracellular Membrane Vesicles from Lactobacilli Dampen IFN-gamma Responses in a Monocyte-Dependent Manner. *Sci Rep*, 9(1), 17109. doi:10.1038/s41598-019-53576-6
- Medina-Contreras, O., Geem, D., Laur, O., Williams, I. R., Lira, S. A., Nusrat, A., Parkos, C. A., & Denning, T. L. (2011). CX3CR1 regulates intestinal macrophage homeostasis, bacterial translocation, and colitogenic Th17 responses in mice. *J Clin Invest*, 121(12), 4787-4795. doi:10.1172/JCI59150
- Meng, D., Sommella, E., Salviati, E., Campiglia, P., Ganguli, K., Djebali, K., Zhu, W., & Walker, W. A. (2020). Indole-3-lactic acid, a metabolite of tryptophan, secreted by *Bifidobacterium longum* subspecies *infantis* is anti-inflammatory in the immature intestine. *Pediatr Res*, 88(2), 209-217. doi:10.1038/s41390-019-0740-x
- Millet, P., Vachharajani, V., McPhail, L., Yoza, B., & McCall, C. E. (2016). GAPDH Binding to TNF-alpha mRNA Contributes to Posttranscriptional Repression in Monocytes: A Novel Mechanism of Communication between Inflammation and Metabolism. *J Immunol*, 196(6), 2541-2551. doi:10.4049/jimmunol.1501345
- Miro-Blanch, J., & Yanes, O. (2019). Epigenetic Regulation at the Interplay Between Gut Microbiota and Host Metabolism. *Front Genet*, 10, 638. doi:10.3389/fgene.2019.00638
- Mitroulis, I., Ruppova, K., Wang, B., Chen, L. S., Grzybek, M., Grinenko, T., Eugster, A., Troullinaki, M., Palladini, A., Kourtzelis, I., Chatzigeorgiou, A., Schlitzer, A., Beyer, M., Joosten, L. A. B., Isermann, B., Lesche, M., Petzold, A., Simons, K., Henry, I., Dahl, A., Schultze, J. L., Wielockx, B., Zamboni, N., Mirtschink, P., Coskun, U., Hajishengallis, G., Netea, M. G., & Chavakis, T. (2018). Modulation of Myelopoiesis Progenitors Is an Integral Component of Trained Immunity. *Cell*, 172(1-2), 147-161 e112. doi:10.1016/j.cell.2017.11.034
- Moreira, L. O., & Zamboni, D. S. (2012). NOD1 and NOD2 Signaling in Infection and Inflammation. *Front Immunol*, 3, 328. doi:10.3389/fimmu.2012.00328
- Mowat, A. M. (2018). To respond or not to respond - a personal perspective of intestinal tolerance. *Nat Rev Immunol*, 18(6), 405-415. doi:10.1038/s41577-018-0002-x
- Mowat, A. M., & Agace, W. W. (2014). Regional specialization within the intestinal immune system. *Nat Rev Immunol*, 14(10), 667-685. doi:10.1038/nri3738

- Mowat, A. M., & Bain, C. C. (2011). Mucosal macrophages in intestinal homeostasis and inflammation. *J Innate Immun*, 3(6), 550-564. doi:10.1159/000329099
- Murofushi, Y., Villena, J., Morie, K., Kanmani, P., Tohno, M., Shimazu, T., Aso, H., Suda, Y., Hashiguchi, K., Saito, T., & Kitazawa, H. (2015). The toll-like receptor family protein RP105/MD1 complex is involved in the immunoregulatory effect of exopolysaccharides from *Lactobacillus plantarum* N14. *Mol Immunol*, 64(1), 63-75. doi:10.1016/j.molimm.2014.10.027
- Nakano, T., Goto, S., Takaoka, Y., Tseng, H. P., Fujimura, T., Kawamoto, S., Ono, K., & Chen, C. L. (2018). A novel moonlight function of glyceraldehyde-3-phosphate dehydrogenase (GAPDH) for immunomodulation. *Biofactors*, 44(6), 597-608. doi:10.1002/biof.1379
- Negi, S., Das, D. K., Pahari, S., Nadeem, S., & Agrewala, J. N. (2019). Potential Role of Gut Microbiota in Induction and Regulation of Innate Immune Memory. *Front Immunol*, 10, 2441. doi:10.3389/fimmu.2019.02441
- Neish, A. S., Gewirtz, A. T., Zeng, H., Young, A. N., Hobert, M. E., Karmali, V., Rao, A. S., & Madara, J. L. (2000). Prokaryotic regulation of epithelial responses by inhibition of IkappaB-alpha ubiquitination. *Science*, 289(5484), 1560-1563. Retrieved from <https://www.ncbi.nlm.nih.gov/pubmed/10968793>
- Nguyen, C. T., Luong, T. T., Lee, S., Kim, G. L., Pyo, S., & Rhee, D. K. (2016). ATF3 provides protection from *Staphylococcus aureus* and *Listeria monocytogenes* infections. *FEMS Microbiol Lett*, 363(10). doi:10.1093/femsle/fnw090
- Nguyen, M. T., Uebele, J., Kumari, N., Nakayama, H., Peter, L., Ticha, O., Woischnig, A. K., Schmalzer, M., Khanna, N., Dohmae, N., Lee, B. L., Bekeredjian-Ding, I., & Gotz, F. (2017). Lipid moieties on lipoproteins of commensal and non-commensal staphylococci induce differential immune responses. *Nat Commun*, 8(1), 2246. doi:10.1038/s41467-017-02234-4
- Nguyen, P. T., Nguyen, T. T., Bui, D. C., Hong, P. T., Hoang, Q. K., & Nguyen, H. T. (2020). Exopolysaccharide production by lactic acid bacteria: the manipulation of environmental stresses for industrial applications. *AIMS Microbiol*, 6(4), 451-469. doi:10.3934/microbiol.2020027
- O'Callaghan, J., Butto, L. F., MacSharry, J., Nally, K., & O'Toole, P. W. (2012). Influence of adhesion and bacteriocin production by *Lactobacillus salivarius* on the intestinal epithelial cell transcriptional response. *Appl Environ Microbiol*, 78(15), 5196-5203. doi:10.1128/AEM.00507-12
- O'Flaherty, S., & Klaenhammer, T. R. (2012). Influence of exposure time on gene expression by human intestinal epithelial cells exposed to *Lactobacillus acidophilus*. *Appl Environ Microbiol*, 78(14), 5028-5032. doi:10.1128/AEM.00504-12
- O'Neill, L. A., Kishton, R. J., & Rathmell, J. (2016). A guide to immunometabolism for immunologists. *Nat Rev Immunol*, 16(9), 553-565. doi:10.1038/nri.2016.70
- Ohland, C. L., & Macnaughton, W. K. (2010). Probiotic bacteria and intestinal epithelial barrier function. *Am J Physiol Gastrointest Liver Physiol*, 298(6), G807-819. doi:10.1152/ajpgi.00243.2009
- Ohoka, N., Yoshii, S., Hattori, T., Onozaki, K., & Hayashi, H. (2005). TRB3, a novel ER stress-inducible gene, is induced via ATF4-CHOP pathway and is involved in cell death. *EMBO J*, 24(6), 1243-1255. doi:10.1038/sj.emboj.7600596

- Orecchioni, M., Ghosheh, Y., Pramod, A. B., & Ley, K. (2020). Corrigendum: Macrophage Polarization: Different Gene Signatures in M1(LPS+) vs. Classically and M2(LPS-) vs. Alternatively Activated Macrophages. *Front Immunol*, *11*, 234. doi:10.3389/fimmu.2020.00234
- Palmieri, E. M., Gonzalez-Cotto, M., Baseler, W. A., Davies, L. C., Ghesquiere, B., Maio, N., Rice, C. M., Rouault, T. A., Cassel, T., Higashi, R. M., Lane, A. N., Fan, T. W., Wink, D. A., & McVicar, D. W. (2020). Nitric oxide orchestrates metabolic rewiring in M1 macrophages by targeting aconitase 2 and pyruvate dehydrogenase. *Nat Commun*, *11*(1), 698. doi:10.1038/s41467-020-14433-7
- Paludan, S. R., Pradeu, T., Masters, S. L., & Mogensen, T. H. (2021). Constitutive immune mechanisms: mediators of host defence and immune regulation. *Nat Rev Immunol*, *21*(3), 137-150. doi:10.1038/s41577-020-0391-5
- Pandey, S., Kawai, T., & Akira, S. (2014). Microbial sensing by Toll-like receptors and intracellular nucleic acid sensors. *Cold Spring Harb Perspect Biol*, *7*(1), a016246. doi:10.1101/cshperspect.a016246
- Papa, S., Zazzeroni, F., Bubici, C., Jayawardena, S., Alvarez, K., Matsuda, S., Nguyen, D. U., Pham, C. G., Nelsbach, A. H., Melis, T., De Smaele, E., Tang, W. J., D'Adamio, L., & Franzoso, G. (2004). Gadd45 beta mediates the NF-kappa B suppression of JNK signalling by targeting MKK7/JNKK2. *Nat Cell Biol*, *6*(2), 146-153. doi:10.1038/ncb1093
- Park, S. H., Do, K. H., Choi, H. J., Kim, J., Kim, K. H., Park, J., Oh, C. G., & Moon, Y. (2013). Novel regulatory action of ribosomal inactivation on epithelial Nod2-linked proinflammatory signals in two convergent ATF3-associated pathways. *J Immunol*, *191*(10), 5170-5181. doi:10.4049/jimmunol.1301145
- Patten, D. A., Leivers, S., Chadha, M. J., Maqsood, M., Humphreys, P. N., Laws, A. P., & Collett, A. (2014). The structure and immunomodulatory activity on intestinal epithelial cells of the EPSs isolated from *Lactobacillus helveticus* sp. Rosyjski and *Lactobacillus acidophilus* sp. 5e2. *Carbohydr Res*, *384*, 119-127. doi:10.1016/j.carres.2013.12.008
- Penkov, S., Mitroulis, I., Hajishengallis, G., & Chavakis, T. (2019). Immunometabolic Crosstalk: An Ancestral Principle of Trained Immunity? *Trends Immunol*, *40*(1), 1-11. doi:10.1016/j.it.2018.11.002
- Peterson, L. W., & Artis, D. (2014). Intestinal epithelial cells: regulators of barrier function and immune homeostasis. *Nat Rev Immunol*, *14*(3), 141-153. doi:10.1038/nri3608
- Philpott, D. J., Sorbara, M. T., Robertson, S. J., Croitoru, K., & Girardin, S. E. (2014). NOD proteins: regulators of inflammation in health and disease. *Nat Rev Immunol*, *14*(1), 9-23. doi:10.1038/nri3565
- Pircalabioru, G., Aviello, G., Kubica, M., Zhdanov, A., Paclat, M. H., Brennan, L., Hertzberger, R., Papkovsky, D., Bourke, B., & Knaus, U. G. (2016). Defensive Mutualism Rescues NADPH Oxidase Inactivation in Gut Infection. *Cell Host Microbe*, *19*(5), 651-663. doi:10.1016/j.chom.2016.04.007
- Pitman, R. S., & Blumberg, R. S. (2000). First line of defense: the role of the intestinal epithelium as an active component of the mucosal immune system. *J Gastroenterol*, *35*(11), 805-814. Retrieved from <https://www.ncbi.nlm.nih.gov/pubmed/11085489>

- Postler, T. S., & Ghosh, S. (2017). Understanding the Holobiont: How Microbial Metabolites Affect Human Health and Shape the Immune System. *Cell Metab*, 26(1), 110-130. doi:10.1016/j.cmet.2017.05.008
- Qin, Y., & Wade, P. A. (2018). Crosstalk between the microbiome and epigenome: messages from bugs. *J Biochem*, 163(2), 105-112. doi:10.1093/jb/mvx080
- Qin, Z. Y. (2012). The use of THP-1 cells as a model for mimicking the function and regulation of monocytes and macrophages in the vasculature. *Atherosclerosis*, 221(1), 2-11. doi:DOI 10.1016/j.atherosclerosis.2011.09.003
- Quintin, J., Saeed, S., Martens, J. H. A., Giamarellos-Bourboulis, E. J., Ifrim, D. C., Logie, C., Jacobs, L., Jansen, T., Kullberg, B. J., Wijmenga, C., Joosten, L. A. B., Xavier, R. J., van der Meer, J. W. M., Stunnenberg, H. G., & Netea, M. G. (2012). *Candida albicans* infection affords protection against reinfection via functional reprogramming of monocytes. *Cell Host Microbe*, 12(2), 223-232. doi:10.1016/j.chom.2012.06.006
- Rakoff-Nahoum, S., Paglino, J., Eslami-Varzaneh, F., Edberg, S., & Medzhitov, R. (2004). Recognition of commensal microflora by toll-like receptors is required for intestinal homeostasis. *Cell*, 118(2), 229-241. doi:10.1016/j.cell.2004.07.002
- Ran, R., Lu, A., Zhang, L., Tang, Y., Zhu, H., Xu, H., Feng, Y., Han, C., Zhou, G., Rigby, A. C., & Sharp, F. R. (2004). Hsp70 promotes TNF-mediated apoptosis by binding IKK gamma and impairing NF-kappa B survival signaling. *Genes Dev*, 18(12), 1466-1481. doi:10.1101/gad.1188204
- Rangel, L. B., Agarwal, R., D'Souza, T., Pizer, E. S., Alo, P. L., Lancaster, W. D., Gregoire, L., Schwartz, D. R., Cho, K. R., & Morin, P. J. (2003). Tight junction proteins claudin-3 and claudin-4 are frequently overexpressed in ovarian cancer but not in ovarian cystadenomas. *Clin Cancer Res*, 9(7), 2567-2575. Retrieved from <https://www.ncbi.nlm.nih.gov/pubmed/12855632>
- Regoli, M., Bertelli, E., Gulisano, M., & Nicoletti, C. (2017). The Multifaceted Personality of Intestinal CX3CR1(+) Macrophages. *Trends Immunol*, 38(12), 879-887. doi:10.1016/j.it.2017.07.009
- Reimand, J., Isserlin, R., Voisin, V., Kucera, M., Tannus-Lopes, C., Rostamianfar, A., Wadi, L., Meyer, M., Wong, J., Xu, C., Merico, D., & Bader, G. D. (2019). Pathway enrichment analysis and visualization of omics data using g:Profiler, GSEA, Cytoscape and EnrichmentMap. *Nat Protoc*, 14(2), 482-517. doi:10.1038/s41596-018-0103-9
- Reuter, S., Gupta, S. C., Chaturvedi, M. M., & Aggarwal, B. B. (2010). Oxidative stress, inflammation, and cancer: how are they linked? *Free Radic Biol Med*, 49(11), 1603-1616. doi:10.1016/j.freeradbiomed.2010.09.006
- Rocha-Ramirez, L. M., Perez-Solano, R. A., Castanon-Alonso, S. L., Moreno Guerrero, S. S., Ramirez Pacheco, A., Garcia Garibay, M., & Eslava, C. (2017). Probiotic *Lactobacillus* Strains Stimulate the Inflammatory Response and Activate Human Macrophages. *J Immunol Res*, 2017, 4607491. doi:10.1155/2017/4607491
- Rodriguez, R. M., Suarez-Alvarez, B., & Lopez-Larrea, C. (2019). Therapeutic Epigenetic Reprogramming of Trained Immunity in Myeloid Cells. *Trends Immunol*, 40(1), 66-80. doi:10.1016/j.it.2018.11.006
- Roger, T., Delaloye, J., Chanson, A. L., Giddey, M., Le Roy, D., & Calandra, T. (2013). Macrophage migration inhibitory factor deficiency is associated with impaired

- killing of gram-negative bacteria by macrophages and increased susceptibility to *Klebsiella pneumoniae* sepsis. *J Infect Dis*, 207(2), 331-339. doi:10.1093/infdis/jis673
- Roger, T., Froidevaux, C., Martin, C., & Calandra, T. (2003). Macrophage migration inhibitory factor (MIF) regulates host responses to endotoxin through modulation of Toll-like receptor 4 (TLR4). *J Endotoxin Res*, 9(2), 119-123. doi:10.1179/096805103125001513
- Rousset, M. (1986). The human colon carcinoma cell lines HT-29 and Caco-2: two in vitro models for the study of intestinal differentiation. *Biochimie*, 68(9), 1035-1040. doi:10.1016/s0300-9084(86)80177-8
- Russell, D. G., Huang, L., & VanderVen, B. C. (2019). Immunometabolism at the interface between macrophages and pathogens. *Nat Rev Immunol*, 19(5), 291-304. doi:10.1038/s41577-019-0124-9
- Saad, N., Urdaci, M., Vignoles, C., Chaignepain, S., Tallon, R., Schmitter, J. M., & Bressollier, P. (2009). *Lactobacillus plantarum* 299v surface-bound GAPDH: a new insight into enzyme cell walls location. *J Microbiol Biotechnol*, 19(12), 1635-1643. doi:10.4014/jmb.0902.0102
- Salminen, A., Paimela, T., Suuronen, T., & Kaamiranta, K. (2008). Innate immunity meets with cellular stress at the IKK complex: Regulation of the IKK complex by HSP70 and HSP90. *Immunology Letters*, 117(1), 9-15. doi:10.1016/j.imlet.2007.12.017
- Salojin, K. V., Owusu, I. B., Millerchip, K. A., Potter, M., Platt, K. A., & Oravec, T. (2006). Essential role of MAPK phosphatase-1 in the negative control of innate immune responses. *J Immunol*, 176(3), 1899-1907. doi:10.4049/jimmunol.176.3.1899
- Salzman, N. H., & Bevins, C. L. (2008). Negative interactions with the microbiota: IBD. *Adv Exp Med Biol*, 635, 67-78. doi:10.1007/978-0-387-09550-9_6
- Sanders, S. E., Madara, J. L., McGuirk, D. K., Gelman, D. S., & Colgan, S. P. (1995). Assessment of inflammatory events in epithelial permeability: a rapid screening method using fluorescein dextrans. *Epithelial Cell Biol*, 4(1), 25-34. Retrieved from <https://www.ncbi.nlm.nih.gov/pubmed/8563793>
- Sansonetti, P. J. (2004). War and peace at mucosal surfaces. *Nat Rev Immunol*, 4(12), 953-964. doi:10.1038/nri1499
- Saraiva, M., & O'Garra, A. (2010). The regulation of IL-10 production by immune cells. *Nat Rev Immunol*, 10(3), 170-181. doi:10.1038/nri2711
- Scharl, M., Paul, G., Barrett, K. E., & McCole, D. F. (2009). AMP-activated protein kinase mediates the interferon-gamma-induced decrease in intestinal epithelial barrier function. *J Biol Chem*, 284(41), 27952-27963. doi:10.1074/jbc.M109.046292
- Schaupp, L., Muth, S., Rogell, L., Kofoed-Branzk, M., Melchior, F., Lienenklaus, S., Ganal-Vonarburg, S. C., Klein, M., Guendel, F., Hain, T., Schutze, K., Grundmann, U., Schmitt, V., Dorsch, M., Spanier, J., Larsen, P. K., Schwanz, T., Jackel, S., Reinhardt, C., Bopp, T., Danckwardt, S., Mahnke, K., Heinz, G. A., Mashreghi, M. F., Durek, P., Kalinke, U., Kretz, O., Huber, T. B., Weiss, S., Wilhelm, C., Macpherson, A. J., Schild, H., Diefenbach, A., & Probst, H. C. (2020). Microbiota-Induced Type I Interferons Instruct a Poised Basal State of Dendritic Cells. *Cell*, 181(5), 1080-1096 e1019. doi:10.1016/j.cell.2020.04.022

- Seth, A., Yan, F., Polk, D. B., & Rao, R. K. (2008). Probiotics ameliorate the hydrogen peroxide-induced epithelial barrier disruption by a PKC- and MAP kinase-dependent mechanism. *Am J Physiol Gastrointest Liver Physiol*, 294(4), G1060-1069. doi:10.1152/ajpgi.00202.2007
- Sha, H., Zhang, D., Zhang, Y., Wen, Y., & Wang, Y. (2017). ATF3 promotes migration and M1/M2 polarization of macrophages by activating tenascinC via Wnt/betacatenin pathway. *Mol Med Rep*, 16(3), 3641-3647. doi:10.3892/mmr.2017.6992
- Shannon, P., Markiel, A., Ozier, O., Baliga, N. S., Wang, J. T., Ramage, D., Amin, N., Schwikowski, B., & Ideker, T. (2003). Cytoscape: a software environment for integrated models of biomolecular interaction networks. *Genome Res*, 13(11), 2498-2504. doi:10.1101/gr.1239303
- Sharif, O., Bolshakov, V. N., Raines, S., Newham, P., & Perkins, N. D. (2007). Transcriptional profiling of the LPS induced NF-kappaB response in macrophages. *BMC Immunol*, 8, 1. doi:10.1186/1471-2172-8-1
- Sherman, P. M., Johnson-Henry, K. C., Yeung, H. P., Ngo, P. S., Goulet, J., & Tompkins, T. A. (2005). Probiotics reduce enterohemorrhagic *Escherichia coli* O157:H7- and enteropathogenic *E. coli* O127:H6-induced changes in polarized T84 epithelial cell monolayers by reducing bacterial adhesion and cytoskeletal rearrangements. *Infect Immun*, 73(8), 5183-5188. doi:10.1128/IAI.73.8.5183-5188.2005
- Smith, D. W., & Nagler-Anderson, C. (2005). Preventing intolerance: the induction of nonresponsiveness to dietary and microbial antigens in the intestinal mucosa. *J Immunol*, 174(7), 3851-3857. Retrieved from <https://www.ncbi.nlm.nih.gov/pubmed/15778338>
- Smith, S. M., Moran, A. P., Duggan, S. P., Ahmed, S. E., Mohamed, A. S., Windle, H. J., O'Neill, L. A., & Kelleher, D. P. (2011). Tribbles 3: a novel regulator of TLR2-mediated signaling in response to *Helicobacter pylori* lipopolysaccharide. *J Immunol*, 186(4), 2462-2471. doi:10.4049/jimmunol.1000864
- Smolkova, K., Spackova, J., Gotvaldova, K., Dvorak, A., Krenkova, A., Hubalek, M., Holendova, B., Vitek, L., & Jezek, P. (2020). SIRT3 and GCN5L regulation of NADP+- and NADPH-driven reactions of mitochondrial isocitrate dehydrogenase IDH2. *Sci Rep*, 10(1), 8677. doi:10.1038/s41598-020-65351-z
- Stecher, B., Robbiani, R., Walker, A. W., Westendorf, A. M., Barthel, M., Kremer, M., Chaffron, S., Macpherson, A. J., Buer, J., Parkhill, J., Dougan, G., von Mering, C., & Hardt, W. D. (2007). Salmonella enterica serovar typhimurium exploits inflammation to compete with the intestinal microbiota. *PLoS Biol*, 5(10), 2177-2189. doi:10.1371/journal.pbio.0050244
- Stelzer, G., Inger, A., Olender, T., Iny-Stein, T., Dalah, I., Harel, A., Safran, M., & Lancet, D. (2009). GeneDecks: paralog hunting and gene-set distillation with GeneCards annotation. *OMICS*, 13(6), 477-487. doi:10.1089/omi.2009.0069
- Stelzer, G., Rosen, N., Plaschkes, I., Zimmerman, S., Twik, M., Fishilevich, S., Stein, T. I., Nudel, R., Lieder, I., Mazor, Y., Kaplan, S., Dahary, D., Warshawsky, D., Guan-Golan, Y., Kohn, A., Rappaport, N., Safran, M., & Lancet, D. (2016). The GeneCards Suite: From Gene Data Mining to Disease Genome Sequence Analyses. *Curr Protoc Bioinformatics*, 54, 1 30 31-31 30 33. doi:10.1002/cpbi.5

- Stetinova, V., Smetanova, L., Kvetina, J., Svoboda, Z., Zidek, Z., & Tlaskalova-Hogenova, H. (2010). Caco-2 cell monolayer integrity and effect of probiotic *Escherichia coli* Nissle 1917 components. *Neuro Endocrinol Lett*, *31 Suppl 2*, 51-56. Retrieved from <https://www.ncbi.nlm.nih.gov/pubmed/21187838>
- Suez, J., Zmora, N., Segal, E., & Elinav, E. (2019). The pros, cons, and many unknowns of probiotics. *Nat Med*, *25*(5), 716-729. doi:10.1038/s41591-019-0439-x
- Sun, K. Y., Xu, D. H., Xie, C., Plummer, S., Tang, J., Yang, X. F., & Ji, X. H. (2017). *Lactobacillus paracasei* modulates LPS-induced inflammatory cytokine release by monocyte-macrophages via the up-regulation of negative regulators of NF-kappaB signaling in a TLR2-dependent manner. *Cytokine*, *92*, 1-11. doi:10.1016/j.cyto.2017.01.003
- Suzuki, T. (2013). Regulation of intestinal epithelial permeability by tight junctions. *Cell Mol Life Sci*, *70*(4), 631-659. doi:10.1007/s00018-012-1070-x
- Svanstrom, A., Boveri, S., Bostrom, E., & Melin, P. (2013). The lactic acid bacteria metabolite phenyllactic acid inhibits both radial growth and sporulation of filamentous fungi. *BMC Res Notes*, *6*, 464. doi:10.1186/1756-0500-6-464
- Szanto, A., Balint, B. L., Nagy, Z. S., Barta, E., Dezso, B., Pap, A., Szeles, L., Poliska, S., Oros, M., Evans, R. M., Barak, Y., Schwabe, J., & Nagy, L. (2010). STAT6 transcription factor is a facilitator of the nuclear receptor PPARgamma-regulated gene expression in macrophages and dendritic cells. *Immunity*, *33*(5), 699-712. doi:10.1016/j.immuni.2010.11.009
- Szklarczyk, D., Gable, A. L., Lyon, D., Junge, A., Wyder, S., Huerta-Cepas, J., Simonovic, M., Doncheva, N. T., Morris, J. H., Bork, P., Jensen, L. J., & Mering, C. V. (2019). STRING v11: protein-protein association networks with increased coverage, supporting functional discovery in genome-wide experimental datasets. *Nucleic Acids Res*, *47*(D1), D607-D613. doi:10.1093/nar/gky1131
- Tafazoli, F., Magnusson, K. E., & Zheng, L. (2003). Disruption of epithelial barrier integrity by *Salmonella enterica* serovar typhimurium requires geranylgeranylated proteins. *Infect Immun*, *71*(2), 872-881. doi:10.1128/IAI.71.2.872-881.2003
- Takeda, N., O'Dea, E. L., Doedens, A., Kim, J. W., Weidemann, A., Stockmann, C., Asagiri, M., Simon, M. C., Hoffmann, A., & Johnson, R. S. (2010). Differential activation and antagonistic function of HIF- α isoforms in macrophages are essential for NO homeostasis. *Genes Dev*, *24*(5), 491-501. doi:10.1101/gad.1881410
- Tannahill, G. M., Curtis, A. M., Adamik, J., Palsson-McDermott, E. M., McGettrick, A. F., Goel, G., Frezza, C., Bernard, N. J., Kelly, B., Foley, N. H., Zheng, L., Gardet, A., Tong, Z., Jany, S. S., Corr, S. C., Haneklaus, M., Caffrey, B. E., Pierce, K., Walmsley, S., Beasley, F. C., Cummins, E., Nizet, V., Whyte, M., Taylor, C. T., Lin, H., Masters, S. L., Gottlieb, E., Kelly, V. P., Clish, C., Auron, P. E., Xavier, R. J., & O'Neill, L. A. (2013). Succinate is an inflammatory signal that induces IL-1beta through HIF-1alpha. *Nature*, *496*(7444), 238-242. doi:10.1038/nature11986
- Tao, Y., Drabik, K. A., Waypa, T. S., Musch, M. W., Alverdy, J. C., Schneewind, O., Chang, E. B., & Petrof, E. O. (2006). Soluble factors from *Lactobacillus GG* activate MAPKs and induce cytoprotective heat shock proteins in intestinal epithelial cells. *Am J Physiol Cell Physiol*, *290*(4), C1018-1030. doi:10.1152/ajpcell.00131.2005

- Tarique, A. A., Logan, J., Thomas, E., Holt, P. G., Sly, P. D., & Fantino, E. (2015). Phenotypic, functional, and plasticity features of classical and alternatively activated human macrophages. *Am J Respir Cell Mol Biol*, *53*(5), 676-688. doi:10.1165/rcmb.2015-0012OC
- Thiennimitr, P., Winter, S. E., Winter, M. G., Xavier, M. N., Tolstikov, V., Huseby, D. L., Sterzenbach, T., Tsohis, R. M., Roth, J. R., & Baumler, A. J. (2011). Intestinal inflammation allows Salmonella to use ethanolamine to compete with the microbiota. *Proc Natl Acad Sci U S A*, *108*(42), 17480-17485. doi:10.1073/pnas.1107857108
- Thomas, C. M., Hong, T., van Pijkeren, J. P., Hemarajata, P., Trinh, D. V., Hu, W., Britton, R. A., Kalkum, M., & Versalovic, J. (2012). Histamine derived from probiotic *Lactobacillus reuteri* suppresses TNF via modulation of PKA and ERK signaling. *PLoS One*, *7*(2), e31951. doi:10.1371/journal.pone.0031951
- Thomas, C. M., & Versalovic, J. (2010). Probiotics-host communication: Modulation of signaling pathways in the intestine. *Gut Microbes*, *1*(3), 148-163. doi:10.4161/gmic.1.3.11712
- Tisza, M. J., Zhao, W., Fuentes, J. S., Prijic, S., Chen, X., Levental, I., & Chang, J. T. (2016). Motility and stem cell properties induced by the epithelial-mesenchymal transition require destabilization of lipid rafts. *Oncotarget*, *7*(32), 51553-51568. doi:10.18632/oncotarget.9928
- Tommassen, J., & Arenas, J. (2017). Biological Functions of the Secretome of *Neisseria meningitidis*. *Front Cell Infect Microbiol*, *7*, 256. doi:10.3389/fcimb.2017.00256
- Tomosada, Y., Villena, J., Murata, K., Chiba, E., Shimazu, T., Aso, H., Iwabuchi, N., Xiao, J. Z., Saito, T., & Kitazawa, H. (2013). Immunoregulatory effect of bifidobacteria strains in porcine intestinal epithelial cells through modulation of ubiquitin-editing enzyme A20 expression. *PLoS One*, *8*(3), e59259. doi:10.1371/journal.pone.0059259
- Tompkins, T. A., Barreau, G., & de Carvalho, V. G. (2012). Draft genome sequence of probiotic strain *Lactobacillus rhamnosus* R0011. *J Bacteriol*, *194*(4), 902. doi:10.1128/JB.06584-11
- Tuo, Y., Song, X., Song, Y., Liu, W., Tang, Y., Gao, Y., Jiang, S., Qian, F., & Mu, G. (2018). Screening probiotics from *Lactobacillus* strains according to their abilities to inhibit pathogen adhesion and induction of pro-inflammatory cytokine IL-8. *J Dairy Sci*, *101*(6), 4822-4829. doi:10.3168/jds.2017-13654
- Vaishnava, S., Behrendt, C. L., Ismail, A. S., Eckmann, L., & Hooper, L. V. (2008). Paneth cells directly sense gut commensals and maintain homeostasis at the intestinal host-microbial interface. *Proc Natl Acad Sci U S A*, *105*(52), 20858-20863. doi:10.1073/pnas.0808723105
- Valladares, R. B., Graves, C., Wright, K., Gardner, C. L., Lorca, G. L., & Gonzalez, C. F. (2015). H₂O₂ production rate in *Lactobacillus johnsonii* is modulated via the interplay of a heterodimeric flavin oxidoreductase with a soluble 28 Kd PAS domain containing protein. *Front Microbiol*, *6*, 716. doi:10.3389/fmicb.2015.00716
- Van den Bossche, J., O'Neill, L. A., & Menon, D. (2017). Macrophage Immunometabolism: Where Are We (Going)? *Trends Immunol*, *38*(6), 395-406. doi:10.1016/j.it.2017.03.001

- Vanamee, E. S., & Faustman, D. L. (2018). Structural principles of tumor necrosis factor superfamily signaling. *Sci Signal*, *11*(511). doi:10.1126/scisignal.aao4910
- Varol, C., Mildner, A., & Jung, S. (2015). Macrophages: development and tissue specialization. *Annu Rev Immunol*, *33*, 643-675. doi:10.1146/annurev-immunol-032414-112220
- Viola, A., Munari, F., Sanchez-Rodriguez, R., Scolaro, T., & Castegna, A. (2019). The Metabolic Signature of Macrophage Responses. *Front Immunol*, *10*, 1462. doi:10.3389/fimmu.2019.01462
- Vivek-Ananth, R. P., Mohanraj, K., Vandanashree, M., Jhingran, A., Craig, J. P., & Samal, A. (2018). Comparative systems analysis of the secretome of the opportunistic pathogen *Aspergillus fumigatus* and other *Aspergillus* species. *Sci Rep*, *8*(1), 6617. doi:10.1038/s41598-018-25016-4
- Vogel, C. F., Khan, E. M., Leung, P. S., Gershwin, M. E., Chang, W. L., Wu, D., Haarmann-Stemann, T., Hoffmann, A., & Denison, M. S. (2014). Cross-talk between aryl hydrocarbon receptor and the inflammatory response: a role for nuclear factor-kappaB. *J Biol Chem*, *289*(3), 1866-1875. doi:10.1074/jbc.M113.505578
- von Schillde, M. A., Hormannspenger, G., Weiher, M., Alpert, C. A., Hahne, H., Bauerl, C., van Huynegem, K., Steidler, L., Hrnir, T., Perez-Martinez, G., Kuster, B., & Haller, D. (2012). Lactocepin secreted by *Lactobacillus* exerts anti-inflammatory effects by selectively degrading proinflammatory chemokines. *Cell Host Microbe*, *11*(4), 387-396. doi:10.1016/j.chom.2012.02.006
- Vong, L., Lorentz, R. J., Assa, A., Glogauer, M., & Sherman, P. M. (2014). Probiotic *Lactobacillus rhamnosus* inhibits the formation of neutrophil extracellular traps. *J Immunol*, *192*(4), 1870-1877. doi:10.4049/jimmunol.1302286
- Vujcic, M., Despotovic, S., Saksida, T., & Stojanovic, I. (2020). The Effect of Macrophage Migration Inhibitory Factor on Intestinal Permeability: FITC-Dextran Serum Measurement and Transmission Electron Microscopy. *Methods Mol Biol*, *2080*, 193-201. doi:10.1007/978-1-4939-9936-1_17
- Vujcic, M., Saksida, T., Despotovic, S., Bajic, S. S., Lalic, I., Koprivica, I., Gajic, D., Golic, N., Tolinacki, M., & Stojanovic, I. (2018). The Role of Macrophage Migration Inhibitory Factor in the Function of Intestinal Barrier. *Sci Rep*, *8*(1), 6337. doi:10.1038/s41598-018-24706-3
- Wallace, T. D., Bradley, S., Buckley, N. D., & Green-Johnson, J. M. (2003). Interactions of lactic acid bacteria with human intestinal epithelial cells: effects on cytokine production. *J Food Prot*, *66*(3), 466-472. Retrieved from <http://www.ncbi.nlm.nih.gov/pubmed/12636302>
- Wan, M. L., Chen, Z., Shah, N. P., & El-Nezami, H. (2018). Effects of *Lactobacillus rhamnosus* GG and *Escherichia coli* Nissle 1917 Cell-Free Supernatants on Modulation of Mucin and Cytokine Secretion on Human Intestinal Epithelial HT29-MTX Cells. *J Food Sci*, *83*(7), 1999-2007. doi:10.1111/1750-3841.14168
- Warde-Farley, D., Donaldson, S. L., Comes, O., Zuberi, K., Badrawi, R., Chao, P., Franz, M., Grouios, C., Kazi, F., Lopes, C. T., Maitland, A., Mostafavi, S., Montojo, J., Shao, Q., Wright, G., Bader, G. D., & Morris, Q. (2010). The GeneMANIA prediction server: biological network integration for gene prioritization and

- predicting gene function. *Nucleic Acids Res*, 38(Web Server issue), W214-220. doi:10.1093/nar/gkq537
- Wentworth, C. C., Alam, A., Jones, R. M., Nusrat, A., & Neish, A. S. (2011). Enteric commensal bacteria induce extracellular signal-regulated kinase pathway signaling via formyl peptide receptor-dependent redox modulation of dual specific phosphatase 3. *J Biol Chem*, 286(44), 38448-38455. doi:10.1074/jbc.M111.268938
- Whitmore, M. M., Iparraguirre, A., Kubelka, L., Weninger, W., Hai, T., & Williams, B. R. (2007). Negative regulation of TLR-signaling pathways by activating transcription factor-3. *J Immunol*, 179(6), 3622-3630. Retrieved from <https://www.ncbi.nlm.nih.gov/pubmed/17785797>
- Wikoff, W. R., Anfora, A. T., Liu, J., Schultz, P. G., Lesley, S. A., Peters, E. C., & Siuzdak, G. (2009). Metabolomics analysis reveals large effects of gut microflora on mammalian blood metabolites. *Proc Natl Acad Sci U S A*, 106(10), 3698-3703. doi:10.1073/pnas.0812874106
- Winter, S. E., Thiennimitr, P., Winter, M. G., Butler, B. P., Huseby, D. L., Crawford, R. W., Russell, J. M., Bevins, C. L., Adams, L. G., Tsohis, R. M., Roth, J. R., & Baumler, A. J. (2010). Gut inflammation provides a respiratory electron acceptor for Salmonella. *Nature*, 467(7314), 426-429. doi:10.1038/nature09415
- Wong, C. B., Tanaka, A., Kuhara, T., & Xiao, J. Z. (2020). Potential Effects of Indole-3-Lactic Acid, a Metabolite of Human Bifidobacteria, on NGF-induced Neurite Outgrowth in PC12 Cells. *Microorganisms*, 8(3). doi:10.3390/microorganisms8030398
- Wood, C., Keeling, S., Bradley, S., Johnson-Green, P., & Green-Johnson, J. M. (2007). Interactions in the mucosal microenvironment: vasoactive intestinal peptide modulates the down-regulatory action of Lactobacillus rhamnosus on LPS-induced interleukin-8 production by intestinal epithelial cells. *Microbial Ecology in Health and Disease*, 19(3), 191-200. doi:10.1080/08910600701278722
- Wu, M., Xu, L. G., Zhai, Z., & Shu, H. B. (2003). SINK is a p65-interacting negative regulator of NF-kappaB-dependent transcription. *J Biol Chem*, 278(29), 27072-27079. doi:10.1074/jbc.M209814200
- Wu, R. Y., Jeffrey, M. P., Johnson-Henry, K. C., Green-Johnson, J. M., & Sherman, P. M. (2016). Impact of prebiotics, probiotics, and gut derived metabolites on host immunity. *LymphoSign Journal*, 4(1), 1-24. doi:10.14785/lymphosign-2016-0012
- Xu, Q., Mengin-Lecreulx, D., Liu, X. W., Patin, D., Farr, C. L., Grant, J. C., Chiu, H. J., Jaroszewski, L., Knuth, M. W., Godzik, A., Lesley, S. A., Elsliger, M. A., Deacon, A. M., & Wilson, I. A. (2015). Insights into Substrate Specificity of NlpC/P60 Cell Wall Hydrolases Containing Bacterial SH3 Domains. *MBio*, 6(5), e02327-02314. doi:10.1128/mBio.02327-14
- Xue, J., Schmidt, S. V., Sander, J., Draffehn, A., Krebs, W., Quester, I., De Nardo, D., Gohel, T. D., Emde, M., Schmidleithner, L., Ganesan, H., Nino-Castro, A., Mallmann, M. R., Labzin, L., Theis, H., Kraut, M., Beyer, M., Latz, E., Freeman, T. C., Ulas, T., & Schultze, J. L. (2014). Transcriptome-based network analysis reveals a spectrum model of human macrophage activation. *Immunity*, 40(2), 274-288. doi:10.1016/j.immuni.2014.01.006

- Yadav, M., Verma, M. K., & Chauhan, N. S. (2018). A review of metabolic potential of human gut microbiome in human nutrition. *Arch Microbiol*, *200*(2), 203-217. doi:10.1007/s00203-017-1459-x
- Yan, F., Cao, H., Cover, T. L., Whitehead, R., Washington, M. K., & Polk, D. B. (2007). Soluble proteins produced by probiotic bacteria regulate intestinal epithelial cell survival and growth. *Gastroenterology*, *132*(2), 562-575. doi:10.1053/j.gastro.2006.11.022
- Yoo, H., Antoniewicz, M. R., Stephanopoulos, G., & Kelleher, J. K. (2008). Quantifying reductive carboxylation flux of glutamine to lipid in a brown adipocyte cell line. *J Biol Chem*, *283*(30), 20621-20627. doi:10.1074/jbc.M706494200
- Yu, W., Dittenhafer-Reed, K. E., & Denu, J. M. (2012). SIRT3 protein deacetylates isocitrate dehydrogenase 2 (IDH2) and regulates mitochondrial redox status. *J Biol Chem*, *287*(17), 14078-14086. doi:10.1074/jbc.M112.355206
- Yue, Y., Huang, W., Liang, J., Guo, J., Ji, J., Yao, Y., Zheng, M., Cai, Z., Lu, L., & Wang, J. (2015). IL4I1 Is a Novel Regulator of M2 Macrophage Polarization That Can Inhibit T Cell Activation via L-Tryptophan and Arginine Depletion and IL-10 Production. *PLoS One*, *10*(11), e0142979. doi:10.1371/journal.pone.0142979
- Zanello, G., Goethel, A., Rouquier, S., Prescott, D., Robertson, S. J., Maisonneuve, C., Streutker, C., Philpott, D. J., & Croitoru, K. (2016). The Cytosolic Microbial Receptor Nod2 Regulates Small Intestinal Crypt Damage and Epithelial Regeneration following T Cell-Induced Enteropathy. *J Immunol*, *197*(1), 345-355. doi:10.4049/jimmunol.1600185
- Zargar, A., Quan, D. N., Carter, K. K., Guo, M., Sintim, H. O., Payne, G. F., & Bentley, W. E. (2015). Bacterial secretions of nonpathogenic *Escherichia coli* elicit inflammatory pathways: a closer investigation of interkingdom signaling. *MBio*, *6*(2), e00025. doi:10.1128/mBio.00025-15
- Zelante, T., Iannitti, R. G., Cunha, C., De Luca, A., Giovannini, G., Pieraccini, G., Zecchi, R., D'Angelo, C., Massi-Benedetti, C., Fallarino, F., Carvalho, A., Puccetti, P., & Romani, L. (2013). Tryptophan catabolites from microbiota engage aryl hydrocarbon receptor and balance mucosal reactivity via interleukin-22. *Immunity*, *39*(2), 372-385. doi:10.1016/j.immuni.2013.08.003
- Zhao, H., Zhao, C., Dong, Y., Zhang, M., Wang, Y., Li, F., Li, X., McClain, C., Yang, S., & Feng, W. (2015). Inhibition of miR122a by *Lactobacillus rhamnosus* GG culture supernatant increases intestinal occludin expression and protects mice from alcoholic liver disease. *Toxicol Lett*, *234*(3), 194-200. doi:10.1016/j.toxlet.2015.03.002
- Zheng, D., Liwinski, T., & Elinav, E. (2020). Interaction between microbiota and immunity in health and disease. *Cell Res*. doi:10.1038/s41422-020-0332-7
- Zhou, S., Zhao, L., Liang, Z., Liu, S., Li, Y., Liu, S., Yang, H., Liu, M., & Xi, M. (2019). Indoleamine 2,3-dioxygenase 1 and Programmed Cell Death-ligand 1 Co-expression Predicts Poor Pathologic Response and Recurrence in Esophageal Squamous Cell Carcinoma after Neoadjuvant Chemoradiotherapy. *Cancers (Basel)*, *11*(2). doi:10.3390/cancers11020169
- Zhou, Y., Zhou, B., Pache, L., Chang, M., Khodabakhshi, A. H., Tanaseichuk, O., Benner, C., & Chanda, S. K. (2019). Metascape provides a biologist-oriented resource for

the analysis of systems-level datasets. *Nat Commun*, 10(1), 1523.
doi:10.1038/s41467-019-09234-6